Untersuchung des Einflusses von Ladungsträgerdelokalisation und Grenzflächendipolen auf die Dissoziationswahrscheinlichkeit von Exzitonen in organischen Solarzellen

zur Erlangung des akademischen Grades eines

Doktors der Naturwissenschaften (Dr. rer. nat.)

im Promotionsprogramm

Photophysik synthetischer und biologischer multichromophorer Systeme

der Bayreuther Graduiertenschule für Mathematik und Naturwissenschaften

Von der Universität Bayreuth genehmigte Abhandlung von

Steffen Tscheuschner

geboren in Bayreuth, Deutschland

Bayreuth 2017

Die vorliegende Arbeit wurde in der Zeit von Januar 2013 bis Dezember 2016 am Lehrstuhl für Experimentalphysik II an der Universität Bayreuth unter der Betreuung von Prof. Dr. Anna Köhler angefertigt.

Amtierender Direktor der Graduiertenschule: Prof. Dr. Dirk Schüler

Prof. Dr. Stephan Kümmel (bei Einreichung)

Datum der Einreichung der Dissertation: 22.12.2016

Datum des wissenschaftlichen Kolloquiums: 14.06.2017

Prüfungsausschuss:

Prof. Dr. Anna Köhler	(Erstgutachter)
PD Dr. Richard Hildner	(Zweitgutachter)
Prof. Dr. Walter Zimmermann	(Vorsitz)
Prof. Dr. Mukundan Thelakkat	(Drittprüfer)

Inhaltsverzeichnis

1. Zusammenfassung

Die von der Bundesregierung beschlossene Energiewende zielt auf die Verwendung und Speicherung von regenerativer Energie hin. Solarenergie spielt dabei eine wichtige Rolle. Solarzellen mit organischen Halbleitermaterialien sind dabei von besonderem Interesse, weil sie die Herstellung von leichten und flexiblen oder beliebig geformten Bauteilen ermöglichen. Um die Effizienz organischer Solarzellen - derzeit nicht über 12% - weiter zu steigern, müssen daher die grundlegenden intrinsischen Prozesse, wie Ladungsträgertrennung und -rekombination, genauer untersucht werden.

Die vorliegende Doktorarbeit beschäftigt sich mit der Frage, wie die Trennung von Elektron-Loch-Paaren in organischen Solarzellen funktioniert. Der entscheidende Verlustkanal bei der Ladungsträgergeneration ist die Rekombination der gegensätzlichen Ladungsträger an der Donor-Akzeptor-Grenzfläche. Zunächst wurden in diesem Zusammenhang die Beiträge und Auswirkungen von geminaler und nicht geminaler Rekombination analysiert. Im Laufe dieser Untersuchungen stellte sich heraus, dass die Reduzierung der Bindungsenergie durch die Delokalisierung der Ladungsträger im Donor bzw. Akzeptor einen entscheidender Aspekt darstellt. Der Zusammenhang zwischen lokaler Ordnung und Delokalisation sowie ihre Auswirkung auf die Trennungswahrscheinlichkeit von Elektron-Loch-Paaren waren jedoch nicht vollständig verstanden. Ebenso war nicht verstanden, inwieweit Grenzflächendipole zusätzlich helfen können die Bindungsenergie weiter zu reduzieren.

Die Effizienz einer Solarzelle wird durch die Konkurrenz der Rekombination von Elektron-Loch-Paaren und der Dissoziation in freie Ladungsträger bestimmt. Es wird angenommen, dass Ladungen frei sind, wenn ihre potentielle Coulomb-Energie gleich der thermischen Energie ist. Diese freien Ladungen können dann entweder an den Elektroden extrahiert werden oder mit einem gegensätzlichen Ladungsträger eines anderen Elektron-Loch-Paares einen gebundenen Zustand bilden und nicht geminal rekombinieren. Letzteres ist von der Ladungsträgerdichte abhängig. Daher kann dieser Beitrag durch die eingestrahlte Lichtintensität identifiziert werden. Variiert man nun die Schichtdicke der Polymerschicht, stellt man eine Dickenabhängigkeit der geminalen Rekombination fest. In dieser Dissertation wird gezeigt, dass diese Abhängigkeit nur über eine Rückdiffusion von bereits freien Ladungsträgern zu ihrem eigenen Partner erklärt werden kann. Dieser häufig nicht berücksichtigte Verlustkanal trägt entscheidend zum maximal erreichbaren Füllfaktor und somit zur Gesamteffizienz bei. Dies wird besonders bei Materialien, die eine reduzierte Beweglichkeit eines der beiden Ladungsträger besitzen, deutlich.

Um die Parameter, die die geminale Rekombination bestimmen, genauer zu identifizieren, habe ich kinetische Monte-Carlo-Simulationen mit nur einem Ladungsträgerpaar durchgeführt. Dadurch können der Einfluss der Beweglichkeit der einzelnen Ladungsträger, die Dimensionalität des Transports und der Einfluss von Delokalisierung auf die Effizienz des Trennungsprozesses untersucht werden. Es stellt sich heraus, dass die Effizienz erheblich

gesteigert werden kann, wenn man von einem 1D- zu einem 2D-Transport übergeht. Diese Erkenntnis ist für das Design von Solarzellen wichtig, da man sicherstellen muss, dass durch Aggregation und Phasenseparation von Donor- und Akzeptor-Materialien die Dimensionalität des Transportes nicht reduziert wird. Des Weiteren stellt sich heraus, dass eine nahezu ausgeglichene Ladungsträgerbeweglichkeit die Trennung, insbesondere im Bereich kleiner Felder, ebenfalls begünstigt. In diesem Bereich dominiert die Diffusion der Ladungsträger und nicht der Drift, der durch das Feld in der Solarzelle bestimmt wird. Ein weiterer wichtiger Punkt ist, dass die Delokalisierung von Ladungsträgern sowohl die Dissoziationswahrscheinlichkeit im Bereich kleiner Felder steigert, als auch die Sättigungsfeldstärke reduziert. Diese beschreibt die Feldstärke im Device, bei der nahezu alle Elektron-Loch-Paare getrennt werden können. Somit kann durch die Delokalisierung der Ladungsträger ebenfalls der Füllfaktor und dadurch die Effizienz der Solarzelle gesteigert werden.

Um die Delokalisierung im Akzeptor bzw. Donor getrennt voneinander zu untersuchen, wurden im Rahmen dieser Doktorarbeit Solarzellen gemessen, bei denen die aktive Schicht nur aus einer einzelnen Schicht besteht. Diese wurden dann bei verschiedenen Energien angeregt, um unterschiedlich stark delokalisierte Zustände besetzen zu können. Als Akzeptoren wurden C_{60} und $PC_{61}BM$ verwendet. Regt man diese unterhalb von 2.25 eV an, so befinden sie sich anschließend in einem stark gebundenen S_1-Zustand. Regt man mit einer höheren Energie an, so kann man einen stärker delokalisierten und schwächer gebundenen Charge-Transfer-Zustand (CT-Zustand) erhalten. Dieser kann dann mit einer, im Vergleich zu anderen Polymeren, hohen Wahrscheinlichkeit in freie Ladungsträger dissoziieren. Dieses Verhalten ist im C_{60} stärker ausgeprägt als im $PC_{61}BM$. Somit tragen, insbesondere bei Verwendung von C_{60} als Akzeptor, diese CT-Zustände zum Photostrom und somit zur Effizienz der Solarzelle bei. Es kann gezeigt werden, dass die Bindungsenergie dieser Zustände ungefähr 100 meV beträgt.

Um hingegen die Delokalisation im Donor zu untersuchen, wurden zwei Low-Bandgap-Polymere verwendet, PCDTBT und PCPDTBT. Auch hier konnte gezeigt werden, dass eine Anregung in einen stärker delokalisierten Zustand mit Hilfe von zusätzlicher Energie helfen kann die erzeugten Ladungsträger leichter zu trennen. Dies wird deutlich, wenn sowohl die Sättigungsfeldstärke von Zweischicht-Solarzellen, als auch die interne Quanteneffizienz von Einzelschicht-Solarzellen in Abhängigkeit der Anregungsenergie betrachtet wird. Hier erkennt man, dass die Sättigungsfeldstärke sinkt und die Quanteneffizienz steigt und somit die Trennung der gebundenen Zustände erleichtert wird, sobald man einen stärker delokalisierten Zustand anregt. Um den Unterschied der Delokalisierung für verschiedene verwendete Donatoren zu verdeutlichen, wurde eine Reihe von Polyparaphenylenen untersucht. Hierbei wurde die Steifigkeit des Poylmerrückgrats variiert. Die unterschiedlichen Konjugationslängen der verwendeten Polymere konnten über die Blauverschiebung im Absorptionsspektrum nachgewiesen werden. Die geordneten Polymere zeigen mehr Struktur in den Absorptionsspektren, so dass ebenfalls eine höhere

Ordnung angenommen werden kann. Die feldabhängige Trennungswahrscheinlichkeit konnte von mir mit Hilfe eines analytischen Modells beschrieben werden. Die Delokalisierung der Ladungsträger wird hierbei durch einen zusätzlichen energetischen Beitrag zur potentiellen Energie des Elektron-Loch-Paares berücksichtigt. Dieser Beitrag wird durch die Lösung der 1D-Schrödinergleichung bestimmt. Die Delokalisierung kann dabei über die Variation der effektiven Masse des Ladungsträgers berücksichtigt werden. Dadurch wird es anhand der feldabhängigen Dissoziationswahrscheinlichkeit möglich die Delokalisierung der Ladungsträger über die effektive Masse zu beschreiben.

Damit kann dieses Modell verwendet werden, um die Auswirkungen der Delokalisation auf die Ladungsträgertrennung genauer zu untersuchen. Bei den im Rahmen dieser Dissertation durchgeführten numerischen Simulationen stellt sich heraus, dass die Delokalisierung von Ladungsträgern in Verbindung mit Dipolen an der Donor-Akzeptor-Grenzfläche genügt, um die experimentellen Daten zu beschreiben. Über Dipole und die Delokalisierung wird die Bindungsenergie des Elektron-Loch-Paares verringert, wodurch die Sättigungsfeldstärke reduziert wird. Aus diesen Gründen lässt sich der Trennungsmechanismus mit einem relaxierten CT-Zustand über einen Hüpfprozess beschreiben. Die so theoretisch gefundene Bindungsenergie kann auch über eine kombinierte Messung von externer Quanteneffizienz und Elektrolumineszenz sowie über temperaturabhängige Messungen der Leerlaufspannung experimentell bestätigt werden. Mit diesem Modell lässt sich zudem die Sättigungsfeldstärke in Abhängigkeit der einzelnen Parameter vorhersagen. Somit kann ein Bild gewonnen werden, wie sich die Delokalisierung, die Dipole an der Donor-Akzeptor Grenzfläche und die Lebenszeit des CT-Zustandes in Kombination mit der Ladungsträgerbeweglichkeit auf die Sättigungsfeldstärke auswirken. In diesem Zusammenhang kann die Steigerung des Füllfaktors mit zunehmender Delokalisation gezeigt werden.

1. Summary

The energy transition, enacted by the German Federal Government, aims for the use and storage of renewable energies. Solar energy plays a major role in this context. Solar cells using organic semiconductors are of peculiar interest, because they enable the production of light, flexible and arbitrary shaped modules. To further enhance the efficiency of organic solar cells – not above 13% - the intrinsic processes, like charge separation and recombination, have to be investigated in more detail.

This work addresses the question, how electron hole separation takes place in an organic semiconductor. The main loss, during the separation of an electron hole pair, is the recombination of opposite charged carriers at the donor acceptor interface. Firstly, the contributions and the impact of geminate and nongeminate recombination are analyzed. In the course of these investigations it turns out, that the reduction of the coulomb binding energy due to the delocalization of the charge carriers in the donor or acceptor is a crucial issue. The correlation of local order and delocalization and their impact on the dissociation probability is not fully understood yet, nor is the supplementary reduction of binding energy mediated by additional interfacial dipoles.

The efficiency of a solar cell is determined by the competition of the recombination of electron hole pairs with the dissociation into free charges. It is assumed, that charges are free, if their potential coulomb energy is equal or less the thermal energy. These free charges could either be extracted at the electrodes or recombine nongeminately with an opposite charge of another electron hole pair. The latter is dependent on the charge carrier concentration. Therefore, this contribution could be identified by modifying the light intensity. By varying the thickness of the polymer layer, one could identify a thickness dependence of the geminate recombination. In this dissertation it is pointed out, that this relationship could only be explained by back diffusion of free charge carriers to their siblings. This underestimated loss plays an important role for the maximum achievable fill factor as well as the overall power conversion efficiency. This is particularly notable in materials, where one of the charge carriers has a significantly reduced mobility.

I carried out kinetic Monte-Carlo-simulations with only one pair of charge carriers to identify the parameters for geminate recombination. With this I was able to investigate the impact of mobility of the respective charge carriers, the dimensionality of the transport, as well as the effect of delocalization on the efficiency of charge separation. It turns out, that this efficiency could be increased significantly, when going from a 1D to a 2D transport regime. This is an important insight for the design of solar cells. In this context, it is noteworthy that Aggregation and phase separation in donor and acceptor materials should not reduce the dimensionality of the transport. Furthermore, it turns out, that nearly balanced charge carrier mobility enhances charge separation, especially at low electric fields. In this case, diffusion instead of drift, caused by the applied field, dominates the charge carrier

movement. Another important point is that delocalization of charge carriers enhances the dissociation probability in the low field regime and reduces the saturation field. The latter corresponds to the field strength in the device at which nearly every electron hole pair can be separated. Thus, delocalization of charge carriers will also increase the fill factor and as a consequence the efficiency of the solar cell.

In this thesis, single layer solar cells, in which the active layer only consist of one material, were measured to investigate the influence of delocalization in the donor and in the acceptor separately. These cells were excited at different energies to populate different delocalized states. C_{60} and $PC_{61}BM$ were used as acceptors. Using energies below 2.25 eV, only the S_1 state of the fullerene is excited. When pumping at higher energies, a more delocalized and weaker bound charge transfer (CT) state is populated. In contrast to polymers, this state could dissociate into free charge carriers at a higher yield. In $C_{60,}$ this behaviour is more pronounced than in $PC_{61}BM$. As a consequence, especially when using C_{60} as acceptor, these CT-state contributes to the total photocurrent and therefore to the power conversion efficiency of the solar cell. It can be shown, that the binding energy of these states is approximately 100 meV.

Two different low-band-gap polymers, PCDTBT as well as PCPDTBT, were used to investigate the delocalization on the donor. In the same way as before it can be shown, that an excitation into a more delocalized state with additional energy, can help for an easier dissociation. This was figured out, when the saturation field strength, as well as the internal quantum efficiency, were investigated in dependence of the excitation energy. It can be seen, that the saturation field decreases, the internal quantum efficiency increases and therefore the dissociation is enhanced, as soon as a more delocalized state is excited. To point out the difference in delocalization for different donors, a series of several poly-para-phenylenes were investigated. In the course of this study, the stiffness of the polymer backbone was varied. The different conjugation lengths could be identified by a blue shift of the absorption and the fact, that higher ordered polymers also show more structured absorption spectra. The field dependent dissociation probability could be fitted with an analytical model. Delocalization of the charge carriers was included with an additional term for the potential energy of the electron hole pair. This contribution is determined from the 1D-Schrödinger equation. Different delocalization could be considered by varying the effective mass. In summary, the delocalization can now be described by the effective mass derived from field dependent dissociation probabilities.

As a result, this model can be used to investigate the impact of delocalization on the charge separation process. Within the framework of the numerical simulations in this thesis it turns out, that delocalization in combination with dipoles at the donor acceptor interface suffices the description of experimental data. The binding energy of the electron hole pair can be decreased with interfacial dipoles and delocalization, so that the saturation field is reduced. These are the reasons, why the mechanism of charge separation can be described by a

hopping transport from relaxed CT-states. The theoretically derived binding energy could be verified by a combined measurement of the external quantum efficiency and electroluminescence as well as using a temperature dependent measurement of the open circuit voltage. Within this model, the saturation field can now be predicted in dependence of different parameters. By doing this, it is possible to get an idea of the influence of delocalization, dipoles at the donor acceptor interface, and the combination of lifetime and charge carrier mobility on the saturation field. In this context, the increase of the fill factor with increasing delocalization can be shown.

2. Einleitung

2.1. Motivation

Die globale Erderwärmung ist ein ernstzunehmendes Thema. Deshalb hat die Bundesregierung beschlossen die Energiewende einzuleiten. [1] Neben der Reduzierung des Energiebedarfs, zum Beispiel durch die Einführung von Energiesparlampen, ist der Ausbau der erneuerbaren Energien ein wichtiger Punkt. Hierzu zählen Wind-, Wasser-, und Sonnenenergie. Solarkraftwerke konnten ihre Kapazität vom Jahr 2000 bis zum Jahr 2013 verdoppeln. [2] Um Solarzellen herzustellen, werden jedoch große Mengen an Energie benötigt. Dies widerspricht den zuvor genannten Zielen der Energiewende. Daher sind Alternativen nötig, welche die zur Produktion notwendige Energie reduzieren und dennoch bezahlbaren Strom liefern. Eine Möglichkeit sind organische Solarzellen, da bei ihrer Herstellung im Vergleich zu anorganischen Solarzellen deutlich weniger Energie aufgebracht werden muss. Der größte Nachteil ist jedoch, dass die Effizienz organischer Solarzellen bei maximal 13.2% im Labor liegt und damit unterhalb ihrer anorganischen Pendants. [3] Multischicht-Solarzellen (GaInP/GaAs/Ge) erreichen bis zu 44%, wohingegen die meisten auf dem Markt erhältlichen Module eine Effizienz in der Größenordnung von 15% besitzen. [4] Der Vorteil organischen Solarzellen ist der, dass diese leicht und flexibel gebaut werden können. Daher können sie auch an Gebäudefassaden eingesetzt werden, an denen anorganische Module zu schwer wären. Ein weiterer Vorteil ist, dass organische Solarzellen semitransparent gebaut werden können, wodurch diese prinzipiell in Fenstern oder als schattenspendendes Designelement einsetzbar sind. [5] Um dieses Ziel zu erreichen, muss die Effizienz jedoch weiter verbessert werden. Als theoretisches oberes Limit erhält man für Einzelschicht-Solarzellen, wie es die meisten siliziumbasierten Module sind, das sogenannte Shockley-Queisser-Limit von 30%. [6] Dieses kann auch für organische Solarzellen adaptiert werden. Organische Solarzellen bestehen aus einem Donor- und einem Akzeptor-Material. Bei diesen Materialien gibt es jedoch einen Energieverlust, damit freie Elektronen und Löcher gebildet werden können. Das modifizierte Shockley-Queisser-Limit ergibt bei einem angenommenen Energieverlust von 0.5 eV in diesem Fall eine obere Grenze von 23%. [7-9] Um dieser Grenze näher zu kommen, müssen die intrinsischen Prozesse bei der Erzeugung freier Ladungsträger verstanden werden. Die gewonnenen Erkenntnisse können dann bei der Entwicklung neuer Materialien oder Geometrien genutzt werden, um die Verluste zu reduzieren und somit die Effizienz der organischen Solarzellen weiter zu steigern.

Die Ladungsträgertrennung erfolgt in organischen Solarzellen in mehreren Schritten. Zunächst fällt ein Photon in die Solarzelle ein und kann dort absorbiert werden, um so ein Exziton zu erzeugen. Dieses Exziton kann anschließend diffundieren, um eine Grenzfläche zwischen Donor und Akzeptor zu finden. Die typische Diffusionslänge beträgt ungefähr 10 nm. An der Grenzfläche kann ein ladungsgetrennter Zustand (Charge-Transfer-Zustand, CT-Zustand) gebildet werden. Befindet sich das Exziton auf dem Donor (Akzeptor), so wird

das Elektron (Loch) auf den Akzeptor (Donor) übertagen und das Loch (Elektron) verbleibt auf dem Donor (Akzeptor). Bei diesem Prozess wird die Differenz der beiden HOMOs (Highest Occupied Molecular Orbital) bzw. LUMOs (Lowest Unoccupied Molecular Orbital) frei und ist damit verloren. Dennoch werden hier typischerweise 0.5 eV benötigt, damit der entstandene CT-Zustand stabil ist und nachfolgend getrennt werden kann. [10] Elektron und Loch können anschließend versuchen, mittels thermisch aktivierter Sprünge, aus diesem metastabilen Zustand entgegen der Coulombanziehung zu entkommen. Hierbei können sie innerhalb ihrer Lebenszeit mehrere Versuche unternehmen. Sind sie schließlich entkommen, so müssen die nun freien Ladungsträger an die entsprechenden Elektroden transportiert werden. Dabei können sie wieder in die Nähe von Ladungsträgern mit entgegengesetzter Ladung gelangen und mit diesem rekombinieren.[11-13]

Die hier vorliegende Doktorarbeit beschäftigt sich hauptsächlich mit der Ladungsträgertrennung an der Donor-Akzeptor-Grenzfläche. Im ersten Teil der Arbeit wird die Trennung allgemein betrachtet. Hierbei wird ein besonderes Augenmerk darauf gelegt, welche Rolle die Rekombination spielt, da sie den Hauptverlustprozess in organischen Solarzellen darstellt. Es ist daher besonders wichtig zu verstehen, wie sie sich beeinflussen lassen. Ein Aspekt, der hier zum Tragen kommt, ist die Frage, ab wann ein Ladungsträger als frei angesehen werden kann. Der zweite Teil der Arbeit beschäftigt sich damit, wie die Bindungsenergie zwischen Donor und Akzeptor reduziert werden kann, um so eine höhere Effizienz der Solarzellen zu erhalten. Dies kann über die Delokalisierung der Ladungsträger und über Grenzflächendipole erreicht werden. Ein weiterer Aspekt in diesem Zusammenhang ist die Beschreibung und Modellierung des Trennungsprozesses in Abhängigkeit dieser Parameter, da es bisher fast keine experimentellen Studien gibt, die erfolgreich Theorie und Experiment verbinden.

In Abschnitt 2.2 werden daher verschiedene Modelle zur Ladungsträgertrennung vorgestellt. Die wichtigsten in der Arbeit verwendeten Modelle werden dort kurz erläutert und ihre Annahmen beschrieben. Zunächst werden im Abschnitt 2.2.1 und 2.2.2 die historisch genutzten Modelle erläutert und ihre Anwendbarkeit und Grenzen aufgezeigt. Abschnitt 2.2.3 bis 2.2.5 erläutern dann die modifizierten Modelle, bei denen die Delokalisierung mit berücksichtigt werden kann. Es können nicht alle in dieser Doktorarbeit betrachteten Fälle abgedeckt werden, weil diese Modelle nur eine analytische Lösung liefern und daher nicht immer auf die entsprechenden Probleme angepasst werden können. Aus diesem Grund wird in Abschnitt 2.3 eine Möglichkeit erläutert, wie diese Lücke geschlossen werden kann. Dort werden die den Modellen zugrunde liegenden Ratengleichungen mit Hilfe einer dynamischen Monte-Carlo-Simulation gelöst.

2.2. Modelle zur Ladungsträgertrennung

Der elementare Prozess in einer organischen Solarzelle ist die Erzeugung freier Ladungsträger. Der größte Unterschied zwischen anorganischen und organischen Solarzellen ist dabei die Bindungsenergie E_b. Diese bestimmt sich aus dem Abstand r der beiden Ladungsschwerpunkte und der effektiven Dielektrizitätskonstante ϵ_r.

$$E_b = \frac{e^2}{4\pi\epsilon_0\epsilon_r r} \tag{1}$$

Während die Bindungsenergie bei anorganischen Solarzellen wegen der hohen Dielektrizitätskonstante fast verschwindet, ist sie in organischen Solarzellen um den Faktor 20 größer als die thermisch zu Verfügung stehende Energie. Bei einem Abstand von ungefähr 1 nm liegt die Bindungsenergie im Bereich von 0.4-0.5 eV. Dies sind typische Werte für einen CT-Zustand in *einem* Material. Werden unterschiedliche Materialien als Donor und Akzeptor verwendet, so reduziert sich die Bindungsenergie auf ca. 0.2 eV. Dieser Energiebetrag muss aufgebracht werden, um die Ladungsträger unendlich weit voneinander zu entfernen. Er ergibt sich aus der Differenz von elektrischer Lücke und optischer Bandlücke. Die optische Bandlücke ist die Energie, die benötigt wird, um das Material optisch anzuregen. Das elektrische Gap hingegen ist die Differenz zwischen dem Ionisationspotential des Donors und der Elektronenaffinität des Akzeptors. Das Ionisationspotential ist die Energie, die benötigt wird, um ein Elektron in das Vakuumniveau anzuheben. Dahingegen ist die Energie, die frei wird, wenn ein Elektron aus dem Vakuumniveau aufgenommen wird, wird als Elektronaffinität bezeichnet.

Da die Bindungsenergie deutlich größer ist als die thermische Energie, sind Elektron und Loch stark gebunden. Elektron und Loch gelten als frei, wenn seine Bindungsenergie kleiner oder gleich der thermischen Energie ist. Der Abstand, ab welchem Elektron und Loch als frei betrachtet werden, ist der Coulomb-Capture-Radius.

$$r_c = \frac{e^2}{4\pi\epsilon_0\epsilon_r kT} \tag{2}$$

Dies bedeutet jedoch nicht, dass Elektron und Loch nicht mehr in ihrem gegenseitigen Coulombfeld sind, wenn der Abstand größer als r_c ist. Um die Ladungen leichter dissoziieren zu können, kann zusätzlich ein elektrisches Feld angelegt werden, welches die Coulombbarriere reduziert und somit dazu beiträgt, die Trennungswahrscheinlichkeit zu erhöhen.

Als Erster hat Onsager die Trennungswahrscheinlichkeit von Ionen beschrieben. [14] Dies wurde dann von Pai und Enk für Elektron-Loch-Paare adaptiert (Siehe Abschnitt 2.2.1). [15] Braun hat schließlich Onsagers Theorie weiterentwickelt und um einen stabilen Grundzustand erweitert (Siehe Abschnitt 2.2.2). [16] Diese Modelle berücksichtigen jedoch nicht die Delokalisation der Ladungen in Donor und Akzeptor. Deibel konnte diesen Sachverhalt mit Monte-Carlo-Simulationen untersuchen, bei denen das Loch über bis zu 10 Moleküle gleichzeitig verteilt war. [17] Der Nachteil hierbei ist jedoch, dass eine Gleichverteilung der Ladung in dem entsprechenden Segment angenommen wurde, die nicht der tatsächlichen Ladungsverteilung auf der Polymerkette entspricht. Arkhipov konnte dies umgehen, indem er die Delokalisierung über eine zusätzliche quantenmechanische kinetische Energie mit berücksichtigte. [18] Diese Idee hat Nenashev aufgegriffen und das Modell weiterentwickelt. [19] (siehe Abschnitt 2.2.3). Zusätzliche Dipole können die Ladungsträgertrennung begünstigen. [20] Diese wurden schon von Arkhipov berücksichtigt. Wiemer et al. konnten die Dipole in das Modell mit einbinden, indem sie dieses erweiterten (siehe Abschnitt 2.2.4). [21] Die Unordnung, welche beim Ladungstransport eine entscheidende Rolle spielt, wurde von Offermanns und van Eersel untersucht. [22,23] Neuere Studien beziehen zusätzlich noch den Effekt der Entropie mit ein. [24] Eine weiterhin mögliche Trennung an Verunreinigungen, wurde schließlich von Arkhipov untersucht (siehe Abschnitt 2.2.5). [25]

All diese Modelle bestimmen die Trennungswahrscheinlichkeit in Abhängigkeit von verschiedenen Parametern. Diese werden meistens nicht ausgehend von der Molekülstruktur berechnet, sondern sind Fitparameter, mit denen das Modell an die gemessenen Kurven angepasst werden kann. Es gibt aber auch Ansätze einzelne Parameter oder sogar den gesamten Trennungsmechanismus *ab initio* zu berechnen. Dazu müssen zunächst die elektronischen Zustände an der Grenzfläche berechnet werden. Hierfür werden meist DFT-Rechnungen (density functional theory) durchgeführt. Um einen angeregten Zustand in einem System berechnen zu können, müssen aber TDDFT (time dependent DFT)-Rechnungen durchgeführt werden. Der Nachteil hierbei ist, dass die Bindungsenergie nicht ausreichend genau bestimmt werden kann. [26-28] Mit der Entwicklung neuer Funktionale konnte dieses Problem jedoch reduziert werden. [29,30] Eine andere Möglichkeit ist die Verwendung der Bethe-Salpeter-Gleichung, welche eine höhere Vorhersagekraft besitzt, aber bisher nur auf relativ kleine Systeme angewendet werden kann. [31-36] Um mehrere Donor- und Akzeptor-Moleküle betrachten zu können, müssen Vereinfachungen gemacht werden. Die Moleküle werden daher nur noch als eine Einheit auffassen, wobei aber die quantenmechanische Wechselwirkung mit ihren Nachbarn dennoch berücksichtigt wird. [37] In einem größeren Maßstab können Monte-Carlo-Simulationen eingesetzt werden, um den entsprechenden Trennungsvorgang zu beschreiben (Siehe Abschnitt 2.3). [22,23,38-40] Diese Vorgehensweisen benötigen sehr viel Rechenzeit und können daher nur bedingt den Einfluss makroskopischer Größen beschreiben. Aus diesem Grund werden in dieser Arbeit nur die oben genannten

analytischen Modelle verwendet. Die erwähnten theoretischen Methoden werden, wenn möglich, zur Unterstützung eingesetzt.

2.2.1. Onsager-Modell

Dieses Modell wurde von Onsager 1938 für die Trennung von Ionen in schwachen Elektrolyten entwickelt. [14] Es kann aber auch auf die Trennung von gebundenen Ladungsträgern in Einzelschicht-Solarzellen aus einem Material verwendet werden. Ein wichtiges Beispiel ist hier die Trennung von Ladungsträgern in Anthracen-Einkristall-Solarzellen. [41] Chance und Braun konnten zeigen, dass die Quanteneffizienz der Ladungsträger in den Solarzellen vom angeregten Zustand abhängt. Die höheren energetischen Zustände besitzen eine niedrigere Bindungsenergie und dadurch auch einen größeren Abstand zwischen Elektron und Loch. Ähnliche Untersuchungen gab es auch für andere Molekülkristalle, wie Tetracen und Pentacen, bei denen auch ein sich über mehrere Moleküle erstreckender CT-Zustand gemessen und festgestellt wurde. [42-45]

Onsager geht in seinem Modell von der braunschen Bewegung in einem externen elektrischen Feld aus. Die Diffusionsgleichung hierfür lautet wie folgt:

$$\frac{\partial f}{\partial t} = \frac{kT}{e}(\mu_e + \mu_h)\mathrm{div}\left(\exp\left(-\frac{U}{kT}\right)\cdot \mathrm{grad}\,\left(f\exp\left(\frac{U}{kT}\right)\right)\right) \tag{3}$$

Hierbei ist f die Konzentration der Ladungsträger, kT die thermische Energie, U die Überlagerung des Coulombpotentials mit dem angelegten elektrischen Feld und μ_e und μ_h sind die Elektron- und Lochbeweglichkeit. Die Lösung für diese Gleichung konnte Onsager in seiner Arbeit von 1934 über das ohmsche Gesetz in schwachen Elektrolyten unter der Annahme eine Senke im Unendlichen (*„infinite sink approximation“)* bestimmen. Damit konnte die Steigerung der Gleichgewichtskonstanten $\frac{K(F)}{K(0)}$ für die Trennung mit zusätzlichem elektrischen Feld hergeleitet werden: [46]

$$\frac{K(F)}{K(0)} = \frac{J_1\left(2\sqrt{-2b}\right)}{\sqrt{-2b}} = \frac{I_1\left(2\sqrt{2b}\right)}{\sqrt{2b}} \quad \text{mit } b = \frac{e^3F}{8\pi\epsilon_0\epsilon_r k^2T^2} \tag{4}$$

Hierbei ist F das elektrische Feld, ϵ_r die relative Dielektrizitätskonstante und J_1 (I_1) die (modifizierte) Besselfunktion erster Ordnung. Wird nun ein Ladungsträgerpaar im Abstand r unter dem Winkel θ zum elektrischen Feld erzeugt, so ergibt sich folgende Trennungswahrscheinlichkeit φ:

$$\varphi(F,\theta,r) = \exp(-A)\exp(-B)\sum_{m=0}^{\infty}\sum_{n=0}^{\infty}\frac{A^m}{m!}\frac{B^{m+n}}{(m+n)!} \tag{5}$$

$$\text{mit } A = \frac{e^2}{4\pi\epsilon_0\epsilon_r kTr} \text{ und } B = \frac{eFr}{2kT}(1+\cos\theta) \tag{6}$$

Eine Schematische Darstellung des Modells ist in Abbildung 1 zu sehen. Pai und Enck haben diese Wahrscheinlichkeit über alle möglichen Orientierungen der Erzeugung eines Ladungsträgerpaares mit dem Radius r_0 gemittelt und folgende Wahrscheinlichkeit erhalten: [15]

$$\varphi(F) = \varphi_0\frac{kT}{eFr_0}e^{-A}\exp\left(-\frac{eFr_0}{kT}\right)\sum_{m=0}^{\infty}\frac{A^m}{m!}\sum_{n=0}^{\infty}\sum_{l=m+n+1}^{\infty}\left(\frac{eFr_0}{kT}\right)^l\frac{1}{l!} \tag{7}$$

Der zusätzliche Faktor φ_0 bestimmt die maximale Effizienz bei hohen angelegten Feldern. Diesen Ausdruck haben sie erfolgreich auf amorphes Selen angewendet. Chance und Braun haben diese Mittelung verwendet, um die Aktivierungsenergie aus temperaturabhängigen Messungen zu erhalten. [41]

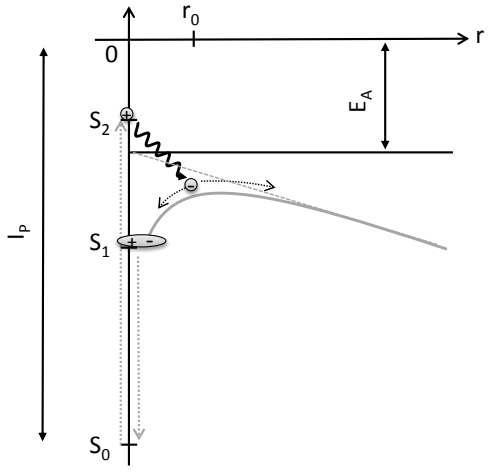

Abbildung 1: *Schematische Darstellung des Onsager-Modells. Ein Elektron wird in den S_2-Zustand angeregt und relaxiert im Abstand r_0. Von dort kann es entweder dissoziieren oder in den S_1-Zustand zurückfallen und von dort in den S_0-Zustand rekombinieren. Ein angelegtes elektrisches Feld kann die Dissoziation begünstigen. Ebenfalls angetragen sind die Ionisierungsenergie I_p und die Elektronaffinität E_A des verwendeten Materials.*

2.2.2. Onsager-Braun-Modell

Das in Abschnitt 2.2.1 beschriebene Modell nimmt wegen der infinite-sink-approximation keinen stabilen Zustand an, von dem eine Trennung erfolgen kann, da CT-Zustände in einem Material energetisch höher sind, als der erste angeregte Zustand. In Zweikomponenten-Solarzellen gibt es jedoch CT-Zustände, die energetisch niedriger liegen als der erste angeregte Zustand in jedem der beiden Materialien. Ein solcher CT-Zustand hat eine endliche Lebenszeit, die in diesem Modell nicht berücksichtigt wird. [16,42] Mit der Einführung eines metastabilen CT-Zustands kann das Elektron-Loch-Paar mehrere Versuche unternehmen bis es in den Grundzustand rekombiniert. Dies ist in Abbildung 2 veranschaulicht. Die Wahrscheinlichkeit φ zu dissoziieren ist somit über folgende Ratengleichung gegeben:

$$\varphi(F) = \frac{k_d(F)}{k_f + k_d(F)} \tag{8}$$

$k_f = \frac{1}{\tau}$ ist die Rate, mit der der CT-Zustand in den Grundzustand zurückkehrt, wobei τ die CT-Lebenszeit ist. $k_d(F)$ ist die feldabhängige Rate der Dissoziation. Die Gleichgewichtskonstante $K(F)$ für den Prozess der Ladungsträgererzeugung ist bestimmt durch das Verhältnis der Rate für die Dissoziation und der Rate ihrer Rekombination k_r zurück zu einem Elektron-Loch-Paar.

$$K(F) = \frac{k_d(F)}{k_r} \tag{9}$$

Die Rekombination von zwei freien Ladungsträgern zu einem neuen Elektron-Loch-Paar kann über eine Langevin-Rekombination beschrieben werden: [47]

$$k_r = \frac{\mu e}{\epsilon_r \epsilon_0} \tag{10}$$

Hierbei ist μ die Summe aus Elektron- und Lochbeweglichkeit. Die feldabhängige Gleichgewichtskonstante $K(F)$ kann über Gleichung (4) mit der feldunabhängigen Gleichgewichtskonstante $K(0)$ verknüpft werden. Diese lässt sich nach Accasina und Fuoss für stark gebundene Ionenpaare wie folgt darstellen: [48]

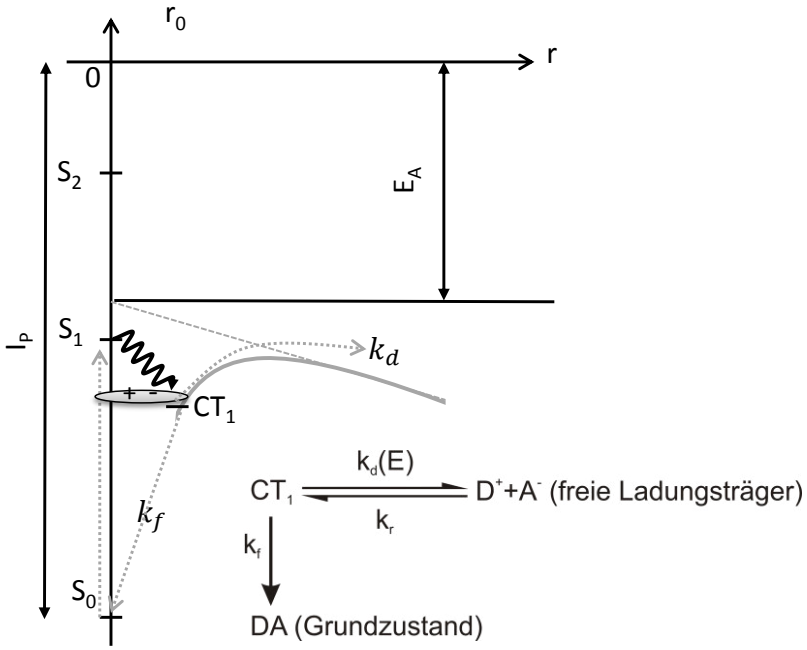

Abbildung 2: *Schematische Darstellung des Onsager-Braun-Modells. Ein Elektron wird in den S_1-Zustand angeregt und relaxiert im Abstand r_0 in einen CT-Zustand. Von dort kann es entweder mit der Rate k_d dissoziieren oder in den Grundzustand mit der Rate k_f rekombinieren. Ein angelegtes elektrisches Feld kann die Dissoziation begünstigen. Zusätzlich können freie Ladungsträger wieder zu einem CT-Zustand mit der Rate k_r rekombinieren. Ebenfalls angetragen sind die Ionisierungsenergie I_p des Donors und die Elektronaffinität E_A des Akzeptors.*

$$K(0) = \frac{3}{4\pi r_0^3} \cdot \exp\left(-\frac{\Delta E}{kT}\right) \tag{11}$$

ΔE ist die nach Gleichung (1) bestimmte Bindungsenergie des Elektron-Loch-Paars im Abstand r_0. Damit lässt sich die feldabhängige Trennungswahrscheinlichkeit wie folgt schreiben:

$$\varphi(F) = \frac{1}{1 + \frac{3e}{4\pi\epsilon_0\epsilon_r r_0^3} \cdot \mu\tau \cdot \exp\left(-\frac{\Delta E}{kt}\right) \cdot \frac{I_1\left(2\sqrt{2b}\right)}{\sqrt{2b}}} \tag{12}$$

$$\text{mit: } b = \frac{e^3 F}{8\pi\epsilon_0\epsilon_r k^2 T^2} \text{ und } \Delta E = \frac{e^2}{4\pi\epsilon_0\epsilon_r r_0}$$

Dieser Formalismus konnte erfolgreich auf molekulare Systeme angewandt [49] und auf

Polymer-Solarzellen erweitert werden. [50] Es wird jedoch nicht mit einbezogen, dass die Rekombinationsrate abstandsabhängig ist. Dies konnten Wojcik und Tachyia über eine erweiterte Version des Braun-Formalismus berücksichtigen. [51]

2.2.3. Effektive-Masse-Modell

Bisher wurde in den betrachteten Modellen angenommen, dass die behandelten Teilchen punktförmig sind. Die Wellenfunktionen können im Polymer jedoch über mehrere Monomereinheiten delokalisiert sein. [52] Dieser Effekt der Kopplung zwischen Wiederholeinheiten wurde von Arkhipov et al. über die Einführung einer effektiven Masse berücksichtigt. [18] Diese Idee wurde von Nenashev et al. weiterentwickelt. [19] Dabei werden im Modell mehrere Polymerketten parallel zur Grenzfläche angeordnet (siehe Abbildung 3a). Das Loch kann sich dann zwischen diesen über temperaturaktivierte Sprünge bewegen. Die Sprünge folgen hierbei den Miller-Abrahams-Raten: [53]

$$a_{n\to n+1} = \nu_0 \exp(-2\gamma r) \begin{cases} \exp\left(-\dfrac{E_{n+1}-E_n}{kT}\right) & E_{n+1} > E_n \\ 1 & E_{n+1} \leq E_n \end{cases} \tag{13}$$

Hierbei ist ν_0 die attempt-to-hop-frequency, γ der inverse Lokalisationsradius und r der Abstand zwischen zwei Ketten. Wird ein Sprung zu einer energetisch höher liegenden Kette ausgeführt, so muss die Differenz der Energie zwischen den Ketten thermisch aufgebracht werden. E_n bezeichnet hierbei die Energie auf der Kette n. Damit kann die Änderung der Konzentration der Ladungsträger f_i auf der Kette i auf folgende Weise geschrieben werden:

$$\frac{\mathrm{d}f_i}{\mathrm{d}t} = f_{j-1}a_{j-1\to j} - f_j\left(a_{j\to j-1} + a_{j\to j+1}\right) + f_{j+1}a_{j+1\to j} + g_0\delta_{1j} - \frac{f_j}{\tau}\delta_{1j} \tag{14}$$

Dies entspricht einem 1-dimensionalen Random Walk. Die Generation von Ladungsträgern an der Grenzfläche wird durch die Rate g_0 und die Rekombination durch die inverse Lebenszeit $\frac{1}{\tau}$ berücksichtigt. Rubel et al. konnten diese 1-dimensionale Ratengleichung lösen und haben die Dissoziationsrate k_d wie folgt berechnet:

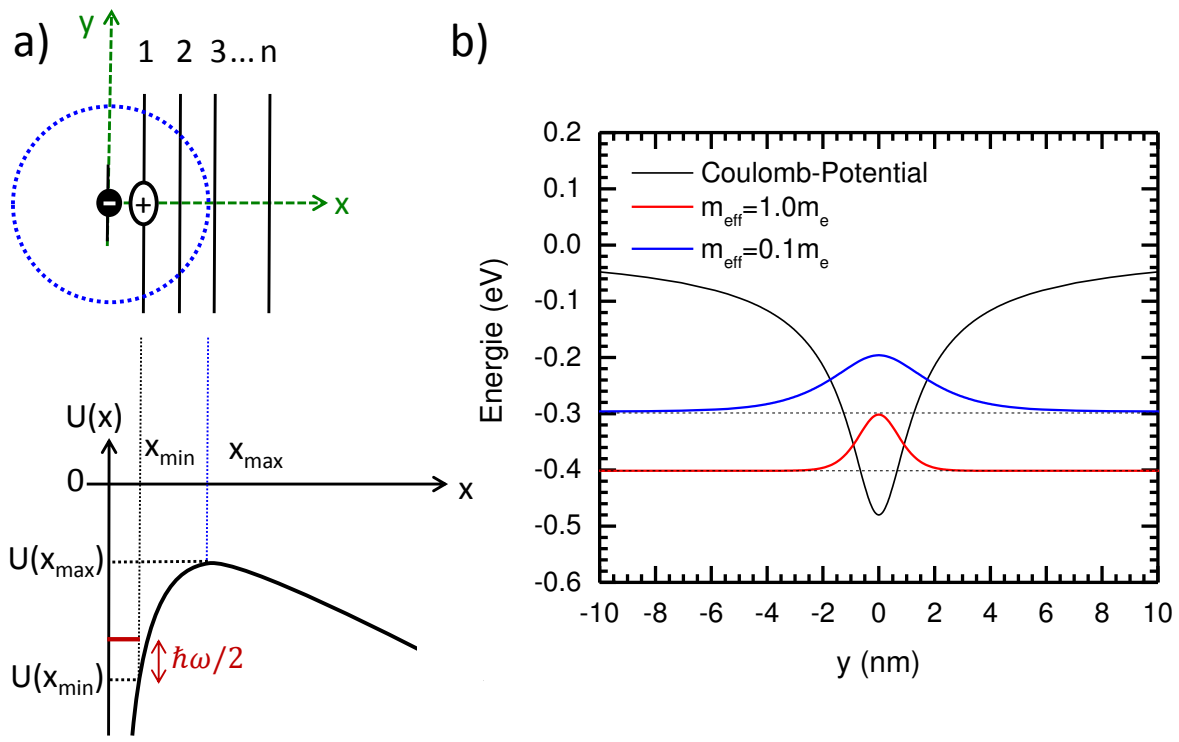

Abbildung 3: *a) Schematische Darstellung des Effektive-Masse-Modells. Die Ketten 1…n sind parallel zur Grenzfläche angeordnet. Das Loch kann sich zwischen diesen bewegen um über die Potentialbarriere U(x_{max}) zu kommen. Die Energie auf den Ketten wird durch die klassische potentielle Energie und die quantenmechanische Nullpunktschwingungsenergie bestimmt. b) Potential entlang der ersten Kette im Abstand x=1 nm. Die Wellenfunktion ist für zwei verschiedene effektive Massen gezeigt. Die Position entspricht der Bindungsenergie E_n auf der Kette. Man erkennt, dass mit sinkender Bindungsenergie die Delokalisation zunimmt.*

$$k_d = \left(\sum_{n=1}^{N-1} a_{n\to n+1}^{-1} \exp\left(\frac{E_n - E_1}{kT}\right) \right)^{-1} \tag{15}$$

Damit kann analog zu Gleichung (8) die Dissoziationswahrscheinlichkeit φ auf folgende Art angegeben werden:

$$\varphi(F) = \frac{1}{1 + \sum_{n=1}^{N-1} \tau^{-1} a_{n\to n+1}^{-1} \exp\left(\frac{E_n - E_1}{kT}\right)} \tag{16}$$

Um diese berechnen zu können, müssen die Energien E_n der einzelnen Ketten bekannt sein. Hier muss analog zu den Überlegungen von Arkhipov nicht die klassische Coulombenergie,

sondern die quantenmechanisch berechnete Energie benutzt werden. [18] Diese kann durch Lösung der Schrödingergleichung bestimmt werden.

$$-\frac{\hbar^2}{2m_{eff}}\frac{\mathrm{d}^2}{\mathrm{d}y^2}\,|\Psi\rangle + U_n(y)|\Psi\rangle = E_n|\Psi\rangle \tag{17}$$

$$U_n(y) = \frac{e^2}{4\pi\epsilon_0\epsilon_r\sqrt{y^2+x_n^2}} - eFx_n \tag{18}$$

Das Polymer wird in diesem Fall als 1-dimensionaler Raum angenommen. Die Kette befindet sich im Abstand x_n zu dem im Ursprung liegenden Elektron. Das Polymer ist in y-Richtung orientiert. $U_n(y)$ bezeichnet somit das Potential auf der n-ten Polymerkette. Die Delokalisierung kann hier über die effektive Masse m_{eff} bestimmt werden. Die Energieeigenwerte E_n der n-ten Kette wiederrum können näherungsweise über eine harmonische Approximation des Potentials berechnet werden.

$$E_{n,approx} = U_n(0) + \frac{\hbar}{2\sqrt{m_{eff}}}\sqrt{\frac{\mathrm{d}^2}{\mathrm{d}y^2}U_n(y)\Big|_{y=0}} \tag{19}$$

Hier erkennt man, dass zusätzlich zur klassischen Energie $U_n(0)$ ein weiterer Term hinzukommt. Dies ist die kinetische Energie, die dem Loch zusätzlich aufgrund seiner Delokalisation zur Verfügung steht und somit die Trennung begünstigen kann. Dies ist in Abbildung 3b für zwei verschiedene effektive Massen gezeigt. Für eine genaue Bestimmung der Quanteneffizienz sollte jedoch die numerische Lösung der Schrödingergleichung verwendet werden, da die harmonische Näherung nur in einem kleinen Parameterbereich vergleichbar mit der exakten Lösung ist. [19,54]

2.2.4. Dipol-Modell

Eine weitere Möglichkeit die experimentell beobachtete Dissoziationswahrscheinlichkeit zu erklären ist die Annahme von zusätzlichen Dipolen an der Donor-Akzeptor-Grenzfläche, welche die Gegenladung abschirmen können. [18,20,55-57] Hierfür muss Gleichung (18) modifiziert werden, um diese partiellen Dipole zu berücksichtigen (siehe Abbildung 4). [21]

$$U_{n,Dipol}(y) = U_n(y) + \frac{e^2}{4\pi\epsilon_0\epsilon_r} \cdot \sum_{i=-N/2}^{i=N/2} \left(\frac{\alpha}{\sqrt{(x_n - d)^2 + \left(y - \left(i + \frac{1}{2}\right)d\right)^2}} + \frac{-\alpha}{\sqrt{x_n^2 + \left(y - \left(i + \frac{1}{2}\right)d\right)^2}} \right) \quad (20)$$

Die Gitterkonstante in diesem Modell ist d. Sie bestimmt den Abstand zwischen Donor und Akzeptor sowie den Abstand der N Dipole untereinander. Die Stärke der Dipole α wird in Vielfachen der Elementarladung e angegeben. Das Potential $U_n(y)$ wird durch Gleichung (18) bestimmt.

Um die Schrödingergleichung (17) mit dem modifizierten Potential (20) zu lösen, kann die harmonische Approximation, durch Gleichung (19) gegeben, verwendet werden. Wiemer et al. haben jedoch gezeigt, dass diese Näherung fast nicht mehr gültig ist. [54] Aus diesem Grund sollte eine numerische Lösung der Schrödingergleichung verwendet werden, sobald Grenzflächendipole in Betracht gezogen werden.

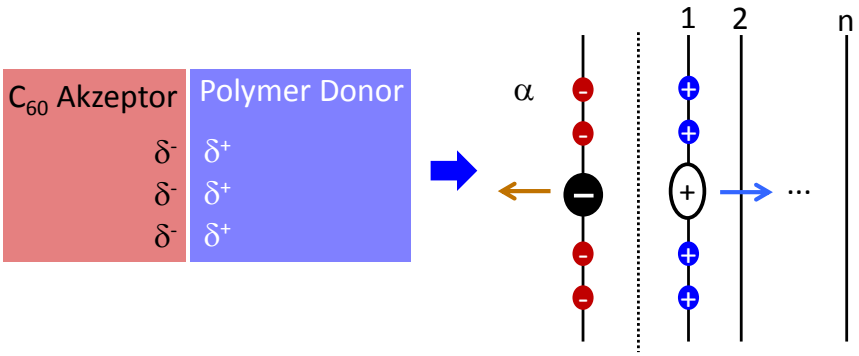

Abbildung 4: *Schematische Erweiterung des Effektive-Masse-Modells mit Grenzflächendipolen. Die zwischen Donor und Akzeptor entstandenen Dipole werden im Modell gelichmäßig an der Grenzfläche angeordnet. Das Loch kann sich nun im modifizierten Potential zwischen den einzelnen Ketten bewegen um zu dissoziieren.*

2.2.5. Fehlstellen-Modell

Neuere Studien konnten zeigen, dass C_{60} in eine Polymerschicht eindiffundieren kann. [58] In dieser wird dann die Lumineszenz gequenched, indem ein Elektron auf das C_{60} übertragen wird. Dieser Mechanismus kann aber auch genutzt werden, um ein Exziton zu trennen. Die

Trennung so entstandenen CT-Zustände kann über ein zusätzlich angelegtes elektrisches Feld erleichtert werden. Das zurückbleibende Elektron kann anschließend von Fallenzustand zu Fallenzustand hüpfen, bis es die Donor-Akzeptor-Grenzfläche erreicht hat. Diese Idee wurde von Arkhipov et al. verfolgt, so dass sie daraus das nachfolgend erklärte Fehlstellen-Modell entwickelten, welches in Abbildung *5* schematisch gezeigt ist. [25]

Ein im Donor angeregtes Exziton kann über einen Tunnelprozess sein Elektron auf den Akzeptor übertragen und so einen CT-Zustand bilden. Die Wahrscheinlichkeit einen solchen Zustand zu bilden, hängt von der Wahrscheinlichkeit ab, einen Akzeptor im Abstand r zu finden und der Wahrscheinlichkeit einen solchen Tunnelprozess auszuführen (Analog zu Gleichung (8) mit $k_d = \nu_0 \exp(-2\gamma r)$ und $k_f = \tau^{-1}$).

$$\varphi(F) = 2\pi l N_d \cdot \exp\left(-\pi l N_d (r^2 - r_{min}^2)\right) \cdot \frac{1}{1 + \nu_0^{-1}\tau^{-1}\exp(2\gamma r)} \tag{21}$$

Der Akzeptor muss mindestens den Abstand r_{min} von der Polymerkette besitzen. Nach diesem Tunnelprozess befindet sich das Loch auf dem Polymer in einem Potential, welches durch Gleichung (18) bestimmt ist. Der Unterschied ist jedoch, dass nur die Projektion des Feldes auf die Polymerkette betrachtet wird, da die Polymerkette nicht senkrecht zum Feld F_0 stehen muss.

$$F_x = \cos(\theta)\, F_0 \tag{22}$$

Der Winkel zwischen elektrischem Feld und Polymerkette beträgt θ. Um die Delokalisierung zu berücksichtigen, wurde das Potential nach Gleichung (19) entwickelt. Aus dieser Entwicklung konnte die minimale Energie im Potential E_{min} und die Potentialbarriere E_{max} bestimmt werden. Ab einem gewissen Abstand $r_0(\theta)$ gibt es kein Minimum des Potentials mehr. Dadurch driftet das Loch auf der Polymerkette entlang und kann so erfolgreich dissoziieren. Im anderen Fall kann das Loch entweder durch thermische Energie über die Potentialbarriere hinwegkommen oder über einen weiteren Tunnelprozess ein Exziton bilden. Die feldabhängige Dissoziationswahrscheinlichkeit erhält man schließlich, wenn über alle oben genannten Prozesse aufsummiert wird.

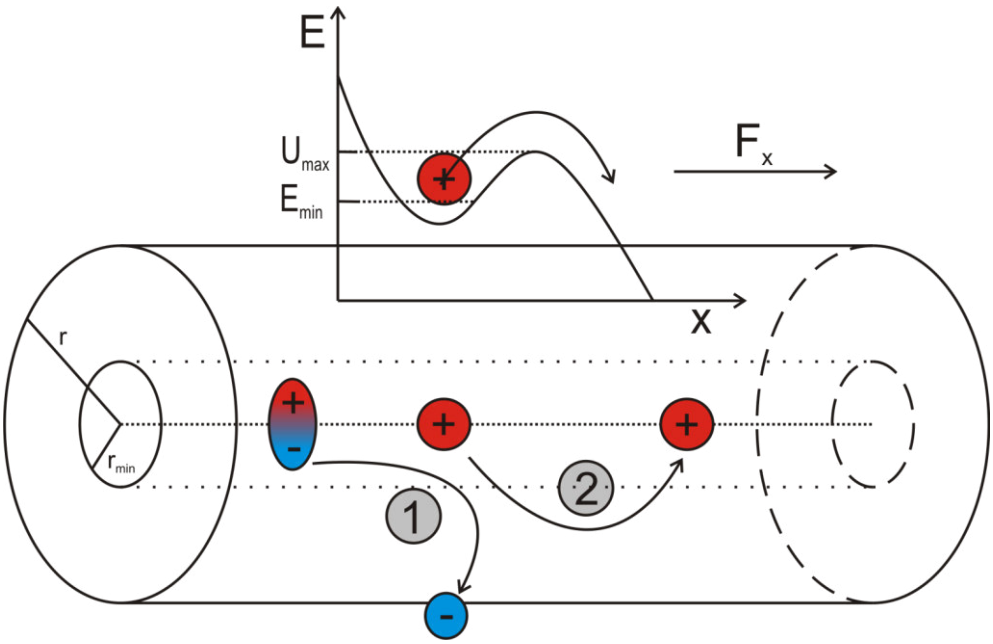

Abbildung 5: *Schematische Darstellung des Fehlstellen-Modells. (1) Das Elektron tunnelt in den Fallenzustand im Abstand r. (2) Das zurückbleibende Loch versucht über die Energiebarriere U_{max}-E_{min} zu dissoziieren. Die Projektion des Feldes auf das Polymer F_x kann diese Energiebarriere reduzieren. In dem Modell wird die Delokalisierung des Loches auf dem Polymer durch zusätzliche kinetische Energie mit berücksichtigt.*

$$\varphi(F) = 2\pi l N_d \int_0^1 dz \left(\int_{\max(r_{min}, r_0(z))}^{\infty} drr \cdot \exp\left(-\pi l N_d (r^2 - r_{min}^2)\right) \cdot \frac{1}{1 + \nu_0^{-1}\tau^{-1}\exp(2\gamma r)} + \int_{r_{min}}^{\max(r_{min}, r_0(z))} drr \cdot \exp\left(-\pi l N_d (r^2 - r_{min}^2)\right) \cdot \frac{1}{1 + \nu_0^{-1}\tau^{-1}\exp(2\gamma r)} \cdot \frac{1}{1 + \exp(-2\gamma r)\exp\left(\frac{E_{max}(z,r) - E_{min}(z,r)}{kT}\right)} \right) \tag{23}$$

2.3. Monte-Carlo-Simulation

Eine weitere Möglichkeit ist, neben den analytischen Lösungen, die in Abschnitt 2.2 vorgestellt wurden, die Dissoziationswahrscheinlichkeit über eine Monte-Carlo-Simulation zu bestimmen. Damit können Ratengleichungen, wie im 1-dimensionalen Fall

Gleichung (14), behandelt werden, ohne diese analytisch lösen zu müssen. Denn dies ist nicht mehr ohne weiteres möglich, wenn sich beide Ladungsträger bewegen können, oder, wenn eine 2- oder 3-dimensionale Bewegung angenommen wird. Zudem kann der Einfluss von energetischer Unordnung berücksichtigt werden.

In diesem Abschnitt sollen die Grundzüge der verwendeten Monte-Carlo-Simulation erläutert werden, die für die in Kapitel 4 aufgeführten Publikationen verwendet wurde. Der zugrunde liegende Code basiert auf einer Adaption des Codes für bereits durchgeführten Monte-Carlo-Simulationen für Triplett-Exzitonen. So konnte die Temperaturabhängigkeit der allgemeinen Bewegung sowie die spektrale Diffusion von Tripletts untersucht und mit experimentellen Daten verglichen werden. [59,60]

In dieser Dissertation wird eine dynamische Monte-Carlo-Simulation verwendet, die an den Metropolis-Algorithmus angelehnt ist. Die Simulation findet auf einem kubischen Gitter statt. Jedem Punkt auf dem Gitter wird eine bestimmte Eigenschaft zugewiesen (zum Beispiel: Donor- oder Akzeptor-Molekül/Monomer). Der Algorithmus hat folgenden Aufbau:

1. Erzeuge ein Elektron-Loch-Paar zufällig an der Grenzfläche (Startbedingung).
2. Berechne alle Raten, welche das System in einen neuen Zustand überführen.
3. Wähle eine Rate entsprechend ihrer Wahrscheinlichkeit aus.
4. Überführe das System in den neuen Zustand.
5. Überprüfe, ob die Abbruchbedingungen erfüllt sind.
    - Wenn Ja: dann weiter mit Schritt 6
    - Wenn Nein: dann zurück zu Schritt 2
6. Gehe zurück zu Schritt 1 so lange bis das Ergebnis konvergiert.

Die Raten werden durch Miller-Abrahams-Raten (Gleichung (13)) und die inverse Lebenszeit bestimmt. Die Zufallszahl, welche die Rate für die Änderung auswählt, wird aus einer Boxverteilung gezogen. Der Versuch wird abgebrochen, wenn entweder das gewählte Ereignis die Rekombination beider Ladungsträger ist oder, wenn ein Ladungsträger die entsprechende Elektrode erreicht. Der Abstand der Elektrode von der Donor-Akzeptor-Grenzfläche kann dabei variiert werden. Die Größe, welche betrachtet wird, ist die Wahrscheinlichkeit $\varphi(F)$, einen Ladungsträger erfolgreich zu dissoziieren.

$$\varphi(F) = \frac{N_{diss}}{N_{tot}} \tag{24}$$

N_{tot} ist die Gesamtzahl aller durchgeführten Versuche, während N_{diss} die Anzahl erfolgreich dissoziierter Elektron-Loch-Paare bezeichnet. So erhält man eine statistische Mittelung über alle Realisierungen des Systems, die mit ihrer Wahrscheinlichkeit gewichtet sind.

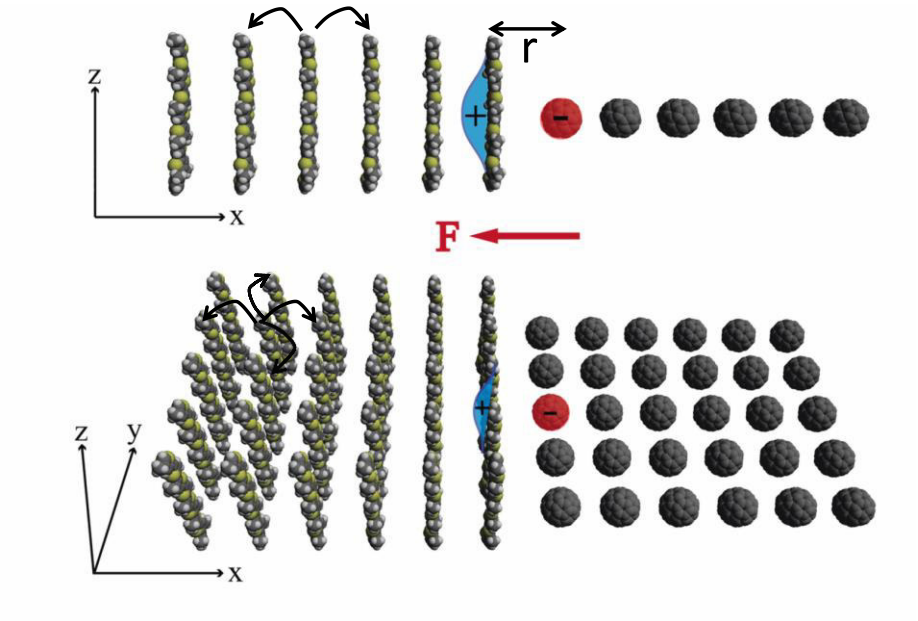

Abbildung 6: *Darstellung der verwendeten Morphologie. Oben: 1-dimensionaler Fall. Das Loch ist auf der Kette delokalisiert und befindet sich im Abstand r zum Elektron. Das Loch hat zwei Sprungmöglichkeiten. Entweder wird ein Sprung auf die Grenzfläche zu der weg durchgeführt. Unten: Erweiterung um eine Dimension. Dadurch können zwei weitere nächste-Nachbar-Sprünge hinzukommen.*

In der Monte-Carlo-Simulation kann auch der Effekt der Delokalisierung untersucht werden. Eine Möglichkeit dazu hat Deibel et al. gezeigt, indem er das Loch über mehrere Monomereinheiten gleichmäßig verteilt hat. [17] In dieser Dissertation wurde sich gegen diesen Ansatz entschieden, um eine bessere Vergleichbarkeit mit dem in Abschnitt 2.2.3 vorgestellten Modell zu erreichen. Deswegen wurde die Delokalisierung stattdessen über einen zusätzlichen energetischen Term berücksichtigt, der sich aus der Schrödingergleichung ergibt. Dieser hängt nur vom Abstand zwischen Elektron und Loch ab, solange die Polymerketten senkrecht zum Feld stehen und die Bewegung in der Monte-Carlo-Simulation nicht entlang der Ketten stattfindet. Dementsprechend können die Ketten wie im Effektive-Masse-Modell angeordnet und die Bewegung als 1-dimensional angenommen werden. Möchte man die Bewegung um eine Dimension erweitern, so stehen alle Polymerketten in der Bewegungsebene (Siehe Abbildung 6). Dies führt dazu, dass mit diesem Modell eine 3-dimensionale Bewegung nicht explizit möglich ist, auch wenn diese Dimension durch die Delokalisierung implizit berücksichtigt wird.

2.4. Literaturverzeichnis

[1] www.bundesregierung.de/Content/DE/StatischeSeiten/Breg/Energiekonzept/0-Buehne/ma%C3%9Fnahmen-im-ueberblick.html abgerufen am 20.12.2016

[2] Z. Er and I. B. Turna, Future Expectation of the Photovoltaics Role in Compensating Energy Demand *Acta Phys Pol A* 2016 129, 865-868.

[3] www.heliatek.com/en/press/press-releases/details/heliatek-sets-new-organic-photovoltaic-world-record-efficiency-of-13-2 abgerufen am 20.12.2016

[4] World Energy Council, *World Energy Resources: Solar*,2013

[5] www.solarte.de/en/#applications abgerufen am 20.12.2016

[6] W. Shockley and H. J. Queisser, Detailed Balance Limit of Efficiency of P-N Junction Solar Cells *J Appl Phys* 1961 32, 510-519.

[7] R. A. J. Janssen and J. Nelson, Factors Limiting Device Efficiency in Organic Photovoltaics *Adv Mater* 2013 25, 1847-1858.

[8] M. Gruber, J. Wagner, K. Klein, U. Hörmann, A. Opitz, M. Stutzmann, and W. Brütting, Thermodynamic Efficiency Limit of Molecular Donor-Acceptor Solar Cells and its Application to Diindenoperylene/C_{60}-Based Planar Heterojunction Devices *Adv Energy Mater* 2012 2, 1100-1108.

[9] N. C. Giebink, G. P. Wiederrecht, M. R. Wasielewski, and S. R. Forrest, Thermodynamic Efficiency Limit of Excitonic Solar Cells *Phys Rev B* 2011 83

[10] A. Köhler and H. Bässler, *Electronic Processes in Organic Semiconductors: An Introduction*. Wiley VCH, 2015.

[11] K. Vandewal, S. Albrecht, E. T. Hoke, K. R. Graham, J. Widmer, J. D. Douglas, M. Schubert, W. R. Mateker, J. T. Bloking, and G. F. Burkhard, Efficient Charge Generation by Relaxed Charge-Transfer States at Organic Interfaces *Nature Materials* 2014 13, 63-68.

[12] C. M. Proctor, M. Kuik, and T.-Q. Nguyen, Charge Carrier Recombination in Organic Solar Cells *Progress in Polymer Science* 2013 38, 1941-1960.

[13] D. Veldman, S. C. Meskers, and R. A. Janssen, The Energy of Charge-Transfer States in Electron Donor–Acceptor Blends: Insight into the Energy Losses in Organic Solar Cells *Advanced Functional Materials* 2009 19, 1939-1948.

[14] L. Onsager, Initial Recombination of Ions *Phys Rev* 1938 54, 554.

[15] D. Pai and R. Enck, Onsager Mechanism of Photogeneration in Amorphous Selenium *Phys Rev B* 1975 11, 5163.

[16] C. L. Braun, Electric Field Assisted Dissociation of Charge Transfer States as a Mechanism of Photocarrier Production *The Journal of Chemical Physics* 1984 80, 4157-4161.

[17] C. Deibel, T. Strobel, and V. Dyakonov, Origin of the Efficient Polaron-Pair Dissociation in Polymer-Fullerene Blends *Phys Rev Lett* 2009 103

[18] V. Arkhipov, P. Heremans, and H. Bässler, Why is Exciton Dissociation so efficient at the Interface between a Conjugated Polymer and an Electron Acceptor? *Applied Physics Letters* 2003 82, 4605-4607.

[19] A. Nenashev, S. Baranovskii, M. Wiemer, F. Jansson, R. Österbacka, A. Dvurechenskii, and F. Gebhard, Theory of Exciton Dissociation at the Interface between a Conjugated Polymer and an Electron Acceptor *Phys Rev B* 2011 84, 035210.

[20] H. D. de Gier, F. Jahani, R. Broer, J. C. Hummelen, and R. W. A. Havenith, Promising Strategy To Improve Charge Separation in Organic Photovoltaics: Installing Permanent Dipoles in PCBM Analogues *J Phys Chem A* 2016 120, 4664-4671.

[21] M. Wiemer, A. Nenashev, F. Jansson, and S. Baranovskii, On the Efficiency of Exciton Dissociation at the Interface between a Conjugated Polymer and an Electron Acceptor *Applied Physics Letters* 2011 99, 013302.

[22] T. Offermans, S. C. Meskers, and R. A. Janssen, Monte-Carlo Simulations of Geminate Electron–Hole Pair Dissociation in a Molecular Heterojunction: A two-Step Dissociation Mechanism *Chemical Physics* 2005 308, 125-133.

[23] H. van Eersel, R. A. Janssen, and M. Kemerink, Mechanism for Efficient Photoinduced Charge Separation at Disordered Organic Heterointerfaces *Advanced Functional Materials* 2012 22, 2700-2708.

[24] S. N. Hood and I. Kassal, Entropy and Disorder enable Charge Separation in Organic Solar Cells *arXiv preprint arXiv:1603.06304* 2016

[25] V. Arkhipov, E. Emelianova, and H. Bässler, Dopant-assisted Charge Carrier Photogeneration in Conjugated Polymers *Chem Phys Lett* 2003 372, 886-892.

[26] T. Ziegler, M. Seth, M. Krykunov, J. Autschbach, and F. Wang, Is Charge Transfer Transitions really too difficult for Standard Density Functionals or are they just a Problem for Time-Dependent Density Functional Theory based on a linear Response Approach *Journal of Molecular Structure: Theochem* 2009 914, 106-109.

[27] D. J. Tozer, Relationship Between Long-Range Charge-Transfer Excitation Energy Error and Integer Discontinuity in Kohn–Sham Theory *The Journal of Chemical Physics* 2003 119, 12697-12699.

[28] A. Dreuw and M. Head-Gordon, Failure of Time-Dependent Density Functional Theory for long-Range Charge-Transfer Excited States: The Zincbacteriochlorin-Bacteriochlorin and Bacteriochlorophyll-Spheroidene Complexes *J Am Chem Soc* 2004 126, 4007-4016.

[29] R. Baer and D. Neuhauser, Density Functional Theory with correct Long-Range Asymptotic Behavior *Phys Rev Lett* 2005 94, 043002.

[30] E. Livshits and R. Baer, A well-tempered density functional theory of electrons in molecules *Physical Chemistry Chemical Physics* 2007 9, 2932-2941.

[31] L. Hedin, New Method for Calculating the One-Particle Green's Function with Application to the Electron-Gas Problem *Phys Rev* 1965 139, A796.

[32] E. E. Salpeter and H. A. Bethe, A Relativistic Equation for Bound-State Problems *Phys Rev* 1951 84, 1232.

[33] Y. Ma, M. Rohlfing, and C. Molteni, Excited States of Biological Chromophores studied using Many-Body Perturbation Theory: Effects of Resonant-Antiresonant Coupling and dynamical Screening *Phys Rev B* 2009 80, 241405.

[34] B. Baumeier, D. Andrienko, and M. Rohlfing, Frenkel and Charge-Transfer Excitations in Donor–Acceptor Complexes from Many-Body Green's Functions Theory *Journal of Chemical Theory and Computation* 2012 8, 2790-2795.

[35] B. Baumeier, D. Andrienko, Y. Ma, and M. Rohlfing, Excited States of Dicyanovinyl-Substituted Oligothiophenes from Many-Body Green's Functions Theory *Journal of Chemical Theory and Computation* 2012 8, 997-1002.

[36] D. Niedzialek, I. Duchemin, T. B. de Queiroz, S. Osella, A. Rao, R. Friend, X. Blase, S. Kümmel, and D. Beljonne, First Principles Calculations of Charge Transfer Excitations in Polymer–Fullerene Complexes: Influence of Excess Energy *Advanced Functional Materials* 2015 25, 1972-1984.

[37] G. Raos, M. Casalegno, and J. Idé, An Effective Two-Orbital Quantum Chemical Model for Organic Photovoltaic Materials *Journal of Chemical Theory and Computation* 2013 10, 364-372.

[38] P. K. Watkins, A. B. Walker, and G. L. Verschoor, Dynamical Monte Carlo Modelling of Organic Solar Cells: The Dependence of Internal Quantum Efficiency on Morphology *Nano Lett* 2005 5, 1814-1818.

[39] R. Marsh, C. Groves, and N. Greenham, A microscopic Model for the Behavior of Nanostructured Organic Photovoltaic Devices *J Appl Phys* 2007 101, 083509.

[40] M. C. Heiber, T.-Q. Nguyen, and C. Deibel, Charge Carrier Concentration Dependence of Encounter-limited Bimolecular Recombination in Phase-separated Organic Semiconductor Blends *Phys Rev B* 2016 93, 205204.

[41] R. Chance and C. Braun, Temperature Dependence of Intrinsic Carrier Generation in Anthracene Single Crystals *The Journal of Chemical Physics* 1976 64, 3573-3581.

[42] H. Bässler and A. Köhler, "Hot or cold": How do Charge Transfer States at the Donor–Acceptor Interface of an Organic Solar Cell Dissociate? *Physical Chemistry Chemical Physics* 2015 17, 28451-28462.

[43] E. Silinsh and A. Jurgis, Photogenerated Geminate Charge-Pair Separation Mechanisms in Pentacene Crystals *Chemical Physics* 1985 94, 77-90.

[44] L. Sebastian, G. Weiser, G. Peter, and H. Bässler, Charge-Transfer Transitions in Crystalline Anthracene and their role in Photoconductivity *Chemical Physics* 1983 75, 103-114.

[45] L. Sebastian, G. Weiser, and H. Bässler, Charge transfer transitions in solid tetracene and pentacene studied by electroabsorption *Chemical Physics* 1981 61, 125-135.

[46] L. Onsager, Deviations from Ohm's Law in Weak Electrolytes *The Journal of Chemical Physics* 1934 2, 599-615.

[47] P. Langevin, Recombinaison et Mobilités des Ions Dans les Gaz *Annales de Chimie et de Physique* 1903 28, 433-530.

[48] M. Fuoss and F. Accascina, *Electrolytic Conductance* Interscience, 1959.

[49] T. Goliber and J. Perlstein, Analysis of Photogeneration in a Doped Polymer System in Terms of a Kinetic Model for Electric-Field-assisted Dissociation of Charge-Transfer States *The Journal of Chemical Physics* 1984 80, 4162-4167.

[50] P. Peumans and S. R. Forrest, Separation of Geminate Charge-Pairs at Donor–Acceptor Interfaces in disordered Solids *Chem Phys Lett* 2004 398, 27-31.

[51] M. Wojcik and M. Tachiya, Accuracies of the Empirical Theories of the Escape Probability based on Eigen Model and Braun Model compared with the exact Extension of Onsager Theory *The Journal of Chemical Physics* 2009 130, 104107.

[52] Z. Guan, H.-W. Li, J. Zhang, Y. Cheng, Q. Yang, M.-F. Lo, T.-W. Ng, S.-W. Tsang, and C.-S. Lee, Evidence of Delocalization in Charge-Transfer State Manifold for Donor: Acceptor Organic Photovoltaics *Acs Appl Mater Inter* 2016 8, 21798-21805.

[53] A. Miller and E. Abrahams, Impurity Conduction at low Concentrations *Phys Rev* 1960 120, 745.

[54] M. Wiemer, M. Koch, U. Lemmer, A. Pevtsov, and S. Baranovskii, Efficiency of Exciton Dissociation at Internal Organic Interfaces beyond Harmonic Approximation *Organic Electronics* 2014 15, 2461-2467.

[55] I. Avilov, V. Geskin, and J. Cornil, Quantum-Chemical Characterization of the Origin of Dipole Formation at Molecular Organic/Organic Interfaces *Advanced Functional Materials* 2009 19, 624-633.

[56] S. Verlaak, D. Beljonne, D. Cheyns, C. Rolin, M. Linares, F. Castet, J. Cornil, and P. Heremans, Electronic Structure and Geminate Pair Energetics at Organic–Organic Interfaces: The Case of Pentacene/C_{60} Heterojunctions *Advanced Functional Materials* 2009 19, 3809-3814.

[57] H. Aarnio, P. Sehati, S. Braun, M. Nyman, M. P. de Jong, M. Fahlman, and R. Österbacka, Spontaneous Charge Transfer and Dipole Formation at the Interface between P3HT and PCBM *Adv Energy Mater* 2011 1, 792-797.

[58] F. Fischer, T. Hahn, H. Bässler, I. Bauer, P. Strohriegl, and A. Köhler, Measuring reduced C_{60} Diffusion in Crosslinked Polymer Films by Optical Spectroscopy *Advanced Functional Materials* 2014 24, 6172-6177.

[59] S. Athanasopoulos, S. T. Hoffmann, H. Bässler, A. Köhler, and D. Beljonne, To Hop or not to Hop? Understanding the Temperature Dependence of Spectral Diffusion in Organic Semiconductors *The Journal of Physical Chemistry Letters* 2013 4, 1694-1700.

[60] S. T. Hoffmann, S. Athanasopoulos, D. Beljonne, H. Bässler, and A. Köhler, How do Triplets and Charges move in Disordered Organic Semiconductors? A Monte Carlo Study comprising the Equilibrium and Nonequilibrium Regime *The Journal of Physical Chemistry C* 2012 116, 16371-16383.

3. Überblick über die Publikationen

3.1. Zentrale Fragestellung

Die vorliegende Arbeit beschäftigt sich mit der Fragestellung, warum in organischen Solarzellen eine effiziente Trennung von Elektron-Loch-Paaren an der Grenzfläche stattfindet, obwohl einfache Abschätzungen eine deutlich geringere Effizienz vorhersagen. Hierbei wird meist von einem Elektron-Loch-Paar ausgegangen, welches sich im Abstand von 1 nm in einem dielektrischen Medium mit ε=3-4 befindet. Dadurch errechnet sich eine Bindungsenergie, die die thermische Energie um den Faktor 20 übersteigt. Aus diesem Grund sollte ohne beziehungsweise bei geringer elektrischer Feldstärke, wie es im Betrieb einer Solarzelle am „Maximum-Power-Point“ vorkommt, keine Trennung stattfinden. Dennoch kann man organische Solarzellen mit einer Effizienz (Power conversion efficiency) von über 10% bauen. Diese Diskrepanz wird mithilfe von theoretischen Modellen und einer systematischen Variation der einzelnen Schichten in Solarzellen untersucht. Hierbei werden entscheidende Faktoren, die die Effizienz der Solarzelle beeinflussen, herausgearbeitet und der hohe Wirkungsgrad anhand einer Modellvorstellung erklärt.

Diese Arbeit besteht aus 6 Publikationen, die sich in zwei Bereiche einteilen lassen. Der erste Teilbereich beschäftigt sich allgemein mit dem Trennungs- und Rekombinationsprozess an der Donor-Akzeptor-Grenzfläche. Hierbei wird insbesondere ein Augenmerk darauf gelegt, welchen Einfluss auf die Strom-Spannungskennlinie die Rekombination von zwei Ladungsträgern hat, die von der selben Anregung stammen. Der zweite Bereich zeigt, wie sich die Delokalisierung der Ladungsträger in Donor und Akzeptor auf die Ladungstrennung auswirken und entwickelt eine Beschreibung, welche diese Delokalisierung mit berücksichtigt. Dabei wird die Auswirkung der chemischen Modifikation von Donor oder Akzeptor auf die Delokalisierung der Ladungsträger und somit auch auf die Trennungswahrscheinlichkeit untersucht. Außerdem werden die Parameter erläutert, die einen großen Einfluss auf die Dissoziationswahrscheinlichkeit haben. Im Nachfolgenden werden die Fragestellungen für die einzelnen Publikationen herausgearbeitet und in das Gesamtkonzept der Arbeit eingeordnet. Im Abschnitt 3.2 erfolgt schließlich eine genauere Beschreibung der Ergebnisse.

Wird ein Photon in einer Solarzelle absorbiert, so kann die so erzeugte Anregung (Exziton) an die Donor-Akzeptor-Grenzfläche wandern, um dort einen ladungsgetrennten Zustand („Charge-Transfer“-Zustand, CT-Zustand) zu bilden. Das so entstandene Elektron-Loch-Paar kann nun entweder rekombinieren oder im Laufe mehrerer Trennungsversuche dissoziieren. Dazu vollführen Elektron und Loch eine Überlagerung aus Diffusions- und Driftbewegung in Gegenwart eines elektrischen Feldes. Die Diffusion wird durch einen Hüpftransport zwischen den einzelnen Sites (Hüpfstellen, wie zum Beispiel einzelne Moleküle oder Wiederholeinheiten einer Polymerkette) des Donors oder Akzeptors beschrieben. Hierbei beeinflussen die Temperatur der Solarzelle und die Unordnung der einzelnen Sites den

Diffusionsprozess. Der Drift hingegen wird durch das in der Solarzelle herrschende elektrische Feld bestimmt. Hierbei kommt sowohl in der Modellierung von Solarzellen als auch in ihrer Konzeptionierung häufig die Frage auf, ab welcher Distanz zwischen Elektron und Loch die Ladungsträger frei sind und sich dadurch selber nicht wieder treffen können. Diese Frage wird experimentell in Kapitel 4.1 und theoretisch mit Hilfe von Monte-Carlo-Simulationen in Kapitel 4.2 beantwortet. Zudem können sich zwei Ladungsträger treffen, die nicht von derselben Anregung abstammen (bimolekulare Rekombination). Diese zusätzlichen Rekombinationen hängen von der Ladungsträgerdichte der Elektronen und Löcher ab und können darauf hindeuten, dass sich in der Solarzelle energetische Barrieren befinden, die den Abtransport verhindern. Wie man den Anteil dieser bimolekularen Rekombination bestimmen kann, ist ebenfalls Gegenstand von Kapitel 4.1. Die Rekombination kann von der Ladungsträgerbeweglichkeit abhängen, aber auch von der Bindungsenergie des Zustandes, der Dimensionalität des Transportes und der Lebenszeit des CT-Zustandes. Wie die einzelnen Parameter die Rekombination und damit auch den Trennungsprozess im Detail beeinflussen, wird in Kapitel 4.2 dargestellt.

Ein wichtiger Parameter für die Dissoziation ist die Bindungsenergie des Elektron-Loch-Paares. Diese wird im klassischen Fall vom Abstand zwischen Elektron und Loch und der umgebenden dielektrischen Konstanten bestimmt. Die so berechnete Bindungsenergie ist zu groß, um eine effiziente Trennung von Elektron-Loch-Paaren bei kleinen Feldstärken zu ermöglichen. Ein Aspekt, der bei dieser Betrachtung außer Acht gelassen wird, ist, dass Elektron und Loch keine Punktteilchen sind, sondern auf Donor bzw. Akzeptor delokalisiert sein können. Welche Rolle eine solche Delokalisation spielt, ist bisher unklar. Um eine geänderte Delokalisation untersuchen zu können, muss diese extern verändert werden können. Dies ist zum Beispiel möglich, indem man einen höheren energetischen Zustand anregt, der stärker delokalisiert ist, und dann die Dissoziationswahrscheinlichkeit als Funktion der Anregungsenergie misst. In C_{60} kann gezeigt werden, dass neben der Anregung in den ersten angeregten Zustand auch eine Anregung in einen CT-Zustand möglich ist, wenn genügend Energie zur Verfügung steht. Daher wird die Auswirkung dieser beiden unterschiedlichen Zustände auf die Dissoziation in Kapitel 4.3 untersucht. Hierbei wird auch die Frage adressiert, wie groß die Bindungsenergie des so erzeugten Charge-Transfer-Zustandes ist. Außerdem kann man den Einfluss der Kristallinität auf die Dissoziation mit Hilfe von zwei fast identischen Akzeptoren untersuchen, die sich nur in ihrer Neigung zur Kristallisation unterscheiden, wenn man zusätzlich $PC_{61}BM$ betrachtet.

Neben dem Akzeptor können auch im Donor zwei unterschiedliche elektronische Zustände angeregt werden. Dies wird mit den beiden Low-Bandgap-Polymeren PCDTBT und PCPDTBT in Kapitel 4.4 behandelt. Im Zuge dessen wird die Änderung der Delokalisierung des Exzitons in Abhängigkeit der Anregungsenergie mit Hilfe von theoretischen Berechnungen untersucht, um Rückschlüsse auf das Trennungsverhalten der unterschiedlich delokalisierten Zustände zu erhalten. Eine unterschiedliche Delokalisation kann jedoch auch chemisch erreicht werden. Hierfür müssen die verwendeten Polymere bei ähnlich

bleibendem Polymerrückgrat, eine unterschiedliche Steifigkeit besitzen. Dafür wird die Kopplung zwischen den einzelnen Phenylringen variiert, wodurch sich unterschiedlich stark delokalisierte Anregungen entlang des Polymers ergeben. Dieser Ansatz wird in Kapitel 4.5 genauer thematisiert. Damit soll ein Zusammenhang zwischen Delokalisation und Sättigungsfeldstärke, die wiederum ein Maß dafür ist, wie leicht die Anregungen getrennt werden können, hergestellt werden.

Um diesen Zusammenhang genauer untersuchen zu können, kann ein theoretisches Modell zur Beschreibung der Trennungswahrscheinlichkeit in Abhängigkeit des angelegten Feldes verwendet werden. Mit Hilfe dessen können weitere Fragen adressiert werden und weitere Vorhersagen über das Verhalten des Systems bei Änderung spezifischer Parameter getroffen werden. Um zunächst die Richtigkeit des in Abschnitt 2.2.4 beschriebenen Modells zeigen zu können, wird dieses auf die bereits erwähnte Serie von Polymeren mit unterschiedlicher Steifigkeit angewandt. In diesem Fall wird gezeigt, dass die experimentell beobachtete Veränderung der Sättigungsfeldstärke mit der im theoretischen Modell berücksichtigten Delokalisation erklärt werden kann. Dies wird in Kapitel 4.5 genauer betrachtet. Darüber hinaus ist es ebenfalls wichtig, dass die Temperaturabhängigkeit der Dissoziation richtig vorhergesagt werden kann, was schließlich in Kapitel 4.6 untersucht wird.

Damit lassen mit diesem Modell Vorhersagen treffen, wie sich die Sättigungsfeldstärke bei unterschiedlichen Graden der Delokalisation verhalten sollte. Auch können die Auswirkungen der Veränderung weiterer Parameter wie der Stärke der Dipole an der Grenzfläche zwischen Donor und Akzeptor auf die Sättigungsfeldstärke untersucht werden. Weiterhin ist es möglich die Temperaturabhängigkeit der Dissoziationsrate, wie sie bei experimentellen Messungen festgestellt werden kann, zu reprodozieren. Diese entsprechende Analyse befindet sich in Kapitel 4.6. Mit diesen Betrachtungen können nun Aussagen getroffen werden, welche Eigenschaften von Polymeren eine wichtige Rolle für die hohe Effizienz organischer Solarzellen spielen.

Eine wichtige Kerngröße, die sich dabei herauskristallisiert, ist die Bindungsenergie. Um diese bestimmen zu können, müssen sowohl die Energie des gebundenen CT-Zustandes als auch die Differenz zwischen Ionisationspotential des Donors und Elektronaffinität des Akzeptors bekannt sein. Das Ionisationspotential kann über die Photoionisierung des Donors bestimmt werden, dahingegen kann die Elektronaffinität von C_{60} zum Beispiel über Cyclovoltammetrie gemessen werden. Die experimentelle Bestimmung der Energie des gebundenen CT-Zustands benötigt die Messung der Elektrolumineszenz des CT-Zustandes. Die CT-Zustandsenergie kann außerdem bestimmt werden, wenn die Leerlaufspannung gegen 0 K extrapoliert wird. Derartige Messungen wurden ebenfalls in Kapitel 4.6 durchgeführt, um damit die Bindungsenergie des CT-Zustandes zu bestimmen. Diese experimentell bestimmte Bindungsenergie kann dann mit der theoretisch bestimmten verglichen werden. Infolgedessen ist es möglich eine Korrelation zwischen der Ordnung und

Delokalisation in Verbindung mit der Stärke der Grenzflächendipole und der Sättigungsfeldstärke und somit der Effizienz der Solarzelle herzustellen.

3.2. Inhalt der Publikationen

Monomolecular and bimolecular recombination of electron-hole pairs at the interface of a bilayer organic solar cell

Diese Publikation beschäftigt sich mit der Rekombination von Ladungsträgern und der Frage, ab wann diese als frei angesehen werden können. Dies spielt vor allem in der Modellierung des Ladungsträgertrennungsprozesses eine große Rolle.

In dieser Publikation wird hauptsächlich ein PCDTBT-Derivat ($PCDTBT_{stat}$) verwendet. Zum Vergleich dient hier das kleine Molekül p-DTS($FBTTh_2$)$_2$. Die HOMO- und LUMO-Level der beiden verwendeten Donor-Materialien sind ähnlich, so dass der Hauptunterschied zwischen beiden Materialien die Beweglichkeit ist, die sich um zwei Größenordnungen unterscheidet. Man kann erkennen, dass bei Verwendung von zwei gleich dicken Schichten (ungefähr 60 nm) p-DTS($FBTTh_2$)$_2$ keinen „s-shape“ zeigt, wohingegen dieser bei der Solarzelle mit dem Polymer deutlich zu sehen ist. Dies lässt sich auch deutlich erkennen, wenn die Kennlinien als feldabhängige Quanteneffizienzen dargestellt werden. Während p-DTS($FBTTh_2$)$_2$ kaum eine Feldabhängigkeit zeigt, ist hingegen bei $PCDTBT_{stat}$ eine starke Feldabhängigkeit zu erkennen und damit verbunden eine deutlich höhere Sättigungsfeldstärke. Diese sagt aus, wie groß das Feld in der Solarzelle sein muss, um eine vollständige Trennung von Elektron-Loch-Paaren zu erhalten.

Um zu verstehen, warum die Polymer-Solarzelle mit der niedrigeren Beweglichkeit einen „s-shape“ zeigt, werden Solarzellen mit verschiedenen Schichtdicken des Donors gebaut. Hierbei sieht man, dass, sobald die Schichtdicke von 66 nm auf 36 nm reduziert wird, ebenfalls der „s-shape“ zurückgeht, bis dieser bei 14 nm vollständig verschwunden ist. Damit lassen sich Injektions- und Extraktionsprobleme ausschließen, da diese ansonsten auch bei den dünnen Zellen zu erkennen gewesen wären. Auch die Dunkelströme für alle Zellen verhalten sich wie erwartet, so dass hier ebenfalls Probleme auszuschließen sind. Die Dunkelströme setzen sich aus einem ohmschen Leckstrom und einem Injektionsstrom, der bei ungefähr 0.6 V einsetzt, zusammen. Der Injektionsstrom ist dabei feld- und damit auch dickenabhängig und weist somit auf einen space-charge-limited-current hin.

Dies lässt sich genauer untersuchen, wenn die Solarzellen zusätzlich intensitätsabhängig gemessen werden. Es zeigt sich, dass der Kurzschlussstrom linear von der eingestrahlten Intensität abhängt. Dies deutet darauf hin, dass unter Kurzschlussbedingungen alle erzeugten Ladungsträgerpaare getrennt werden können und nicht rekombinieren. Reduziert

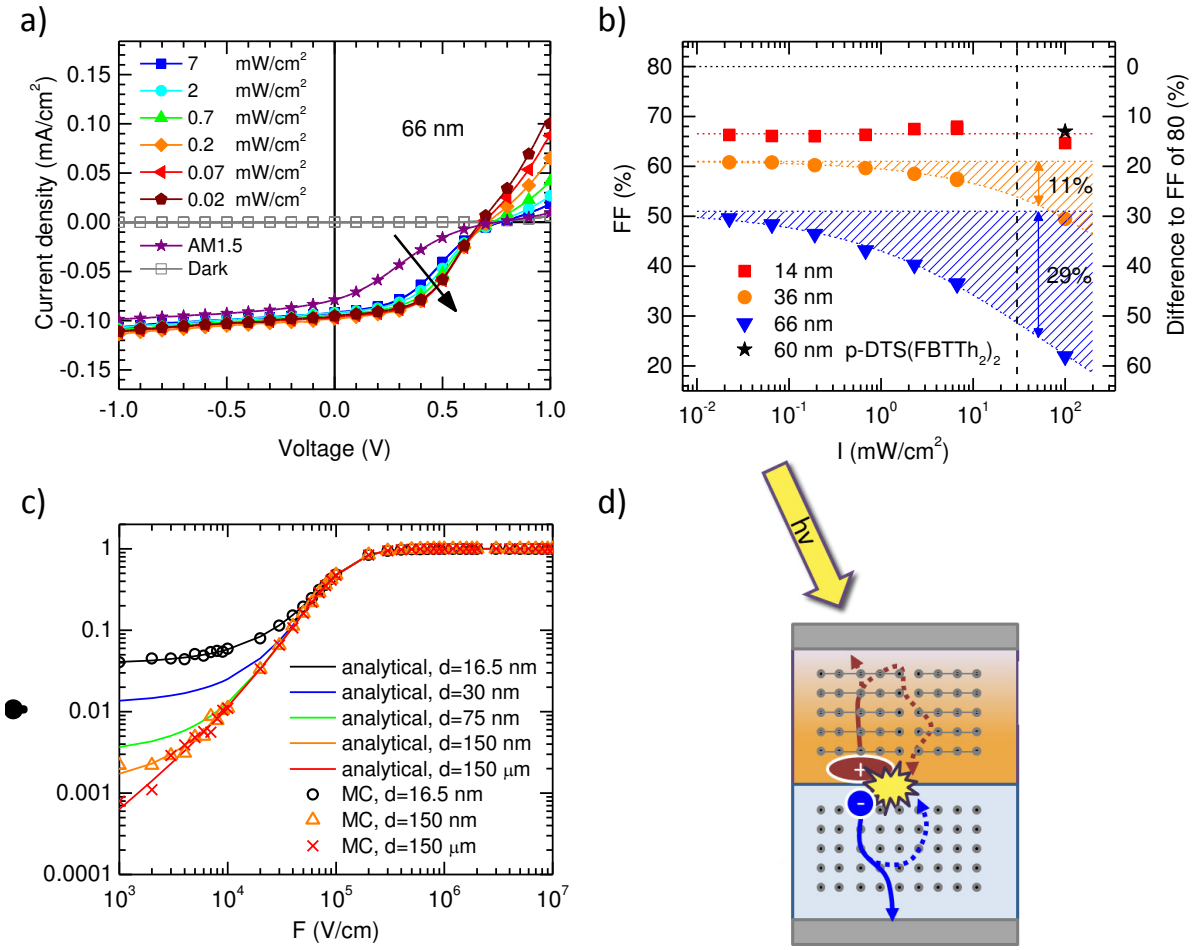

Abbildung 7: *a) Normierte Strom-Spannungs-Kennlinie für einen 66 nm dicken Polymerfilm für verschiedene Lichtintensitäten bei 580 nm und unter AM1.5. Die Normierung ist in Kapitel 4.1 beschrieben. b) Füllfaktor für Schichtdicken von 14, 36 und 66 nm für verschiedene Lichtintensitäten bei 580 nm und unter AM1.5 Bedingungen. Der Füllfaktor wurde aus den normierten Strom-Spannungs-Kennlinien, wie in a) zu sehen, berechnet. Ebenso zu sehen ist der Füllfaktor für eine identische Bilayer-Solarzelle mit 60 nm p-DTS(FBTTh$_2$)$_2$ (schwarzer Stern). Die rechte Achse zeigt die Differenz zu einem idealen Füllfaktor von 80%. Die Differenz der horizontalen Linien wird der geminalen Rekombination zugeschrieben, die schraffierte Fläche der non-geminalen Rekombination. Die eingezeichneten Pfeile und Prozentwerte zeigen die non-geminalen Verluste unter AM1.5 Bedingung an. c) Wahrscheinlichkeit ein Elektron-Loch-Paar zu trennen als Funktion des Feldes berechnet aus Monte-Carlo-Simulationen (Symbole) und einem analytischen Modell (Linien) für unterschiedliche Schichtdicken. d) Schematische Darstellung des Trennungsprozesses für die Konkurrenz zwischen Rekombination und Dissoziation*

man jedoch das Feld, indem man die Spannung in Richtung der Leerlaufspannung erhöht, ergeben sich Unterschiede für die einzelnen Schichtdicken. Während der Strom für die dünnste Schicht noch immer fast linear auf alle Intensitäten reagiert, ergeben sich bei den dickeren Schichten größere Abweichungen. Dies deutet darauf hin, dass in den dickeren Solarzellen bei hohen Intensitäten Rekombinationsverluste die Effizienz verringern. Damit

ist auch der zuvor beobachtete „s-shape“ verbunden, den man erkennen kann, wenn der Photostrom auf die Intensität korrigiert wird. So normiert, bleibt die Form der Kennlinie bei der dünnsten Zelle unverändert, wenn man die Lichtintensität ändert. Die mittlere Schichtdicke zeigt erst Abweichungen, wenn die Intensität Sonnenstärke erreicht (100 mW/cm^2). Die dickste Zelle weicht schon deutlich früher von der üblichen Form ab und zeigt unter Sonnenbedingungen einen deutlich zu erkennenden „s-shape“ (siehe Abbildung 7a). Daraus lässt sich schließen, dass in den dünnsten Zellen bimolekulare Rekombination keine Rolle spielt. Dieser Verlustkanal wird jedoch umso wichtiger, je dicker die Zelle ist.

Um die Rekombination genauer untersuchen zu können, wird der Füllfaktor als Funktion der Lichtintensität dargestellt (siehe Abbildung 7b). Die dünnste Zelle zeigt auch hier keine Veränderung des Füllfaktors, welcher bei ungefähr 67% liegt. Deshalb können bimolekulare Rekombinationen (non-geminale Rekombination) hier keine Rolle spielen. Bei den Solarzellen, welche 36 nm dick sind, sieht man einen Füllfaktor, welcher bei niedrigen Intensitäten bei 61% liegt, und sobald die Intensität bis auf 100 mW/cm^2 erhöht wird, auf 50% abnimmt. Bei den 66 nm dicken Zellen beträgt der Verlust unter Sonnenlicht bereits 29% bezüglich des Füllfaktors bei niedrigen Intensitäten. Daher erkennt man zum einen, dass die Verluste durch die non-geminale Rekombination dominanter werden je dicker die Solarzelle wird. Zum anderen ist aber auch zu erkennen, dass der maximal zu erreichende Füllfaktor dickenabhängig ist. Um dies zu verdeutlichen, kann man den Füllfaktor in Abhängigkeit der Dicke für verschiedene Intensitäten betrachten. Alle Verluste, die bei niedrigster Intensität auftreten, können der geminaler Rekombination zugeordnet werden. Die zusätzlichen Verluste, die auftreten, wenn die Intensität erhöht wird, werden folglich durch non-geminale Rekombination verursacht.

Die non-geminale Rekombination ist, wie erwartet, dickenabhängig. Hier führen die freien Elektronen und Löcher eine durch Diffusion bestimmte Bewegung aus. Im Verlauf dieser Bewegung können Elektronen und Löcher wieder an die Grenzfläche zurück diffundieren und eine Gegenladung treffen. Es wird angenommen, dass diese nicht von demselben Elektron-Loch-Paar stammt. Dies ist der Grund für die Intensitätsabhängigkeit der non-geminalen Rekombination. Durch die dickere Schicht wird die Diffusionszeit erhöht und damit auch die Wahrscheinlichkeit wieder zurück an die Grenzfläche zu kommen. Bei der geminalen Rekombination hingegen wird davon ausgegangen, dass diese signifikant ist, solange die Ladungsträger gebunden sind. Dies ist der Fall, solange die Coulombbindungsenergie $E_b = \frac{e^2}{4\pi\epsilon_0\epsilon_r r_{e-h}}$ größer als die thermische Energie $E_T = kT$ ist. Ist der Abstand zwischen Elektron und Loch größer als der Langevinradius (auch „Coulomb-Capture“-Radius), welcher durch $E_b = E_T$ definiert ist, so gelten die Ladungsträger als frei und können nicht mehr zu dieser primären geminalen Rekombination beitragen. Der Coulombradius beträgt bei einer angenommenen Dielektrizitätskonstante von 3.5 ungefähr 16 nm. Dies ist in der Größenordnung der dünnsten verwendeten Schicht. Daher sollte die geminale Rekombination dickenunabhängig sein. Da aber auch diese mit dicker werdenden

Donor-Schichten zunimmt, muss gefolgert werden, dass die freien Ladungsträger wieder zu ihrem ursprünglichen Partner zurück diffundieren und mit diesem rekombinieren können. Diese Art von Rekombination wird sekundäre geminale Rekombination genannt und kann die Effizienz der Solarzelle weiter reduzieren.

Dieser Prozess kann genauer untersucht werden, wenn nur ein Elektron-Loch-Paar betrachtet wird. Am einfachsten lässt sich das mit Hilfe einer Monte-Carlo-Simulation realisieren, bei der nur ein Elektron-Loch-Paar erzeugt wird und die Dicke des Donors variiert wird. Zusätzlich kann man diese Ergebnisse mit einem analytischen Modell, welches als Grundlage der in Kapitel 2.2.3 und 2.2.4 beschriebenen Modelle dient, bestätigen (siehe Abbildung 7c). Bei diesen Berechnungen sieht man, dass bei hohen Feldern die Dissoziationswahrscheinlichkeit unabhängig von der Dicke des Donors ist. Dies reproduziert auch die experimentell gemessenen Daten, dass sich der Kurzschlussstrom linear mit der Intensität verhält. Bei kleineren Feldern hingegen spielt die Rückdiffusion von freien Ladungsträgern zur Grenzfläche eine entscheidende Rolle und dadurch auch für den Füllfaktor und die Effizienz der Solarzelle. Bei dünnen Zellen können die freien Ladungsträger schneller extrahiert werden. Aus diesem Grund haben diese nicht mehr die Möglichkeit zur Grenzfläche zurück zu diffundieren und mit ihrem Partner zu rekombinieren (siehe Abbildung 7d). Dies erklärt die erhöhte Effizienz der Solarzellen, bei denen die Donor-Schicht in der Größenordnung des Langevinradius ist.

Diese Ergebnisse erweiterten das Verständnis der für die Effizienz in der Solarzelle wichtigen Rekombinationsprozesse. Es gibt die primäre geminale Rekombination, die die Rekombination von gebundenen Ladungsträgern beschreibt, und die non-geminale Rekombination, welche die Rekombination von freien Elektronen und Löchern beschreibt und hauptsächlich bei hohen Ladungsträgerdichten auftritt. Zusätzlich konnte gezeigt werden, dass die Rückdiffusion von freien Ladungsträgern zu ihrem ursprünglichen Partner ebenfalls eine große Rolle spielt und die Effizienz signifikant reduzieren kann. Dies kann die Abhängigkeit der Effizienz von der Ladungsträgerbeweglichkeit auch bei niedrigen Anregungsdichten erklären.

Efficient Charge Separation in organic photovoltaics through incoherent hopping

Diese Publikation untersucht die Frage, wie die Ladungsträgertrennung und -rekombination von der Delokalisierung der Ladungsträger, der Dimensionalität des Transportes und der Beweglichkeit abhängt. Dies wird mit Hilfe kinetischer Monte-Carlo-Simulationen untersucht.

Für die in dieser Arbeit verwendete Monte-Carlo-Simulation wurde entweder eine 1-dimensionale Kette oder ein 2-dimensionales Netzwerk an Sites angenommen. Auf der einen Seite befindet sich das Donor-Polymer, auf der anderen Seite der molekulare Akzeptor. An der Grenzfläche wird ein Elektron-Loch-Paar erzeugt, in dem sich das Elektron

F

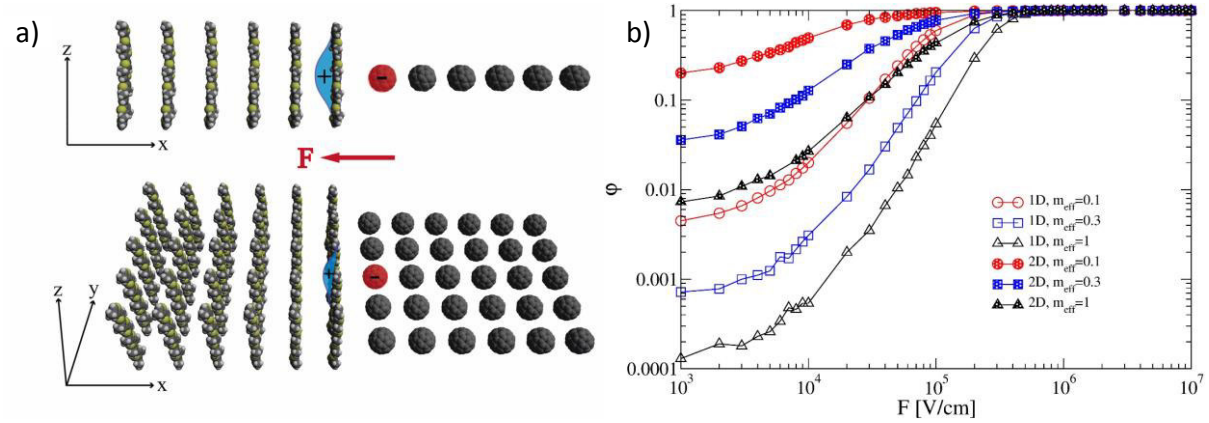

Abbildung 8: *a) Schematische Darstellung der 1D (obere Hälfte) und 2D (untere Hälfte) der Zweischicht Morphologie, welche für die Monte-Carlo-Simulation verwendet wurde. Jeder Punkt besteht entweder aus einem C_{60}-Akzeptor-Molekül oder einem Donor-Polymer mit unendlich langer Kettenlänge. Die Delokalisation entlang der Kette wurde über die effektive Masse mit berücksichtigt. b) Dissoziationswahrscheinlichkeit als Funktion des Feldes berechnet mit 1D und 2D Monte-Carlo-Simulationen für verschiedene effektive Massen des Lochs auf dem Donor.*

auf dem Akzeptor und das Loch auf dem Donor befinden, wie in Abbildung 8a zu sehen ist. Das Loch kann zusätzlich noch im Potential des Elektrons delokalisiert sein und so eine zusätzliche kinetische Energie besitzen. Elektron und Loch können im Potential des anderen Ladungsträgers, überlagert mit dem elektrischen Feld, einen Random Walk ausführen. Die Sprünge von einer Site zur nächsten Site werden über Miller-Abrahams-Raten beschrieben und zufällig aus allen möglichen Ereignissen ausgewählt. Elektron und Loch können entweder rekombinieren oder an ihren jeweiligen Elektroden extrahiert werden. Genauere Informationen zu der dynamischen Monte-Carlo-Simulation befinden sich in Kapitel 2.3.

Zunächst wird die Auswirkung der Änderung der Delokalisierung, welche durch die effektive Masse beschrieben wird, auf den Trennungsprozess betrachtet. Hierfür wird die feldabhängige Quanteneffizienz des Trennungsprozesses untersucht. Zunächst wird das Elektron stationär gewählt, so dass nur die Änderungen der Eigenschaften des Lochs relevant werden. Außerdem wird zunächst nur ein 1-dimensionaler Transport angenommen. Erhöht man die Delokalisierung des Loches auf dem Polymer, indem man die effektive Masse reduziert, so sind die Änderungen in Abbildung 8b zu sehen. Zunächst reduziert sich die Sättigungsfeldstärke, was mit einer Reduzierung der Bindungsenergie gleichzusetzen ist. Einhergehend damit erhöht sich ebenfalls die Effizienz bei niedrigen Feldstärken. In diesem Bereich wird die Bewegung der Ladungsträger hauptsächlich durch die Diffusion in der gegebenen Energielandschaft bestimmt und weniger über den Drift des angelegten Feldes. Daher kann die Reduzierung der Barriere des Coulombfeldes die Reduzierung der Sättigungsfeldstärke und die Steigerung der Effizienz bei kleinen Feldern erklären.

Des Weiteren kann der Effekt der Erhöhung der Dimensionalität des Transportes betrachtet werden. Hierfür werden Berechnungen analog zu den oben genannten Überlegungen durchgeführt. Diesmal wird aber ein 2-dimensionales Gitter an möglichen Sites angenommen. Dadurch stehen dem Ladungsträger mehr Möglichkeiten zur Verfügung einen Sprung auszuführen. Man kann in Abbildung 8b erkennen, dass dies einen erheblichen Einfluss auf das Trennungsverhalten des Elektron-Loch-Paares hat. Die Erhöhung der Dimensionalität hat einen ähnlichen Einfluss wie eine starke Delokalisierung, die durch eine effektive Masse von 0.1 m_e charakterisiert ist. Eine weitere erhebliche Reduzierung der Sättigungsfeldstärke und damit eine Steigerung der Dissoziationswahrscheinlichkeit bei niedrigen Feldern kann erreicht werden, wenn ein 2-dimensionaler Transport in Verbindung mit einer starken Delokalisierung angenommen wird.

Wie in der vorherigen Publikation zu sehen war, wird die Effizienz der Solarzelle ebenfalls stark durch unausgeglichene Mobilität der Ladungsträger bestimmt. So besteht eine starke Feldabhängigkeit, wenn nur ein Ladungsträger als mobil und der andere im Verhältnis dazu als stationär angenommen werden kann. Die Simulationen, die in dieser Publikation durchgeführt wurden, zeigen, dass sobald sich die Beweglichkeiten beider Ladungsträger angleichen, sich die Trennungswahrscheinlichkeit im Diffusionsregime erhöht. Ebenfalls erniedrigt sich die Sättigungsfeldstärke, so dass bei stark delokalisierten Ladungsträgern, 2-dimensionalem Transport und ausgeglichenen Mobilitäten eine feldunabhängige Trennung vorausgesagt wird. Es wurde ein Vergleich zwischen den experimentellen Daten von p-DTS($FBTh_2$)$_2$, welches in der vorherigen Publikation verwendet wurde, und den Simulationen dieser Publikation durchgeführt. Die gemessene Mobilität ist um zwei Größenordnungen kleiner als die in der Literatur angegebene von C_{60}. Verwendet man diese Information und eine effektive Masse von 0.1 m_e, so kann mit der 2-dimensionale Monte-Carlo-Simulation die Feldabhängigkeit der p-DTS($FBTh_2$)$_2$/C_{60}-Solarzelle gut reproduzieren.

Die Daten der Publikation zeigen, dass die Erhöhung der Lebenszeit des CT-Zustandes, einen ähnlichen Effekt hat wie die Erhöhung der Beweglichkeit. Dies ist analog zu der Erhöhung des Produktes aus Lebenszeit und Mobilität im Onsager-Braun-Modell. Dies kann dadurch erklärt werden, dass das Elektron-Loch-Paar während seiner Lebenszeit mehr Versuche hat aus dem wechselseitigen Coulombfeld zu entkommen.

The role of intrinsic photogeneration in single layer and bilayer solar cells with C_{60} and PCBM

In dieser Publikation wird die Frage beantwortet, welchen Einfluss die Akzeptor-Schicht in der Solarzelle auf das Photostromspektrum hat. Hierbei werden insbesondere der Trennungsmechanismus und dessen Beschreibung dargelegt.

Die Trennung im Akzeptor lässt sich am Besten durch die interne Quanteneffizienz (IQE) charakterisieren, da in diesem Fall nur das Verhältnis aus getrennten Elektron-Loch-Paaren

zu den Erzeugten betrachtet wird. Dieses Verhältnis kann man berechnen, wenn die externe Quanteneffizienz (EQE) um die Transmission des Glassubstrats und die Absorption der aktiven Schicht korrigiert wird. Die EQE kann gemessen werden, indem der Strom in Abhängigkeit der Spannung aufgenommen wird, wodurch wiederum das Feld in der Solarzelle variiert wird. Da die Messung der Absorption in einer einzelnen Schicht in einer vollständigen Solarzelle schwierig und dadurch sehr fehlerbehaftet ist, wird der Anteil der absorbierten Photonen mit Hilfe der Transfermatrixmethode berechnet. Diese kann bei bekannten komplexen Brechungsindizes n, k die elektrische Feldstärkenverteilung für verschiedene Anregungswellenlängen bestimmen, so dass die Absorption ortsabhängig

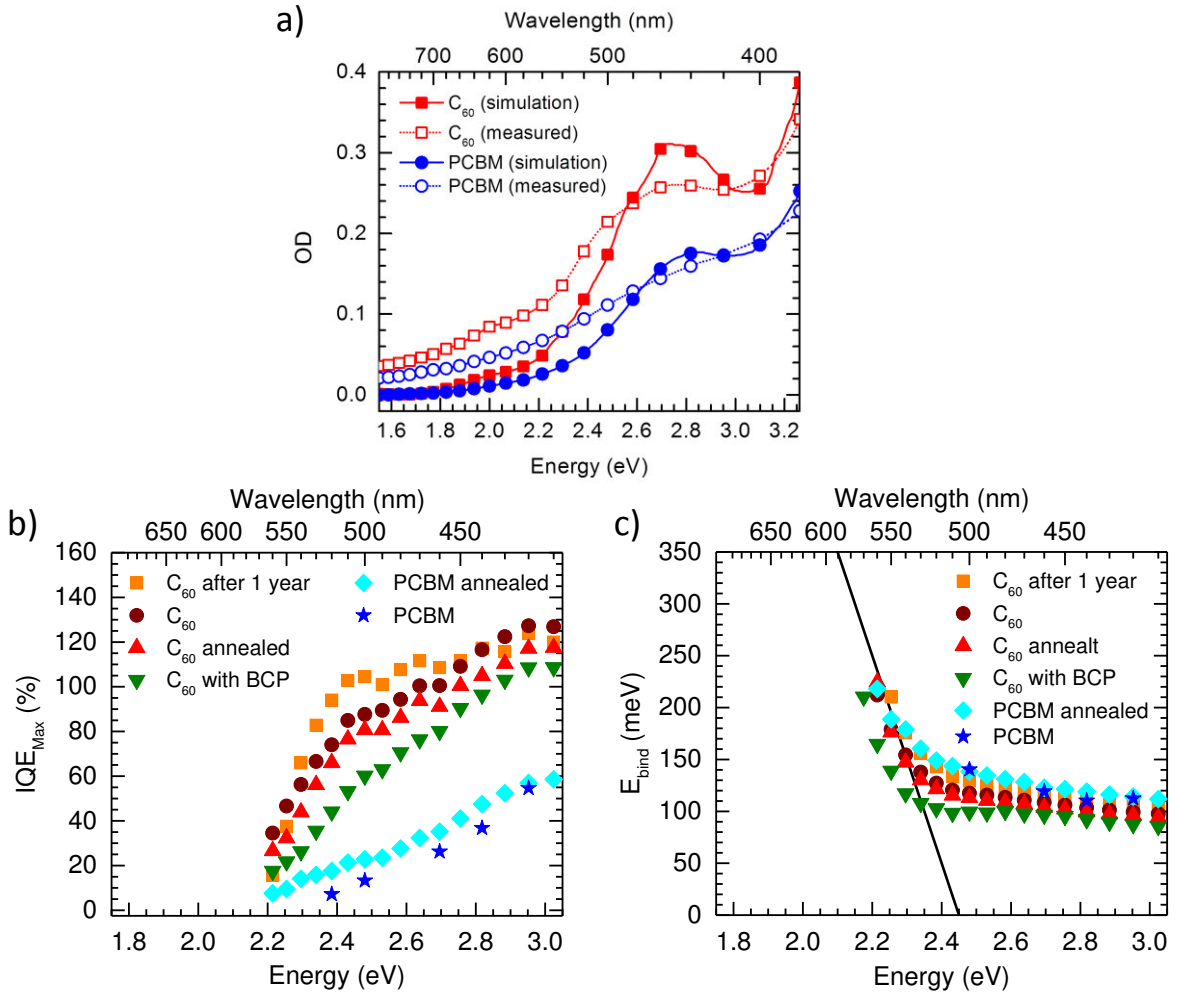

Abbildung 9: *a) Optische Dichte von C_{60} (rote Vierecke) und $PC_{61}BM$ (blaue Kreise) gemessen auf einem Quarzglassubstrat (offene Symbole) und berechnet (geschlossene Symbole). In der Berechnung war die Schicht von C_{60} bzw. $PC_{61}BM$, wie in der Solarzelle, zwischen ITO/MoO_3 und Aluminium eingebettet. b) Maximale Interne Quanteneffizienz für hohe Felder und c) Coulombbindungsenergie als Funktion der Anregungsenergie für Einzelschicht-Solarzellen. Die eingezeichnete Linie in c) zeigt die Coulombbindungsenergie ohne Verluste an, bei einer angenommenen elektrischen Lücke von 2.45 eV.*

angegeben werden kann. Die Brechungsindizes können aus der Literatur entnommen werden. Die gemessenen und berechneten optischen Dichten befinden sich in Abbildung 9a.

Es wurden Einzelschicht-Solarzellen verwendet, um den Einfluss des Akzeptor-Materials C_{60} und $PC_{61}BM$ zu bestimmen. Es zeigt sich, dass die EQE bei diesen Zellen zweigeteilt ist. Daraus kann man schließen, dass unterhalb von 2.25 eV zwar Photonen absorbiert werden können, diese aber nicht innerhalb des Fullerens getrennt werden. Oberhalb dieser Kante können zusätzlich Charge-Transfer-Zustände angeregt werden. Diese können leichter getrennt werden und liefern somit einen Beitrag zur Effizienz der Solarzelle. Es wird gezeigt, dass die Effizienz von C_{60} deutlich besser als von $PC_{61}BM$ ist. Die hier beobachtete Tendenz wird deutlich, wenn die feldabhängige IQE bei zwei unterschiedlichen Anregungsenergien betrachtet wird. Unterhalb der Energiekante zeigen C_{60} und $PC_{61}BM$ die gleiche Effizienz und oberhalb den schon beschriebenen Unterschied.

Zusätzlich kann gezeigt werden, dass der Beitrag zur externen Quanteneffizienz in Zweischicht-Solarzellen bei Verwendung von C_{60} nicht vernachlässigbar ist. Dieser Beitrag fällt geringer aus, wenn man stattdessen $PC_{61}BM$ verwendet. Dennoch sollte dieser Beitrag bei der Analyse und Interpretation von Solarzellen, bei denen C_{60} oder $PC_{61}BM$ verwendet wird, berücksichtigt oder durch Anregung unterhalb des niedrigsten CT-Zustandes ausgeschaltet werden. Die feldabhängen Messungen mit einem kleinen Molekül oder einem Polymer als Donor zeigen, dass es einen signifikanten Unterschied zwischen der Anregung unterhalb und oberhalb von 2.25 eV gibt.

Die Messungen der Einzelschicht-Solarzellen können verwendet werden, um den Trennungsprozess zu modellieren. Hierfür wird analog zu den Arbeiten an Anthrazenkristallen das 1938 entwickelte Modell von Onsager verwendet. Dieses wird ausführlich in Abschnitt 2.2.1 beschrieben. Die entscheidenden Parameter, die durch die Fits der feldabhängigen internen Quanteneffizienz gewonnen werden können, sind der Sättigungswert für die interne Quantenausbeute bei hohen elektrischen Feldern, IQE_{max}, und die Coulombbindungsenergie des zu trennenden Zustands, E_{coul}. Man kann auch hier erkennen, dass die Trennung erst ab 2.25 eV einsetzt. Die unterschiedlich behandelten Solarzellen zeigen fast keinen Unterschied, wohingegen eine deutliche Differenz zwischen C_{60} und $PC_{61}BM$ für IQE_{max} zu erkennen ist (siehe Abbildung 9b). Dieses Verhalten bestätigt das schon in den Zweischicht-Solarzellen gesehene Verhalten. Dahingegen kann man keinen Unterschied zwischen den beiden Akzeptoren erkennen, wenn man sich die Coulombbindungsenergie in Abhängigkeit der Anregungsenergie anschaut. Es lässt sich erkennen, dass die Bindungsenergie linear mit steigender Energie sinkt. Dies deutet darauf hin, dass es keinen Energieverlust im Rahmen der Thermalisierung des Elektron-Loch-Paares gibt. Damit ergibt sich die elektronische Bandlücke als Summe von Anregungsenergie und Bindungsenergie (siehe Abbildung 9c). Diese stimmt mit durch andere Techniken bestimmten Werten überein, wenn man die Unsicherheit der einzelnen Methoden berücksichtigt. Regt man oberhalb dieser Energie an, so sättigt die Bindungsenergie auf

100 meV, was darauf hindeutet, dass die überschüssige Energie über Phononen abgegeben wird. Die Bindungsenergie kann auch in mittlere Elektron-Loch-Abstände umgerechnet werden. Hier lässt sich erkennen, dass der Abstand bei Anregungen oberhalb von 2.25 eV mit steigender Anregungsenergie von ungefähr 2.0 nm auf 2.5 nm anwächst.

Aus diesen Ergebnissen lässt sich ein Bild für die intrinsische Ladungsträgertrennung in Fullerenen ableiten. Werden Fullerene unterhalb von 2.25 eV angeregt, so können die entstehenden stark gebundenen Elektron-Loch-Paare nur an Grenzflächen oder an Fehlstellen getrennt werden. Ungefähr zwischen 2.25 eV und 2.45 eV können eine Serie kalter CT-Zustände angeregt werden, deren mittlerer Bindungsabstand von ungefähr 2.0 nm auf 2.5 nm zunimmt. Durch Änderung des Elektron-Loch Abstands sinkt die Bindungsenergie von 220 meV auf 100 meV. Oberhalb von 2.45 eV relaxieren die optisch angeregten CT-Zustände in CT-Zustände mit einer Bindungsenergie von ebenfalls 100 meV. Um diese Zustände trennen zu können, müssen diese durch thermische Anregung an die Transportzustände koppeln. Diese Kopplung spiegelt sich in IQE_{max} wider. Der Unterschied der IQE_{max} zwischen C_{60} und $PC_{61}BM$ deutet darauf hin, dass diese Kopplung in C_{60} stärker ist.

Does Excess Energy Assist Photogeneration in an Organic Low-Bandgap Solar Cell?

Diese Publikation soll zur Ergänzung der vorangegangen dienen. Sie behandelt die Prozesse in der Donor-Schicht und ihre Auswirkungen auf die Solarzelle.

Die betrachteten Materialien sind zwei unterschiedliche Donor-Akzeptor-Polymere, zum einen PCDTBT und zum anderen PCPDTBT. Beide Materialien zeigen eine energieabhängige Dissoziationswahrscheinlichkeit, wenn diese in Zweischichtzellen mit C_{60} prozessiert werden. Es ist zu erkennen, dass eine starke Feldabhängigkeit zu erkennen ist, solange man in den S_1 Zustand anregt. Diese wird deutlich schwächer ausgeprägt, wenn man in den nächst höher erlaubten elektronischen Zustand anregt. Die Daten von PCDTBT sind in Abbildung 10a zu sehen. Wie zuvor gezeigt, kann jedoch C_{60} eine starke Feldabhängigkeit besitzen, die den hier betrachteten Effekt überdeckt. Da dieses Wissen erst nach dieser Publikation zur Verfügung stand, wurden nachträglich Messungen durchgeführt, die diesen Einfluss eliminieren sollten. Hierfür wurden anstatt der normalerweise üblicherweise 30 nm C_{60} nur 6 nm verwendet. Dies ist notwendig, damit es in der Solarzelle keine intrinsische Ladungsträgergeneration im C_{60} gibt. Dennoch ist in beiden Materialkombinationen weiterhin die Änderung der Feldabhängigkeit zu beobachten (siehe Extension). Zusätzlich zu der Verhinderung der intrinsischen Generation von Ladungen im C_{60} konnte durch den verbesserten Aufbau der Solarzelle eine konstante Leerlaufspannung in Verbindung mit einer guten Auskopplung der Ladungen sichergestellt werden. Damit ist ein Vergleich der feldabhängigen IQE für alle verschiedenen Anregungsenergien möglich.

Damit war es nun möglich, die Sättigungsfeldstärke eindeutig im gesamten Anregungsbereich zu bestimmen. Hier ist eine Erniedrigung der Sättigungsfeldstärke zu erkennen, sobald der energetisch höhere Übergang angeregt wird. Dieses Verhalten konnte zwar auch mit den dicken C_{60}-Schichten beobachtet werden, aber nur mit den dünnen Schichten kann der störende Einfluss von C_{60} verhindert werden. Dies kann zusätzlich untermauert werden, wenn man sich die Polymere, analog zu den C_{60}-Zellen, in einer Einzelschicht-Solarzelle anschaut. Auch hier sieht man für die beiden Polymere mehrere unterschiedliche Bereiche im IQE-Spektrum, welches in Abbildung 10b für PCDTBT zu sehen ist. Es sind zwei Stufen zu erkennen. Die erste beginnt, sobald die Absorption des $S_1 \leftarrow S_0$ 0-0 Übergang einsetzt. Ungefähr 0.5 eV oberhalb dieser Energie erhöht sich die IQE, wenn die Absorption in den nächst höheren Zustand einsetzt. Analog zu der Argumentation mit C_{60} kann auch hier die Annahme gemacht werden, dass es sich um zwei unterschiedliche Zustände handelt, die unterschiedlich leicht getrennt werden können.

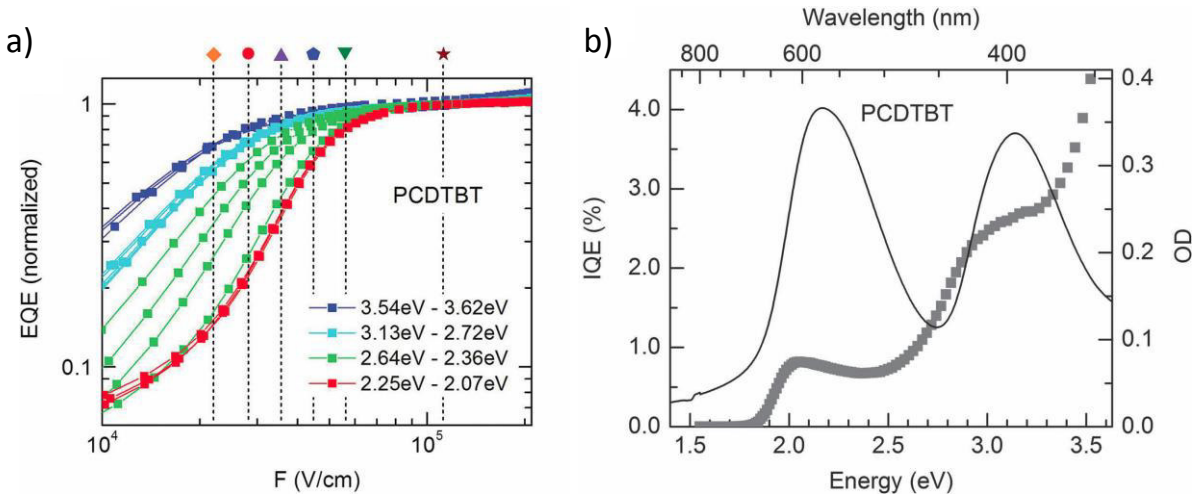

Abbildung 10: *a) Normierte externe Quanteneffizienz einer PCDTBT/C_{60} Bilayer Solarzelle in Abhängigkeit des Feldes parametrisch für verschiedene Anregungsenergien. b) Interne Quanteneffizienz einer PCDTBT Einzelschicht-Solarzelle ohne Akzeptor in Abhängigkeit der Anregungsenergie. Die rechte Achse zeigt die optische Dichte der verwendeten PCDTBT-Schicht.*

Die beobachtete Reduzierung der Sättigungsfeldstärke für höhere Anregungsenergien deutet auf eine geringere Bindungsenergie hin. Diese kann erreicht werden, indem der Elektron-Loch-Abstand durch die zusätzlich verfügbare Energie größer wird. Außerdem ist mit der Anregung eines höheren Zustandes meist eine Delokalisierung der Anregung verbunden, wodurch die Bindungsenergie zusätzlich gesenkt werden kann. Mit Hilfe von „many-body Green's function Bethe-Salpeter"-Berechnungen wird diese Delokalisierung gezeigt. Damit diese Rechnungen durchgeführt werden können, wurde das betrachtete System vereinfacht. Es wurde nur ein C_{60}-Molekül und ein PCDTBT-Polymer berücksichtigt. Zusätzlich wurde das Polymer durch ein Dimer approximiert. Bei den Rechnungen, die nur das Polymer berücksichtigen, ist zu sehen, dass sowohl der $S_1 \leftarrow S_0$-, als auch der $S_2 \leftarrow S_0$-Übergang eine ähnliche Energie besitzen und auf einer Monomereinheit lokalisiert sind. Der

$S_3 \leftarrow S_0$-Übergang besitzt eine deutlich höhere Übergangsenergie und ist zudem noch über das gesamte betrachtete Dimer delokalisiert. Die Differenz der beiden berechneten Übergangsenergien stimmt mit der gemessenen Differenz zwischen den beiden sichtbaren Übergängen überein. Die absoluten Energien sind jedoch ins Rote verschoben, was daran liegen kann, dass hier nur ein Dimer und kein Polymer betrachtet wird. Außerdem wird die Umgebung in der Berechnung nicht mit berücksichtigt. Ein ähnliches Verhalten ist zu beobachten, wenn das C_{60}-Molekül in der Berechnung mit berücksichtigt wird. Hier ändert sich die Delokalisierung von einer Monomereinheit nicht nur auf das gesamte Dimer, sondern es wird zusätzlich auf das benachbarte C_{60} ausgeweitet. Dies ist noch kein Charge-Transfer-Zustand, da sowohl die Elektron- als auch die Lochwellenfunktion über den gesamten Komplex delokalisiert sind. Erst durch die Bildung eines Charge-Transfer-Zustandes kann die Trennung stattfinden. Dies wird durch die zusätzliche Energie und damit verbundene Delokalisation der Wellenfunktionen erleichtert. So sind auch die beobachtete Abnahme der Sättigungsfeldstärke und die damit verbundene Bindungsenergie zu erklären.

Role of the effective mass and interfacial dipoles on exciton dissociation in organic donor-acceptor solar cells

In dieser Publikation wird eine weiterführende Studie durchgeführt, welche die bisher gefundenen Ergebnisse zur Delokalisation bestätigen soll. Zusätzlich wird ein theoretisches Modell einführt, welches diese Ergebnisse in den Trennungsprozess mit einbezieht.

Um die Delokalisation genauer zu charakterisieren und ihren Einfluss auf die Effizienz von Solarzellen festzustellen, wird hier eine Serie von unterschiedlich steifen Polymeren benutzt. Diese Polymere besitzen ein chemisch fast identisches Rückgrat, das aus unterschiedlich vielen miteinander steif verbunden Phenylringen besteht. Zum ersten gibt es das vollkommen versteifte MeLPPP. Das nächst flexiblere Polymer ist PIF, welches drei Phenylringe miteinander verbunden hat. PF2/6 besitzt zwei miteinander verbundene Phenylringe, bei DOOPPP dahingegen können sich alle Phenylringe frei drehen. Zusätzlich wird das in der zuvor schon verwendeten Arbeit Low-Bandgap-Polymer PCDTBT zum Vergleich mit hinzugezogen. In einer früheren Arbeit konnte bereits über Absorptions- und Emissionsmessungen gezeigt werden, dass diese chemische Verknüpfung der Phenylringe mit einer steigenden Konjugationslänge gleichzusetzen ist. In Zweischicht-Solarzellen mit C_{60} ist zu sehen, dass die Sättigungsfeldstärke mit steigender Konjugationslänge abnimmt und somit die Bindungsenergie sinkt (siehe Abbildung 11a). Zudem kann in den Materialkombinationen eine Verschiebung des Vakuumlevels festgestellt werden. Diese deuten auf Dipole an der Grenzfläche zwischen Polymer und C_{60} hin.

Um die gemessene feldabhängige Quanteneffizienz genauer beschreiben zu können, kann das Onsager-Braun-Modell herangezogen werden (siehe Kapitel 2.2.2). Dieses Modell wurde schon auf kleine Moleküle erfolgreich angewendet. Die entscheidenden Parameter für die

Beschreibung nach diesem Modell sind der Elektron-Loch-Abstand des Charge-Transfer-Zustandes sowie das Produkt aus der Lebenszeit jenes Zustandes und der Ladungsträgerbeweglichkeit. Dieses Modell ist jedoch nicht für die Beschreibung des Trennungsprozesses geeignet. Zum einen kann die Feldabhängigkeit der Ladungsträgerseparation, insbesondere für die Materialien mit niedriger Sättigungsfeldstärke, nur unzureichend beschrieben werden, zum anderen sind die erhaltenen Parameter in einem Bereich, in dem entweder die Ladungsträgerbeweglichkeit oder die Lebenszeit zu groß gewählt werden müssen. Da das Produkt nur in Kombination der beiden Parameter vorkommt, muss zum Beispiel die Ladungsträgerbeweglichkeit angenommen werden, um die Lebenszeit zu erhalten. So berechnet man bei DOOPPP bei einer angenommenen Beweglichkeit von ungefähr 10^{-5} cm^2/Vs eine Lebenszeit von 30 ms, die um mehrere Größenordnungen zu groß ist. Typischerweise liegen die Lebenszeiten im Bereich einiger zehn Nanosekunden. Im Onsager-Braun-Modell wird weder eine Delokalisierung entlang einer Kette, noch die Möglichkeit des Vorhandenseins möglicher Grenzflächendipole, welche die Gegenladung abschirmen können, mit einbezogen.

Das Effektive-Masse-Modell, welches die Delokalisation mit berücksichtigt, sollte daher besser geeignet sein die hier verwendeten Polymere und ihre unterschiedliche Delokalisation zu beschreiben. Die schematische Darstellung dieses Modells ist in Abbildung 11b zu sehen. In diesem Modell wird die Delokalisation mit Hilfe einer effektiven Masse des Lochs auf dem Polymer beschrieben, wie es schon von Arkhipov vorgeschlagen wurde. Das Loch kann temperaturaktivierte Sprünge zwischen benachbarten Ketten, die parallel zur Grenzfläche liegen, ausführen. Die Sprungrate wird mithilfe von Miller-Abrahams-Raten ermittelt. Die potentielle Energie auf den einzelnen Ketten kann durch die Lösung der 1D-Schrödingergleichung berechnet werden. Diese Energie kann in zwei Teile aufgeteilt werden. Der größte Teil entspricht der klassischen potentiellen Energie auf dieser Kette. Hinzu kommt die quantenmechanisch bestimmte kinetische Energie. Diese Nullpunktenergie reduziert die Bindungsenergie und hängt von der Krümmung des Potentials ab. Sie wird größer, wenn die effektive Masse kleiner und somit die Wellenfunktion stärker delokalisiert ist.

Wie in der Publikation gezeigt, kann mit diesem Modell der Feldverlauf der Trennung von Elektron–Loch-Paaren, vor allem für die effizienten Materialien mit einer niedrigen Sättigungsfeldstärke, gut beschrieben werden. Für die Materialien mit einer höheren Bindungsenergie kann zwar der Feldverlauf bei hohen Feldern gut rekonstruiert werden, jedoch erkennt man, dass bei kleinen Feldern die Quanteneffizienz unterschätzt wird. Ein weiterer Punkt, der beachtet werden muss, ist, dass die gewählte effektive Masse für PCDTBT und MeLPPP im Bereich von 0.06 Elektronenmassen liegt. Vergleicht man diesen Wert mit Messungen und Berechnungen bei gestreckten Polydiacetylenketten, welche im Bereich von 0.1 bis 0.05 liegen, so sieht man, dass dieser Wert zu klein ist. Deshalb wird als untere Grenze 0.1 m_e angenommen.

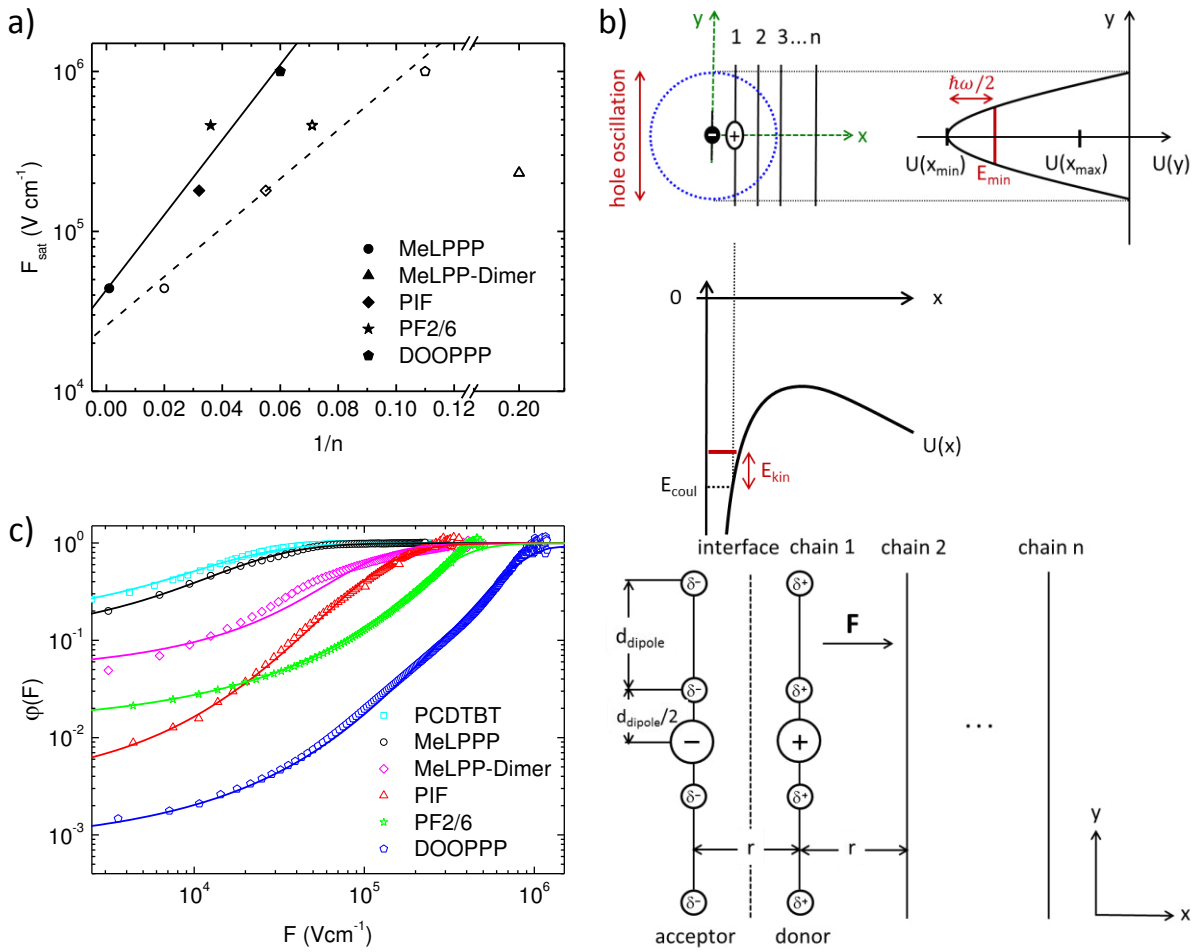

Abbildung 11: *a) Sättigungsfeldstärke in Abhängigkeit der inversen effektiven Konjugationslänge des Donors für die Grundzustandsgeometrie (Daten aus Absorption, offene Symbole) und die Geometrie des angeregten Zustandes (Daten aus Emission, geschlossene Symbole). Die Linien dienen der graphischen Veranschaulichung. b) Schematische Darstellung des verwendeten Modells für die Elektron-Loch-Trennung an einer Bilayer-Grenzfläche. Das Elektron befindet fest sich auf einem C_{60}-Molekül während das Loch zwischen den Ketten 1 bis n hüpfen kann. Das Loch kann auf den Ketten eine Nullpunktschwingung ausführen, mit der eine entsprechende kinetische Energie verknüpft ist. Zusätzlich wird das Potential durch das elektrische Feld beeinflusst, so dass die Barriere weiter reduziert wird. Unterhalb befindet sich eine genauere Ansicht der Grenzfläche bei der neben Elektron und Loch auch Grenzflächendipole eingezeichnet sind, welche das Potential weiter beeinflussen können. c) Dissoziationswahrscheinlichkeit als Funktion des elektrischen Feldes für Donor/C_{60}-Bilayer-Solarzellen unter Anregung bei 2.2 eV. Die experimentellen Daten (Symbole) der Polymere (PCDTBT, MeLPPP, PIF, PF2/6 und DOOPPP) und das MeLPPP-Dimer wurden mit einer Kombination aus dem Effektive-Masse-Modell und dem Fehlstellen-Modell gefittet (Linien).*

Als Ursache für die zu geringe effektive Masse wurde von uns die Vernachlässigung von Grenzflächendipolen in diesem Modell identifiziert. Solche Grenzflächendipole können die Gegenladung abschirmen und somit die Trennung begünstigen. Daher kann man das Effektive-Masse-Modell erweitern und zusätzlich die Grenzflächendipole mit berücksichtigen (siehe Kapitel 2.2.4). In diesem Fall wird eine geringere Delokalisation

angenommen, um eine ähnliche Bindungsenergie zu erhalten. Im Gegensatz zu dem Effektive-Masse-Modell war zu diesem Zeitpunkt nur eine Näherung der Lösung der Schrödingergleichung verfügbar. Aus diesem Grund ist ein direkter Vergleich schwierig. Dieses Problem wird in der darauffolgenden Arbeit gelöst. Dennoch findet man, dass es im niedrigen Feldbereich bei beiden Modellen eine Unterschätzung der Dissoziationswahrscheinlichkeit gibt. Insbesondere gilt dies für die Polymere mit einer höheren Sättigungsfeldstärke.

Der zusätzliche Trennungsmechanismus, der vorkommen kann, beruht auf einer Trennung von Elektron-Loch-Paaren an zusätzlich in das Polymer eindiffundierten C_{60}-Molekülen. Zu diesem Zweck wird das ebenfalls von Arkhipov entwickelte Fehlstellen-Modell verwendet, welches in Kapitel 2.2.5 beschrieben wird. Die Idee dieses Modells ist, dass ein Elektrontransfer auf ein eindiffundiertes C_{60}-Molekül stattfindet, welches zunächst als Elektronenfalls fungiert. Das zurückbleibende Loch wird auf dem Polymer delokalisiert. Das Loch versucht im Anschluss auf dem Polymer mit Hilfe des elektrischen Feldes der Coulombanziehung des Elektrons zu entkommen. Ist die Konzentration der Elektronfallenzustände groß genug, so kann das Elektron im Anschluss eine Fallen-zu-Fallen Bewegung ausführen und so die entsprechende Elektrode erreichen. Da es sich hier um einzelne Fallenzustände handelt, gibt es keine Grenzflächen, an denen sich Dipole bilden können, so dass diese nicht mit berücksichtigt werden müssen. Da zusätzlich der Abstand und die Orientierung zwischen Polymerkette und Fallenzustand zufällig verteilt sind, muss noch darüber gemittelt werden.

Das Fehlstellen-Modell kann mit dem Dipol-Modell kombiniert werden. Die erzeugten Exzitonen können über den Mechanismus, der durch das Dipol-Modell beschrieben wird, getrennt werden. Die Exzitonen, die nicht erfolgreich getrennt werden konnten, können aber zusätzlich über den Mechanismus des Fehlstellen-Modells getrennt werden. Die so erhaltenen feldabhängigen Wahrscheinlichkeiten können den gemessenen Verlauf im gesamten Feldbereich für alle verwendeten Materialkombinationen wiedergeben, welche in Abbildung 11c zu sehen ist. Dies zeigt, dass neben der Trennung an der Grenzfläche zwischen Donor und Akzeptor auch die eindiffundierten C_{60}-Moleküle mit berücksichtigt werden müssen, um eine vollständige Beschreibung des Trennungsmechanismus zu erhalten. Zusätzlich müssen für eine erfolgreiche Modellierung sowohl die Grenzflächendipole als auch eine mögliche Delokalisation der Elektronen, beziehungsweise der Löcher, mit berücksichtigt werden.

A Combined Theoretical and Experimental Study of Dissociation of Charge Transfer States at the Donor-Acceptor Interface of Organic Solar Cells

Die Bindungsenergie und, damit verbunden, auch die Energie des Charge-Transfer-Zustandes werden in dieser Publikation genauer betrachtet. Zusätzlich wird untersucht,

durch welche Parameter sich die Bindungsenergie beeinflussen lässt und damit eine erfolgreiche Dissoziation von einem kalten Charge-Transfer-Zustand ermöglicht wird.

Um aussagekräftigere Ergebnisse zu bekommen, wird die zuvor verwendete Approximation der Lösung der Schrödingergleichung durch eine numerische Lösung ersetzt. Das bedeutet, dass das Potential nicht länger als harmonisch angenähert wird, sondern das exakte Coulombpotential verwendet wird. Die Änderungen in der Feldabhängigkeit fallen je nach verwendeten Parametern unterschiedlich stark aus. Man kann jedoch zeigen, dass für die bisher verwendeten Parametersätze die Änderung deutlich geringer ausfällt, als sie in anderen Arbeiten abgeschätzt wird.

Damit kann die Sättigungsfeldstärke in Abhängigkeit des Feldes betrachtet werden. Setzt man das Produkt aus Lebenszeit und inverser Hüpfzeit fest, so kann man die effektive Masse variieren, welche ein Maß für die Delokalisation ist. Wie schon aus experimentellen Daten bekannt ist, verringert sich die Sättigungsfeldstärke mit kleiner werdender effektiver Masse. Ermöglicht man nun dem Elektron-Loch-Paar mehr Versuche zu entkommen, indem man die Lebenszeit oder die Hüpfrate erhöht, so lässt sich erkennen, dass die Sättigungsfeldstärke abnimmt und sich der gesamte Kurvenverlauf zu niedrigeren Feldstärken verschiebt. Ebenfalls lässt sich erkennen, dass die Abschirmung der Gegenladung durch Grenzflächendipole bei fester effektiver Masse und dem Produkt aus Lebenszeit und Hüpfrate ebenfalls die Trennung begünstigt und so die Sättigungsfeldstärke reduziert. Reduziert man zusätzlich die effektive Masse, so erhält man für starke Grenzflächendipole eine fast feldunabhängige Trennung der Exzitonen. Dies gilt insbesondere für Feldstärken, die gleich oder größer des built-in-fields ($\approx 5 \cdot 10^4$ V/cm) sind. Damit verbunden ist eine weitere Verschiebung der Sättigungsfeldstärke zu kleineren Feldern. Dieses Verhalten kann man deutlich erkennen, wenn man die Sättigungsfeldstärke in Abhängigkeit der Grenzflächendipole parametrisch im Produkt der Lebenszeit und inverser Hüpfzeit betrachtet. Hier lässt sich ein fast exponentieller Zusammenhang aus Sättigungsfeldstärke und Stärke der Grenzflächendipole erkennen. Als nächstes wird die Sättigungsfeldstärke in Abhängigkeit der Delokalisierung, also der effektiven Masse, wieder parametrisch im Produkt aus Lebenszeit und inverser Hüpfzeit betrachtet. Hier lässt sich für den Fall nicht vorhandener Grenzflächendipole erkennen, dass effektive Massen kleiner als $0.1\ m_e$ benötigt werden, um eine Sättigungsfeldstärke im Bereich des built-in-field zu erhalten. Dies ist notwendig, um effiziente Solarzellen erhalten zu können. Da dies, wie vorher beschrieben, die untere Grenze für die effektive Masse ist, wird daraus deutlich, dass zumindest eine geringe Abschirmung durch die Grenzflächendipole vorhanden sein muss, um eine effiziente Trennung erhalten zu können. Werden hingegen stärkere Grenzflächendipole ausgebildet, so kann die Delokalisierung fast vernachlässigt werden. Dies gilt insbesondere dann, wenn die Lebenszeit oder die Hüpfrate hoch ist.

Ein weiterer Aspekt des Modells ist, wie sich die Dissoziationswahrscheinlichkeit mit der Änderung der Temperatur verändert. Um zu überprüfen, ob die Temperaturabhängigkeit

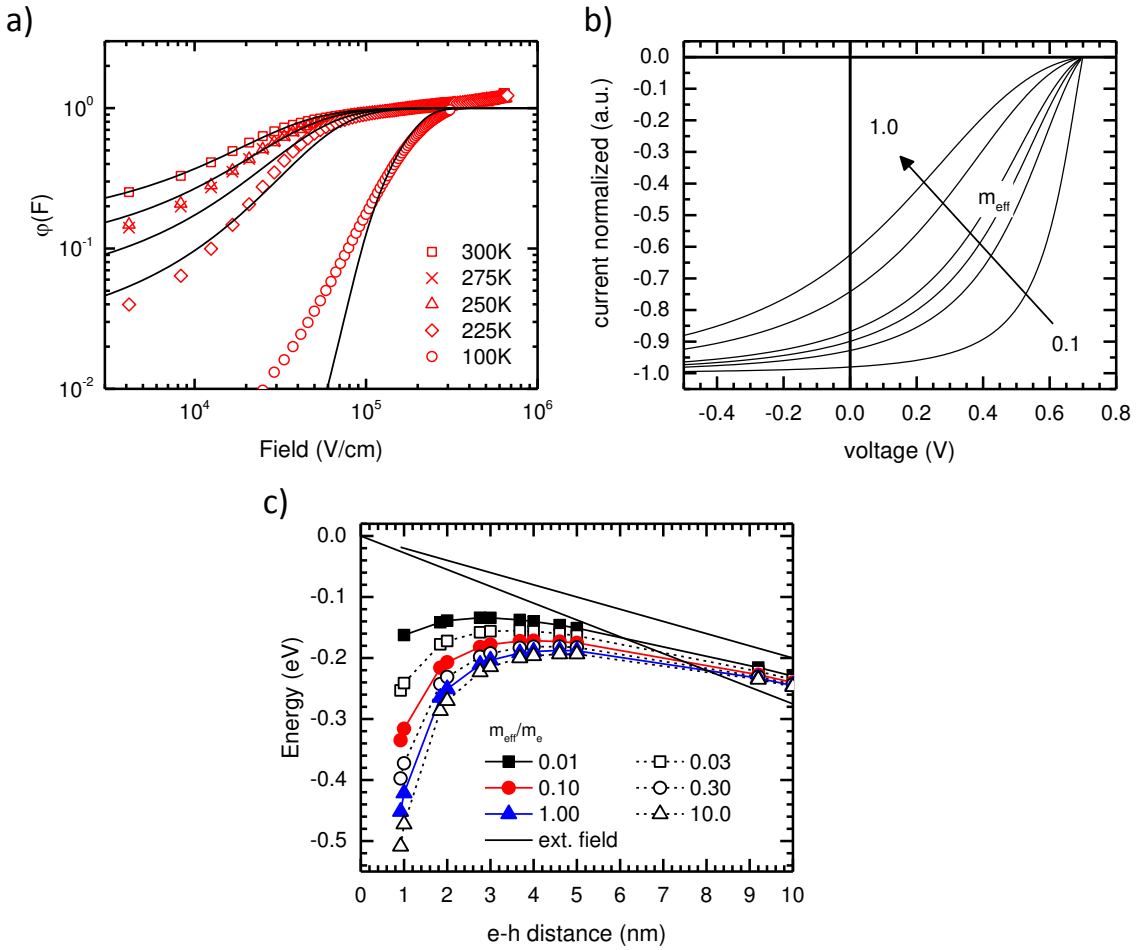

Abbildung 12: *a) Gemessene Dissoziationswahrscheinlichkeit (Symbole) als Funktion des elektrischen Feldes parametrisch für verschiedene Temperaturen. Globaler Fit (Linien) für die gemessenen Daten mit* $\boldsymbol{m_{eff} = 0.112\, m_e, \alpha = 0.0142}$ *und* $\boldsymbol{\nu_0 \tau e^{-2\gamma r} = 2500}$*. Die Temperatur wurde entsprechend der experimentellen Temperatur gewählt. b) Strom-Spannungs-Kennlinien berechnet für eine Bilayer-Solarzelle mit 60 nm Dicke und einer Leerlaufspannung von 0.7 V. Die Grenzflächendipolstärke beträgt* $\boldsymbol{\alpha = 0.02}$ *und die effektive Masse wurde von 0.1* m_e *bis 1.0* m_e *variiert. c) Die Energien (Symbole) der Lochwellenfunktion als Funktion des Elektron-Loch-Abstandes parametrisch in der effektiven Masse. Die Werte wurden als Überlagerung der Coulombwechselwirkung zwischen Elektron und Loch und einer elektrischen Feldstärke von* $\boldsymbol{F = 2 \cdot 10^5\, V/cm}$ *ohne Grenzflächendipole berechnet. Die Linien dienen der graphischen Veranschaulichung.*

des Modells richtig beschrieben wird, werden Zweischicht-Solarzellen mit MeLPPP als Donor und C_{60} als Akzeptor gebaut. Von diesen werden die feldabhängigen Dissoziationswahrscheinlichkeiten bei verschiedenen Temperaturen gemessen. Im Anschluss wird ein globaler Fit an den Messdaten durchgeführt. Der einzige variable Parameter hierbei ist die Temperatur, die explizit in die temperaturaktivierten Sprünge eingeht. Alle anderen Parameter werden gleich gewählt. In Abbildung 12a ist zu erkennen, dass die Wahrscheinlichkeit für eine erfolgreiche Trennung von dem Modell gut beschrieben wird. Die Abweichungen, welche bei niedrigen Temperaturen und kleinen Feldern zu sehen

sind, können darauf zurückgeführt werden, dass in diesem Modell keine Unordnung mit berücksichtigt wird. Diese kann hauptsächlich bei kleinen Feldstärken und niedrigen Temperaturen die Trennung begünstigen. Zusätzlich kann die schwache Temperaturabhängigkeit im Bereich der Sättigungsfeldstärke durch das Modell erklärt werden. Dies ist möglich, ohne dass weitere Annahmen gemacht werden müssen, wie zum Beispiel ein feldabhängiger Tunnelprozess, der den Elektron-Loch-Abstand erhöhen kann. Diese Temperaturunabhängigkeit kann dadurch erklärt werden, dass die Bindungsenergie stark reduziert wird. Bei einer Bindungsenergie von 0.5 eV erhält man eine stark temperaturabhängige Dissoziationswahrscheinlichkeit bei einem festen Feld von $1 \cdot 10^5$ V/cm, welche sich ähnlich zum Onsager-Braun-Modell verhält. Die Bindungsenergie reduziert sich ungefähr um den Faktor zwei im Falle einer starken Delokalisierung, die durch eine effektive Masse von 0.1 m_e charakterisiert wird, oder bei moderaten Grenzflächendipolen, bei denen die fraktionelle Dipolstärke $\alpha = 0.02$ beträgt. Dadurch wird die Trennungswahrscheinlichkeit oberhalb von 250 K fast temperaturunabhängig, wohingegen unterhalb noch eine starke Temperaturabhängigkeit zu beobachten ist. Diese Abhängigkeit verschwindet, wenn die Bindungsenergie noch weiter reduziert wird, dass sowohl das Loch delokalisiert ist, als auch sich moderate Dipole an der Grenzfläche befinden.

Diese Bindungsenergie, welche den Trennungsprozess bestimmt, kann aus dem Modell direkt in Abhängigkeit der verschiedenen Parameter ermittelt werden. Sie nimmt, wie oben schon beschreiben, im Bereich von 1.0 m_e bis 0.1 m_e um den Faktor zwei ab. Die dazu entsprechenden Strom-Spannungs-Kennlinien sind in Abbildung 12b zu finden. Durch das Anlegen eines externen Feldes wird die Energie, die zur Trennung der Elektron-Loch-Paare benötigt wird, weiter reduziert (siehe Abbildung 12c). Bei Bindungsenergien von etwa 0.1 eV und einem angelegten Feld, welches in der Größenordnung des built-in-field ist, wird die Potentialkurve flach. Dadurch sind keine temperaturaktivierte Sprünge nötig. So kann auch die verschwindende, experimentell gemessene, Temperaturabhängigkeit erklärt werden.

Die Bindungsenergie in einer Zweischichtsolarzelle kann auch experimentell gemessen werden. Hierfür wird zunächst die Energie des Charge-Transfer-Zustandes benötigt. Es können zwei Methoden verwendet werden, um diese zu bestimmen. Bei der einen betrachtet man die Elektrolumineszenz und die externe Quanteneffizienz des Photostroms, bei der anderen extrapoliert man die Leerlaufspannung (V_{oc}) auf 0 K. Die Elektrolumineszenz zeigt zwei Peaks. Der hochenergetische Peak bei 1.67 eV verliert an Intensität relativ zu dem niederenergetischen Peak (1.38 eV). Zudem wird der Peak bei 1.67 eV bereits der Fluoreszenz von C_{60} zugeordnet. MeLPPP besitzt ebenfalls keine Emission bei 1.38 eV, wodurch dieser Peak dann der Elektrolumineszenz des CT-Zustandes zugeschrieben werden kann. Bei der externen Quanteneffizienzmessung kann der Photostrom, der bei ungefähr 1.7 eV stark abfällt, der S_1 Absorption des C_{60} zugeordnet werden. Die bei 1.48 eV ausgeprägte Schulter kann nicht durch diese Absorption erklärt werden und muss daher vom CT-Zustand kommen. Durch die Kombination der beiden Messungen ergibt sich eine

Energie des CT-Zustandes von 1.43 eV. Dieser kann mit dem Wert verglichen werden, wenn man V_{oc} in Abhängigkeit der Temperatur misst und dann gegen 0 K extrapoliert. Die Messungen ergeben einen Wert von 1.35 eV für die Kombination von MeLPPP mit C_{60} und ungefähr 1 eV für DOOPPP in Verbindung mit C_{60}. Dies kann auch erklären, warum keine CT-Emission mit der verwendeten CCD-Kamera gesehen werden konnte, da diese nur bis 1.2 eV messen kann.

Die Bindungsenergie ist die Differenz zwischen dem elektronischen Gap (Unterschied des Ionisierungspotentials des Donors und der Elektronaffinität des Akzeptors) und der Energie des Charge-Transfer-Zustandes. Die Elektronaffinität von C_{60} kann mit Hilfe von Cyclovoltammetrie bestimmt werden. Die Ionisierungsenergie der Polymere kann durch Photoionisation ermittelt werden. Diese Methoden wurden schon in der Literatur für die verwendeten Materialien angewendet, weshalb diese nicht extra gemessen wurden. Die CT-Energie wird, wie oben beschrieben, aus den temperaturabhängigen Messungen von V_{oc} sowie der Elektrolumineszenz in Verbindung mit der externen Quanteneffizienz des Photostroms bestimmt. Die Werte der so bestimmten Bindungsenergie stimmen gut mit denen überein, welche sich aus den Rechnungen der Dissoziationswahrscheinlichkeiten ergeben.

Als letztes lässt sich aus den vorliegenden Ergebnissen ableiten, dass es keine Notwendigkeit gibt, heiße, kurzlebige Zustände mit zu berücksichtigen. In diesem Modell wurden nur langlebige gebundene Zustände angenommen. Die Bindungsenergie kann durch Dipole an der Grenzfläche und durch Delokalisierung reduziert werden. Dadurch kann die Bindungsenergie so weit herabgesetzt werden, dass der hohe Füllfaktor und somit auch die hohe Effizienz, welche in organischen Solarzellen gemessen werden kann, erklärbar ist.

3.3. Beiträge zu den Publikationen

1) Tobias Hahn, Steffen Tscheuschner, Julian Kahle, Markus Reichenberger, Stavros Athanasopoulos, Christina Saller, Guillermo C. Bazan, Thuc-Quyen Nguyen, Peter Strohriegl, Heinz Bässler, Anna Köhler

   Monomolecular and bimolecular recombination of electron-hole pairs at the interface of a bilayer organic solar cell

   Advanced Functional Materials (**2017**), 27, 1604906

   Ich habe die Methode zur Normierung der Strom-Spannungskennlinien entwickelt und auf die Daten angewendet. Ich habe die theoretischen Berechnungen zur Dickenabhängigkeit zusammen mit Stavros Athanasopoulos durchgeführt. Bei der

Interpretation von den Ergebnissen habe ich mitgeholfen. Bei der Erstellung und Bearbeitung des Manuskripts habe ich mitgeholfen.

2) Stavros Athanasopoulos, Steffen Tscheuschner, Heinz Bässler, Anna Köhler

Efficient Charge Separation in organic photovoltaics through incoherent hopping

Journal of Physical Chemistry Letters (**2017**), 8, 2093−2098

Bei der Erstellung und Optimierung des Codes habe ich entscheidende Vorarbeit geleistet. Ich habe zusammen mit Stavros Athanasopoulos die Möglichkeit erarbeitet, die effektive Masse in die Monte-Carlo-Simulation einzubinden. Ich habe bei der Analyse der Daten mitgeholfen.

3) Tobias Hahn & Steffen Tscheuschner, Christina Saller, Peter Strohriegl, Puttaraju Boregowda, Tushita Mukhopadhyay, Satish Patil, Dieter Neher , Heinz Bässler, Anna Köhler

The role of intrinsic photogeneration in single layer and bilayer solar cells with C_{60} and PCBM

Journal of Physical Chemistry C (**2016**), 120, 25083-25091

Ich habe die Absorption von C_{60} sowie $PC_{61}BM$ gemessen und berechnet. Ich habe das Programm zur Messung der energieabhängigen Strom-Spannungskennlinien weiterentwickelt und umgeschrieben. Ich habe die Fits und Auswertung der feldabhängigen IQE-Daten durchgeführt. In Zusammenarbeit mit den Coautoren habe ich die Ergebnisse interpretiert und das Manuskript überarbeitet. Tobias Hahn und ich haben zu gleichen Teilen zur vorliegenden Publikation beigetragen.

4) Tobias Hahn , Johannes Geiger , Xavier Blase , Ivan Duchemin , Dorota Niedzialek , Steffen Tscheuschner , David Beljonne , Heinz Bässler , and Anna Köhler

Does Excess Energy Assist Photogeneration in an Organic Low-Bandgap Solar Cell?

Advanced Functional Materials (**2015**), 25, 1287–1295

Ich habe ein Programm zur Auswertung der Daten entwickelt. Ich habe eine Routine zum Auslesen der Sättigungsfeldstärken entworfen. Bei der Auswertung und Interpretation habe ich mitgeholfen.

5) Christian Schwarz, Steffen Tscheuschner, Johannes Frisch, Stefanie Winkler, Norbert Koch, Heinz Bässler, Anna Köhler

Role of the effective mass and interfacial dipoles on exciton dissociation in organic donor-acceptor solar cells

Physical Review B (**2013**), 87, 155205

Ich habe ein Programm entwickelt mit dem die Messdaten durch verschiedene Modelle gefittet werden können. Ich habe alle Fits der Messdaten durchgeführt und ausgewertet. Ich habe die Kombination der Modelle entwickelt. Bei der Erstellung und Bearbeitung des Manuskripts habe ich mitgeholfen.

6) Steffen Tscheuschner, Heinz Bässler, Katja Huber, Anna Köhler

A Combined Theoretical and Experimental Study of Dissociation of Charge Transfer States at the Donor-Acceptor Interface of Organic Solar Cells

Journal of Physical Chemistry B (**2015**), 119, 10359-10371

Ich habe sämtliche Berechnungen durchgeführt. Ich habe den Aufbau zur Messung der Elektrolumineszenz weiterentwickelt und diese gemessen. Ich habe zusammen mit Heinz Bässler die Interpretation der Ergebnisse durchgeführt. Bei der Erstellung und Bearbeitung des Manuskripts habe ich große Teile beigetragen.

4. Publikationen

Publikationen dieser Dissertation

1) Tobias Hahn, Steffen Tscheuschner, Julian Kahle, Markus Reichenberger, Stavros Athanasopoulos, Christina Saller, Guillermo C. Bazan, Thuc-Quyen Nguyen, Peter Strohriegl, Heinz Bässler, Anna Köhler

   Monomolecular and bimolecular recombination of electron-hole pairs at the interface of a bilayer organic solar cell

   Advanced Functional Materials (**2017**), 27, 1604906

2) Stavros Athanasopoulos, Steffen Tscheuschner, Heinz Bässler, Anna Köhler

   Efficient Charge Separation in organic photovoltaics through incoherent hopping

   Journal of Physical Chemistry Letters (**2017**), 8, 2093-2098

3) Tobias Hahn & Steffen Tscheuschner, Christina Saller, Peter Strohriegl, Puttaraju Boregowda, Tushita Mukhopadhyay, Satish Patil, Dieter Neher , Heinz Bässler, Anna Köhler

   The role of intrinsic photogeneration in single layer and bilayer solar cells with C_{60} and PCBM

   Journal of Physical Chemistry C (**2016**), 120, 25083-25091

4) Tobias Hahn , Johannes Geiger , Xavier Blase , Ivan Duchemin , Dorota Niedzialek , Steffen Tscheuschner , David Beljonne , Heinz Bässler , and Anna Köhler

   Does Excess Energy Assist Photogeneration in an Organic Low-Bandgap Solar Cell?

   Advanced Functional Materials (**2015**), 25, 1287–1295

5) Christian Schwarz, Steffen Tscheuschner, Johannes Frisch, Stefanie Winkler, Norbert Koch, Heinz Bässler, Anna Köhler

   Role of the effective mass and interfacial dipoles on exciton dissociation in organic donor-acceptor solar cells

   Physical Review B (**2013**), 87, 155205

6) Steffen Tscheuschner, Heinz Bässler, Katja Huber, Anna Köhler

A Combined Theoretical and Experimental Study of Dissociation of Charge Transfer States at the Donor-Acceptor Interface of Organic Solar Cells

Journal of Physical Chemistry B (**2015**), 119, 10359-10371

Weitere Publikationen

7) Cheng Li, Steffen Tscheuschner, Fabian Paulus, Paul E. Hopkinson, Johannes Kiessling, Anna Köhler,Yana Vaynzof, Sven Hüttner

Iodine Migration and its Effect on Hysteresis in Perovskite Solar Cells

Advanced Materials (**2016**), 28, 2446-2454

Diese bereits veröffentlichte Publikation befindet sich im Anhang dieser Dissertation.

8) Puttaraju Boregowda, Julian Kahle, Tushita Mukhopadhyay, Tobias Hahn, Alexander Rudnick, Steffen Tscheuschner, Anna Köhler and Satish Patil

Synthesis and Chain-length Dependent Photophyscial and Photovoltaic Properties of DPP-DPP based Oligomers

Journal of Materials Chemistry C (**2016**) ready for submission

4.1. Monomolecular and bimolecular recombination of electron-hole pairs at the interface of a bilayer organic solar cell

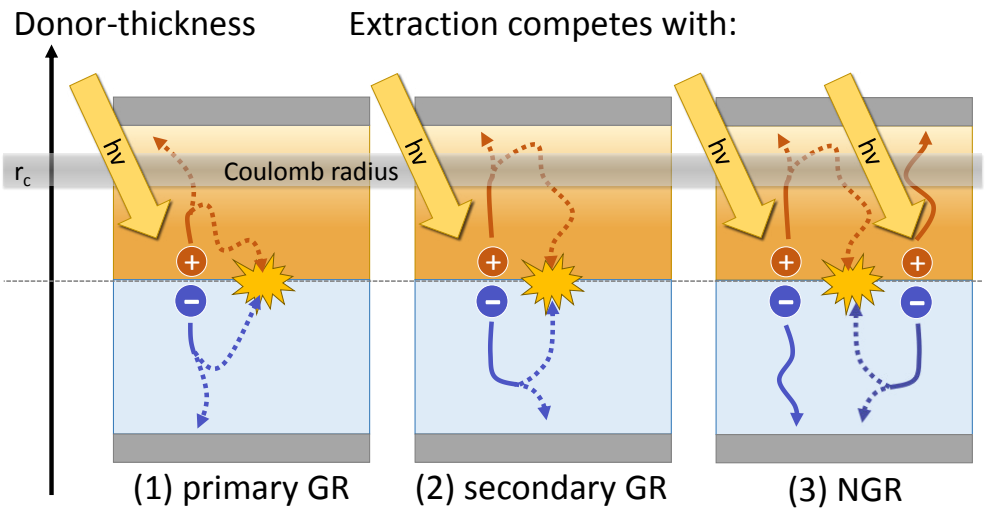

Tobias Hahn, Steffen Tscheuschner, Julian Kahle, Markus Reichenberger, Stavros Athanasopoulos, Christina Saller, Guillermo C. Bazan, Thuc-Quyen Nguyen, Peter Strohriegl, Heinz Bässler, Anna Köhler

Veröffentlicht in

Advanced Functional Materials (**2016**), 27, 1604906

(DOI: https://doi.org/10.1002/adfm.201604906)

ADVANCED FUNCTIONAL MATERIALS
www.afm-journal.de

Monomolecular and Bimolecular Recombination of Electron–Hole Pairs at the Interface of a Bilayer Organic Solar Cell

*Tobias Hahn, Steffen Tscheuschner, Frank-Julian Kahle, Markus Reichenberger, Stavros Athanasopoulos, Christina Saller, Guillermo C. Bazan, Thuc-Quyen Nguyen, Peter Strohriegl, Heinz Bässler, and Anna Köhler**

While it has been argued that field-dependent geminate pair recombination (GR) is important, this process is often disregarded when analyzing the recombination kinetics in bulk heterojunction organic solar cells (OSCs). To differentiate between the contributions of GR and nongeminate recombination (NGR) the authors study bilayer OSCs using either a PCDTBT-type polymer layer with a thickness from 14 to 66 nm or a 60 nm thick p-DTS(FBTTh$_2$)$_2$ layer as donor material and C_{60} as acceptor. The authors measure *JV*-characteristics as a function of intensity and charge-extraction-by-linearly-increasing-voltage-type hole mobilities. The experiments have been complemented by Monte Carlo simulations. The authors find that fill factor (FF) decreases with increasing donor layer thickness (L_p) even at the lowest light intensities where geminate recombination dominates. The authors interpret this in terms of thickness dependent back diffusion of holes toward their siblings at the donor–acceptor interface that are already beyond the Langevin capture sphere rather than to charge accumulation at the donor–acceptor interface. This effect is absent in the p-DTS(FBTTh$_2$)$_2$ diode in which the hole mobility is by two orders of magnitude higher. At higher light intensities, NGR occurs as evidenced by the evolution of s-shape of the *JV*-curves and the concomitant additional decrease of the FF with increasing layer thickness.

T. Hahn, S. Tscheuschner, F.-J. Kahle, M. Reichenberger, Dr. S. Athanasopoulos, Prof. A. Köhler
Experimental Physics II
University of Bayreuth
95440 Bayreuth, Germany
E-mail: Anna.Koehler@uni-bayreuth.de
Dr. S. Athanasopoulos
Departamento de Física
Universidad Carlos III de Madrid
Avenida Universidad 30, 28911 Leganés, Madrid, Spain
C. Saller, Prof. P. Strohriegl
Macromolecular Chemistry I
University of Bayreuth
95440 Bayreuth, Germany
Prof. G. C. Bazan, Prof. T.-Q. Nguyen
Department of Chemistry and Biochemistry
Center for Polymers and Organic Solids
University of California
Santa Barbara, CA 93106-9510, USA
Prof. P. Strohriegl, Prof. H. Bässler, Prof. A. Köhler
Bayreuth Institute of Macromolecular Science (BIMF)
University of Bayreuth
95440 Bayreuth, Germany

DOI: 10.1002/adfm.201604906

1. Introduction

The power conversion efficiency in organic solar cells (OSCs) depends in a complex way on several parameters, i.e., (i) the fraction of the solar spectrum that is absorbed in the cell, (ii) the probability that an absorbed photon creates a Coulomb-bound pair of charge carriers, (iii) the internal electric field needed to dissociate that electron–hole pair (eh-pair), (iv) the fraction of charge carriers that escapes bimolecular recombination before reaching the electrodes, and (v) the contact resistance that can impede charge extraction at the electrodes.[1–3] A measure of the fraction of the photogenerated charges that are actually collected at the electrodes is the fill factor (FF).[4–11] Its value thus directly reflects the mechanism of charge carrier generation, which is a controversially discussed issue in the organic photovoltaic (OPV) community. By definition, the FF gives an indication on the voltage dependence of the photocurrent in the range between zero applied voltage and the open-circuit voltage.

Traditional models for the photogeneration of charges,[12] and thus also for the photocurrent–voltage (*JV*) curves, have always taken into account that an electric field is needed to dissociate the interfacial eh-pair, be it in bulk heterojunction (BHJ)[8,13] or in planar heterojunction (PHJ)[14,15] solar cells. This implies that the inverse process, geminate recombination (GR), plays a role in controlling the shape of the *JV*-curves. The significant influence of electric field assisted dissociation and, conversely, geminate recombination has been well established experimentally for both PHJ cells[16,17] and BHJ cells.[18–20] In recent years, however, there has been an increasing number of reports demonstrating that device performance, and concomitantly the FF, is dominated by nongeminate recombination (NGR) processes such as Langevin or Shockley–Read–Hall-type recombination.[21–26] Moreover, the appearance of an s-shaped kink in the *JV*-curves of PHJ cells has been associated with the prevalence of NGR, provided that injection or extraction barrier effects can be excluded.[27,28] The NGR is considered to arise from charge accumulation at the heterojunction interface.[24] What causes a significant

contribution of either geminate or nongeminate recombination, and which factors determine the relative weight of both recombination pathways has been addressed by a few groups.[19,29–34] These groups find distinct branching ratios between GR and NGR that change with film morphology, so that it can be influenced by appropriate processing conditions. Nevertheless, a microscopic understanding of what controls these recombination pathways is still lacking.

Here we have analyzed *JV*-curves of PHJ cells made with different donor layer thicknesses (L_p) from 14 to 66 nm covered by a 30 nm thick C_{60} layer as acceptor, sandwiched between ITO/MoO_3 and Al electrodes. The donor material $PCZ_{0.3}$ is a statistical low bandgap copolymer of the PCDTBT family shown in **Figure 1**. For brevity, we shall refer to it as $PCDTBT_{stat}$. The results are compared to PHJ cells employing the molecular donor p-DTS$(FBTTh_2)_2$. We show that the branching ratio between GR and NGR depends not only on operational parameters such as light intensity and electric field but also on device parameters such as film thickness. Using Monte Carlo (MC) simulations we illustrate how, close to the open-circuit condition, not only nongeminate recombination, but also the rate of geminate recombination depends on the competition between diffusive motion toward the collecting electrode and toward the sibling countercharge. The role of mobility and delocalization of charges is discussed. These results advance our microscopic understanding of the charge generation process which is the basis for the fabrication of efficient solar cells.

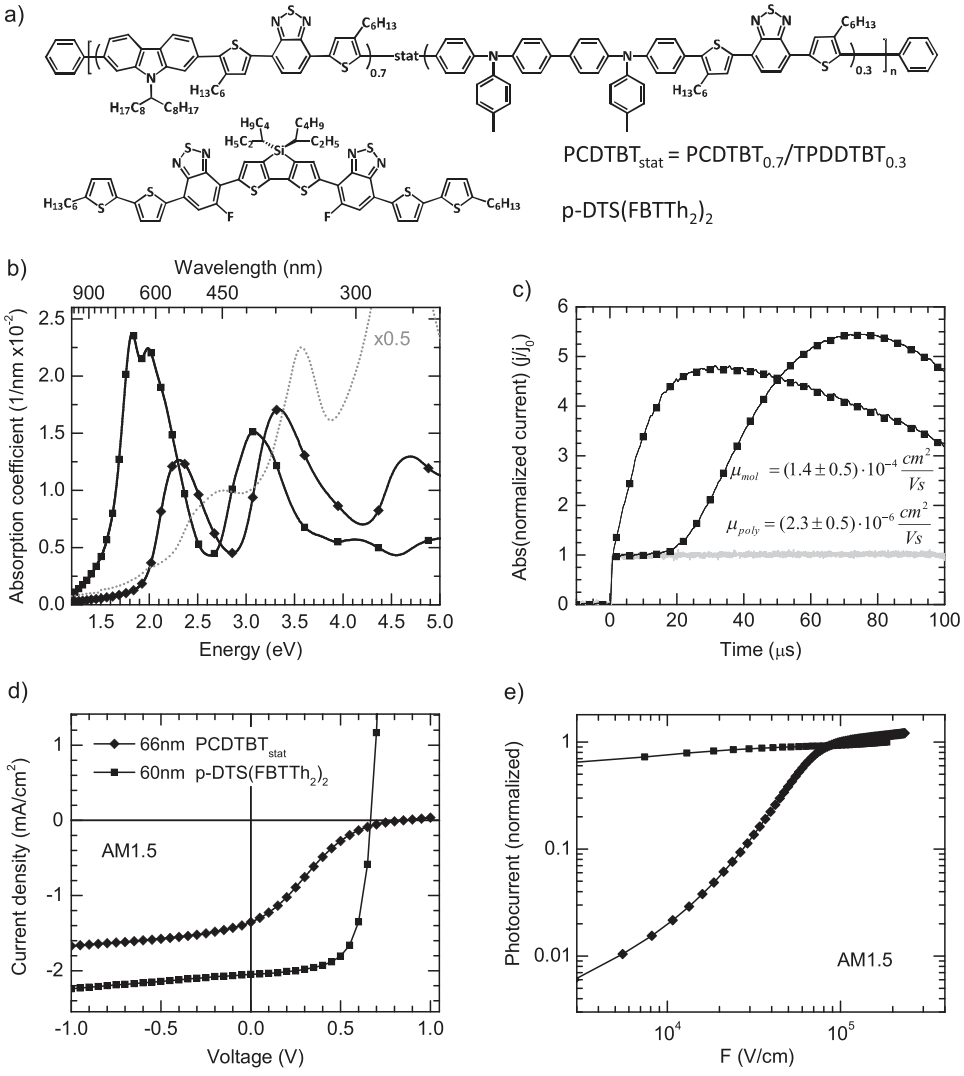

Figure 1. a) Chemical structure of the polymeric $PCDTBT_{stat}$ and the oligomeric p-DTS$(FBTTh_2)_2$ donor materials and b) the absorption coefficients of $PCDTBT_{stat}$ (gray diamonds), p-DTS$(FBTTh_2)_2$ (black squares) and C_{60}, measured from a 30 nm thick film. c) The current–response curves obtained in an MIS-CELIV measurement for $PCDTBT_{stat}$ and for p-DTS$(FBTTh_2)_2$, as well as the response of the samples when no offset is applied (gray line). The extracted mobilities are given in the figure. d) The current as a function of applied voltage under AM1.5 sun light conditions for a bilayer cell with 66 nm of $PCDTBT_{stat}$ donor and for an identical bilayer cell made with 60 nm of p-DTS$(FBTTh_2)_2$ as donor. e) The photocurrent obtained from (d) replotted as a function of internal field.

Adv. Funct. Mater. **2016**,
DOI: 10.1002/adfm.201604906

2. Results

Tress et al. suggested that mobility imbalance between electron and holes would be a major factor contributing to an s-shape in the *JV*-characteristics of PHJ cells.[27] In order to probe this hypothesis and to illustrate its effect we measured the *JV*-characteristics of two bilayer diodes, each made with a 60–66 nm thick low bandgap donor layer covered by a 30 nm thick C_{60} acceptor layer sandwiched between an ITO/MoO_3 anode and an Al cathode. The chemical structures and absorption spectra of the donor materials, i.e., the molecule p-DTS(FBTTh$_2$)$_2$ and the polymer PCDTBT$_{stat}$, are shown in Figure 1a,b. Both materials form suitable heterojunctions with C_{60}, since C_{60} has HOMO and LUMO levels of –6.4 and –3.7 eV, while the corresponding values for the donors are –5.12 and –3.34 eV for the p-DTS(FBTTh$_2$)$_2$ and –5.2 and –2.9 eV for PCDTBT$_{stat}$.[35–40] A key difference between the two materials is their hole mobility. We used the metal–insulator–semiconductor charge-extraction-by-linearly-increasing-voltage (MIS-CELIV) approach to determine specifically the hole mobility in each donor (Figure 1c). For p-DTS(FBTTh$_2$)$_2$, we obtain a value of $1.4 \pm 0.5 \times 10^{-4}$ cm^2 V^{-1} s^{-1}, while only $2.3 \pm 0.5 \times 10^{-6}$ cm^2 V^{-1} s^{-1} are obtained for the hole mobility in PCDTBT$_{stat}$. The latter value is about three orders of magnitude lower than the electron mobility in C_{60}, which is in the range of 10^{-3}–10^{-2} cm^2 V^{-1} s^{-1}.[41] Indeed, under AM1.5 illumination (Figure 1d), the *JV*-characteristics of the bilayer diode with the PCDTBT$_{stat}$ is s-shaped with a fill-factor of merely 22%, in contrast to the diode with p-DTS(FBTTh$_2$)$_2$, that has a fill-factor of 67%. This difference is also evident when replotting the *JV*-curves as field dependence of the photocurrent (Figure 1e), as described further below. While these data clearly confirm the notion that the magnitude of hole mobility has an important bearing of the diode performance, it is not fully understood how this relates to the underlying microscopic mechanism.

To address the microscopic reason, we consider the *JV*-curves of the bilayer as a function of the layer thickness of the donor for the PCDTBT$_{stat}$ (**Figure 2**), in the dark as well as both for broadband excitation at AM1.5 (100 mW cm^{-2}) and for monochromatic excitation. The thickness of the C_{60} acceptor layer was kept at 30 nm while the donor layer thickness was varied from 14 to 66 nm. The dark current characteristics for the diodes (Figure 2a) are a superposition of an ohmic leakage current that is symmetric about $V = 0$ V and an injection current that increases steeply with voltage above ≈ 0.6 V and with decreasing thickness of the donor layer. This strong voltage dependence of the forward current on the donor thickness is an indication that it is controlled by the space charge injected from the ohmic ITO/MoO_3 anode. Thus, the dark *JV*-curves are perfectly "well-behaved" and they are tractable in terms of drift-diffusion theory developed by Wetzelaer et al.[42,43]

Under illumination, the highest short circuit current j_{SC}, 2.2 mA cm^{-2}, is obtained for the thinnest diode using broad band excitation at air mass 1.5 (AM1.5), shown in Figure 2b. Considering that in a bilayer OSC only excitations generated within a 5–10 nm exciton diffusion range to the bilayer contribute to the photocurrent, this is a remarkably high value. The short circuit current decreases slightly when the thickness L_p of the polymer layer increases, approaching a value of

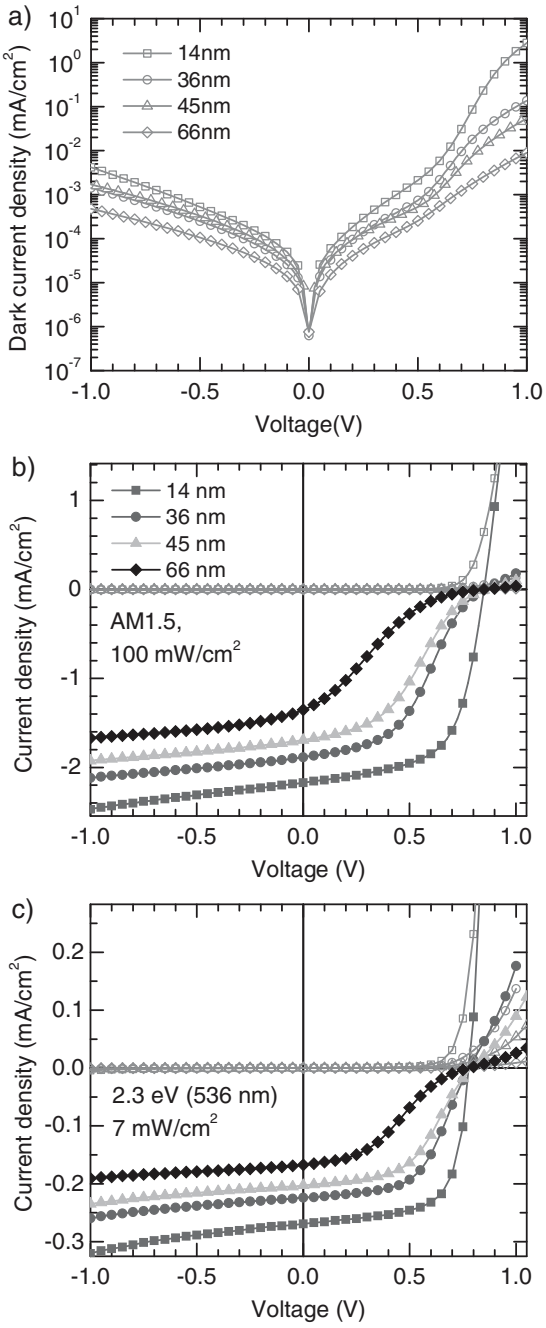

Figure 2. Current–voltage characteristics for different polymer layer thicknesses, i.e., 14 nm (squares), 36 nm (circles), 45 nm (triangles), 66 nm (diamonds), measured a) in the dark, b) under broadband excitation at AM1.5, and c) under monochromatic excitation at 536 nm (2.3 eV) at 7 mW cm^{-2}. The filled symbols show the total current under illumination and the open symbols the dark current for each polymer layer thickness.

1.5 mA cm^{-2} for the diode with L_p = 66 nm. More importantly, with increasing thickness of the donor layer the *JV*-curves acquire an s-shape character. Since the only variable parameter of the diodes is the thickness of the donor layer it appears straightforward to associate the evolution of the s-shape character of the *JV*-curves upon increasing L_p with charge carrier

recombination rather than with injection or extraction barriers.[28] These experimental results at AM1.5 are consistent with reports by Yu et al. for PHJ cells made with SubPc and C_{60}, for donor thicknesses from 10 to 40 nm,[24] and with reports by Petersen et al., for PHJ cells using a merocyanine dye as donor and C_{60} as acceptor.[17] It seems that this recombination effect depends on hole mobility since the s-shape of the *JV*-curve is lost when the $PCDTBT_{stat}$ is replaced by the p-$DTS(FBTTh_2)_2$ that has an almost 100 times higher hole mobility (Figure 1d). A similar thickness-dependence of the s-shape also appears upon monochromatic excitation of 7 mW cm^{-2} of predominantly the donor at the maximum of its first absorption band (536 nm, about 2.3 eV), though it sets in at higher voltages. Similar results are obtained for excitation at 580 nm (2.1 eV, see Figure S2 in the Supporting Information). Since the C_{60} still absorbs weakly at 2.3 eV, yet it does not absorb at 2.1 eV (see Figure 1), all subsequent monochromatic measurements were carried out at 2.1 eV. The radiant flux of 2.1 eV photons impinging on the sample is 6.7 mW cm^{-2}.

A straightforward way to check whether or not the evolution of the s-shape $PCDTBT_{stat}/C_{60}$ diodes is indeed caused by charge carrier recombination is to measure the dependence of the photocurrent as a function of light intensity. **Figure 3**a shows that the short circuit photocurrents, measured at a photon energy of 2.1 eV (580 nm), are perfectly linear with incident light intensity up to 30 mW cm^{-2} and even up to 100 mW cm^{-2} broadband

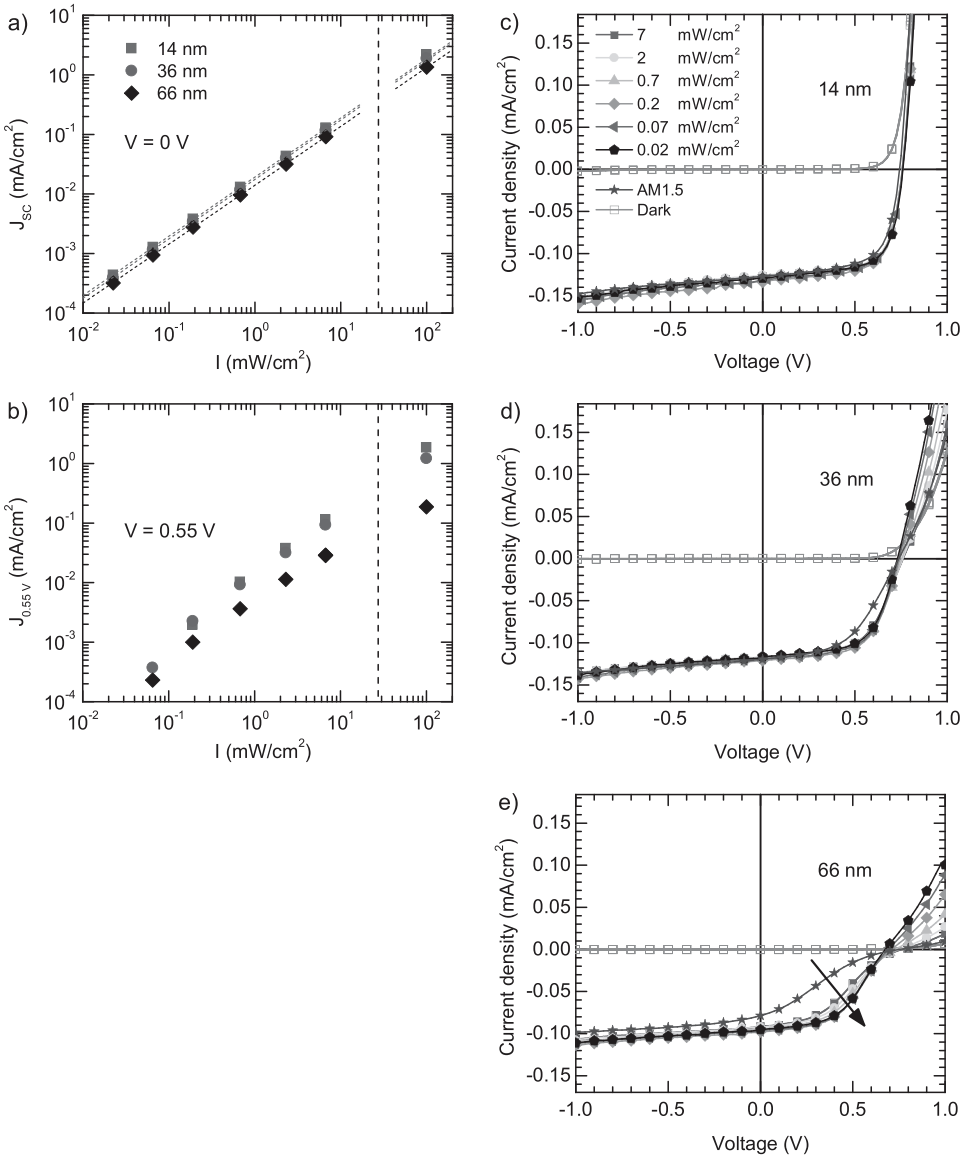

Figure 3. The total current as a function of illumination intensity, measured a) under short-circuit conditions ($V = 0$ V) and b) at $V = 0.55$ V. Values up to 30 mW cm^{-2} are for monochromatic illumination at 580 nm (2.1 eV), and values at 100 mW cm^{-2} are for broadband excitation at AM1.5. The dotted lines indicate a linear fit of the data points below 30 mW cm^{-2}. For a c) 14 nm, d) 36 nm, and e) 66 nm thick polymer layer current–voltage characteristics are shown for different light intensities at 580 nm and AM1.5 illumination. The *JV*-characteristics are normalized as described in the text.

Adv. Funct. Mater. **2016**,
DOI: 10.1002/adfm.201604906

excitation (AM1.5), suggesting that virtually no carriers are lost by bimolecular recombination. In contrast, when measuring the photocurrent closer to the open-circuit voltage, e.g., at 0.55 V (Figure 3b), we observe a deviation from linearity that implies that bimolecular processes are now dominant.

We can use the observed linear dependence of j_{SC} to normalize our *JV*-curves to j_{SC}, such as to compare their shapes. In Figure 3c–e, we thus assess how the light intensity affects the photocurrents as a function of voltage for different film thicknesses. Usually, comparing the *JV*-curves of solar cells under different high intensity illuminations is straightforward since in each case the dark current characteristic is negligible. A negligible contribution of the dark current is also tacitly assumed when calculating the fill factor, usually defined as the product of current and voltage at the maximum power point divided by the product of short-circuit current and open-circuit voltage.[1] However, this assumption is no longer valid when the light intensity decreases by up to three orders of magnitude because the dark current stays constant while the photocurrent decreases until the photocurrent eventually becomes comparable or even smaller than the dark current. In order to avoid any artifacts associated with the dark current we subtracted the dark current from the total current, thus obtaining the photocurrent. This photocurrent was then normalized to the light intensity I_0 = 6.7 mW cm^{-2} and the dark current was added again. Thus, the normalized current is given by

$$j_{\text{normalized}}(\text{V}) = \left[j_{\text{photo}}(V) \cdot \frac{I_0}{I} \right] + j_{\text{dark}} \quad (1)$$

where j_{photo} is the photocurrent obtained under illumination with intensity I, j_{dark} is the dark current, and I_0 is our reference intensity I_0 = 6.7 mW cm^{-2}. Note that if instead we had normalized the *JV*-curves of the total current, we would also have implicitly multiplied the dark current by the normalization factor $\frac{I_0}{I}$, thus introducing an artefact, and this is avoided by subtracting the dark current prior to the normalization and then adding it again afterwards.

Figure 3c–e compares the *JV*-curves obtained for different light intensities, normalized as just described to illumination with I_0 = 6.7 mW cm^{-2}, for different film thicknesses. We focus on the voltage range between V = 0 V and $V = V_{OC}$. It is evident that, as V approaches V_{OC}, the *JV*-characteristics become more intensity dependent as the donor thickness increases. For diodes with 14 nm, the *JV*-curve normalized to light intensity are indistinguishable, indicating that bimolecular effects cannot be important. For L_p = 36 nm diodes, some deviation is seen upon increasing the intensity (Figure 3d) and, for L_p = 66 nm, an s-shape develops (Figure 3e). The effect is more pronounced when the data measured under AM1.5 illumination are included. Figure 3 confirms that in the thicker diode bimolecular recombination becomes a loss process for photocarriers while this is not the case in the thinnest diode.

From Figure 3, we can read out the fill factor as a function of light intensity, shown in **Figure 4**. We find that for the L_p = 14 nm diode, the FF remains constant at about 67% as the illumination intensity changes by four orders of magnitude. For the L_p = 36 nm diode, the FF decreases from 61% to 50%

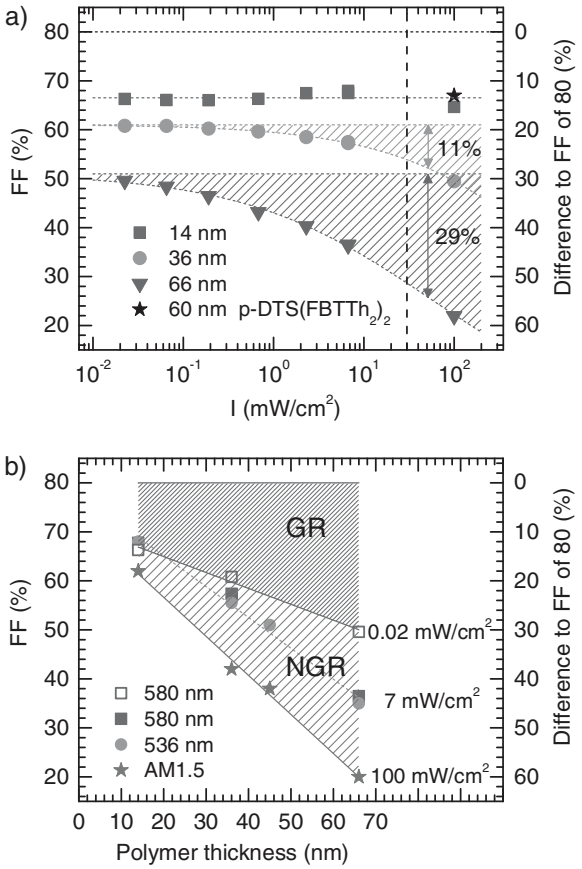

Figure 4. a) Fill factor for a polymer thickness of 14, 36, and 66 nm for different light intensities at an excitation wavelength of 580 nm. Dotted lines serve as guide to the eye. The fill factor obtained with AM1.5 illumination is also shown (on the right side of the dashed vertical line). The FF was calculated using the *JV*-curves shown in Figure 3. The fill factor for an identical bilayer cell made with 60 nm of the oligomer p-DTS(FBTTh$_2$)$_2$ is also shown (black star). On the right axis, the difference to an assumed ideal fill factor of 80% is indicated. The colored horizontal lines indicate the asymptotic value of the data at each thickness for infinitely low illumination, obtained by extrapolation of a fit to the data. The difference between the horizontal lines and 80% is attributed to losses due to geminate recombination, and the difference between the horizontal lines and the data points (shaded area) is attributed to losses by nongeminate recombination. The vertical arrows and associated numbers indicate the NGR losses at AM1.5 (the arrows are slightly offset from 100 mW cm^{-2} for clarity of display). b) Fill factors for different light intensities as a function of polymer layer thickness. The difference in FF between the data obtained at 0.02 mW cm^{-2} to 80% (densely shaded area) is attributed to losses by geminate recombination, and the difference between the data at 0.02 mW cm^{-2} and the data obtained at higher intensities such as 100 mW cm^{-2} is attributed to nongeminate recombination.

while in the 66 nm diode FF drops from 51% to 22% under AM1.5 (Figure 4a). For reference, we also include the FF of the 60 nm p-DTS(FBTTh$_2$)$_2$/C$_{60}$ diode, which is 67%, i.e., the same as in the 14 nm PCDTBT$_{stat}$/C$_{60}$ diode at any intensity.

Figure 4a allows to differentiate between the contributions of geminate and nongeminate recombination to the overall reduction in fill factor. Let us assume that, for an ideal cell in the Shockley–Queisser limit, the maximum obtainable fill factor is

80%, in agreement with simulations of Bartesaghi et al.[5] The difference to the FF actually observed in the limit of the lowest illumination intensity can be assigned to predominantly geminate recombination. In Figure 4a, this value is indicated by a dashed line for each film thickness. The difference to this value that arises with increasing illumination intensity, however, can be attributed to nongeminate recombination losses, indicated by the shaded areas in Figure 4a. Evidently, the FF is reduced by predominantly GR for the thinnest donor layer, while the losses due to GR and NGR are equal at AM1.5 for the thickest layer investigated.

How the fill factor decreases with the thickness of the donor layer is illustrated in Figure 4b. The contributions from GR and from NGR are indicated by the red and green areas. While the FF value for the thin sample is, within the experimental error, independent of intensity, with increasing film thickness a slopes arises not only for broadband illumination at AM1.5 but also for monochromatic illumination at 0.02 mW cm^{-2}, suggesting a thickness dependence of geminate recombination.

For the subsequent analysis it is useful to convert the *JV*-plots into plots of the photocurrent as a function of the internal electric field. We calculated the internal field F according to $F = (V_{build\text{-}in} - V)/(L_p + L_{C60})$, where L_p and L_{C60}, are the thicknesses of the polymer donor layer and the C_{60} layer, V is the voltage applied to the diode and $V_{build\text{-}in}$ is the voltage at which the photocurrent equals zero. In **Figure 5**a, we compare the field dependence of the photocurrents for different thicknesses of the donor layer taken under low light intensity and under AM1.5. The arrows indicate the field strengths corresponding to the short-circuit conditions for the OSCs with L_p = 14 nm and L_p = 66 nm, i.e., corresponding to V = 0 V. While the photocurrent is independent of electric field and illumination intensities for high internal fields, (V < 0 V), there is a strong field dependence of the photocurrent for low internal fields, even at very low illumination intensity, which reflects the field dependence of the dissociation of eh-pairs at the interface.[18] For reference, an internal field of 10^4 V cm^{-1} translates into a difference of less than 0.1 V to $V_{build\text{-}in}$.

This field dependence increases with light intensity and with increasing thickness of the polymer donor layer. The difference between the field dependent photocurrent for low and for high intensity, normalized to the current at AM1.5, is displayed in Figure 5b, from which the strong thickness dependence is particularly evident. Essentially, in Figure 5b, the current is corrected for the field dependence due to the geminate recombination, so that the data reflect the strong field and thickness dependence of the nongeminate recombination pathway. This difference between the photocurrent at high and low illumination intensities vanishes above saturation field F_{sat} of the photocurrent. This is the field at which all primarily generated eh-pairs are dissociated and are extracted by the electrodes. For $F < F_{sat}$ an increasing fraction of eh-pairs execute a diffusive motion inside the coulombic capture sphere. They are thus able to return to their siblings. As their concentration increases due to more intense illumination, they find recombination partners that are not their siblings. Figure 5b shows that this nongeminate recombination is particularly field dependent for thick donor layers.

To further probe the effect of film thickness on the dissociation of CT states, we carried out Monte Carlo simulations. In

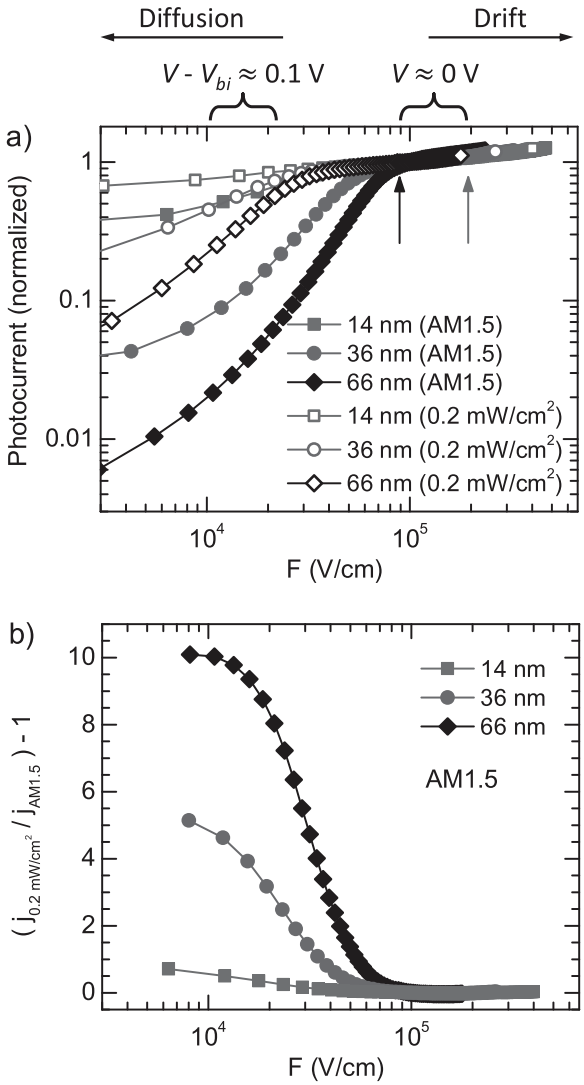

Figure 5. a) Photocurrent as a function of internal field $F = (V_{build\text{-}in} - V)/(L_p + L_{C60})$ for different polymer layer thicknesses, i.e., 14 nm (squares), 36 nm (circles), 45 nm (triangles), 66 nm (diamonds), taken under 580 nm illumination with an intensity of 0.2 mW cm^{-2} (open symbols) and under AM1.5 illumination (filled symbols). The field is calculated using $V_{build\text{-}in}$ = 0.85 V for all thicknesses at AM1.5 and $V_{build\text{-}in}$ = 0.76, 0,74, and 0.71 V for L_p = 14, 36, and 66 nm for 580 nm excitation, respectively. The arrows indicate the field strengths corresponding to the internal field under short-circuit conditions for the OSCs with L_p = 14 nm (right arrow) and L_p = 66 nm (left arrow). b) Difference between photocurrent at 0.2 mW cm^{-2} and at AM1.5, normalized to the photocurrent at AM1.5, $(j_{0.2} - j_{AM1.5})/j_{AM1.5}$, as a function of internal field for different film thicknesses.

order to simplify the simulation we considered a bilayer OSC composed of an array of point sites with variable thickness of the donor layer, assuming that the electron remains stationary in the acceptor layer. As detailed in the methodology, the quantum yield $\varphi(F)$ for electron–hole separation was calculated by averaging over 10^6 individual trials. In each trial, we created a single electron–hole pair at the interface. We kept the electron stationary while allowing the hole to execute a random walk in the potential created by the mutual Coulomb attraction

Adv. Funct. Mater. **2016**,
DOI: 10.1002/adfm.201604906

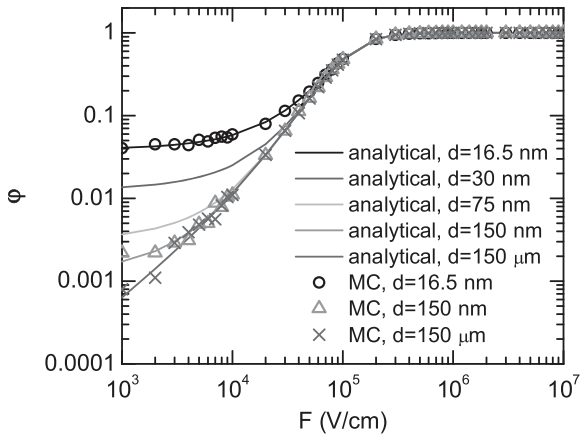

Figure 6. The probability of electron–hole separation as a function of internal field derived by Monte Carlo simulation (symbols) and derived by an analytical model (lines) for different thicknesses L_p of the polymer layer as described in the text.

and the applied field. The trial was over when the hole reached either the collecting electrode or when it recombined with the electron. In this simulation, only monomolecular recombination is taken into account since only one electron–hole pair is considered for each trial. In addition to the MC simulations, we have also used an analytical expression to calculate the field dependent separation efficiency as developed by Rubel et al.[44] (see Section 5) which is in perfect agreement with the MC simulation. Compared to the experiment displayed in Figure 5, **Figure 6** shows that the simulations predict a qualitatively similar shape of the dissociation yield as a function of field and, moreover, a similar evolution with film thickness as observed experimentally. The simulations do, however, predict a larger saturation field than found in experiment because in the simulation we ignored the effect that a low effective mass of the conjugated polymer has on the dissociation yield.[45] However, this does not alter the conclusions regarding the thickness dependence of recombination at low fields. In Figure 6 we see that the photocurrent yield is enhanced when the thickness of the donor transport layer is of the order of the Langevin capture radius (≈ 16 nm) and the yield reduces considerably with thicknesses up to ≈ 150 nm.

3. Discussion

Let us first summarize the essential experimental results. (i) In bilayer solar cells made with two different donors yet the same donor layer thickness of about 60 nm, a s-shape occurs for the donor with the lower hole mobility, yet not for the donor with the higher hole mobility, consistent with Tress et al.[27] (ii) The short circuit photocurrent in the bilayer diodes is linear with light intensity but when the applied voltage approaches V_{OC}, the *JV*-curves acquire s-shape character as the thickness of the donor layer increases (Figures 2 and 3). (iii) The fill factors increase and finally saturate at decreasing light intensity, and the saturation values decrease with increasing donor layer thickness (Figure 4). (iv) Losses in FF increase with increasing film thickness for both, geminate recombination and nongeminate recombination. (v) Above a critical electric field, F_{sat}, the photocurrent is saturated. For $F < F_{sat}$, the photocurrent decreases. This effect is stronger (i.e., the slope dj/dF is steeper) with increasing donor layer thickness and with increasing light intensity (Figure 5). (vi) The Monte Carlo simulations carried out in a strictly monomolecular regime reproduce the field and thickness dependence of the photocurrent that is experimentally observed.

Based upon the present experimental results we shall critically examine the role of monomolecular, i.e., geminate, recombination and of bimolecular, nongeminate recombination in organic solar cells, in particular with a view to the thickness dependence of the *JV*-curves.

The basic idea to account for the thickness dependence of the *JV*-curves is to consider the balance between charge extraction at the electrode and recombination of the electron–hole pair.[17,24] We stress that this is a field-dependent process. Let us first attend to the regime of very low excitation density, represented in the Monte Carlo simulation (Figure 6) and in the *JV*-curves under monochromatic illumination as displayed in Figures 2 and 5. After generation of an electron–hole pair, its hole diffuses in the combined potential of the Coulomb attraction by the electron and the internal field. If it does not leave the Langevin capture radius before recombining with the electron, i.e., if it has not truly been separated from its sibling electron, this is termed primary geminate recombination according to the IUPAC goldbook definition.[46] The Coulomb capture radius, i.e., the Langevin radius, is given by $r_{Coul} = \frac{e^2}{4\pi\epsilon\, k_B T}$, and it is about 16 nm for a material with dielectric constant of 3.5. We note that due to energetic disorder and charge delocalization this is not a well-defined, sharp boundary but rather a blurred out range. Primary geminate recombination does not play a role in the thickness dependence of the photocurrent yield, as in our case the polymer donor layer was always equal or larger than the Langevin capture radius. However, in particular at low internal fields, i.e., close to V_{OC}, it is also possible for the hole to separate from the electron by diffusing out of the Langevin capture radius, yet to enter it again at a later stage in its diffusive motion such as to return to its sibling electron. In chemical kinetics, recombination with the initial sibling countercharge after separation is known as secondary geminate recombination.[46]

Clearly, the rate of secondary geminate recombination depends on the thickness of the polymer donor layer. The thinner the polymer layer, the more likely it is that the hole in its diffusive motion meets the extracting electrode rather than returning to the electron. This is particularly true close to V_{OC}, i.e., in the low field regime, where the diffusive regime is prominent. The overall efficiency of geminate recombination is then controlled by the competition between a thickness-dependent charge extraction rate and a recombination rate that is independent of thickness. This is analogous to the well-known competition between NGR and extraction of free charges.[5] We therefore conclude that geminate recombination reduces the photocurrent close to V_{OC}, i.e., for low internal fields (Figure 5a), with this process being particularly important for thicker polymer donor layers. Geminate recombination thus is

also responsible for a reduction in fill factor (Figure 4a) under low light intensities, i.e., in the monomolecular regime.

We shall now discuss the evolution of the shape of the *JV*-curves as well the fill factor at higher light intensities. In addition to the monomolecular, geminate recombination processes, bimolecular processes can occur. The obvious process is nongeminate recombination from charges that, after photoexcitation, diffused out of their Langevin radius and return diffusively to the interface such as to recombine with another opposite charge there. The probability for this process increases with both light intensity and thickness of the donor layer. It will also become more probably for lower fields that enable diffusive return toward the interfacial layer. A further process that is possible is that one geminately bound pair can recombine with another geminately bound pair. While such a recombination of still primarily bound geminate pairs will also depend on intensity and field, it will not depend on film thickness. The ratio in the field dependence of the photocurrent for low and high intensity is displayed in Figure 5b. The stronger sensitivity to field for thick donor layers as compared to thinner donor layers thus directly reflects the increase in nongeminate recombination compared to the geminate recombination channel. For fields exceeding the saturation field, there is no thickness dependence since the charges are free, so that there is neither geminate nor nongeminate recombination.

So far, we have analyzed the *JV*-curve in the framework of considering geminate and nongeminate recombination. The appearance of an s-shape can, however, also be related to other factors. In particular, barriers to charge extraction or injection, as well as low or unbalanced carrier mobilities have been identified as causes for low fill factors and s-shaped *JV*-curves.[27,28,47,48] In our studies, the only parameter that has been varied was the thickness of the donor layer. The appearance of an s-shaped kink can therefore not be attributed to energy barriers or mobilities, as none of these change with film thickness.

Tress et al. further highlighted the role of low mobility and of imbalanced carrier mobility in reducing the fill factor of organic solar cells. Based on drift-diffusion simulations, Tress concludes that low carrier mobilities as well as imbalanced carrier mobilities lead to a high carrier density at the donor–acceptor interface, thus promoting recombination.[27] The key point of his argument is thus based on considering the carrier density. An increased recombination due to charge accumulation at the interface is also brought forward by Yu et al. to account for the appearance of an s-shape with donor layer thickness in SubPc/C_{70} based PHJ cells.[24] Consistent with their reasoning, we also find that an increased excitation density enhances recombination by adding the NGR channel. However, our key argument goes beyond this and also applies in the limit of vanishing carrier density. Charge accumulation at the interface is not required to reduce the fill factor. This is important as it implies that the carrier density does not need to be high or even in the range of the capacitor charge for the FF to be reduced by recombination losses.[7]

Clearly, the rate of carrier extraction, which prevents recombination, increases with mobility, even in the limit of considering a single electron–hole pair prone to geminate recombination. In the diffusive regime near V_{OC}, the diffusion range L_p depends on the diffusivity D by $L_p = \sqrt{D\tau}$, with τ being the carrier lifetime. Diffusivity is directly proportional to the carrier mobility by the Einstein relation $eD = \mu kT$. The probability of a hole to diffuse to the collecting electrode rather than to return to its sibling electron, i.e., the extraction rate, therefore increases with mobility. In this way, increasing mobility increases the photocurrent yield near V_{OC} and improves the fill factor even in the regime of low illumination intensity and in the limit of vanishing carrier density. This microscopic picture accounts for the observation by Proctor et al.,[31] that changes in morphology reduce both losses due to GR and NGR.

In a similar way, increasing the delocalization of charges should, and in fact does, also improve the extraction rate.[45,49–51] One factor that contributes to this is that excited states or charges that are well delocalized, i.e., with an extended wavefunction, can diffuse further in a disordered environment than localized charges due to geometric reasons.[52] A second, and perhaps more important factor relates to the fact that the binding energy of the eh-pair is reduced by an additional energy term when the eh-pair is more delocalized. In the case of on-chain wavefunction delocalization of a hole along a polymer chain, this additional energy arises from the zero-point oscillation of the delocalized hole in the pair potential. Mathematically, it can be expressed via a reduced effective mass of the hole, that can be as low as 0.1 times the electron mass for planarized or well-ordered polymers.[45,53] A similar effect can arise for crystalline assemblies of donor or acceptor molecules. An additional 200 meV of electrostatic energy has, for example, been reported by Gélinas et al. due to electron delocalization in ordered regions of the fullerene acceptor material.[50]

4. Conclusions

The stimulant for this work was that we wondered why in a thin bilayer OSC the fill factor can be as high as about 70% but decreases with increasing thickness of the polymeric donor layer (L_p). To this end we measured the *JV*-characteristics of bilayer diodes composed of $PCDTBT_{stat}$ donor layers with thicknesses ranging from 14 nm and 66 nm and a 30 nm thick C_{60} acceptor layer and light intensities ranging from 0.02 to 100 mW cm^{-2}. We find that at low light intensities the diode characteristics is strictly linear in intensity but the fill factor decreases from 67% to 50% when the thickness of the donor layer L_p increases from 14 nm to 66 nm. Supported by Monte Carlo simulations we argue that this decrease of FF is a signature of GR of holes that initially escaped from the Langevin capture sphere but can diffuse back toward the interface and can recombine with their siblings. The presence of an exit electrode prevents back diffusion. Therefore the trade-off between GR and charge extraction becomes thickness dependent up to a layer thickness of a multiple of the Langevin capture radius.

Since GR is ultimately limited by the nonradiative decay of the charge transfer states at the donor–acceptor interface, the efficiency of hole extraction should increase with hole diffusivity, i.e., hole mobility. Experiments with a diode in which the polymeric donor has been replaced by a 60 nm thick p-DTS$(FBTTh_2)_2$ layer that has an about 100 times higher hole mobility confirms this expectation. The FF of a 60 nm

Adv. Funct. Mater. **2016**,
DOI: 10.1002/adfm.201604906

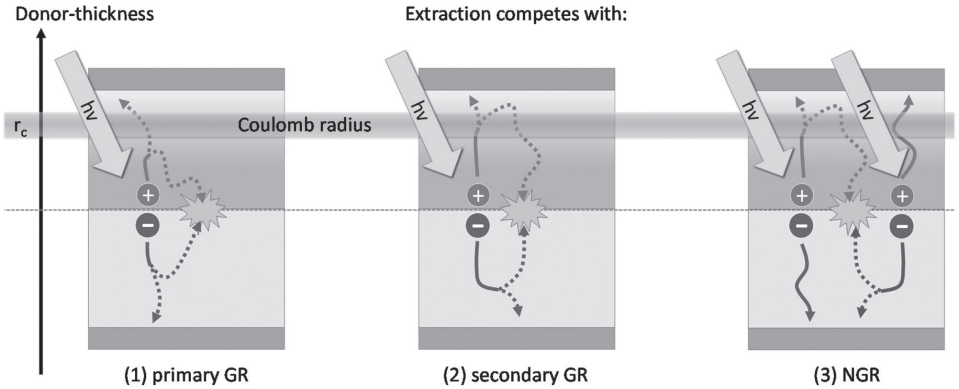

Figure 7. Schematic illustrating the competition between recombination at the donor–acceptor interface and extraction at the electrode for the monomolecular process of geminate recombination and for the bimolecular process of nongeminate recombination. r_c denotes the Coulomb capture radius (Langevin radius).

OSC with p-DTS(FBTTh$_2$)$_2$ at AM1.5 has a higher value than the FF of a PCDTBT$_{stat}$ OSC with same thickness at 0.02 mW cm^{-2}. Hence, the total losses of the p-DTS(FBTTh$_2$)$_2$ cell, i.e., GR and NGR, must be lower than the GR of the PCDTBT$_{stat}$ OSC (Figure 4). Thus, our results show that the limitation to the FF that is imposed by GR can be overcome by increasing the charge mobility. However, we stress that this effect is diffusion controlled, and consequently mobility controlled rather than controlled by interfacial charging, as is the case of NGR.[24]

As the light intensity increases and finally approaches AM1.5 the *JV*-curves acquire an s-shape that becomes more pronounced as the layer thickness increases. This is a signature of the onset of bimolecular, i.e., nongeminate recombination, at the donor–acceptor interface. As is well known, ultimately the diode efficiency is controlled by the trade-off between – the thickness dependent – extraction and NGR. The effect of NGR depends strongly on the internal electric field and film thickness (Figure 5b) due to interfacial charging.[24] Since the primary dissociation of charge transfer states at the interface is a field-assisted process, at lower electric field more eh-pairs exist near the donor–acceptor interface, so that a back-diffusing charge can easily find a recombination partner other than their siblings.

The overall picture is summarized in **Figure 7**. At low light intensity, a hole executing a random walk within the Coulomb capture radius of its electron may recombine with its sibling prior to any escape (primary GR). If it diffuses out of the Coulomb capture radius, it may be extracted at the electrode or it may diffuse back into the Coulomb capture radius such as to recombine with its sibling (secondary GR). Both processes are monomolecular. At high intensity, NGR will occur as additional, bimolecular process, as described above. In the framework of this microscopic picture it becomes evident why any process that improves charge carrier mobility, e.g., increasing the degree of (short-range) order in a film by processing, reduces not only losses due to NGR but also losses due to GR through enhancing the extraction rate.[31]

Our results show that simple *JV*-experiments of bilayer OSCs with variable layer thickness and variable light intensity provide a simple tool to quantify the effect of GR and NGR because the origins of recombination – be it geminate or nongeminate – and charge extraction are spatially separated.

5. Experimental Section

The compound p-DTS(FBTTh$_2$)$_2$ was synthesized as described by van der Poll et al.[35]

Synthesis of the Polymer PCDTBT$_{0.7}$/TPDDTBT$_{0.3}$ (PCDTBT$_{stat}$): PCDTBT$_{stat}$ (poly[(*N*-heptadecan-9′-yl)-2,7-carbazole-*alt*-5,5-(4′,7′-bis-(4-hexylthien-2-yl)-2′,1′,3′-benzothiadiazole)]$_{0.7}$-*stat*-[*N*,*N*′-bis(4-methylphenyl)-*N*,*N*′-diphenylbenzidine-*alt*-5,5-(4′,7″-bis-(4-hexylthien-2-yl)-2′,1′,3′-benzothiadiazole)]$_{0.3}$) was synthesized via Suzuki coupling according to the following procedure. The molar ratio of the carbazole, the phenyl-substituted benzidine, and the bisthienyl-benzothiadiazole units in PCDTBT$_{stat}$ was 0.7:0.3:1.

A Schlenk flask was charged with the monomers 2,7-bis-(4′,4′,5′,5′-tetramethyl-1′,3′,2′-dioxaborolan-2′-yl)-*N*-(heptadecan-9″-yl)-carbazole (0.368 g, 0.560 mmol), *N*,*N*′-bis(4-methylphenyl)-*N*,*N*′-bis((4′,4′,5′,5′-tetramethyl-1′,3′,2′-dioxaborolan-2′-yl)phenyl)-benzidine (0.184 g, 0.239 mmol), 4,7-bis(5′-bromo-4′-hexylthien-2′-yl)-2,1,3-benzothiadiazole (0.501 g, 0.800 mmol) and 12 mL of toluene under argon. One drop of Aliquat 336 and 20 mL of 2 M Na_2CO_3 solution were added and the mixture was degassed by three freeze–thaw cycles. Afterward 14 mg of tetrakis(triphenylphosphine)palladium(0) were added and followed by again three freeze–thaw cycles. The reaction mixture was then stirred under reflux in an argon atmosphere for 90 h before bromobenzene (0.126 g, 0.800 mmol) was added. After 2 h phenylboronic acid (0.098 g, 0.800 mmol) was added and the reaction mixture was again refluxed overnight. The reaction mixture was allowed to cool to room temperature and the polymer was precipitated into methanol/water (10:1). Soxhlet extraction was carried out using acetone and toluene. The reduced toluene fraction was precipitated into methanol/water (10:1) and dried in vacuum overnight, yielding 0.669 g (93%) of PCDTBT$_{stat}$ as a dark-red powder. A molecular weight of 47 000 gmol^{-1} (M_w) and 18 000 gmol^{-1} (M_n) was determined by size exclusion chromatography in THF solution with a polydispersity index of 2.56 (polystyrene calibration). The ionization potential was determined by photoelectron spectroscopy to be –5.2 eV. Adding the photon energy at maximum of the first absorption band yields –2.9 eV as a rough estimate for the ionization potential.

^{1}H NMR (300 MHz, $C_2D_2Cl_4$, 120 °C): δ = 0.75–0.95 (m, CH_3), 1.05–1.55 (m, CH_2), 1.75 (br, thiophene—CH_2), 2.04 (br, carbazole—CH_2), 2.23–2.44 (m, benzidine—CH_3, carbazole—CH_2), 2.63–2.95 (m, thiophene—CH_2), 4.62 (br, CH), 6.92–8.22 (m, ar—CH). Broadened and multiple signals were due to atropisomerism. From the integration of the signal for the CH_2 group in the swallow-tail spacer of the carbazole unit (2.04 ppm), the combined signal for the methyl group in the benzidine units and the other CH_2 group in the carbazole spacer (2.23–2.44 ppm), and the signal for the CH_2 groups in the hexyl spacer of the thiophene (1.75 ppm), a molar ratio of 0.7:0.3:1 was calculated (for ^{1}H NMR spectrum see the Supporting Information).

Experiments: To fabricate the bilayer solar cells, ITO-coated substrates were covered with a patterned photoresist as described by Schwarz et al.[54] A 15 nm thick MoO_3 (Sigma Aldrich) layer was evaporated on top of it. The donor ($PCDTBT_{stat}$ or p-DTS$(FBTTh_2)_2$) was spun onto this from chlorobenzene solution (7.0 mg mL^{-1}). The thickness of the donor layer was controlled with a Dektak (Veeco) profilometer. The donor was covered by subsequent thermal evaporation of a 30 nm thick C_{60} layer and a 100 nm thick aluminium cathode. The devices were annealed at 140 °C for 15 min. The complete solar cell fabrication was done in a nitrogen atmosphere using a glovebox with direct access to the evaporation chamber. In Figure S1 in the Supporting Information, additional measurements were also carried out on samples where (i) the annealing step was omitted, or (ii) annealing was omitted and a 5 nm thick BCP layer was evaporated between C_{60} and aluminum, or (iii) annealing was carried out for 15 min after C_{60} evaporation, prior to deposition of a 5 nm thick BCP layer and aluminum. Since it turned out that the shape of the *JV*-curves is in dependent on the diode preparation the authors used annealed samples with the structure ITO/MoO_3/donor/C_{60}/Al since these feature particularly low dark current.

The current–voltage characteristics were measured in vacuum at room temperature under either broad band AM1.5 illumination employing a Newport sun simulator or under monochromatic illumination at 536 nm (2.3 eV) or 580 nm (2.1 eV), provided by a 450 W Xenon lamp (Osram) using a commercial monochromator. In the latter case the incident light intensity was varied by neutral optical density (OD) filters with optical densities of 0.5, 1.0, 1.5, 2.0, and 2.5. The light intensity impinging on the diode was measured using a Hamamatsu S1337-33BQ photodiode. Without OD filter, it was 7.1 mW cm^{-2} for 536 nm and 6.7 mW cm^{-2} for 580 nm. The photocurrents were measured with a Keithley 236 and 238 source-measure-unit.

To determine the fill factor of the photodiode at variable light intensities, both the dark current $j_{dark}(V)$ as well as the total current $j(V)$ under illumination were measured. The difference is the photocurrent $j_{photo}(V) = j(V) - j_{dark}(V)$. At low light intensities, one needs to take account of the fact that the dark current is independent on intensity while the photocurrent decreases with decreasing intensity. The authors did this by normalizing the photocurrent to the monochromatic light intensity without optical density (OD) filter. To do this, the photocurrent is multiplied by the ratio of the light intensity of monochromatic light without and with OD filters, and the dark current is added subsequently

$$j_{normalized}(V) = \left[j_{photo}(V) \cdot \frac{I_0}{I} \right] + j_{dark} \tag{2}$$

When the photocurrent is displayed as a function of internal field, the field was determined according to $F = (V_{build\text{-}in} - V)/(L_p - L_{C60})$, with L_p being the layer of the polymer donor layer and L_{C60} being the thickness of the C_{60} acceptor layer (30 nm). The fields in the solar cells were calculated using $V_{build\text{-}in}$ which was approximated by the voltage at which the photocurrent equals zero.

MIS-CELIV measurements were performed according to the procedure described in literature.[55,56] For both materials the same parameters were used. The layer thickness of p-DTS$(FBTTh_2)_2$ was 100 nm and for $PCDTBT_{stat}$ 121 nm. A hole injection layer of 6 nm MoO_3 was used. The voltage was supplied by a Rigol DG4102 function generator. The slope of the voltage ramp, the offset voltage, and the length of the voltage pulse were fixed to 0.1 V μs^{-1}, 7 V, and 100 µs, respectively, for all measurements, to make sure that experimental conditions are identical for all compounds and samples. This ensures that observed trends and effects may be attributed to materials. The resulting current response signal was amplified using a Femto DHPCA-100 current amplifier and recorded with a Tektronix TDS3000 digital phosphor oscilloscope. In all the measurements the authors applied a prebias voltage of 7 V for one minute to ensure equilibrium conditions.

Monte Carlo Simulations: The authors performed Monte Carlo simulations to model the extraction efficiency in a bilayer device as a function of the electric field for different donor layer thicknesses. The system consisted of a 1D array of points with a separation distance a = 1.5 nm and an interface at origin. At t = 0 a hole and an electron were placed in an adjacent configuration at the interface with a minimal separation. The electron position was fixed while the hole was allowed to move between neighboring points with a hopping rate $\nu_{i,j}$ given by a Miller–Abrahams expression

$$\nu_{i,j} = \begin{cases} \nu_0 e^{-2\alpha r_{ij}} e^{-\left(\frac{\varepsilon_j - \varepsilon_i}{k_B T}\right)}, & \varepsilon_j > \varepsilon_i \\ \nu_0 e^{-2\alpha r_{ij}}, & \varepsilon_j \le \varepsilon_i \end{cases} \tag{3}$$

where i is the hole residence site and j the target neighboring site, separated by a distance r_{ij}. The site energies ε_i and ε_j include contributions from the Coulomb potential due to the presence of the electron at the interface and the voltage drop due to the externally applied field. The attempt-to-hop frequency was set to ν_0 = 10 ps^{-1}, the relative permittivity to ϵ_r = 4, and the inverse localization length to α = 2 nm^{-1}. At each Monte Carlo step the authors calculate a waiting time for each hopping event: $\tau_{ij} = -\frac{1}{\nu_{i,j}} \ln X$ and a waiting time for recombination between the electron–hole pair: $\tau_r = -\tau \ln X$, where τ is the electron–hole pair lifetime that increases exponentially with electron hole distance r_{eh} as $\tau = \tau_0 e^{2\alpha(r_{eh}-a)}$ and X is a random number from a box distribution between 0 and 1. The lifetime at close proximity is $\tau_0 = 1000 t_0$ with t_0 being the minimum hopping time $t_0 = \frac{1}{\nu_0} e^{2\alpha a}$.

The event with the smallest waiting time is is selected and executed. If the accepted event was a hop, then the authors updated the site of the hole and recalculated waiting times. If the chosen event was recombination, the authors removed the charges and started a new trial. Each trial terminated successfully when the electron–hole distance was larger than a given separation distance d, ranging from 16.5 nm to 150 µm. By averaging over 10^6 trials the authors calculated the quantum yield for separation as: $\varphi(F) = \frac{N_{sep}(F)}{N_{tot}(F)}$, where $N_{sep}(F)$ is the number of successful trials for an applied field F and $N_{tot}(F)$ the total number of trials.

The authors also used an analytical expression to calculate the field dependent separation efficiency $\varphi(F)$ as developed by Rubel et al.[44] This is derived from a rate equation model and reads

$$\varphi(F) = 1 - \frac{\sum_{i=1}^{n-1} \nu_{i,i+1}^{-1} e^{\left(\frac{\varepsilon_i - \varepsilon_1}{k_B T}\right)}}{\tau_0 + \sum_{i=1}^{n-1} \nu_{i,i+1}^{-1} e^{\left(\frac{\varepsilon_i - \varepsilon_1}{k_B T}\right)}} \tag{4}$$

where ε_1 is the energy of the initially placed hole site at the interface right next to the electron and the index i runs from 1 to $n - 1$ with n being the site at distance d from the interface at which the authors considered that the hole was separated. The forward, with respect to the field direction, hopping rates $\nu_{i,i+1}$ were given by the Miller–Abrahams expression described above.

Supporting Information

Supporting Information is available from the Wiley Online Library or from the author.

Acknowledgements

The authors acknowledge financial support by the Bavarian State Ministry of Science, Research, and the Arts through the Collaborative Research Network "Solar Technologies go Hybrid", by the Volkswagen foundation and by the German Science Foundation DFG through the doctoral training center "GRK 1640." This project further received funding from the Universidad Carlos III de Madrid, the European Union's Seventh Framework Programme for research, technological development and demonstration under grant agreement no. 600371, el Ministerio de

Economía y Competitividad (COFUND2014-51509), el Ministerio de Educación, cultura y Deporte (CEI-15-17), and Banco Santander. M.R. additionally acknowledges support from the Hanns Seidel Foundation for a stipend through funds from the German Ministry of Education and Research (BMBF). T.-Q.N. thanks the Office of Naval Research (#N000141410076) for the support. Furthermore, the authors would like to thank the anonymous referees for helpful suggestions.

Received: September 21, 2016
Published online:

[1] A. Köhler, H. Bässler, *Electronic Processes in Organic Semiconductors: An Introduction*, Wiley-VCH, Weinheim, Germany, **2015**.
[2] P. Würfel, *Physics of Solar Cells*, Wiley-VCH, Weinheim, Germany, **2005**.
[3] N. C. Giebink, G. P. Wiederrecht, M. R. Wasielewski, S. R. Forrest, *Phys. Rev. B* **2011**, *83*, 195326.
[4] B. Liu, R. Q. Png, J. K. Tan, P. K. H. Ho, *Adv. Energy Mater.* **2014**, *4*, 1200972.
[5] D. Bartesaghi, I. D. Perez, J. Kniepert, S. Roland, M. Turbiez, D. Neher, L. J. A. Koster, *Nat. Commun.* **2015**, *6*, 7083.
[6] M. Stolterfoht, A. Armin, B. Philippa, R. D. White, P. L. Burn, P. Meredith, G. Juska, A. Pivrikas, *Sci. Rep.* **2015**, *5*, 9949.
[7] M. Stolterfoht, B. Philippa, S. Shoaee, H. Jin, W. Jiang, R. D. White, P. L. Burn, P. Meredith, A. Pivrikas, *J. Phys. Chem. C* **2015**, *119*, 26866.
[8] L. J. A. Koster, E. C. P. Smits, V. D. Mihailetchi, P. W. M. Blom, *Phys. Rev. B* **2005**, *72*, 085205.
[9] L. J. A. Koster, V. D. Mihailetchi, P. W. M. Blom, *Appl. Phys. Lett.* **2006**, *88*, 093511.
[10] P. W. M. Blom, V. D. Mihailetchi, L. J. A. Koster, D. E. Markov, *Adv. Mater.* **2007**, *19*, 1551.
[11] N. Christ, S. W. Kettlitz, S. Valouch, J. Mescher, M. Nintz, U. Lemmer, *Org. Electron* **2013**, *14*, 973.
[12] C. L. Braun, *J. Chem. Phys.* **1984**, *80*, 4157.
[13] V. D. Mihailetchi, L. J. A. Koster, J. C. Hummelen, P. W. M. Blom, *Phys. Rev. Lett.* **2004**, *93*, 216601.
[14] J. A. Barker, C. M. Ramsdale, N. C. Greenham, *Phys. Rev. B* **2003**, *67*, 075205.
[15] N. C. Giebink, B. E. Lassiter, G. P. Wiederrecht, M. R. Wasielewski, S. R. Forrest, *Phys. Rev. B* **2010**, *82*, 155306.
[16] A. Ojala, A. Petersen, A. Fuchs, R. Lovrincic, C. Polking, J. Trollmann, J. Hwang, C. Lennartz, H. Reichelt, H. W. Hoffken, A. Pucci, P. Erk, T. Kirchartz, F. Würthner, *Adv. Funct. Mater.* **2012**, *22*, 86.
[17] A. Petersen, A. Ojala, T. Kirchartz, T. A. Wagner, F. Würthner, U. Rau, *Phys. Rev. B* **2012**, *85*, 245208.
[18] R. A. Marsh, J. M. Hodgkiss, R. H. Friend, *Adv. Mater.* **2010**, *22*, 3672.
[19] S. Albrecht, W. Schindler, J. Kurpiers, J. Kniepert, J. C. Blakesley, I. Dumsch, S. Allard, K. Fostiropoulos, U. Scherf, D. Neher, *J. Phys. Chem. Lett.* **2012**, *3*, 640.
[20] D. Veldman, O. Ipek, S. C. J. Meskers, J. Sweelssen, M. M. Koetse, S. C. Veenstra, J. M. Kroon, S. S. van Bavel, J. Loos, R. A. J. Janssen, *J. Am. Chem. Soc.* **2008**, *130*, 7721.
[21] C. G. Shuttle, R. Hamilton, B. C. O'Regan, J. Nelson, J. R. Durrant, *Proc. Natl. Acad. Sci. USA* **2010**, *107*, 16448.
[22] T. M. Clarke, J. R. Durrant, *Chem. Rev.* **2010**, *110*, 6736.
[23] M. Gluecker, A. Foertig, V. Dyakonov, C. Deibel, *Phys. Status Solidi RRL* **2012**, *6*, 337.
[24] H. M. Yu, R. C. Yi, J. W. Zhang, A. R. Yu, H. Peng, J. J. Qin, X. Y. Hou, *J. Phys. D: Appl. Phys.* **2016**, *49*, 205105.
[25] D. Credgington, Y. Kim, J. Labram, T. D. Anthopoulos, J. R. Durrant, *J. Phys. Chem. Lett.* **2011**, *2*, 2759.
[26] R. Mauer, I. A. Howard, F. Laquai, *J. Phys. Chem. Lett.* **2010**, *1*, 3500.
[27] W. Tress, A. Petrich, M. Hummert, M. Hein, K. Leo, M. Riede, *Appl. Phys. Lett.* **2011**, *98*, 063301.
[28] W. Tress, A. Merten, M. Furno, M. Hein, K. Leo, M. Riede, *Adv. Energy Mater.* **2013**, *3*, 631.
[29] F. Etzold, I. A. Howard, R. Mauer, M. Meister, T. D. Kim, K. S. Lee, N. S. Baek, F. Laquai, *J. Am. Chem. Soc.* **2011**, *133*, 9469.
[30] A. Foertig, J. Kniepert, M. Gluecker, T. Brenner, V. Dyakonov, D. Neher, C. Deibel, *Adv. Funct. Mater.* **2014**, *24*, 1306.
[31] C. M. Proctor, S. Albrecht, M. Kuik, D. Neher, T. Q. Nguyen, *Adv. Energy Mater.* **2014**, *4*, 1400230.
[32] S. Albrecht, J. R. Tumbleston, S. Janietz, I. Dumsch, S. Allard, U. Scherf, H. Ade, D. Neher, *J. Phys. Chem. Lett.* **2014**, *5*, 1131.
[33] S. Albrecht, S. Janietz, W. Schindler, J. Frisch, J. Kurpiers, J. Kniepert, S. Inal, P. Pingel, K. Fostiropoulos, N. Koch, D. Neher, *J. Am. Chem. Soc.* **2012**, *134*, 14932.
[34] F. Gao, J. P. Wang, J. C. Blakesley, I. C. Hwang, Z. Li, N. C. Greenham, *Adv. Energy Mater.* **2012**, *2*, 956.
[35] T. S. van der Poll, J. A. Love, T. Q. Nguyen, G. C. Bazan, *Adv. Mater.* **2012**, *24*, 3646.
[36] M. A. Faist, T. Kirchartz, W. Gong, R. S. Ashraf, I. McCulloch, J. C. de Mello, N. J. Ekins-Daukes, D. D. C. Bradley, J. Nelson, *J. Am. Chem. Soc.* **2012**, *134*, 685.
[37] J. H. Seo, S. J. Kang, C. Y. Kim, S. W. Cho, K. H. Yoo, C. N. Whang, *Appl. Surf. Sci.* **2006**, *252*, 8015.
[38] J. Niederhausen, P. Amsalem, A. Wilke, R. Schlesinger, S. Winkler, A. Vollmer, J. P. Rabe, N. Koch, *Phys. Rev. B* **2012**, *86*, 081411.
[39] K. Akaike, K. Kanai, H. Yoshida, J. Tsutsumi, T. Nishi, N. Sato, Y. Ouchi, K. Seki, *J. Appl. Phys.* **2008**, *104*, 023710.
[40] Z. L. Guan, J. B. Kim, H. Wang, C. Jaye, D. A. Fischer, Y. L. Loo, A. Kahn, *Org. Electron* **2010**, *11*, 1779.
[41] B. P. Rand, J. G. Xue, S. Uchida, S. R. Forrest, *J. Appl. Phys.* **2005**, *98*, 124902.
[42] G. A. H. Wetzelaer, M. Kuik, M. Lenes, P. W. M. Blom, *Appl. Phys. Lett.* **2011**, *99*, 153506.
[43] P. de Bruyn, A. H. P. van Rest, G. A. H. Wetzelaer, D. M. de Leeuw, P. W. M. Blom, *Phys. Rev. Lett.* **2013**, *111*, 186801.
[44] O. Rubel, S. D. Baranovskii, W. Stolz, F. Gebhard, *Phys. Rev. Lett.* **2008**, *100*, 196602.
[45] C. Schwarz, S. Tscheuschner, J. Frisch, S. Winkler, N. Koch, H. Bässler, A. Köhler, *Phys. Rev. B* **2013**, *87*, 155205.
[46] K. J. Laidler, *Pure Appl. Chem.* **1996**, *68*, 149.
[47] J. Wagner, M. Gruber, A. Wilke, Y. Tanaka, K. Topczak, A. Steindamm, U. Hormann, A. Opitz, Y. Nakayama, H. Ishii, J. Pflaum, N. Koch, W. Brütting, *J. Appl. Phys.* **2012**, *111*, 054509.
[48] J. Nelson, J. Kirkpatrick, P. Ravirajan, *Phys. Rev. B* **2004**, *69*, 035337.
[49] S. Tscheuschner, H. Bässler, K. Huber, A. Köhler, *J. Phys. Chem. B* **2015**, *119*, 10359.
[50] S. Gelinas, A. Rao, A. Kumar, S. L. Smith, A. W. Chin, J. Clark, T. S. van der Poll, G. C. Bazan, R. H. Friend, *Science* **2014**, *343*, 512.
[51] A. A. Bakulin, A. Rao, V. G. Pavelyev, P. H. M. van Loosdrecht, M. S. Pshenichnikov, D. Niedzialek, J. Cornil, D. Beljonne, R. H. Friend, *Science* **2012**, *335*, 1340.
[52] S. Athanasopoulos, S. T. Hoffmann, H. Bässler, A. Köhler, D. Beljonne, *J. Phys. Chem. Lett.* **2013**, *4*, 1694.
[53] B. B. Y. Hsu, C. M. Cheng, C. Luo, S. N. Patel, C. Zhong, H. T. Sun, J. Sherman, B. H. Lee, L. Ying, M. Wang, G. C. Bazan, M. Chabinyc, J. L. Brédas, A. Heeger, *Adv. Mater.* **2015**, *27*, 7759.
[54] C. Schwarz, H. Bässler, I. Bauer, J. M. Koenen, E. Preis, U. Scherf, A. Köhler, *Adv. Mater.* **2012**, *24*, 922.
[55] G. Juska, N. Nekrasas, K. Genevicius, *J. Non-Cryst. Solids* **2012**, *358*, 748.
[56] A. Armin, G. Juska, M. Ullah, M. Velusamy, P. L. Burn, P. Meredith, A. Pivrikas, *Adv. Energy Mater.* **2014**, *4*, 1300954.

ADVANCED FUNCTIONAL MATERIALS

Supporting Information

for *Adv. Funct. Mater.*, DOI: 10.1002/adfm.201604906

Monomolecular and Bimolecular Recombination of Electron-Hole Pairs at the Interface of a Bilayer Organic Solar Cell

*Tobias Hahn, Steffen Tscheuschner, Frank-Julian Kahle, Markus Reichenberger, Stavros Athanasopoulos, Christina Saller, Guillermo C. Bazan, Thuc-Quyen Nguyen, Peter Strohriegl, Heinz Bässler, and Anna Köhler**

Supporting Information to:

Monomolecular and bimolecular recombination of electron-hole pairs at the interface of a bilayer organic solar cell

Tobias Hahn[1], Steffen Tscheuschner[1], Frank-Julian Kahle[1], Markus Reichenberger[1], Stavros Athanasopoulos[1,2], Christina Saller[3], Guillermo C. Bazan[4], Thuc-Quyen Nguyen[4], Peter Strohriegl[3,5], Heinz Bässler[5], Anna Köhler[1,5]*

[1] Experimental Physics II, University of Bayreuth, 95440 Bayreuth, Germany

[2] Departamento de Física, Universidad Carlos III de Madrid, Avenida Universidad 30, 28911 Leganés, Madrid, Spain

[3] Macromolecular Chemistry I, University of Bayreuth, 95440 Bayreuth, Germany

[4] Department of Chemistry and Biochemistry, Center for Polymers and Organic Solids, University of California, Santa Barbara, California 93106-9510, United States

[5] Bayreuth Institute of Macromolecular Science (BIMF), University of Bayreuth, 95440 Bayreuth, Germany

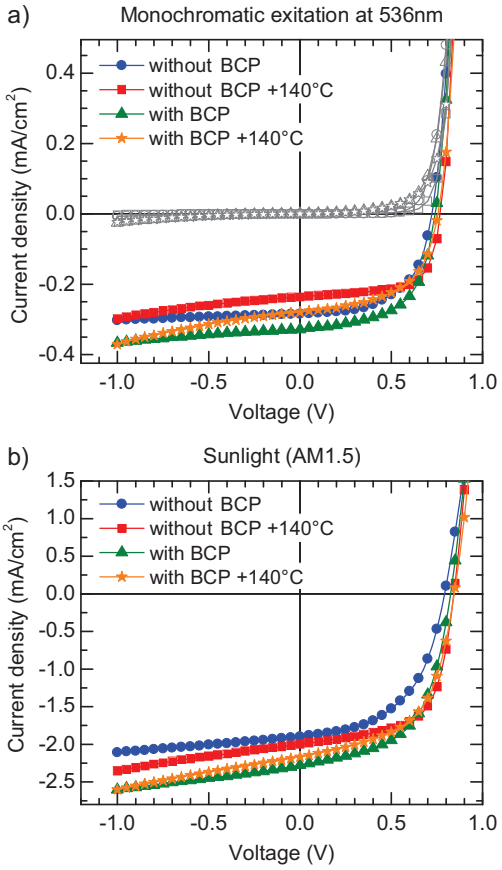

Figure S1: (a) Current-voltage characteristics of ITO/MoO_3/$PCDTBT_{stat}$/C_{60}/(BCP/)Al bilayer solar cells measured with or without BCP interlayer and with or without annealing step for monochromatic excitation at 536 nm. Open grey symbols indicate the associated dark current. (b) The same for AM1.5 sun light conditions.

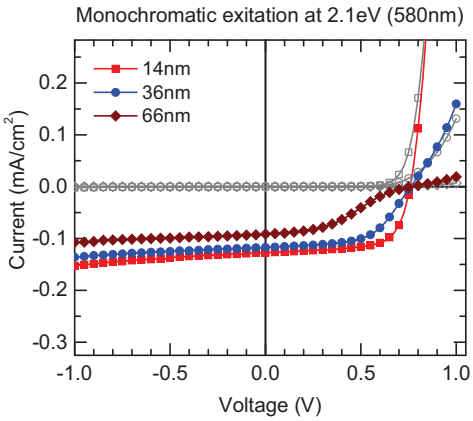

Figure S2: Current-voltage characteristics of ITO/MoO_3/$PCDTBT_{stat}$/C_{60}/Al bilayer solar cells for different film thicknesses taken for monochromatic excitation at 580 nm (2.1 eV).

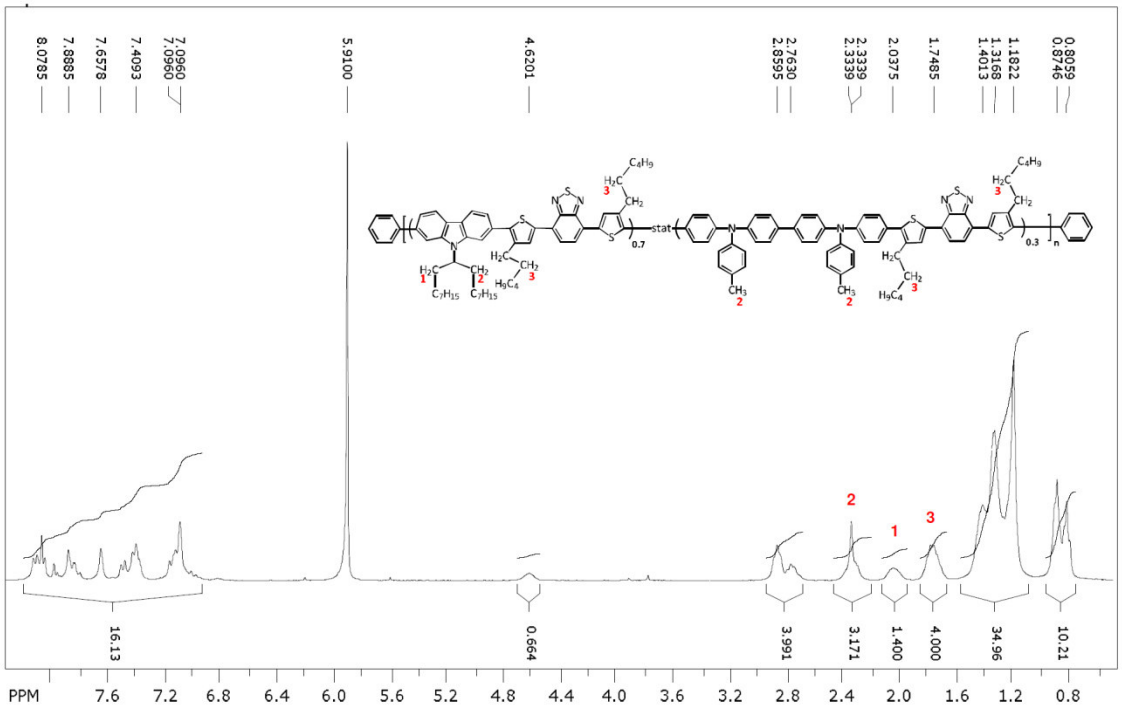

Figure S3: ^{1}H NMR spectrum of PCDTBT$_{0.7}$/TPDDTBT$_{0.3}$ (300 MHz) in $C_2D_2Cl_4$ at 120 °C. For the calculation of the molar ratio see Experimental Section.

4.2. Efficient Charge Separation in organic photovoltaics through incoherent hopping

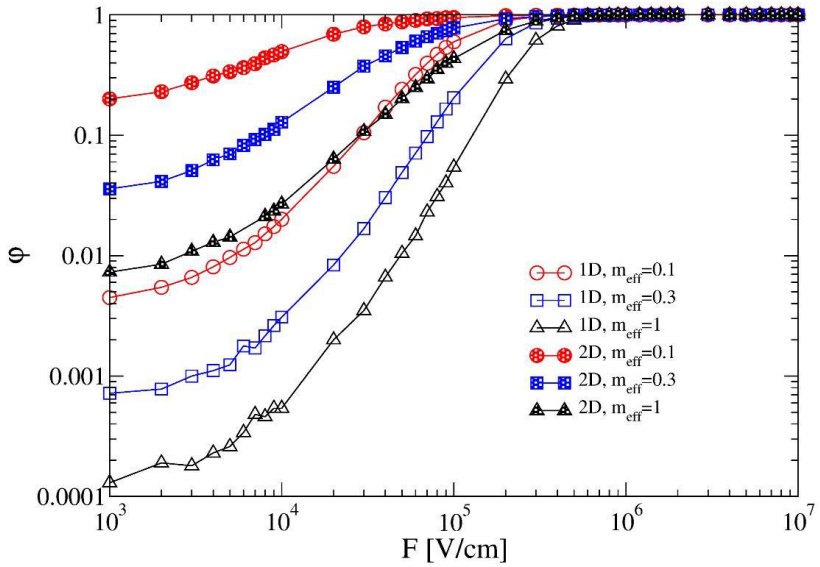

Stavros Athanasopoulos, Steffen Tscheuschner, Heinz Bässler, Anna Köhler

Veröffentlicht in

Journal of Physical Chemistry Letters (**2017**), 8, 2093-2098

(DOI: 10.1021/acs.jpclett.7b00595)

THE JOURNAL OF PHYSICAL CHEMISTRY Letters

Letter

pubs.acs.org/JPCL

Efficient Charge Separation of Cold Charge-Transfer States in Organic Solar Cells Through Incoherent Hopping

Stavros Athanasopoulos,*[,†] Steffen Tscheuschner,[‡] Heinz Bässler,[§] and Anna Köhler[‡,§]

[†]Departamento de Física, Universidad Carlos III de Madrid, Avenida Universidad 30, Leganés 28911, Madrid, Spain

[‡]Experimental Physics II and [§]Bayreuth Institute of Macromolecular Research (BIMF), University of Bayreuth, Bayreuth 95440, Germany

ABSTRACT: We demonstrate that efficient and nearly field-independent charge separation of electron−hole pairs in organic planar heterojunction solar cells can be described by an incoherent hopping mechanism. Using kinetic Monte Carlo simulations that include the effect of on-chain delocalization as well as entropic contributions, we simulate the dissociation of the charge-transfer state in polymer−fullerene bilayer solar cells. The model further explains experimental results of almost field independent charge separation in bilayers of molecular systems with fullerenes and provides important guidelines at the molecular level for maximizing the efficiencies of organic solar cells. Thus, utilizing coherent phenomena is not necessarily required for highly efficient charge separation in organic solar cells.

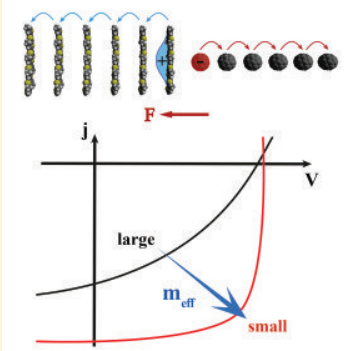

Charge separation in solar cells is a key process for extracting carriers that contribute to a photocurrent. While in traditional inorganic solar cells the available thermal energy provides enough kinetic energy in order to overcome the Coulomb interaction between geminate electron−hole pairs, in new-generation organic solar cells, separation of charges is a cumbersome process.[1−3] As a first step, it usually requires the presence of interfaces between an electron transporting and a hole transporting material that facilitates the transfer of the electron to the acceptor material by formation of a charge-transfer (CT) state,[4] provided that the exciton diffusion length is large enough to reach such interfaces.[5−7] Second, once the charges are in separate phases, they need to overcome their mutual Coulomb attraction, which is much larger than the thermal energy, due to the low dielectric constant of organic materials, which is in the range of 3−5.[8] This charge separation process can be assisted by an electric field, although in some materials the process occurs with high efficiency even at low electric fields. A great deal of attention has been drawn recently on the mechanism of charge separation, and a number of possible scenarios have been suggested to explain the large variability in dissociation efficiencies for chemically similar molecular systems.[9] These include dissociation via delocalized or hot states,[10−12] ultrafast separation via band-type states,[13,14] the presence of interfacial dipoles,[15−19] entropic contributions,[20−22] and coherence effects.[23−26] Thus, there is much interest in efficiently predicting under which conditions the efficiency of separation is maximized using computer experiments.

In organic solar cells, both geminate recombination, i.e., the recombination of electron−hole carriers that trace back to the same parent exciton, and nongeminate (bimolecular) recombination, i.e., recombination of electron−hole carriers from two different parent excitons, are important loss mechanisms that reduce the quantum efficiency of the device.[27] It has recently been demonstrated that geminate recombination in molecule-based solar cells can be controlled by thermal annealing and chemical treatment of spin coated devices with the amount of recombination being accessible experimentally by time-delayed collection field measurements (TDCF).[28] Recently, we have reported that the dissociation efficiency in bilayer films of molecule donor with a C_{60} acceptor layer can be very efficient, with the separation yield exceeding 70% at low electric fields.[29] Moreover, we have shown that recombination near the open circuit voltage (V_{OC}) increases with the donor layer thickness in polymer devices, and we have elaborated on the role of diffusion with Monte Carlo simulations and an analytical model. That work has also highlighted that once the limiting to efficiency contribution of geminate recombination reduces then nongeminate recombination losses are also minimized.

The central question of this Letter is the following: Is dissociation of an optical excitation an instantaneous or a sequential process and, if so, is the rate-limiting step the creation of a charge-transfer state or its subsequent dissociation? Can we achieve efficient charge separation through incoherent hopping of Coulombically bound charges that start off from tightly bound, cold CT states, or are coherence and ultrafast separation a prerequisite for high carrier generation yields in organic solar cells? Earlier transient absorption experiments suggested that the excess energy of

Received: March 10, 2017
Accepted: April 24, 2017
Published: April 24, 2017

DOI: 10.1021/acs.jpclett.7b00595
J. Phys. Chem. Lett. 2017, 8, 2093−2098

vibrationally hot charge-transfer states drives charge separation.[30,31] Meanwhile, there is growing evidence that delocalization effects are more important and they could involve delocalized states either in a polymeric donor[15,32] or in an aggregated acceptor such as PCBM.[14,19,33−35] There are also a number of previous Monte Carlo (MC) simulations that address this issue.[36−38] For example, Jones et al. have investigated whether "hot" delocalized charge transfer (CT) states are responsible for the high quantum efficiency in some polymer:fullerene blend heterojunction cells. They implemented the effect of the hot CT state in a bulk heterojunction (BHJ) morphology by considering the already cooled down geminate electron−hole pair, with electron and hole separated by a certain distance r. They found that most of them collapse back to a tight bound pair at the interface, unless an unphysically large initial separation r, e.g., in excess of 10 nm, is assumed. From this they concluded that hot CT states are unlikely to be the dominant factor for high solar cell efficiencies. Rather, they speculate whether it could be that a "variation in energy levels close to the heterojunction plays a more significant role".[36] Volpi and co-workers consider this implicitly by studying the effect of interfacial polarization on the dissociation of cold CT states for the case of the anthracene−C_{60} interface.[38] They find that, while polarization helps, the effect is not sufficient to account for the observed dissociation, so they speculate whether "charge delocalization in the polymer plays an important role". Burke and McGehee, in contrast, consider the role of the local charge carrier mobility on the separation efficiency.[37] In their MC simulation for three-phase BHJ, they find that high mobility-lifetime-products are required to account for experimentally found quantum yields. This could be reconciled with experimental lifetimes if the relevant mobility is a high local one, e.g., as probed by time-resolved terahertz conductivity. In their work, the effect of delocalization is not explicitly included, though one might consider the high mobility as an incoherent delocalization effect. Also, attempts have been made to model the electron transfer dynamics by quantum mechanical models.[13,14,24]

In order to decide whether the primary dissociation event (the creation of a CT state by charge transfer) or rather the subsequent secondary dissociation limits the overall yield of photogenerated carriers, we shall focus on the charge separation process following the electron transfer step, and we consider a "cold", vibrationally relaxed e−h pair CT state as the initial condition.[32] In so doing, we treat the dynamics of simultaneous electron and hole transport in the donor and acceptor phase, respectively, at equal grounds. In this Letter, we shed light on the mechanism of charge extraction in bilayer donor−acceptor devices by using Monte Carlo simulations[11,39−41] to calculate the charge collection efficiency as a function of externally applied field. Entropic contributions to charge separation are naturally included within the kinetic model.[22] We lay emphasis on the role of dimensionality, disorder, and bipolar transport. In addition, we examine in particular the question of delocalization, whereby the spatial extent of a charge wave function over a segment is parametrized by an effective mass of the polymer/oligomer. It is well-known that those factors have an influence on charge carrier mobility and recombination.[41−44] Here we unravel the impact of each of those physical parameters on the JV curves and quantify their relative importance. This approach goes beyond existing one-dimensional models[15,16,44,45] by incorporating the effect of delocalization and bipolar transport in a kinetic model that is able to quantify the separation efficiency and relate it to device parameters under experimentally relevant conditions.

In what follows, we compute the probability that an electron−hole pair separates over a given distance of 100 nm. We use a discrete lattice of points with donor polymers as the basis with their molecular axis extending parallel to each other and to the interface with the acceptor. The hole can only make interchain hops between π-conjugated polymers. The extent of the hole wave function along the polymer chain is taken into account using an effective mass model.[16,44,46] The main idea of the model is that the zero-point oscillations of the delocalized hole modify the potential energy of the hole by an additional kinetic energy term in the Hamiltonian. The potential energy of the hole is determined by the Coulomb potential well due to the presence of the electron and the external electric field. The more delocalized the hole is, the larger the kinetic energy term and therefore the shallower the potential. The degree of delocalization can be described by an on-chain effective mass for the hole m_{eff}, given in units of the free electron rest mass. In our simulation, this is implemented by adding the associated additional kinetic energy term to the site energy (see below).[47]

We consider a linear one-dimensional (Figure 1 top panel) and a square two-dimensional lattice (Figure 1 bottom panel)

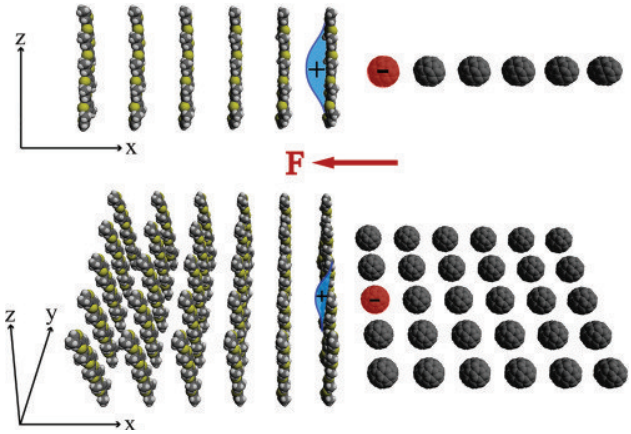

Figure 1. Schematics of the 1D (top panel) and 2D (bottom panel) bilayer lattice morphologies used for the Monte Carlo simulations. Each grid point consists of either a donor polymer chain of infinite length or a C_{60} acceptor molecule. The effect of on-chain hole delocalization is taken into account using an effective mass model.

with a constant a = 1 nm. For simplicity, the lattice constant remains the same for the acceptor phase, representing a fullerene based molecule, and energetic disorder is neglected. The initial condition for each independent Monte Carlo trial sets a photogenerated electron−hole pair at the interface, in a nearest neighbor charge-transfer configuration with an initial separation of 1 nm. Since we focus on geminate recombination, at every Monte Carlo trial we follow only one pair of charges. An external electric field of strength F is applied perpendicular to the DA interface with a vector direction antiparallel to the electron−hole Coulomb field.

Charge hopping rates follow the Miller−Abrahams formulation:

$$\nu_{ij} = \begin{cases} \nu_0 e^{-2\gamma r_{ij}} e^{-(\varepsilon_j - \varepsilon_i)/k_B T} & \text{for } \varepsilon_j > \varepsilon_i \\ \nu_0 e^{-2\gamma r_{ij}} & \text{for } \varepsilon_j \le \varepsilon_i \end{cases} \quad (1)$$

DOI: 10.1021/acs.jpclett.7b00595
J. Phys. Chem. Lett. 2017, 8, 2093−2098

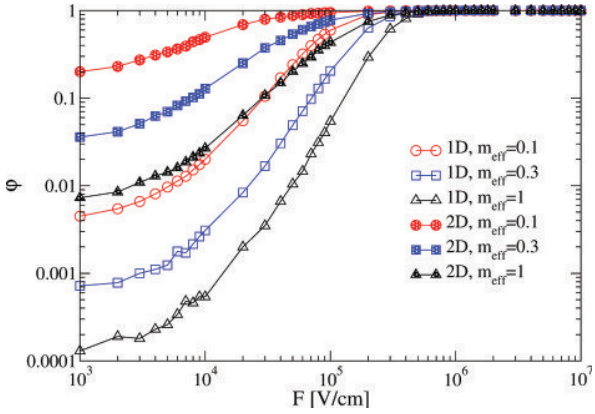

Figure 2. 1D and 2D Monte Carlo simulations for different effective mass of the donor molecules. Electron extraction efficiency φ as a function of an internal electric field F.

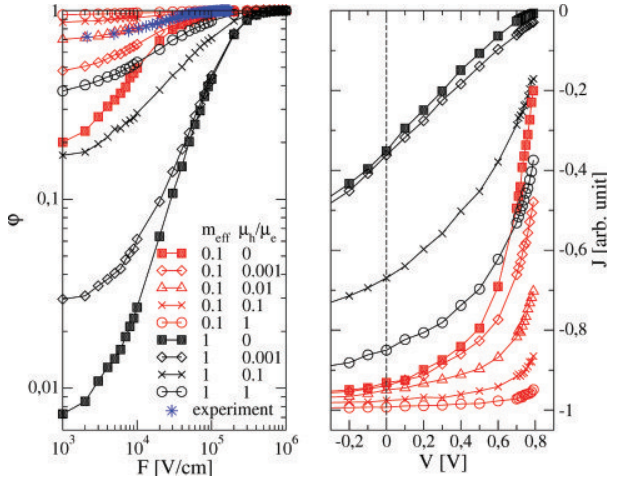

Figure 3. 2D Monte Carlo simulations, influence of imbalanced e and h mobilities. Left panel: Electron−hole separation efficiency φ as a function of an externally applied field and experimental data for a bilayer consisting of 60 nm thick layer of the T1 molecule as donor and 30 nm thick layer of C_{60} as acceptor. Right panel: resulting photocurrent JV curves for a purely geminate recombination regime.

where i denotes the residence site of the charge and j the target site, and the two sites are separated by a distance r_{ij}. Site energies ε_i and ε_j include contributions from the electron−hole Coulomb interaction potential including the kinetic energy term resulting from the delocalization of the hole wave function calculated by numerically solving the Schrödinger equation (see ref 16) and the voltage drop due to the applied field. Unless stated, the inverse localization length $\gamma = 2$ nm^{-1}, the frequency prefactor $\nu_0 = 10^{12}$ s^{-1}, and $T = 300$ K. We consider hopping events up to second nearest-neighbor distances, i.e., $r_{ij,\max} = 2$ nm, which is a sufficient cutoff distance for moderate values of temperature normalized disorder $\sigma/kT < 4$. From a simulation point of view, the parameters ν_0 and γ define the minimum hopping time, and their value does not influence the presented results since it is the relative ratio of the CT lifetime to the minimum hopping time that controls the probability for recombination (see below). In practice, these parameters determine the equilibrium charge carrier diffusion coefficient and mobility values.

At each Monte Carlo step, we calculate a waiting time for each hopping event: $\tau_{ij} = -(1/\nu_{ij}) \ln X$. In addition, we calculate a waiting time for recombination events between the electron−hole pair: $\tau_r = -\tau \ln X$, where τ is the electron−hole pair lifetime that increases exponentially with electron−hole distance r_{eh} as $\tau = \tau_{CT} e^{2\gamma(r_{eh}-a)}$, and X is a random number drawn from a box distribution between 0 and 1. The lifetime at close proximity is a parameter that we allow to vary from a minimum value of $\tau_{CT} = 35t_0$ to a maximum value of $\tau_{CT} = 3000t_0$, with t_0 being the minimum hopping time $t_0 = \frac{1}{\nu_0} e^{2\gamma a}$. The event with the smallest waiting time is selected and executed, and the interaction potential is updated. If the accepted event is a hop, then we update the site of the hole or electron and recalculate waiting times. If the chosen event is recombination, we remove the charges and start a new trial. Each trial terminates successfully when the electron−hole distance is larger or equal to 100 nm. The influence of the donor−acceptor thickness has been considered elsewhere.[29] The statistical quantity of interest is the separation yield calculated as $\varphi(F) = \frac{N_{sep}(F)}{N_{tot}(F)}$, where $N_{sep}(F)$ the number of successful trials (trials with $r_{eh} \geq 100$ nm) for an applied field F and $N_{tot}(F)$ the total number of trials of the order of 10^4. Thus, N_{tot} is the total number of e−h pairs considered.

At first we consider that only one of the carriers is mobile, e.g., only the electron is allowed to hop and the hole position is fixed. This situation could also be modeled analytically in one dimension,[45] and we have tested that the results for the field dependence of the separation yield are in perfect agreement with the analytical solution. Figure 2 shows that reducing the effective mass of the donor results in higher electron extraction efficiencies at intermediate and low fields. This is a straightforward result, because a lower effective mass, i.e., a longer hole delocalization along the polymer chain, translates into a smaller barrier for the e−h interaction potential (see ref 16). Let us now consider the two-dimensional case where the electron has more routes available to escape the e−h interaction potential while the hole is still stationary at the interface. Simulations reveal that φ increases by more than 1 order of magnitude for $m_{eff} = 0.1m_e$ at low fields where the driving force for electron extraction is dominated by the diffusion of the electron rather than the electric field (Figure 2). This is a remarkable result that highlights the important role of dimensionality on diffusion limited charge extraction.

Let us now lift up the restriction of immobilizing the hole and further allow for imbalanced electron and hole mobilities. Both experimental and theoretical works have indicated that this can have a significant impact on dissociation.[48,49] Results from our Monte Carlo calculations in the 2D case depicted in Figure 3 show a striking increase in the e−h separation yield when both the hole and the electron particle are allowed to hop. For a hole effective mass $m_{eff} = 0.1$, φ becomes virtually field independent even at the diffusive regime at low electric fields. We note that there are several reports of organic solar cells with molecular oligomers as the donor material that exhibit high external quantum efficiencies[28,50,51] and we have recently reported high separation yields in bilayer cells using the p-DTS(FBTTh$_2$)$_2$ oligomer (T1 molecule) as donor with C_{60} as acceptor.[29] These data are included at the left panel of Figure 3, and it is noteworthy that the field dependence can be well reproduced from the Monte Carlo simulations for $m_{eff} = 0.1$ and a mobility imbalance ratio $\mu_h/\mu_e = 10^{-2}$. Such a ratio is consistent with photo-CELIV measurements of hole mobility

DOI: 10.1021/acs.jpclett.7b00595
J. Phys. Chem. Lett. 2017, 8, 2093−2098

$1.4 \pm 0.5 \times 10^{-4}$ $cm^2/(V\ s)$ for the T1 oligomer while the electron mobility in C_{60} is of the order of 10^{-2} $cm^2/(V\ s)$.[29] We can further translate the obtained Monte Carlo results to photocurrent JV curves, assuming a thickness of the active layer (electron and hole transporting material) of d = 100 nm in total, and an open-circuit voltage V_{oc} = 0.8 V. The simulated JV characteristics are depicted at the right panel of Figure 3. They represent purely geminate recombination limited JV curves. These results highlight that bipolar transport dramatically increases the fill factors (FF) by lowering geminate recombination. Importantly, equal mobilities are not even required, and mobility differences of 1−2 orders of magnitude are tolerable. The geminate recombination regime can be partly accessed experimentally via time-delayed collection field measurements.[28] Experiments in as-cast and thermally annealed T1:$PC_{70}BM$ film blends have shown that annealed films exhibit phases with higher crystalline domains of T1 that improve hole mobilities by an order of magnitude as measured by photo-CELIV and TDCF transients. Consequently, the fill factors for annealed films have been shown to improve. This is therefore in accordance with the predictions of the Monte Carlo model.

Next, we consider the influence of varying the charge-transfer state lifetime with respect to the minimum hopping time that determines the magnitude of the mobility of the particles.[52] This can be achieved by either increasing the charge-transfer state lifetime of the pair, which corresponds to decreasing the electron−hole wave function overlap, or by decreasing the minimum hopping time, equivalent to increasing the coupling between the molecular units. When the ratio τ_{CT}/t_0 of the CT state lifetime over minimum hopping time increases, this corresponds to increasing the $\mu\tau$ product in a Braun−Onsager model.[53] Consequently, the separation yield increases since the electron and hole are given more chances to make hops and can get far-off in the course of their lifetime. Figure 4 shows the

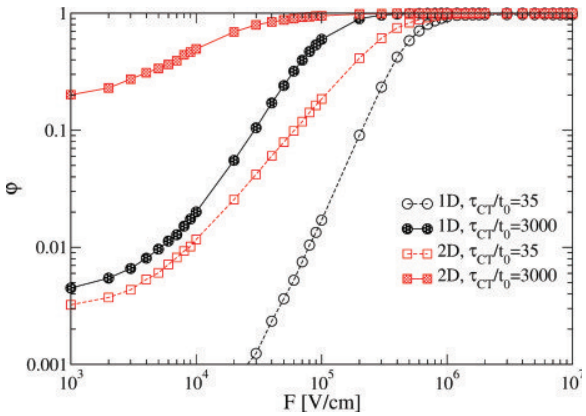

Figure 4. 1D and 2D Monte Carlo simulations of electron−hole separation efficiency φ as a function of an internal electric field F for m_{eff} = 0.1 and different CT state lifetime over minimum hopping time ratios.

changes in φ for the 1D and 2D cases. At the low field regime, φ increases by the same order of magnitude that τ_{CT}/t_0 increases. The role of energetic disorder has also been investigated, and we find that the inclusion of Gaussian disorder does not alter the conclusions presented here. A detailed study on the influence of disorder will be presented elsewhere.

We are now in a position to answer the pertinent question of whether we can achieve efficient charge separation of cold CT states through incoherent hopping of Coulombically bound charges. Based upon the main results obtained in this Letter, we are not only able to simulate experimental photocurrent JV curves dominated by geminate recombination by considering only incoherent hopping processes, but we can also quantify the contribution of important parameters, which independently lead to higher charge separation yields with weaker field dependence. These parameters include transport dimensionality, bipolar transport, effective mass, and the ratio of minimum hopping time over CT state lifetime, i.e., the $\mu\tau$ product. Given that typically CT state lifetimes do not vary dramatically in most organic blends, overall increase in transport dimensionality has the strongest effect following by bipolar transport and lowering the effective mass. Although bipolar transport is crucial, we find that fully balanced mobilities is less important.[54] Given that typically electron mobilities can be one or 2 orders of magnitude higher than hole mobilities this is a favorable result. The value of the effective mass is mainly controlled by molecular design with m_{eff} varying from about 0.1 in well-conjugated polymers[55,56] to values on the order of 1 in disordered molecules exhibiting strong hole localization. We stress that our results are also relevant to recent experiments showing that both delocalized hole states as well as fullerene aggregation improve charge separation.[13,32] In comparison with published experimental results, our simulations explain the increase of fill factors with increased crystallinity obtained by thermal annealing or chemical treatment. Paradoxically, the delocalization of the *hole* wave function also assists the transport of the *electron* in the acceptor phase by lowering the Coulomb interaction potential, whereas fullerene aggregation is expected to increase the hopping rates of the electron. It is also gratifying that our results consistently confirm and further complement previous MC calculations that focused, e.g., on the role of mobility or polarization.[37,38] Moreover, the implementation of the delocalization through a (site-specific) additional kinetic energy term corresponds, in a way, to the suggestion made by Jones et al. that the variation in energy levels close to the interface might be crucial.[36] Our findings also have the following consequences for optimizing organic solar cell devices: First, for the design of organic solar cells, it is not sufficient to focus on only one material in which the transport states are efficiently delocalized. Rather, both materials need to display either high charge delocalization or high carrier mobilities, ideally both. Second, morphologies that promote filamentary 1D transport are detrimental for charge separation, whereas architectures that favor transport with increased dimensionality (even at the expense of localization) are superior. It is also important to highlight that our results were obtained within an incoherent hopping formalism of vibrationally relaxed CT states[32] where the initial electron−hole pair has a close proximity of only 1 nm. Therewithal, we find that an incoherent transport model can describe efficient charge separation without the need to invoke "hot" processes, in agreement with ref 57. Coherence is therefore not the only route toward improving the efficiencies of organic solar cells. More consideration should be given to the fact that optimally efficient devices can be realized with simple material architectures that utilize incoherent hopping.

DOI: 10.1021/acs.jpclett.7b00595
J. Phys. Chem. Lett. 2017, 8, 2093−2098

AUTHOR INFORMATION

Corresponding Author

*E-mail: astavros@fis.uc3m.es.

ORCID

Stavros Athanasopoulos: 0000-0003-0753-2643

Anna Köhler: 0000-0001-5029-4420

Notes

The authors declare no competing financial interest.

ACKNOWLEDGMENTS

This project has received funding from the Universidad Carlos III de Madrid, the European Union's Seventh Framework Programme for research, technological development, and demonstration under Grant Agreement No. 600371, el Ministerio de Economía, Industria y Competitividad (COFUND2014-51509), el Ministerio de Educación, cultura y Deporte (CEI-15-17), and Banco Santander. We also acknowledge additional funding from the German Research Foundation DFG (GRK1640) and the Bavarian University Centre for Latin America (BAYLAT).

REFERENCES

(1) Mihailetchi, V. D.; Koster, L. J. A.; Hummelen, J. C.; Blom, P. W. M. Photocurrent Generation in Polymer-Fullerene Bulk Heterojunctions. *Phys. Rev. Lett.* **2004**, *93*, 216601.

(2) Köhler, A.; Bässler, H. *Electronic Processes in Organic Semiconductors: An Introduction*; Wiley-VCH: Weinheim, Germany, 2015; pp 1−86.

(3) Laquai, F.; Andrienko, D.; Deibel, C.; Neher, D. In *Elementary Processes in Organic Photovoltaics*; Leo, K., Ed.; Springer International Publishing: Cham, Switzerland, 2017; pp 267−291.

(4) Sariciftci, N. S.; Smilowitz, L.; Heeger, A. J.; Wudl, F. Photoinduced Electron Transfer from a Conducting Polymer to Buckminsterfullerene. *Science* **1992**, *258*, 1474−1476.

(5) Athanasopoulos, S.; Emelianova, E. V.; Walker, A. B.; Beljonne, D. Exciton diffusion in energetically disordered organic materials. *Phys. Rev. B: Condens. Matter Mater. Phys.* **2009**, *80*, 195209.

(6) Athanasopoulos, S.; Hennebicq, E.; Beljonne, D.; Walker, A. B. Trap Limited Exciton Transport in Conjugated Polymers. *J. Phys. Chem. C* **2008**, *112*, 11532−11538.

(7) Mikhnenko, O. V.; Blom, P. W. M.; Nguyen, T.-Q. Exciton diffusion in organic semiconductors. *Energy Environ. Sci.* **2015**, *8*, 1867.

(8) Deibel, C.; Dyakonov, V. Polymer-fullerene bulk heterojunction solar cells. *Rep. Prog. Phys.* **2010**, *73*, 096401.

(9) Few, S.; Frost, J. M.; Nelson, J. Models of charge pair generation in organic solar cells. *Phys. Chem. Chem. Phys.* **2015**, *17*, 2311−2325.

(10) Nayak, P. K.; Narasimhan, K. L.; Cahen, D. Separating Charges at Organic Interfaces: Effects of Disorder, Hot States, and Electric Field. *J. Phys. Chem. Lett.* **2013**, *4*, 1707−1717.

(11) Peumans, P.; Forrest, S. R. Separation of geminate charge-pairs at donor-acceptor interfaces in disordered solids. *Chem. Phys. Lett.* **2004**, *398*, 27−31.

(12) Clarke, T. M.; Durrant, J. R. Charge Photogeneration in Organic Solar Cells. *Chem. Rev.* **2010**, *110*, 6736−6767.

(13) Gélinas, S.; Rao, A.; Kumar, A.; Smith, S. L.; Chin, A. W.; Clark, J.; van der Poll, T. S.; Bazan, G. C.; Friend, R. H. Ultrafast Long-Range Charge Separation in Organic Semiconductor Photovoltaic Diodes. *Science* **2014**, *343*, 512−516.

(14) Savoie, B. M.; Rao, A.; Bakulin, A. A.; Gélinas, S.; Movaghar, B.; Friend, R. H.; Marks, T. J.; Ratner, M. A. Unequal Partnership: Asymmetric Roles of Polymeric Donor and Fullerene Acceptor in Generating Free Charge. *J. Am. Chem. Soc.* **2014**, *136*, 2876−2884.

(15) Schwarz, C.; Tscheuschner, S.; Frisch, J.; Winkler, S.; Koch, N.; Bässler, H.; Köhler, A. Role of the effective mass and interfacial dipoles on exciton dissociation in organic donor-acceptor solar cells. *Phys. Rev. B: Condens. Matter Mater. Phys.* **2013**, *87*, 155205.

(16) Tscheuschner, S.; Bässler, H.; Huber, K.; Köhler, A. A Combined Theoretical and Experimental Study of Dissociation of Charge Transfer States at the Donor-Acceptor Interface of Organic Solar Cells. *J. Phys. Chem. B* **2015**, *119*, 10359−10371.

(17) Verlaak, S.; Beljonne, D.; Cheyns, D.; Rolin, C.; Linares, M.; Castet, F.; Cornil, J.; Heremans, P. Electronic Structure and Geminate Pair Energetics at Organic-Organic Interfaces: The Case of Pentacene/C60 Heterojunctions. *Adv. Funct. Mater.* **2009**, *19*, 3809−3814.

(18) Ryno, S. M.; Fu, Y.-T.; Risko, C.; Brédas, J.-L. Energies at Organic-Organic Interfaces Impact on the Charge Separation Barrier at Donor-Acceptor Interfaces in Organic Solar Cells. *ACS Appl. Mater. Interfaces* **2016**, *8*, 15524−15534.

(19) D'Avino, G.; Muccioli, L.; Olivier, Y.; Beljonne, D. Charge Separation and Recombination at Polymer-Fullerene Heterojunctions: Delocalization and Hybridization Effects. *J. Phys. Chem. Lett.* **2016**, *7*, 536−540.

(20) Gregg, B. A. Entropy of Charge Separation in Organic Photovoltaic Cells: The Benefit of Higher Dimensionality. *J. Phys. Chem. Lett.* **2011**, *2*, 3013−3015.

(21) Gao, F.; Tress, W.; Wang, J.; Inganäs, O. Temperature Dependence of Charge Carrier Generation in Organic Photovoltaics. *Phys. Rev. Lett.* **2015**, *114*, 128701.

(22) Hood, S. N.; Kassal, I. Entropy and Disorder Enable Charge Separation in Organic Solar Cells. *J. Phys. Chem. Lett.* **2016**, *7*, 4495−4500.

(23) Song, Y.; Clafton, S. N.; Pensack, R. D.; Kee, T. W.; Scholes, G. D. Vibrational coherence probes the mechanism of ultrafast electron transfer in polymer-fullerene blends. *Nat. Commun.* **2014**, *5*, 4933.

(24) Bittner, E. R.; Silva, C. Noise-induced quantum coherence drives photo-carrier generation dynamics at polymeric semiconductor heterojunctions. *Nat. Commun.* **2014**, *5*, 3119.

(25) Kocherzhenko, A. A.; Lee, D.; Forsuelo, M. A.; Whaley, K. B. Coherent and Incoherent Contributions to Charge Separation in Multichromophore Systems. *J. Phys. Chem. C* **2015**, *119*, 7590−7603.

(26) Brédas, J.-L.; Sargent, E. H.; Scholes, G. D. Photovoltaic concepts inspired by coherence effects in photosynthetic systems. *Nat. Mater.* **2017**, *16*, 35−44.

(27) Proctor, C. M.; Kuik, M.; Nguyen, T.-Q. Charge carrier recombination in organic solar cells. *Prog. Polym. Sci.* **2013**, *38*, 1941−1960.

(28) Proctor, C. M.; Albrecht, S.; Kuik, M.; Neher, D.; Nguyen, T.-Q. Overcoming Geminate Recombination and Enhancing Extraction in Solution-Processed Small Molecule Solar Cells. *Adv. En. Mater.* **2014**, *4*, 1400230.

(29) Hahn, T.; Tscheuschner, S.; Kahle, J.; Reichenberger, M.; Athanasopoulos, S.; Saller, C.; Bazan, G. C.; Nguyen, T.-Q.; Strohriegl, P.; Bässler, H.; et al. Monomolecular and bimolecular recombination of electron-hole pairs at the interface of a bilayer organic solar cell. *Adv. Funct. Mater.* **2017**, *27*, 1604906.

(30) Ohkita, H.; Cook, S.; Astuti, Y.; Duffy, W.; Tierney, S.; Zhang, W.; Heeney, M.; McCulloch, I.; Nelson, J.; Bradley, D. D. C.; et al. Charge Carrier Formation in Polythiophene/Fullerene Blend Films Studied by Transient Absorption Spectroscopy. *J. Am. Chem. Soc.* **2008**, *130*, 3030−3042.

(31) Bakulin, A. A.; Rao, A.; Pavelyev, V. G.; van Loosdrecht, P. H. M.; Pshenichnikov, M. S.; Niedzialek, D.; Cornil, J.; Beljonne, D.; Friend, R. H. The Role of Driving Energy and Delocalized States for Charge Separation in Organic Semiconductors. *Science* **2012**, *335*, 1340−1344.

(32) Bässler, H.; Köhler, A. Hot or cold": how do charge transfer states at the donor-acceptor interface of an organic solar cell dissociate? *Phys. Chem. Chem. Phys.* **2015**, *17*, 28451−28462.

(33) Zusan, A.; Vandewal, K.; Allendorf, B.; Hansen, N. H.; Pflaum, J.; Salleo, A.; Dyakonov, V.; Deibel, C. The Crucial Influence of Fullerene Phases on Photogeneration in Organic Bulk Heterojunction Solar Cells. *Adv. Energy Mater.* **2014**, *4*, 1400922.

(34) Gehrig, D. W.; Howard, I. A.; Sweetnam, S.; Burke, T. M.; McGehee, M. D.; Laquai, F. The Impact of Donor-Acceptor Phase

DOI: 10.1021/acs.jpclett.7b00595
J. Phys. Chem. Lett. 2017, 8, 2093−2098

Separation on the Charge Carrier Dynamics in pBTTT:PCBM Photovoltaic Blends. *Macromol. Rapid Commun.* **2015**, *36*, 1054−1060.
(35) Jakowetz, A. C.; Böhm, M. L.; Zhang, J.; Sadhanala, A.; Huettner, S.; Bakulin, A. A.; Rao, A.; Friend, R. H. What Controls the Rate of Ultrafast Charge Transfer and Charge Separation Efficiency in Organic Photovoltaic Blends. *J. Am. Chem. Soc.* **2016**, *138*, 11672−11679.
(36) Jones, M. L.; Dyer, R.; Clarke, N.; Groves, C. Are hot charge transfer states the primary cause of efficient free-charge generation in polymer:fullerene organic photovoltaic devices? A kinetic Monte Carlo study. *Phys. Chem. Chem. Phys.* **2014**, *16*, 20310−20320.
(37) Burke, T. M.; McGehee, M. D. How High Local Charge Carrier Mobility and an Energy Cascade in a Three-Phase Bulk Heterojunction Enable > 90% Quantum Efficiency. *Adv. Mater.* **2014**, *26*, 1923−1928.
(38) Volpi, R.; Nassau, R.; Nørby, M. S.; Linares, M. Theoretical Study of the Charge-Transfer State Separation within Marcus Theory: The C60-Anthracene Case Study. *ACS Appl. Mater. Interfaces* **2016**, *8*, 24722−24736.
(39) Watkins, P. K.; Walker, A. B.; Verschoor, G. L. B. Dynamical Monte Carlo Modelling of Organic Solar Cells: The Dependence of Internal Quantum Efficiency on Morphology. *Nano Lett.* **2005**, *5*, 1814−1818.
(40) Marsh, R. A.; Groves, C.; Greenham, N. C. A microscopic model for the behavior of nanostructured organic photovoltaic devices. *J. Appl. Phys.* **2007**, *101*, 083509.
(41) Groves, C.; Marsh, R. A.; Greenham, N. C. Monte Carlo modeling of geminate recombination in polymer-polymer photovoltaic devices. *J. Chem. Phys.* **2008**, *129*, 114903.
(42) Onsager, L. Initial Recombination of Ions. *Phys. Rev.* **1938**, *54*, 554−557.
(43) Pope, M.; Swenberg, C. E. Electronic Processes in Organic Solids. *Annu. Rev. Phys. Chem.* **1984**, *35*, 613−655.
(44) Arkhipov, V. I.; Heremans, P.; Bässler, H. Why is exciton dissociation so efficient at the interface between a conjugated polymer and an electron acceptor? *Appl. Phys. Lett.* **2003**, *82*, 4605−4607.
(45) Rubel, O.; Baranovskii, S. D.; Stolz, W.; Gebhard, F. Exact Solution for Hopping Dissociation of Geminate Electron-Hole Pairs in a Disordered Chain. *Phys. Rev. Lett.* **2008**, *100*, 196602.
(46) Nenashev, A. V.; Baranovskii, S. D.; Wiemer, M.; Jansson, F.; Österbacka, R.; Dvurechenskii, A. V.; Gebhard, F. Theory of exciton dissociation at the interface between a conjugated polymer and an electron acceptor. *Phys. Rev. B: Condens. Matter Mater. Phys.* **2011**, *84*, 035210.
(47) The Coulomb interaction potential between the hole−electron pair is modified for different m_{eff}. We have not considered any other additional influence on the hole hopping rate. For different values of the effective mass, the hopping prefactor remains the same, v_0. In other words, the bulk hole mobility is kept constant.
(48) Stolterfoht, M.; Armin, A.; Shoaee, S.; Kassal, I.; Burn, P.; Meredith, P. Slower carriers limit charge generation in organic semiconductor light-harvesting systems. *Nat. Commun.* **2016**, *7*, 11944.
(49) Wojcik, M.; Michalak, P.; Tachiya, M. Geminate electron-hole recombination in organic solids in the presence of a donor-acceptor heterojunction. *Appl. Phys. Lett.* **2010**, *96*, 162102.
(50) Zhang, Q.; Kan, B.; Liu, F.; Long, G.; Wan, X.; Chen, X.; Zuo, Y.; Ni, W.; Zhang, H.; Li, M.; et al. Small-molecule solar cells with efficiency over 9%. *Nat. Photonics* **2015**, *9*, 35−41.
(51) Kan, B.; Zhang, Q.; Li, M.; Wan, X.; Ni, W.; Long, G.; Wang, Y.; Yang, X.; Feng, H.; Chen, Y. Solution-Processed Organic Solar Cells Based on Dialkylthiol-Substituted Benzodithiophene Unit with Efficiency near 10%. *J. Am. Chem. Soc.* **2014**, *136*, 15529−15532.
(52) Hong, K. M.; Noolandi, J. Solution of the Smoluchowski equation with a Coulomb potential. II. Application to fluorescence quenching. *J. Chem. Phys.* **1978**, *68*, 5172−5176.
(53) Braun, C. L. Electric field assisted dissociation of charge transfer states as a mechanism of photocarrier production. *J. Chem. Phys.* **1984**, *80*, 4157−4161.
(54) Tress, W.; Petrich, A.; Hummert, M.; Hein, M.; Leo, K.; Riede, M. Imbalanced mobilities causing S-shaped IV curves in planar heterojunction organic solar cells. *Appl. Phys. Lett.* **2011**, *98*, 063301.
(55) Northrup, J. E. Atomic and electronic structure of polymer organic semiconductors: P3HT, PQT, and PBTTT. *Phys. Rev. B: Condens. Matter Mater. Phys.* **2007**, *76*, 245202.
(56) Hsu, B. B.-Y.; Cheng, C.-M.; Luo, C.; Patel, S. N.; Zhong, C.; Sun, H.; Sherman, J.; Lee, B. H.; Ying, L.; Wang, M.; et al. The Density of States and the Transport Effective Mass in a Highly Oriented Semiconducting Polymer: Electronic Delocalization in 1D. *Adv. Mater.* **2015**, *27*, 7759−7765.
(57) Vandewal, K.; Albrecht, S.; Hoke, E. T.; Graham, K. R.; Widmer, J.; Douglas, J. D.; Schubert, M.; Mateker, W. R.; Bloking, J. T.; Burkhard, G. F.; et al. Efficient charge generation by relaxed charge-transfer states at organic interfaces. *Nat. Mater.* **2014**, *13*, 63−68.

DOI: 10.1021/acs.jpclett.7b00595
J. Phys. Chem. Lett. 2017, 8, 2093−2098

4.3. The role of intrinsic photogeneration in single layer and bilayer solar cells with C_{60} and PCBM

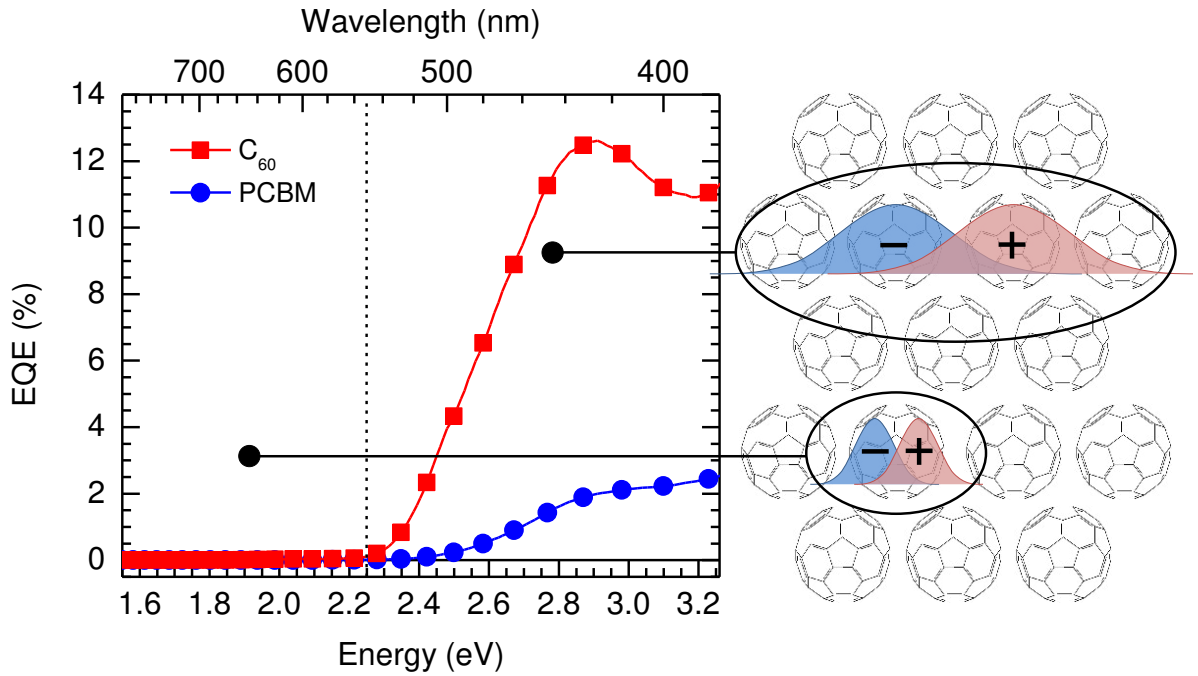

Tobias Hahn & Steffen Tscheuschner, Christina Saller, Peter Strohriegl, Puttaraju Boregowda, Tushita Mukhopadhyay, Satish Patil, Dieter Neher , Heinz Bässler, Anna Köhler

Veröffentlicht in

Journal of Physical Chemistry C (**2016**), 120, 25083-25091

(DOI: https://doi.org/10.1021/acs.jpcc.6b08471)

THE JOURNAL OF PHYSICAL CHEMISTRY C

Article

pubs.acs.org/JPCC

Role of Intrinsic Photogeneration in Single Layer and Bilayer Solar Cells with C_{60} and PCBM

Tobias Hahn,[†,▽] Steffen Tscheuschner,[†,▽] Christina Saller,[‡] Peter Strohriegl,[‡,⊥] Puttaraju Boregowda,[§] Tushita Mukhopadhyay,[§] Satish Patil,[§] Dieter Neher,[∥] Heinz Bässler,[⊥] and Anna Köhler*[,†,⊥]

[†]Experimental Physics II, University of Bayreuth, 95440 Bayreuth, Germany

[‡]Macromolecular Chemistry I, University of Bayreuth, 95440 Bayreuth, Germany

[§]Solid State and Structural Chemistry Unit, Indian Institute of Science, Bangalore, 560012 India

[∥]Institute for Physics and Astronomy, University of Potsdam, 14476 Potsdam-Golm, Germany

[⊥]Bayreuth Institute of Macromolecular Science (BIMF), University of Bayreuth, 95440 Bayreuth, Germany

Supporting Information

ABSTRACT: In an endeavor to examine how optical excitation of C_{60} and PCBM contribute to the photogeneration of charge carriers in organic solar cells, we investigated stationary photogeneration in single-layer C_{60} and PCBM films over a broad spectrum as a function of the electric field. We find that intrinsic photogeneration starts at a photon energy of about 2.25 eV, i.e., about 0.4 eV above the first singlet excited state. It originates from charge transfer type states that can autoionize before relaxing to the lower-energy singlet S_1 state, in the spirit of Onsager's 1938 theory. We analyze the internal quantum efficiency as a function of electric field and photon energy to determine (1) the Coulombic binding and separation of the electron−hole pairs, (2) the value of the electrical gap, and (3) which fraction of photoexcitations can fully separate at a given photon energy. The latter depends on the coupling between the photogenerated charge transfer states and the eventual charge transporting states. It is by a factor of 3 lower in PCBM. Close to the threshold energy for intrinsic photoconduction (2.25 eV), the generating entity is a photogenerated electron−hole pair with roughly 2 nm separation. At higher photon energy, more expanded pairs are produced incoherently via thermalization.

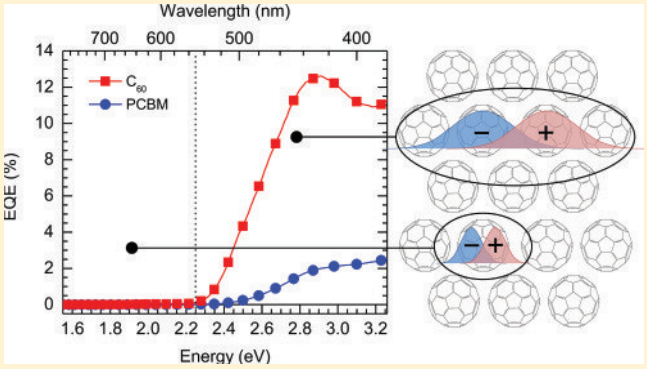

1. INTRODUCTION

It is a generally accepted notion that in single component molecular solids photogeneration of charge carriers is inefficient because the Coulombic binding energy of singlet excitons is large.[1] This process becomes efficient only if an electron donor material is blended with an electron accepting material. If the offset between the highest occupied molecular orbital (HOMO) and the lowest unoccupied molecular orbital (LUMO) levels of the constituents is sufficiently large, the charge transfer (CT) state at the donor−acceptor interface becomes the lowest excited state of the system and can act as a precursor for photogeneration.[2−9] These CT states are populated by singlet excitons, usually generated in the donor phase, that diffuse toward the donor−acceptor interface. Efficient power conversion in an organic solar cell (OSC) requires that the subsequent dissociation of the CT state or, more generally, the electron−hole pair (eh-pair), is an efficient process. The reason why the escape of the eh-pair from the Coulomb potential can be efficient is subject of current research.[10−20] There is growing evidence, though, that delocalization of the charges comprising the eh-pair plays a major role.[21−27]

Optimal power conversion efficiency of an OSC requires an optimal overlap between the absorption spectrum of the solar cell materials and the solar spectrum. This condition is satisfied when using donor materials with high oscillator strength and an absorption edge near 700 nm (1.8 eV) or above. Prototypical donor materials are donor−acceptor type conjugated oligomers or polymers. They are usually combined with C_{60} or PCBM ((6,6)-phenyl-C_{61}-butyric acid methyl ester) as acceptors. The absorption spectra of these donor materials commonly feature a minimum somewhere around 450 nm (2.7 eV), where a film of C_{60} absorbs strongly. In bulk heterojunction donor−acceptor blends C_{60} or PCBM forms aggregates, unless only very small amounts are incorporated that are often not sufficient for efficient OSC operation.[28] It is therefore of primary importance to identify the role of optical excitations in these fullerene domains for the operation of such OSCs. There is indeed experimental evidence that optical excitation of C_{60} or PCBM

Received: August 22, 2016
Revised: October 11, 2016
Published: October 12, 2016

DOI: 10.1021/acs.jpcc.6b08471
J. Phys. Chem. C 2016, 120, 25083−25091

has a significant effect on the performance of donor−acceptor OSCs.[29−33] However, the underlying mechanism is discussed controversially. From the analysis of the current−voltage ($j(V)$) dependence of a bilayer OSC with a C_{60} layer as electron acceptor, Jeong et al.[32] conclude that excited C_{60} creates an additional photocurrent while Tress et al.[33] argue that the excited C_{60} introduces a loss mechanism, caused by an additional hole injection current that leads to a so-called photoshunt. Li et al.[31] attribute the continuous increase of the photocurrent in CuPc/C_{60} diodes upon increasing negative bias to an enhancement of hole injection from the cathode due to the interaction of triplet excitons with electrons in C_{60}. On the other hand, Zou and Holmes[30] conjecture that in the C_{60} rich phase a virtually temperature independent bulk ionization process occurs because singlet excitons in C_{60} are believed to be only very weakly bound. This conclusion is in disagreement with the observation of Mort et al.,[34] who have found that photoconduction in a neat C_{60} film is thermally activated. An in-depth study of photogeneration in a neat C_{60} and PCBM films should resolve these controversies.

There is a further motivation for studying photogeneration in C_{60} or PCBM films. There is abundant evidence that charge generation in bulk heterojunction OSCs depends critically on the extent of aggregation of the electron acceptor.[26,28,35−37] A suggested reason for this charge generation efficiency is associated with an increasing electron delocalization with increasing content of PCBM in bulk-heterojunction cells. This ought to be dependent on the degree of structural order and should therefore be reflected in an analysis of photogeneration of differently prepared films of C_{60} and PCBM.

Photogeneration in C_{60} is not a new subject. Early on, Mort el al.[34,38,39] investigated photogeneration in C_{60} films employing the xerographic method. In subsequent work, Kazaoui et al. focused on spectrally dependent photoconduction combined with studies of electroabsorption and field assisted photoluminescence using a coplanar interdigitated electrode arrangement and constant electric field.[40] They observed a weak photocurrent with a threshold energy that is close to the 0−0 feature of the photoluminescence spectrum (1.84 eV) that increases steeply above 2.3 eV. This increase correlates with the onset of electroabsorption that features a maximum at 2.45 eV. The main conclusion of this work is that the source of the intrinsic photocurrent in C_{60} is a charge transfer state. However, the mechanism of the dissociation of the CT state has not been elucidated and the estimated bandgap of about 3 eV is incompatible with experimental results on the ionization energy and the electron affinity.[6,41−44]

The aim of the current work is to identify the mechanism of optical photogeneration in bulk films of C_{60} or PCBM by measuring and analyzing the photocurrent over a broad range of electric fields and photon energies. The experiments were done on a sandwich-type diode with a 30 nm thick C_{60} or PCBM layer. The advantage of a sandwich arrangement as compared to a gap arrangement, used by Kazaoui et al.,[40] is that both bimolecular charge recombination is greatly reduced and surface effects are avoided. Moreover, the use of electrodes with different workfunctions allows the operation of the diodes under reverse bias. This prevents exciton induced charge injection from the electrode(s) that might otherwise obscure weak intrinsic photogeneration at low photon energies.[45]

In brief, we find that in C_{60} and PCBM films intrinsic photogeneration occurs above a photon energy of 2.2−2.3 eV. It originates from charge transfer states that couple efficiently to charge transporting states and that can escape from their Coulomb potential via an Onsager-like process. Close to the threshold photon energy, eh-pairs with eh-separation of about 2 nm are generated resonantly while at higher $h\nu$ they are produced via an incoherent thermalization process.

2. EXPERIMENTAL METHODS

To fabricate single component C_{60} or PCBM diodes, ITO-coated substrates were covered with a patterned photoresist as described by Schwarz et al. such as to leave round openings for the active area.[46] A 15 nm thick MoO_3 (Sigma-Aldrich) layer was evaporated on top of the ITO openings using a shadow mask. C_{60} (Sigma-Aldrich) films with a thickness of 30 nm were vapor deposited with an evaporation rate of 1 Å/s. Alternatively, 30 nm thick PCBM films (99.5% purity, Sigma-Aldrich) were spin coated from chlorobenzene solution (20 mg/mL). The thickness of the PCBM layer was verified with a Dektak (Veeco) profilometer. Finally, the films were covered by a thermally evaporated 100 nm thick aluminum cathode. The complete diode fabrication was done in a nitrogen atmosphere using a glovebox with direct access to the evaporation chamber. Measurements of the photocurrent were carried out for (i) a single layer C_{60} (thereafter referred to as C_{60}-only) device measured immediately after fabrication ("C_{60}"), (ii) a C_{60}-only device stored in a nitrogen glovebox for one year ("after 1 year"), (iii) a C_{60}-only device annealed at 140 °C for 26 h under nitrogen ("C_{60} annealed"), (iv) a PCBM-only device annealed at 140 °C for 30 min and afterward cooled down to 60 °C in a time range of 30 min ("PCBM annealed"), and (v) for a PCBM-only device which was not annealed and measured as cast ("PCBM"). In addition to single layer fullerene diodes, bilayer donor−acceptor type cells were also investigated (shown in Figure 4,) in which a x nm thick donor layer was combined with 30 nm C_{60} acceptor layer. As a donor, we used once a PCDTBT derivative ($PCDTBT_{co}$; x = 14 nm) and once the small molecule Ph-TDPP-Ph (x = 25 nm). Their chemical structures are shown in Figure 4 below. The Ph-TDPP-Ph donor layer was spin coated from a chloroform/chlorobenzene (3:2) solution (7 mg/mL) and the $PCDTBT_{co}$ from a chlorobenzene solution (6 mg/mL) before the C_{60} layer was vapor deposited. Ph-TDPP-Ph and $PCDTBT_{co}$ were synthesized as described in the Supporting Information (SI). $PCDTBT_{co}$ was synthesized by Strohriegl et al. as described in the SI.

The current−voltage characteristics of the diodes in the dark and upon illumination were measured under vacuum at room temperature. Monochromatic illumination was provided by a 450 W xenon lamp (Osram) using a commercial monochromator. The light intensity impinging on the diode was measured using a Hamamatsu S1337-33BQ photodiode. It was 7.1 mW/cm^2 for 536 nm irradiation and 6.7 mW/cm^2 for 580 nm irradiation. The photocurrents were measured with a Keithley 236 source-measure unit.

The electric field in the active layer of the solar cells was taken as $(V_{bi} - V)/d$ where d is the thickness of the active layer, V is the applied voltage, and V_{bi} is the built-in voltage, approximated by the voltage at which the photocurrent is zero. V_{bi} was typically 0.9 ± 0.1 V. The photocurrent was calculated from the difference between the total current under illumination and the dark current.

Calculating the internal quantum efficiency (IQE) of the solar cells requires the absorption spectra of the thin C_{60} or PCBM films in the diode structures, which is not trivial due to optical effects.[47] To circumvent this problem, we calculated the effective absorption spectrum of the film embedded in the

DOI: 10.1021/acs.jpcc.6b08471
J. Phys. Chem. C 2016, 120, 25083−25091

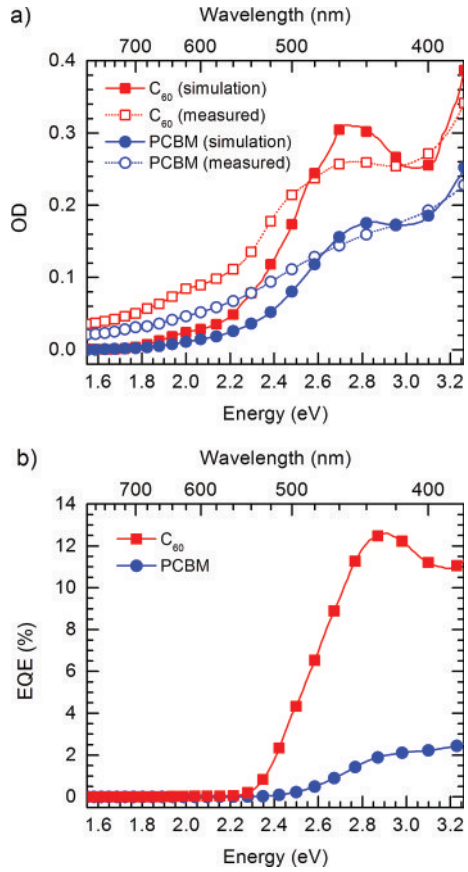

Figure 1. (a) Optical density of C_{60} (red squares) and PCBM (blue circles) measured from a film on quartz glass (open symbols) and simulated (filled symbols). In the simulation, the absorption of C_{60} or PCBM was calculated for a layer embedded between ITO/MoO_3 and aluminum, as is the case in a solar cell. (b) EQE measured under short-circuit conditions for a C_{60}-only device (red squares) and a PCBM-only device (blue circles). Both devices were not annealed and measured as cast.

ITO(250 nm)/MoO_3(15 nm)/C_{60}(30 nm)/Al(100 nm) assembly using a transfer matrix approach[48,49] implemented by Burkhard et al.[47] For this, we used the literature values for the real and imaginary part of the complex refractive index, n and k, for C_{60}[50] or PCBM (provided by Burkhard et al.[47]). A comparison of the calculated spectrum and the measured absorption spectrum of a C_{60} or PCBM film deposited on a quartz substrate illustrates the importance of eliminating interference effects (Figure 1). We therefore used the calculated absorption for calculating the IQE. Figure 1 also shows that the oscillator strength of the optical transition of PCBM between 2.3 and 3.2 eV is by a factor of 2 lower than that of C_{60}. We estimate that the absolute IQE values have an experimental error of about 20%.

3. EXPERIMENTAL RESULTS

In addition to the calculated and measured absorption spectra for C_{60} and PCBM, Figure 1 shows the external quantum efficiency (EQE) of single layer solar cells made from C_{60} or PCBM. By correcting the EQE for the absorption of the C_{60} or PCBM layer and the transmission of the glass/ITO/MoO_3 substrate, we obtain the internal quantum efficiencies (IQE). In Figure 2a we compare the IQE of differently treated C_{60} and PCBM films as a function of photon energy, taken under short-

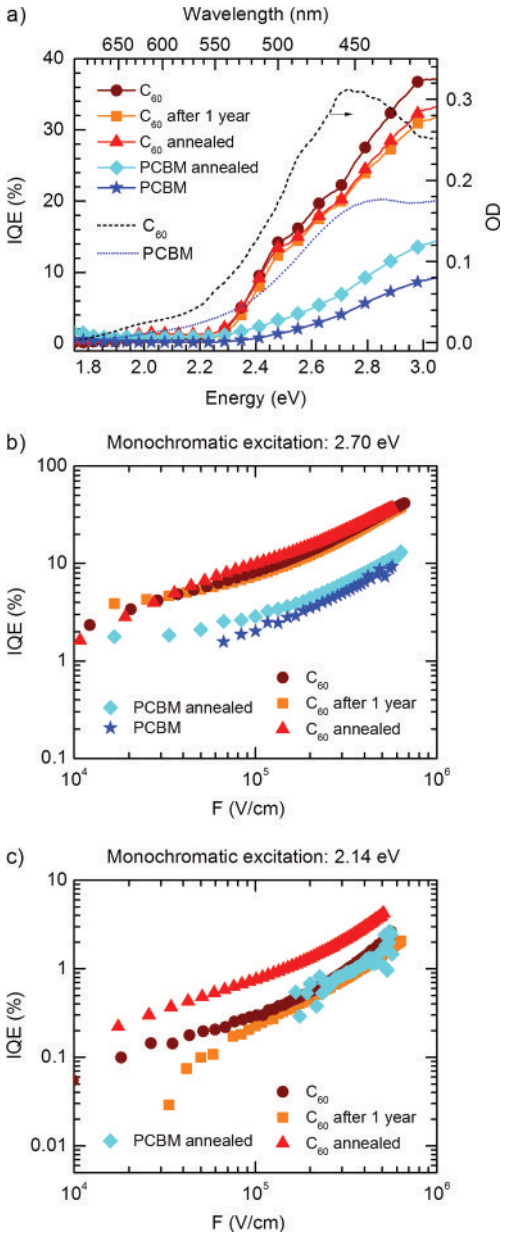

Figure 2. Internal quantum efficiency (IQE) spectra for a C_{60}-only device measured immediately after fabrication (wine circles), a C_{60}-only device after one year (orange squares), a C_{60}-only device annealed at 140 °C (red triangles), a PCBM-only device annealed at 140 °C (cyan diamonds) and for a PCBM-only device measured as cast (blue stars) (a) under short-circuit conditions, (b) as a function of field for a monochromatic excitation energy of 2.70 eV, and (c) as a function of field for a monochromatic excitation energy of 2.14 eV. In (c) the not annealed PCBM sample had an insufficient ratio of photocurrent to dark current at low excitation energies and is therefore not shown. Additionally, on the right axis in (a) the absorption of C_{60} and PCBM is shown.

circuit conditions. The field dependent photocurrent of the different samples is shown in Figure 2b,c. It turns out that in C_{60} films neither annealing at 140 °C nor storage during a year have major effects. The IQE of PCBM films is by roughly a factor of 3 lower than that of C_{60} films when exciting at 2.70 eV. In both materials, the IQE is strongly dependent on the operating voltage at reverse bias ($V \leq V_{bi}$) (Figure 3). Consistent with earlier work,[40] there is weak photogeneration starting at the

DOI: 10.1021/acs.jpcc.6b08471
J. Phys. Chem. C 2016, 120, 25083−25091

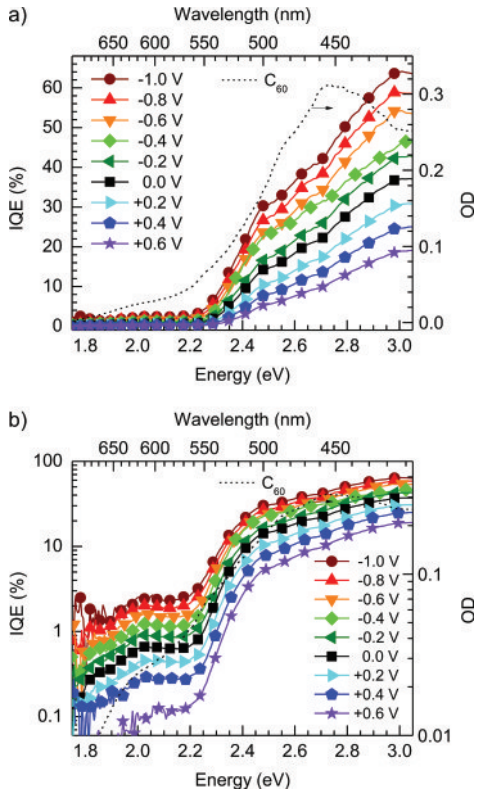

Figure 3. Internal quantum efficiency (IQE) of a C_{60}-only device measured immediately after preparation for different external voltages (symbols) and the associated optical density of the 30 nm thick C_{60} layer used for calculating the IQE (dashed line) (a) on a linear scale and (b) on a logarithmic scale. Only a quarter of the data points are shown as symbols for clarity of display.

photon energy of about 1.85 eV, i.e., coincident with the onset of the 0−0 feature of the absorption spectrum, and increasing strongly above 2.2−2.3 eV. Below 2.25 eV, the IQE is only about 0.001−0.01 and almost independent of photon energy. At an applied voltage of −1.0 V, corresponding to a field of 6.6×10^5 V/cm, and at a photon energy of 3.0 eV, the IQE is about 60%. Above a photon energy of 2.3 eV, V_{bi} is about 0.9 V ± 0.1 V.

In order to find out in which way optical excitation of C_{60} contributes to the efficiency of an OSC, we studied also the field dependence of photogeneration in bilayer diodes with a donor material combined with C_{60} as an acceptor (Figure 4). We chose two donor materials, that is Ph-TDPP-Ph as an example for a molecular donor and $PCDTBT_{co}$ as an example for a low-bandgap polymer. The chemical structures and thin film absorption spectra of the donors are shown in Figure 4a,b, along with the thin film absorption of C_{60} for ease of comparison. We excited both diodes, once at 2.14 eV where the absorption is dominated by the donor and which is below the threshold energy for significant intrinsic C_{60} photocurrent generation (cf. Figure 3) and once at 2.94 or 3.35 eV where both donor and C_{60} absorb and where the intrinsic photocurrent generation of C_{60} is significant, e.g., with about 30% IQE at 0 V, i.e., for internal fields of about 3×10^5 V/cm. Figure 4c shows how the EQEs evolve as a function of field for the two different excitation ranges, while Figure 4d shows the current−voltage curve, exemplarily for a planar heterojunction made with $PCDTBT_{co}$ and C_{60}.

Upon 2.14 eV excitation, the EQEs nearly ($PCDTBT_{co}$) or fully (Ph-TDPP-Ph) saturate above 10^5 V/cm. In contrast, for the high energy excitation, the EQE increases monotonously, with a change of slope at about 10^5 V/cm. This increase in photocurrent for fields above 10^5 V/cm resembles the field dependent intrinsic photocurrent in a single-layer C_{60} diode as shown in Figure 2. The difference in field-dependent photocurrent that is seen when both, donor and fullerene, are excited compared to donor-only excitation is therefore clear evidence that the extra contribution to the EQE is caused by intrinsic charge carrier generation inside the C_{60} layer, consistent with the findings by Jeong et al.[32] In passing, we comment on the perfect saturation of the EQE at high electric fields upon selective Ph-TDPP-Ph excitation combined with the fact that we could not observe any photocurrent in single layer Ph-TDPP-Ph devices (not shown). This is in contrast to experiments on single layer PCDTBT devices that reveal an intrinsic photogeneration above a threshold photon energy at 2.6 eV.[51] The reason is that in the molecule Ph-TDPP-Ph the singlet exciton is too strongly bound in order to allow the escape from the Coulomb potential while in the donor−acceptor polymer PCDTBT some intrinsic dissociation can ocur, albeit only at high electric fields because it proceeds from an on-chain charge transfer state. This explains why in diodes made with C_{60} and PCDTBT or a PCDTBT derivative there is always a residual increase (see Figure 4) of photogeneration above the electric field at which dissociation of eh-pairs at the donor−acceptor interface already saturates.

For C_{60}-only devices, experimental current−voltage $j(V)$) data taken for different excitation energies are presented in Figure 5, converted into plots of IQE as a function of electric field. Also shown are fits according to the Onsager 1938 model[52] using eq 17 in reference 53. For reference, representative $j(V)$ curves are available as Supporting Information.

4. DISCUSSION

The kind of field dependence of the intrinsic photogeneration yield, i.e. the IQE, in a neat C_{60} film shown in Figure 2 is reminiscent of an Onsager-type dissociation process by autoionization.[1,52] In his 1938 treatise, Onsager considered that a high-energy photon ionizes a molecule and creates a Coulomb-bound pair of a radical cation and anion with an intrapair separation r_0 after thermalization. The medium is considered homogeneous and has a dielectric constant ε_r. The cation and the anion undergo a Brownian diffusive motion within the superimposed Coulomb potential and the potential due to the applied electric field. In the course of their motion, the pair has the option to fully dissociate or to recombine geminately upon their encounter. The essential parameters in the Onsager formalism are

i. the intrapair separation r_0 and
ii. the initial yield of eh-pairs with separation of r_0 that are able to fully separate in the high field limit.

In the limit of low fields, the dissociation yield of the eh-pairs is constant. It is simply given by the Boltzmann factor for the thermally activated dissociation of eh-pairs at a distance r_0 with a Coulomb binding energy $E_{coul} = \frac{e^2}{4\pi\varepsilon_r\varepsilon_0} \cdot \frac{1}{r_0}$, noting that $\frac{E_{coul}}{kT} = \frac{r_{coul}}{r_0}$, where r_{coul} is the Coulomb capture radius, i.e., the radius at which the thermal energy kT equals the Coulomb energy. The textbook example for successful application of Onsager's 1938 theory is the work of Chance and Braun on crystalline anthracene.[54]

DOI: 10.1021/acs.jpcc.6b08471
J. Phys. Chem. C 2016, 120, 25083−25091

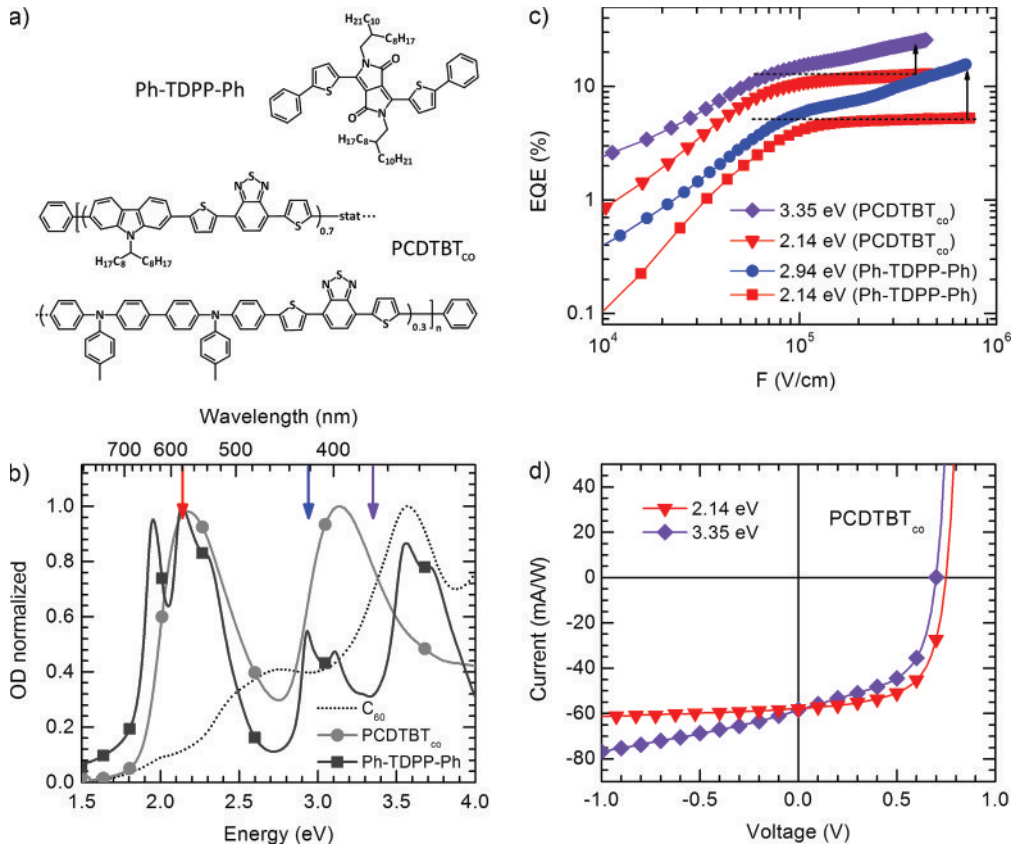

Figure 4. (a) Chemical structure of the copolymer PCDTBT$_{co}$ and the small molecule Ph-TDPP-Ph. (b) Normalized absorption spectra for C_{60}, the copolymer PCDTBT$_{co}$, and the small molecule Ph-TDPP-Ph measured from a quartz glass substrate. The arrows indicate the excitation energies for the photocurrent measurements. (c) External quantum efficiency (EQE) as a function of internal field for the planar heterojunction solar cells (ITO/MoO_3/Ph-TDPP-Ph(25 nm)/C_{60}(30 nm)/Al) excited at 2.94 and 2.14 eV, and for (ITO/MoO_3/ PCDTBT$_{co}$(14 nm)/C_{60}(30 nm)/Al) excited at 3.35 and 2.14 eV. The black arrows indicate the intrinsic contribution of the C_{60} layer for 2.94 or 3.35 eV excitation. (d) Corresponding current–voltage curves exemplarily for the PCDTBT$_{co}$ corrected by the spectral intensity of the used xenon lamp as described in the experimental section.

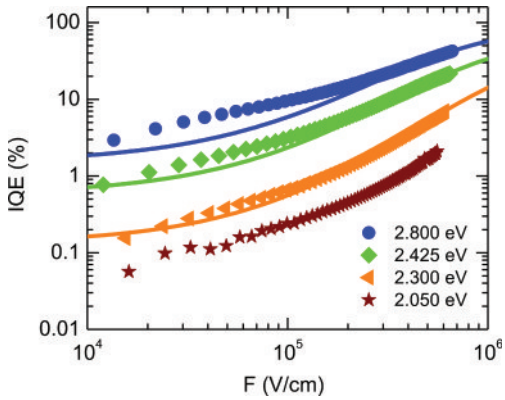

Figure 5. Internal quantum efficiency (IQE) as a function of internal field for a C_{60}-only device (ITO/MoO_3/C_{60}/Al) with a C_{60} layer thickness of 30 nm for different excitation energies (symbols). The solid lines indicate the Onsager fit to the data points. No Onsager fit is shown for 2.050 eV data points since for this energy the Onsager theory does not apply here.

The facts that (1) the action spectrum of intrinsic photogeneration in C_{60} features a threshold near 2.2–2.3 eV, i.e., roughly 0.4 eV above the singlet exciton, and (2) the field dependence of the IQE resembles typical Onsager plots of the field dependent yield of photogeneration (e.g., refs 38, 39, and 53), prompted us to analyze the data in terms of Onsager's 1938 theory. Representative plots of experimental IQE data and fits to the Onsager formalism are shown in Figure 5. The data were fitted according to eq 17 in ref 53. Considering that in the original version of the theory neither the distribution of the r_0 values[55] nor disorder are considered, the agreement between theory and experiment is satisfactory. In the following, we shall first consider the results for the photon energies above 2.25 eV where IQE rises sharply. We associate this regime with intrinsic photogeneration while below 2.25 eV extrinsic photogeneration prevails (vide infra).

Two essential outcomes of the Onsager 1938 theory are the yield of the quantum efficiency of photogeneration extrapolated to infinite electric field (IQE_{max}), and the Coulomb binding energy (E_{coul}) of the eh-pair that translates into the electron–hole separation of the pair (r_0). E_{coul} is inferred, for different energies of the exciting photon, from the ratio of the photogeneration yields at zero and at infinite field, i.e., $\frac{IQE(F_0, h\nu)}{IQE_{max}} = \exp\left(-\frac{E_{coul}}{kT}\right)$. We shall first consider the dependence of E_{coul} on photon energy above the intrinsic photogeneration threshold at about 2.25 eV. $IQE(F_0, h\nu)$ was approximated by the asymptotic value at a field strength of 10^4 V/cm in Figure 5, and IQE_{max} was taken from the Onsager fits in the limit of infinitely high field. We find that $E_{coul}(h\nu)$ decreases linearly with photon energy from about 2.25 eV up to about 2.35 eV and levels off at higher $h\nu$ (Figure 6a), with no systematic difference between the data taken from diodes

DOI: 10.1021/acs.jpcc.6b08471
J. Phys. Chem. C 2016, 120, 25083–25091

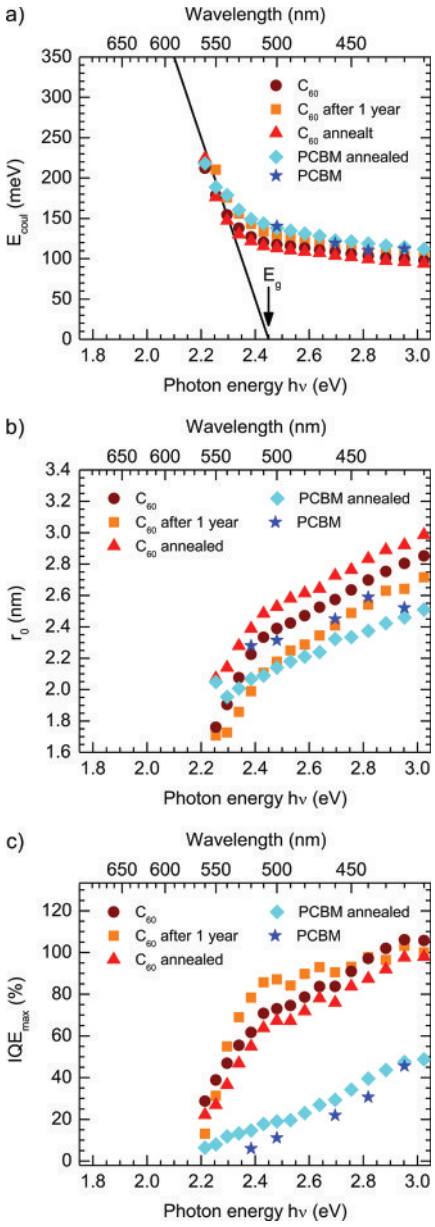

Figure 6. (a) Coulomb binding energy (E_{coul}), (b) eh-distance (r_0), and (c) maximal internal quantum efficiency (IQE_{max}) in the limit of infinite field, all as a function of the excitation energy for differently prepared fullerene single-layer devices. The solid line in (a) indicates the fit according to $E_{coul} = E_g - h\nu$, with E_g = 2.45 eV.

prepared in different ways. The linear decrease of $E_{coul}(h\nu)$ with increasing $h\nu$ close to the onset of intrinsic photogeneration implies that the dissociating eh-pair is generated resonantly, so that no energy is lost in the course of a thermalization process. Therefore, $E_g = h\nu + E_{coul}$ should apply where E_g is the electrical gap. This is illustrated in Figure 7. It is gratifying that the range of the $E_{coul}(h\nu)$ values, 0.10−0.22 eV, is in excellent agreement with the temperature dependence of the photocurrent generated by white light irradiation shown by Mort et al.[34] In that work, the curvature of the pertinent Arrhenius graphs are indicative of a distribution of activation energies ranging from 0.15 to 0.25 eV. At photon energies above 2.4 eV, the $E_{coul}(h\nu)$ dependence acquires a reduced slope. This indicates that above 2.4 eV, the eh-pairs are generated via a thermalization process in which the initially hot eh-pair loses energy by phonon

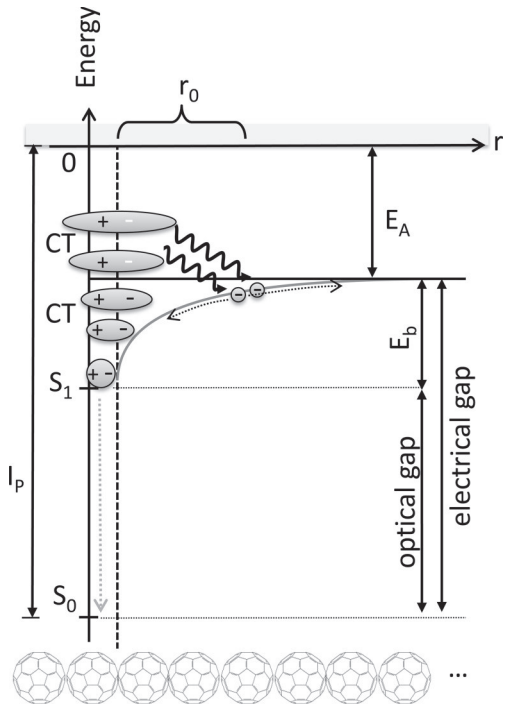

Figure 7. Schematic illustrating the process of eh-separation in a bulk fullerene phase as described in the text. I_p and E_a denote the ionization potential and electron affinity of the fullerene, and r_0 is the separation between the center of mass of the electron and hole wave functions after thermalization. Thermalization only occurs for CT states excited at energies exceeding that of the electrical gap.

emission. This process is well-known from work on molecular crystals.[54]

When fitting the experimental data for $E_{coul}(h\nu)$ asymptotically to $E_{coul}(h\nu) = E_g - h\nu$, we obtain an electrical gap of 2.45 ± 0.05 eV (Figure 6a). This is in good agreement with the value of 2.52 eV calculated by Shirley et al.[56] but in disagreement with the value of 2.98 eV reported by Kazaoui et al.[40] Since the energy of the singlet exciton in C_{60} is 1.85 eV, an electrical gap of 2.45 eV implies its binding energy is as large as 0.6 eV, at variance with ref 30. This means the intrinsic dissociation yield at 1.85 eV at room temperature is as low as 10^{-10}. The weak photocurrent we observed below a photon energy of 2.25 eV must therefore be of extrinsic origin, possibly caused by unidentified impurities with higher lying HOMO levels or by exciton dissociation at the electrode(s) under reverse bias.

The above value for E_g for C_{60} has to be compared to the value that can be derived from photoemission data. The value for ionization energies I_p of C_{60} in the gas phase is 7.59 eV.[57] Reported values of I_p for a C_{60} film are 6.4 ± 0.05 eV.[41−44] The difference between the gas phase values and the thin-film values is the polarization energy of a hole in solid C_{60}, P^+ = 1.2 ± 0.05 eV. Based upon the gas phase value for the electron affinity E_A = 2.65 eV[58] and assuming that the polarization energies of an electron and a hole in solid C_{60} are the same, the electron affinity in solid C_{60} should be about 3.65−3.75 eV. This would be consistent with the value inferred from cyclic voltammetry[6] and would predict an electrical gap of 2.65−2.75 eV. However, from both photoemission and inverse photoemission, Guan et al.[44] derived E_g = 2.37 eV. Given the uncertainties of the various techniques, we consider this consistent with our value of 2.45 eV.

DOI: 10.1021/acs.jpcc.6b08471
J. Phys. Chem. C 2016, 120, 25083−25091

For PCBM, the E_{coul} values above threshold are identical with those for C_{60}, which indicates that the spectral dependence of the photocurrent in C_{60} and PCBM is similar. This is plausible because photoemission experiments indicate that in PCBM both the HOMO and LUMO levels only experience an upward shift by 0.4−0.5 eV relative to those of C_{60}.[43] Therefore, the value of the band gap is retained.

The activation energies for photogeneration in C_{60} translates into the values for the intrapair eh-separation r_0 as a function of photon energy by $E_{coul} = \frac{e^2}{4\pi\varepsilon_r\varepsilon_0}\cdot\frac{1}{r_0}$. Figure 6b shows the data calculated using the value for the low frequency dielectric permittivity of $\varepsilon_r = 5$.[59] When the photon energy increases from 2.25 to 2.4 eV, r_0 increases approximately linearly. Above 2.4 eV the $r_0(h\nu)$ dependence becomes weaker. This is the spectral range in which thermalization occurs. Taking into account an experimental uncertainty of ±10%, there is no significant difference between differently prepared samples and between C_{60} and PCBM.

We now turn to the IQE at infinite electric field (IQE_{max}) (Figure 6c) that can be inferred from Onsager fits to the experimental $IQE(F,h\nu)$ plots. The IQE_{max} values of C_{60} increase with photon energy and reach, within experimental uncertainty, 100% at $h\nu = 3$ eV. This indicates that there is efficient coupling between the charge transfer states and charge transporting states, and that this coupling increases with quantum energy. Evidently, the coupling strength first rises strongly with photon energy for the CT states below the electrical gap, symbatic with the strong increase in the electron−hole separation. The weaker increase in coupling strength above the electrical gap mirrors the weaker increase in r_0. For PCBM, the coupling between the photoexcited CT states and the charge transporting states is weaker as evident by the significantly lower IQE_{max} values, even though the binding energy and electron−hole separation in the CT state in PCBM is comparable to C_{60}. We conjecture that this reflects a lesser coupling to the charge transporting states within the PCBM aggregates than within the C_{60} aggregates.

It is plausible that the coupling between two adjacent fullerenes is also reflected in the oscillator strength of the CT state absorptions. For example, in hexane solution, where charge transfer to an adjacent fullerene is not possible due to lack of neighbor, the CT state absorptions below 3 eV cannot be seen[60] while in solid C_{60} these transitions are well visible.[61,62] Similarly, the observed reduced oscillator strength of PCBM relative to C_{60} in the spectral range between 2.3 and 3 eV therefore also suggests a weaker coupling for charge transfer events.

The overall interpretation we present goes beyond the concept suggested by Kazaoui et al.[40] From electroabsorption (EA) spectroscopy, Kazaoui et al. observed that there is an increase of the transition dipole moment above 2.2 eV that is associated with a CT state at 2.43 eV, i.e., resonant with the value we identified for the electrical gap. At first glance, the observation of a discrete CT state appears incompatible with efficient autoionization over a spectral range from above 2.2 eV up to at least 3 eV. However, when modulating a broad absorption spectrum with oscillating electric field, an EA feature can only show up at the lower energy edge of the spectrum. This is reminiscent of a Franz-Keldysh effect on crystalline polydiacetylenes.[63] Therefore, there is indeed consistency between EA spectroscopy and photogeneration interpreted in terms of an Onsager process.

In passing, it appears noteworthy to comment on the different dependences of photogeneration on photon energy in a single phase system like C_{60} compared to a donor−acceptor type heterojunction. While the yield increases with photon energy in the single-phase C_{60}, it is usually observed to be constant in donor−acceptor type heterojunctions.[15] This difference reflects the different generation processes. In the single-phase C_{60} case, the dissociating entity is a short-lived CT state in the framework of the Onsager 1938 approach[52] with energies above the S_1 singlet state. In contrast, in a donor−acceptor type heterojunction, the cold CT state formed between donor and acceptor is the energetically lowest available state that is long-lived and that can make several attempts to fully ionize, as described in the framework of the Onsager-Braun model.[2]

In this context, it is interesting to consider the implication of our results for a donor−acceptor type system. Gelinas et al.[37] explained the observation that in PCDTBT/PCBM bulk heterojunction OCSs the dissociation of geminately bound electron pairs occurs with almost 100% efficiency by ultrafast charge separation through delocalized band-like states in fullerene aggregates. The current results on the spectrally dependent and field assisted photogeneration in C_{60} or PCBM indicate, however, that mean electron−hole separation in fullerenes is about 2.0−2.5 nm. Thus, the center of mass of the delocalized electron wave function is separated from the center of mass of the delocalized hole wave function by no more than about 2.5 nm.

The present results have an important bearing for the interpretation of bulk or planar heterojunction solar cells since they demonstrate that optical excitation of C_{60} or, to a lesser degree, PCBM in the form of clusters or solid films contributes to the overall yield of photogeneration above a photon energy of 2.25 eV (550 nm).[29,32] The photocurrent is therefore a sum of the contribution from dissociation of CT states at the donor−acceptor interface and the intrinsic photocurrent from the fullerene phase. The field dependences of both currents are different. Since the CT state in the bulk fullerene phase is more strongly bound than the CT state at the donor−acceptor interface, the additional current due to the fullerene clusters only saturates at much higher reverse voltages. This yields a higher short circuit current yet a reduced fill factor. These findings provide an alternative explanation to the observation that was recently reported by Tress and co-workers.[33]

5. CONCLUSIONS

The overall picture we obtain from our data on the photogeneration of charges in fullerene films is summarized in Figure 7. Between about 2.25 eV and the electrical gap at 2.45 eV, optical excitation creates charge transfer states. Their binding energies reduce with photon energy from 220 to 100 meV while the mean electron−hole separation r_0 within these CT states increases from 2.0 to 2.5 nm. They are ionized by thermal excitation to the electrical gap so that they can couple to charge transporting states, and the relation $E_g = h\nu + E_{coul}$ applies. For optical excitation exceeding the energy of the electrical gap, photogenerated CT states thermalize to a mean electron−hole distance r_0 that also increases with photon energy, albeit less strongly. Their binding energy, in the range of about 100 meV, also reduces only slightly with photon energy. The thermalized, i.e., cold, CT states, also dissociate by coupling to charge transporting states, again by thermal excitation. The ultimate internal quantum efficiency that can be obtained for infinite field strength depends on the strength of the coupling between

DOI: 10.1021/acs.jpcc.6b08471
J. Phys. Chem. C 2016, 120, 25083−25091

the CT states and the charge transporting states. We find this coupling is stronger for C_{60} than for PCBM.

■ ASSOCIATED CONTENT

Supporting Information

The Supporting Information is available free of charge on the ACS Publications website at DOI: 10.1021/acs.jpcc.6b08471.

$j(V)$ characteristics for monochromatic excitation at 2.7 eV. Synthesis and ^{1}H and ^{13}C NMR spectra of Ph-TDPP-Ph. Synthesis and ^{1}H NMR spectrum of PCDTBT$_{co}$. (PDF)

■ AUTHOR INFORMATION

Corresponding Author

*E-mail: Anna.Koehler@uni-bayreuth.de. Tel: +49 (0)921 55 2600.

Author Contributions

$^{\nabla}$Both authors contributed equally to this work.

Notes

The authors declare no competing financial interest.

■ ACKNOWLEDGMENTS

We acknowledge financial support by the Bavarian State Ministry of Science, Research, and the Arts through the Collaborative Research Network "Solar Technologies go Hybrid" and by the German Science Foundation DFG through the doctoral training center "GRK 1640". Satish Patil thanks the Department of Science and Technology, New Delhi, India for a Swarnajayanti fellowship. We thank Irene Bauer and Frank Schirmer for technical assistance.

■ REFERENCES

(1) Köhler, A.; Bässler, H. *Electronic Processes in Organic Semiconductors: An Introduction*; Wiley: New York, 2015.

(2) Braun, C. L. Electric-Field Assisted Dissociation of Charge-Transfer States as a Mechanism of Photocarrier Production. *J. Chem. Phys.* **1984**, *80*, 4157−4161.

(3) Vandewal, K.; Tvingstedt, K.; Gadisa, A.; Inganäs, O.; Manca, J. V. Relating the Open-Circuit Voltage to Interface Molecular Properties of Donor:Acceptor Bulk Heterojunction Solar Cells. *Phys. Rev. B: Condens. Matter Mater. Phys.* **2010**, *81*, 125204.

(4) Veldman, D.; Ipek, Ö.; Meskers, S. C. J.; Sweelssen, J.; Koetse, M. M.; Veenstra, S. C.; Kroon, J. M.; van Bavel, S. S.; Loos, J.; Janssen, R. A. J. Compositional and Electric Field Dependence of the Dissociation of Charge Transfer Excitons in Alternating Polyfluorene Copolymer/Fullerene Blends. *J. Am. Chem. Soc.* **2008**, *130*, 7721−7735.

(5) Provencher, F.; Sakowicz, M.; Brosseau, C. N.; Latini, G.; Beaupré, S.; Leclerc, M.; Reynolds, L. X.; Haque, S. A.; Leonelli, R.; Silva, C. Slow Geminate-Charge-Pair Recombination Dynamics at Polymer: Fullerene Heterojunctions in Efficient Organic Solar Cells. *J. Polym. Sci., Part B: Polym. Phys.* **2012**, *50*, 1395−1404.

(6) Faist, M. A.; Kirchartz, T.; Gong, W.; Ashraf, R. S.; McCulloch, I.; de Mello, J. C.; Ekins-Daukes, N. J.; Bradley, D. D. C.; Nelson, J. Competition between the Charge Transfer State and the Singlet States of Donor or Acceptor Limiting the Efficiency in Polymer:Fullerene Solar Cells. *J. Am. Chem. Soc.* **2012**, *134*, 685−692.

(7) Albrecht, S.; Vandewal, K.; Tumbleston, J. R.; Fischer, F. S. U.; Douglas, J. D.; Fréchet, J. M. J.; Ludwigs, S.; Ade, H.; Salleo, A.; Neher, D. On the Efficiency of Charge Transfer State Splitting in Polymer: Fullerene Solar Cells. *Adv. Mater.* **2014**, *26*, 2533−2539.

(8) Mendaza, A. D. D.; Melianas, A.; Rossbauer, S.; Bäcke, O.; Nordstierna, L.; Erhart, P.; Olsson, E.; Anthopoulos, T. D.; Inganäs, O.; Müller, C. High-Entropy Mixtures of Pristine Fullerenes for Solution-Processed Transistors and Solar Cells. *Adv. Mater.* **2015**, *27*, 7325−7331.

(9) Halls, J. J. M.; Cornil, J.; dos Santos, D. A.; Silbey, R.; Hwang, D. H.; Holmes, A. B.; Brédas, J. L.; Friend, R. H. Charge- and Energy-Transfer Processes at Polymer/Polymer Interfaces: A Joint Experimental and Theoretical Study. *Phys. Rev. B: Condens. Matter Mater. Phys.* **1999**, *60*, 5721−5727.

(10) Panda, P.; Veldman, D.; Sweelssen, J.; Bastiaansen, J. J. A. M.; Langeveld-Voss, B. M. W.; Meskers, S. C. J. Charge Transfer Absorption for π-Conjugated Polymers and Oligomers Mixed with Electron Acceptors. *J. Phys. Chem. B* **2007**, *111*, 5076−5081.

(11) Clarke, T. M.; Durrant, J. R. Charge Photogeneration in Organic Solar Cells. *Chem. Rev.* **2010**, *110*, 6736−6767.

(12) Servaites, J. D.; Ratner, M. A.; Marks, T. J. Organic Solar Cells: A New Look at Traditional Models. *Energy Environ. Sci.* **2011**, *4*, 4410−4422.

(13) Wiemer, M.; Koch, M.; Lemmer, U.; Pevtsov, A. B.; Baranovskii, S. D. Efficiency of Exciton Dissociation at Internal Organic Interfaces beyond Harmonic Approximation. *Org. Electron.* **2014**, *15*, 2461−2467.

(14) Kaake, L. G.; Zhong, C. M.; Love, J. A.; Nagao, I.; Bazan, G. C.; Nguyen, T. Q.; Huang, F.; Cao, Y.; Moses, D.; Heeger, A. J. Ultrafast Charge Generation in an Organic Bilayer Film. *J. Phys. Chem. Lett.* **2014**, *5*, 2000−2006.

(15) Vandewal, K.; Albrecht, S.; Hoke, E. T.; Graham, K. R.; Widmer, J.; Douglas, J. D.; Schubert, M.; Mateker, W. R.; Bloking, J. T.; Burkhard, G. F.; et al. Efficient Charge Generation by Relaxed Charge-Transfer States at Organic Interfaces. *Nat. Mater.* **2013**, *13*, 63−68.

(16) Few, S.; Frost, J. M.; Nelson, J. Models of Charge Pair Generation in Organic Solar Cells. *Phys. Chem. Chem. Phys.* **2015**, *17*, 2311−2325.

(17) Hendriks, K. H.; Wijpkema, A. S. G.; van Franeker, J. J.; Wienk, M. M.; Janssen, R. A. J. Dichotomous Role of Exciting the Donor or the Acceptor on Charge Generation in Organic Solar Cells. *J. Am. Chem. Soc.* **2016**, *138*, 10026−10031.

(18) Kurpiers, J.; Neher, D. Dispersive Non-Geminate Recombination in an Amorphous Polymer: Fullerene Blend. *Sci. Rep.* **2016**, *6*, 26832.

(19) Ran, N. A.; Love, J. A.; Takacs, C. J.; Sadhanala, A.; Beavers, J. K.; Collins, S. D.; Huang, Y.; Wang, M.; Friend, R. H.; Bazan, G. C.; et al. Harvesting the Full Potential of Photons with Organic Solar Cells. *Adv. Mater.* **2016**, *28*, 1482−1488.

(20) Bartesaghi, D.; Perez, I. D.; Kniepert, J.; Roland, S.; Turbiez, M.; Neher, D.; Koster, L. J. A. Competition between Recombination and Extraction of Free Charges Determines the Fill Factor of Organic Solar Cells. *Nat. Commun.* **2015**, *6*, 7083.

(21) Arkhipov, V. I.; Heremans, P.; Bässler, H. Why is Exciton Dissociation so Efficient at the Interface between a Conjugated Polymer and an Electron Acceptor? *Appl. Phys. Lett.* **2003**, *82*, 4605−4607.

(22) Deibel, C.; Strobel, T.; Dyakonov, V. Origin of the Efficient Polaron-Pair Dissociation in Polymer-Fullerene Blends. *Phys. Rev. Lett.* **2009**, *103*, 036402.

(23) Bakulin, A. A.; Rao, A.; Pavelyev, V. G.; van Loosdrecht, P. H. M.; Pshenichnikov, M. S.; Niedzialek, D.; Cornil, J.; Beljonne, D.; Friend, R. H. The Role of Driving Energy and Delocalized States for Charge Separation in Organic Semiconductors. *Science* **2012**, *335*, 1340−1344.

(24) Schwarz, C.; Tscheuschner, S.; Frisch, J.; Winkler, S.; Koch, N.; Bässler, H.; Köhler, A. Role of the Effective Mass and Interfacial Dipoles on Exciton Dissociation in Organic Donor-Acceptor Solar Cells. *Phys. Rev. B: Condens. Matter Mater. Phys.* **2013**, *87*, 155205.

(25) Niklas, J.; Mardis, K. L.; Banks, B. P.; Grooms, G. M.; Sperlich, A.; Dyakonov, V.; Beaupré, S.; Leclerc, M.; Xu, T.; Yu, L. P.; et al. Highly-Efficient Charge Separation and Polaron Delocalization in Polymer-Fullerene Bulk-Heterojunctions: A Comparative Multi-Frequency EPR and DFT Study. *Phys. Chem. Chem. Phys.* **2013**, *15*, 9562−9574.

(26) Bernardo, B.; Cheyns, D.; Verreet, B.; Schaller, R. D.; Rand, B. P.; Giebink, N. C. Delocalization and Dielectric Screening of Charge

Transfer States in Organic Photovoltaic Cells. *Nat. Commun.* **2014**, *5*, 3245.
(27) Tscheuschner, S.; Bässler, H.; Huber, K.; Köhler, A. A Combined Theoretical and Experimental Study of Dissociation of Charge Transfer States at the Donor-Acceptor Interface of Organic Solar Cells. *J. Phys. Chem. B* **2015**, *119*, 10359−10371.
(28) Im, C.; Tian, W.; Bässler, H.; Fechtenkötter, A.; Watson, M. D.; Müllen, K. Photoconduction in Organic Donor-Acceptor Systems. *J. Chem. Phys.* **2003**, *119*, 3952−3957.
(29) Burkhard, G. F.; Hoke, E. T.; Beiley, Z. M.; McGehee, M. D. Free Carrier Generation in Fullerene Acceptors and Its Effect on Polymer Photovoltaics. *J. Phys. Chem. C* **2012**, *116*, 26674−26678.
(30) Zou, Y. L.; Holmes, R. J. The Role of Exciton Ionization Processes in Bulk Heterojunction Organic Photovoltaic Cells. *Adv. Energy Mater.* **2015**, *5*, 1500019.
(31) Li, W. B.; Yu, H. M.; Zhang, J. W.; Yao, Y.; Wu, C. Q.; Hou, X. Y. Photoinduced Injection Enhancement in Fullerene-Based Organic Solar Cell Originates from Exciton-Electron Interaction. *J. Phys. Chem. C* **2014**, *118*, 11928−11934.
(32) Jeong, W. I.; Lee, Y. E.; Shim, H. S.; Kim, T. M.; Kim, S. Y.; Kim, J. J. Photoconductivity of C_{60} as an Origin of Bias-Dependent Photocurrent in Organic Photovoltaics. *Adv. Funct. Mater.* **2012**, *22*, 3089−3094.
(33) Tress, W.; Leo, K.; Riede, M. Photoconductivity as Loss Mechanism in Organic Solar Cells. *Phys. Status Solidi RRL* **2013**, *7*, 401−405.
(34) Mort, J.; Machonkin, M.; Ziolo, R.; Huffman, D. R.; Ferguson, M. I. Temperature-Dependence of Photoconductivity in Buckminsterfullerene Films. *Appl. Phys. Lett.* **1992**, *60*, 1735−1737.
(35) Jamieson, F. C.; Domingo, E. B.; McCarthy-Ward, T.; Heeney, M.; Stingelin, N.; Durrant, J. R. Fullerene Crystallisation as a Key Driver of Charge Separation in Polymer/Fullerene Bulk Heterojunction Solar Cells. *Chem. Sci.* **2012**, *3*, 485−492.
(36) Hedley, G. J.; Ward, A. J.; Alekseev, A.; Howells, C. T.; Martins, E. R.; Serrano, L. A.; Cooke, G.; Ruseckas, A.; Samuel, I. D. W. Determining the Optimum Morphology in High-Performance Polymer-Fullerene Organic Photovoltaic Cells. *Nat. Commun.* **2013**, *4*, 2867.
(37) Gelinas, S.; Rao, A.; Kumar, A.; Smith, S. L.; Chin, A. W.; Clark, J.; van der Poll, T. S.; Bazan, G. C.; Friend, R. H. Ultrafast Long-Range Charge Separation in Organic Semiconductor Photovoltaic Diodes. *Science* **2014**, *343*, 512−516.
(38) Mort, J.; Machonkin, M.; Chen, I.; Ziolo, R. Charge-Transfer Processes in Buckminsterfullerene Films. *Philos. Mag. Lett.* **1993**, *67*, 77−83.
(39) Mort, J.; Machonkin, M.; Ziolo, R.; Chen, I. Electronic Carrier Transport and Photogeneration in Buckminsterfullerene Films. *Appl. Phys. Lett.* **1992**, *61*, 1829−1831.
(40) Kazaoui, S.; Minami, N.; Tanabe, Y.; Byrne, H. J.; Eilmes, A.; Petelenz, P. Comprehensive Analysis of Intermolecular Charge-Transfer Excited States in C_{60} and C_{70} Films. *Phys. Rev. B: Condens. Matter Mater. Phys.* **1998**, *58*, 7689−7700.
(41) Seo, J. H.; Kang, S. J.; Kim, C. Y.; Cho, S. W.; Yoo, K. H.; Whang, C. N. Energy Level Alignment between C_{60} and Al Using Ultraviolet Photoelectron Spectroscopy. *Appl. Surf. Sci.* **2006**, *252*, 8015−8017.
(42) Niederhausen, J.; Amsalem, P.; Wilke, A.; Schlesinger, R.; Winkler, S.; Vollmer, A.; Rabe, J. P.; Koch, N. Doping of C_{60} (Sub)Monolayers by Fermi-Level Pinning Induced Electron Transfer. *Phys. Rev. B: Condens. Matter Mater. Phys.* **2012**, *86*, 081411.
(43) Akaike, K.; Kanai, K.; Yoshida, H.; Tsutsumi, J.; Nishi, T.; Sato, N.; Ouchi, Y.; Seki, K. Ultraviolet Photoelectron Spectroscopy and Inverse Photoemission Spectroscopy of [6,6]-Phenyl-C_{61}-butyric Acid Methyl Ester in Gas and Solid Phases. *J. Appl. Phys.* **2008**, *104*, 023710.
(44) Guan, Z. L.; Kim, J. B.; Wang, H.; Jaye, C.; Fischer, D. A.; Loo, Y. L.; Kahn, A. Direct Determination of the Electronic Structure of the Poly(3-hexylthiophene):phenyl-[6,6]-C_{61} Butyric Acid Methyl Ester Blend. *Org. Electron.* **2010**, *11*, 1779−1785.
(45) Kalinowski, J.; Giro, G.; Camaioni, N.; Fattori, V.; DiMarco, P. Photoconduction in Solid Films of C_{60}. *Synth. Met.* **1996**, *77*, 181−188.
(46) Schwarz, C.; Bässler, H.; Bauer, I.; Koenen, J. M.; Preis, E.; Scherf, U.; Köhler, A. Does Conjugation Help Exciton Dissociation? A Study on Poly(p-phenylene)s in Planar Heterojunctions with C_{60} or TNF. *Adv. Mater.* **2012**, *24*, 922−925.
(47) Burkhard, G. F.; Hoke, E. T.; McGehee, M. D. Accounting for Interference, Scattering, and Electrode Absorption to Make Accurate Internal Quantum Efficiency Measurements in Organic and Other Thin Solar Cells. *Adv. Mater.* **2010**, *22*, 3293−3297.
(48) Pettersson, L. A. A.; Roman, L. S.; Inganäs, O. Modeling Photocurrent Action Spectra of Photovoltaic Devices Based on Organic Thin Films. *J. Appl. Phys.* **1999**, *86*, 487−496.
(49) Peumans, P.; Yakimov, A.; Forrest, S. R. Small Molecular Weight Organic Thin-Film Photodetectors and Solar Cells. *J. Appl. Phys.* **2003**, *93*, 3693−3723.
(50) Wynands, D.; Erber, M.; Rentenberger, R.; Levichkova, M.; Walzer, K.; Eichhorn, K. J.; Stamm, M. Spectroscopic Ellipsometry Characterization of Vacuum-Deposited Organic Films for the Application in Organic Solar Cells. *Org. Electron.* **2012**, *13*, 885−893.
(51) Hahn, T.; Geiger, J.; Blase, X.; Duchemin, I.; Niedzialek, D.; Tscheuschner, S.; Beljonne, D.; Bässler, H.; Köhler, A. Does Excess Energy Assist Photogeneration in an Organic Low-Bandgap Solar Cell? *Adv. Funct. Mater.* **2015**, *25*, 1287−1295.
(52) Onsager, L. Initial Recombination of Ions. *Phys. Rev.* **1938**, *54*, 554.
(53) Pai, D. M.; Enck, R. C. Onsager Mechanism of Photogeneration in Amorphous Selenium. *Phys. Rev. B* **1975**, *11*, 5163−5174.
(54) Chance, R. R.; Braun, C. L. Temperature-Dependence of Intrinsic Carrier Generation in Anthracene Single-Crystals. *J. Chem. Phys.* **1976**, *64*, 3573−3581.
(55) Borsenberger, P. M.; Weiss, D. S. *Organic Photoreceptors for Imaging Systems*; Taylor and Francis: London, 1993.
(56) Shirley, E. L.; Benedict, L. X.; Louie, S. G. Excitons in Solid C_{60}. *Phys. Rev. B: Condens. Matter Mater. Phys.* **1996**, *54*, 10970−10977.
(57) Steger, H.; Holzapfel, J.; Hielscher, A.; Kamke, W.; Hertel, I. V. Single-Photon Ionization of Higher Fullerenes C_{76}, C_{78} and C_{84} - Determination of Ionization-Potentials. *Chem. Phys. Lett.* **1995**, *234*, 455−459.
(58) Wang, L. S.; Conceicao, J.; Jin, C. M.; Smalley, R. E. Threshold Photodetachment of Cold C_{60}^-. *Chem. Phys. Lett.* **1991**, *182*, 5−11.
(59) Chern, G.; Mathias, H.; Testardi, L. R.; Seger, L.; Schlenoff, J. Low-Frequency Dielectric Permittivity of C_{60}. *J. Supercond.* **1995**, *8*, 207−210.
(60) Leach, S.; Vervloet, M.; Desprès, A.; Bréheret, E.; Hare, J. P.; Dennis, T. J.; Kroto, H. W.; Taylor, R.; Walton, D. R. M. Electronic-Spectra and Transitions of the Fullerene C_{60}. *Chem. Phys.* **1992**, *160*, 451−466.
(61) Kazaoui, S.; Ross, R.; Minami, N. In-Situ Photoconductivity Behavior of C_{60} Thin-Films - Wavelength, Temperature, Oxygen Effect. *Solid State Commun.* **1994**, *90*, 623−628.
(62) Pac, B.; Petelenz, P.; Eilmes, A.; Munn, R. W. Charge-Transfer Exciton Band Structure in the Fullerene Crystal-Model Calculations. *J. Chem. Phys.* **1998**, *109*, 7923−7931.
(63) Weiser, G. Stark-Effect of One-Dimensional Wannier Excitons in Polydiacetylene Single-Crystals. *Phys. Rev. B: Condens. Matter Mater. Phys.* **1992**, *45*, 14076−14085.

DOI: 10.1021/acs.jpcc.6b08471
J. Phys. Chem. C 2016, 120, 25083−25091

Supporting Information:

Role of Intrinsic Photogeneration in Single Layer and Bilayer Solar Cells with C_{60} and PCBM

Tobias Hahn[1,+] & Steffen Tscheuschner[1,+], Christina Saller[2], Peter Strohriegl[2,5], Puttaraju Boregowda[3], Tushita Mukhopadhyay[3], Satish Patil[3], Dieter Neher[4] , Heinz Bässler[5], Anna Köhler[1,5]*

[1] Experimental Physics II, University of Bayreuth, 95440 Bayreuth, Germany

[2] Macromolecular Chemistry I, University of Bayreuth, 95440 Bayreuth, Germany

[3] Solid State and Structural Chemistry Unit, Indian Institute of Science, Bangalore, 560012

[4] Institute for Physics and Astronomy, University of Potsdam, 14476 Potsdam-Golm, Germany

[5] Bayreuth Institute of Macromolecular Science (BIMF), University of Bayreuth, 95440 Bayreuth, Germany

[+] Both authors contributed equally to this work

* Anna.Koehler@uni-bayreuth.de; Tel: +49 (0)921 55 2600

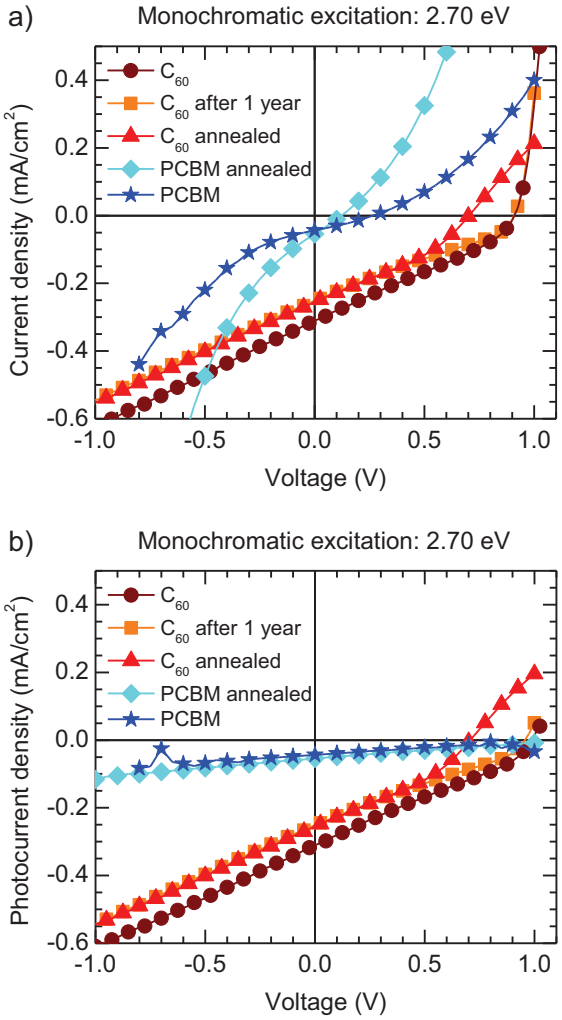

Figure S1: (a) Current and (b) Photocurrent (= Current minus Darkcurrent) for a C_{60}-only device measured immediately (wine circles), a C_{60}-only device stored in a nitrogen glovebox for one year (orange squares), a C_{60}-only device annealed at 140°C for 26 hours under nitrogen (red triangles), a PCBM-only device annealed at 140°C for 30 min and afterwards cooled down to 60°C in a time range of 30 min (cyan diamonds) and for a PCBM-only device which was not annealed and measured as cast (blue stars).

Synthesis of 2,5-bis(2-octyldodecyl)-3,6-bis(5-phenylthiophen-2-yl)pyrrolo[3,4-c]pyrrole-1,4(2H,5H)-dione (Ph-TDPP-Ph)

A mixture of phenylboronic acid (0.079 g, 0.64 mmol) and potassium carbonate (0.089 g, 0.64 mmol) in toluene/ethanol (3:1, 60 mL) was stirred at 50°C for 30 min. Then the compound 3,6-bis(5-bromothiophen-2-yl)-2,5-bis(2-octyldodecyl)pyrrolo[3,4-c]pyrrole-1,4(*2H,5H*)-dione (0.3 g, 0.29 mmol) was added in one portion, the reaction mixture was heated at 110°C for 12 h and then cooled to room temperature. Dichloromethane (100 mL) and water (200 mL) were added and the layers separated. The organic layer was concentrated *in vacuo*. Further purification was carried out by column chromatography on silica gel eluting with hexane/ethyl acetate (5%) to give the compound Ph-TDPP-Ph as a dark blue solid (0.22 g, 75%). ^{1}H NMR (400 MHz, $CDCl_3$), δ = 8.94 (d, *J* = 8 Hz, 2H), 7.67 (dd, *J* = 8.5, 1.3 Hz, 4H), 7.45 (d, *J* = 4.2 Hz, 3H), 7.44 – 7.39 (m, 4H), 7.35 – 7.37 (m, *J* = 7.5 Hz, 1H), 4.06 (d, *J* = 4 Hz, 4H), 1.98 – 2.00 (m, 2H), 1.19 – 1.34 (m, 62H), 0.81 – 0.86 (m, 12H) ppm. ^{13}C NMR (100 MHz, $CDCl_3$) δ 161.82, 149.69, 139.98, 136.84, 133.28, 129.23, 128.92, 126.20, 124.52, 108.28, 46.38, 37.99, 32.01, 31.98, 29.76, 29.74, 29.45, 29.40, 22.78, 22.75, 14.22, 14.21 ppm. ESI-MS calculated for $C_{66}H_{96}N_2O_2S_2$: *m/z*: 1012.69; found: 1014.12.

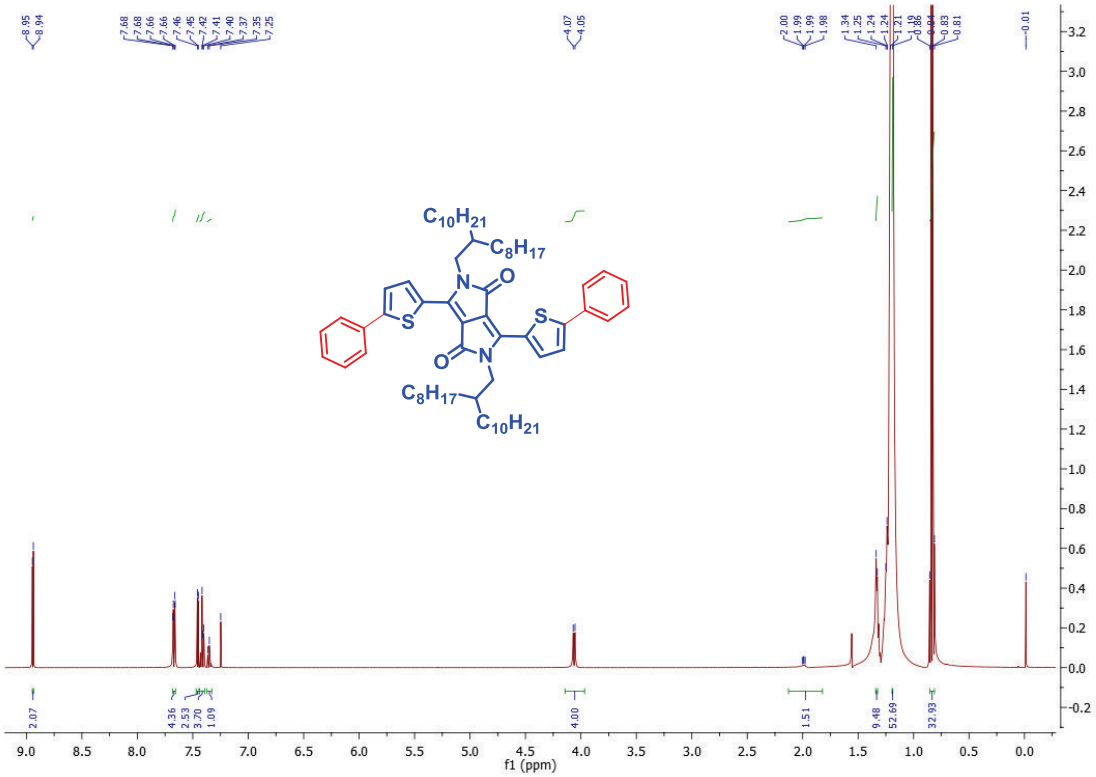

Figure S2: ^{1}H NMR spectrum of Ph-TDPP-Ph

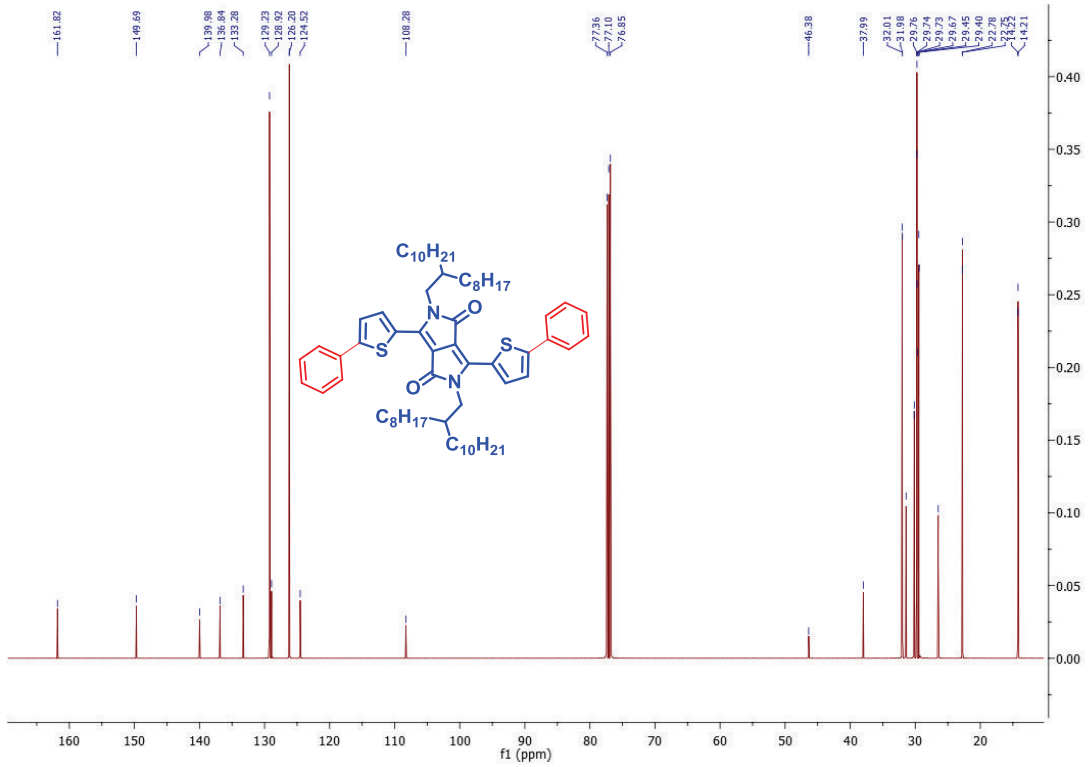

Figure S3: ^{13}C NMR specrum of Ph-TDPP-Ph

Synthesis of the polymer PCDTBT$_{co}$

PCDTBT$_{co}$ (poly[(*N*-heptadecan-9'-yl)-2,7-carbazole-*alt*-5,5-(4',7'-bis(thien-2-yl)-2',1',3'-benzothiadiazole)]$_{0.7}$-*stat*-[*N*,*N'*-bis(4-methylphenyl)-*N*,*N'*-diphenylbenzidine-*alt*-5,5-(4',7'-bis(thien-2-yl)-2',1',3'-benzothiadiazole)]$_{0.3}$) was synthesized via Suzuki coupling according to the following procedure. The molar ratio of the carbazole, the phenyl-substituted benzidine, and the bisthienyl-benzothiadiazole units in PCDTBT$_{co}$ is 0.7:0.3:1.

A Schlenk flask was charged with the monomers 2,7-bis-(4',4',5',5'-tetramethyl-1',3',2'-dioxaborolan-2'-yl)-*N*-(heptadecan-9''-yl)-carbazole (0.368 g, 0.560 mmol), *N*,*N'*-bis(4-methylphenyl)-*N*,*N'*-bis((4',4',5',5'-tetramethyl-1',3',2'-dioxaborolan-2'-yl)phenyl)-benzidine (0.184 g, 0.239 mmol), 4,7-bis(5'-bromo-thien-2'-yl)-2,1,3-benzothiadiazole (0.367 g, 0.800 mmol) and 12 mL of toluene under argon. One drop of Aliquat 336 and 20 mL of 2 M Na_2CO_3 solution were added and the mixture was degassed by three freeze-thaw cycles. Afterwards, 14 mg of tetrakis(triphenylphosphine)palladium(0) were added and followed by again three freeze-thaw cycles. The reaction mixture was then stirred under reflux in an argon atmosphere for 90 h before bromobenzene (0.126 g, 0.800 mmol) was added. After 2 h, phenylboronic acid (0.098 g, 0.800 mmol) was added and the reaction mixture was again refluxed overnight. The reaction mixture was allowed to cool to room temperature and the polymer was precipitated into methanol/water (10:1). Soxhlet extraction was carried out using acetone and toluene. The reduced toluene fraction was precipitated into methanol/water (10:1) and dried in vacuum overnight, yielding 0.163 g (28 %) of PCDTBT$_{co}$ as a dark-red powder. A molecular weight of 45,000 gmol^{-1} (M_w) and 31,000 gmol^{-1} (M_n) was determined by high temperature polymer size exclusion chromatography in trichlorobenzene at 160°C with a polydispersity index of 1.44.

^{1}H NMR (300 MHz, $C_2D_2Cl_4$, 120 °C): δ = 0.66-0.91 (m, CH_3), 0.93 - 1.49 (m, CH_2), 2.08 (br, carbazole-CH_2), 2.22 - 2.48 (m, benzidine-CH_3, carbazole-CH_2), 4.67 (br, CH), 6.76 - 8.27 (m, ar-CH). Broadened and multiple signals are due to atropisomerism. From the integration of the signal for the CH_2 group in the swallow-tail spacer of the carbazole unit (2.08 ppm) and the combined signal for the methyl group in the benzidine units and the other CH_2 group in the carbazole spacer (2.22 - 2.48 ppm), a molar ratio of 0.7:0.3:1 was calculated.

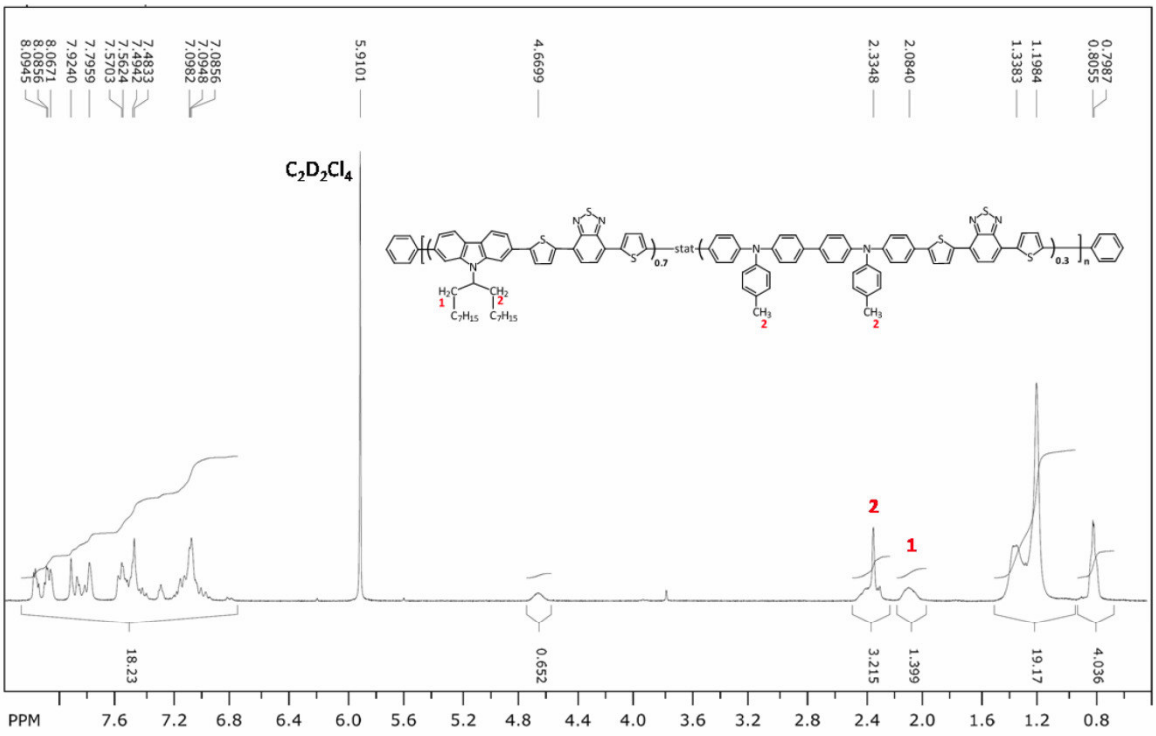

Figure S4: ^{1}H NMR spectrum of PCDTBT$_{co}$ (300 MHz) in $C_2D_2Cl_4$ at 120 °C for the calculation of the molar ratio.

4.4. Does Excess Energy Assist Photogeneration in an Organic Low-Bandgap Solar Cell?

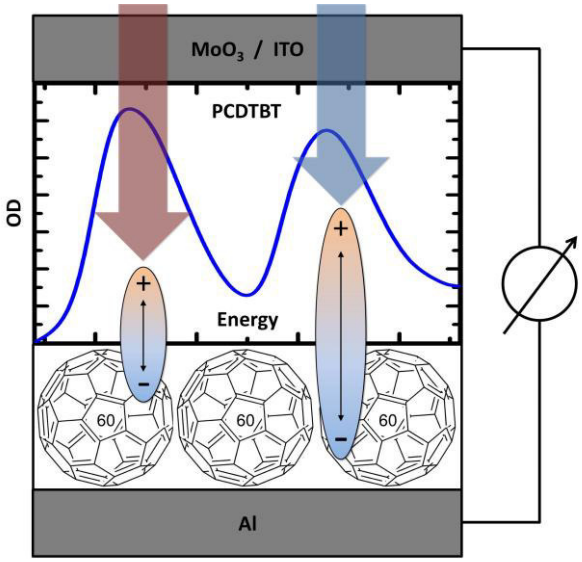

Tobias Hahn , Johannes Geiger , Xavier Blase , Ivan Duchemin , Dorota Niedzialek , Steffen Tscheuschner , David Beljonne , Heinz Bässler , and Anna Köhler

Veröffentlicht in

Advanced Functional Materials (**2015**), 25, 1287–1295

(DOI: https://doi.org/10.1002/adfm.201403784)

ADVANCED FUNCTIONAL MATERIALS
www.afm-journal.de

Does Excess Energy Assist Photogeneration in an Organic Low-Bandgap Solar Cell?

*Tobias Hahn, Johannes Geiger, Xavier Blase, Ivan Duchemin, Dorota Niedzialek, Steffen Tscheuschner, David Beljonne, Heinz Bässler, and Anna Köhler**

The field dependence of the photocurrent in a bilayer assembly is measured with the aim to clarify the role of excess photon energy in an organic solar cell comprising a polymeric donor and an acceptor. Upon optical excitation of the donor an electron is transferred to the acceptor forming a Coulomb-bound electron–hole pair. Since the subsequent escape is a field assisted process it follows that photogeneration saturates at higher electric fields, the saturation field being a measure of the separation of the electron–hole pair. Using the low bandgap polymers, PCDTBT and PCPDTBT, as donors and C_{60} as acceptor in a bilayer assembly it is found that the saturation field decreases when the photon energy is roughly 0.5 eV above the S_1–S_0 0–0 transition of the donor. This translates into an increase of the size of the electron-hole-pair up to about 13 nm which is close to the Coulomb capture radius. This increase correlates with the onset of higher electronic states that have a highly delocalized character, as confirmed by quantum-chemical calculations. This demonstrates that accessing higher electronic states does favor photogeneration yet excess vibrational energy plays no role. Experiments on intrinsic photogeneration in donor photodiodes without acceptors support this reasoning.

1. Introduction

In an organic photovoltaic cell (OPV) the conversion of an optically excited state to a pair of charge carriers is thought to be a multistep process. An electron of the optically excited donor is first transferred to an acceptor with lower lying LUMO (lowest unoccupied molecular orbital) thereby forming a Coulomb-bound electron–hole pair.[1–9] That pair has to escape from the mutual Coulomb potential. While this notion is by now firmly established, the mechanism by which the pair is liberated is heavily debated. It is obvious that in an OPV cell with high quantum efficiency the initial pair must be fairly expanded so that the Coulomb binding energy is small. How can this be accomplished? One possibility is that the excess energy that is dissipated when the excited electron of the donor is transferred to the acceptor is at least partially converted to kinetic energy. This would help generating a weakly bound electron–hole pair. If so, a large energy difference between the LUMOs of donor and acceptor would be of advantage. On the other hand, any energy dissipating process lowers the power efficiency of the cell. Therefore, an optimization of the energy difference between donor and acceptor LUMO is required. Indeed, experimental results seem to corroborate this notion.[10,11] The question is, though, how conclusive this reasoning is.

At this stage it is helpful to recall how the photogeneration of charge carriers in molecular crystals occurs. It had been firmly established that within the spectral regime of the first singlet transition (S_1–S_0) photogeneration is of extrinsic origin, caused by either exciton dissociation at an electrode or at sensitizing impurities. The pioneering work of Chance and Braun[12] and Geacintov and Pope[13] showed that—except for some dissociation of charge–transfer states—intrinsic photogeneration is due to autoionization of higher electronic states of the crystal. Remarkably, for molecular crystals such as anthracene, the photogeneration yield is constant within the spectral range of the S_2–S_0 transition. It does not increase until the S_3–S_0 transition is reached and it saturates again at higher photon energies. This is a clear indication that excess energy of the autoionizing state is helpful, yet that it is the *electronic* excess energy of S_2 and S_3 excitations relative to S_1 exciton that matters rather than any *vibrational* energy coupled to an S_1 exciton. From an analysis of the temperature and field dependence of the photocarrier yield one learns that the autoionization process generates an electron–hole pair with an intrapair separation r_0 = 3–5 nm depending on the kind of electronic excitation. That pair can either fully dissociate in the course on an Onsager-type diffusive random walk

T. Hahn, J. Geiger, S. Tscheuschner,
Prof. H. Bässler, Prof. A. Köhler
Bayreuth Institute of Macromolecular Research (BMBF)
University of Bayreuth
95440 Bayreuth, Germany
E-mail: Anna.Koehler@uni-bayreuth.de
T. Hahn, J. Geiger, S. Tscheuschner, Prof. A. Köhler
Experimental Physics II
University of Bayreuth
95440, Bayreuth, Germany
Dr. X. Blase
CNRS and Grenoble-Alpes University
Inst. NEEL, F-38042 Grenoble, France
Dr. I. Duchemin
INAC, SP2M/L sim
CEA and Grenoble-Alpes University
Cedex 09, 38054 Grenoble, France
Dr. D. Niedzialek,[+] Dr. D. Beljonne
University of Mons
Place du Parc 20
7000 Mons, Belgium
[+]Present address: Experimental Solid State Physics Group, The Blackett Laboratory, Imperial College, Prince Consort Road, London SW7 2BZ, UK

DOI: 10.1002/adfm.201403784

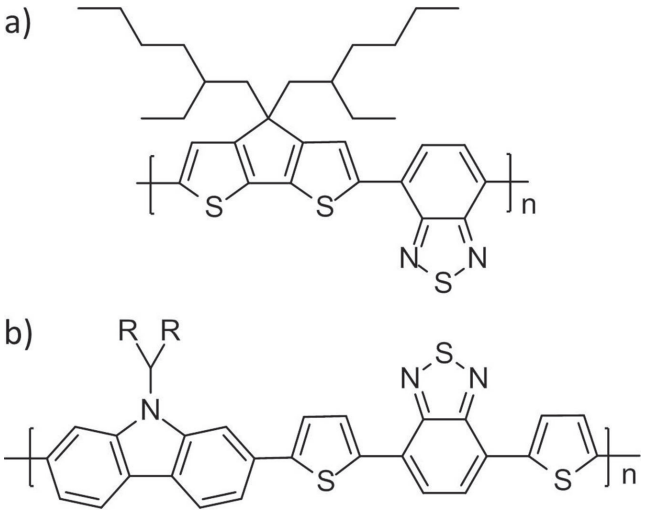

Figure 1. Chemical structures of a) PCPDTBT and b) PCDTBT. R=C_8H_{17}.

or recombine geminately. Photoionization in conjugated polymers is consistent with this notion. In films of MEH-PPV[14,15] and MeLPPP[16] onset of intrinsic photogeneration is coincident with the origin of the S_2–S_0 transition, i.e., energetically above the estimated electrical gap. Confirmed by quantum chemical calculations[14] this proves that it is the spatial extension of the wavefunction of the excited state that determines the yield of dissociation of an excited state.

From this perspective we shall address the question regarding the importance of the excess photon energy on photogeneration in a donor–acceptor OPV cell. Employing ultrafast pump–probe spectroscopy on OPV cell with CuPc as electron donor and C_{60}/C_{70} as an acceptor Jailaubekov et al.[17] showed that within an photon energy range of 1.85–2.10 eV excess vibrational energy has little effect on the yield of formation of primary electron–hole pairs. On the other hand, Grancini et al.[18] studied the evolution of electron–hole pairs in a high efficiency OPV cell with PCPDTBT–PCBM as a donor–acceptor pair (see **Figure 1** for the chemical structure of PCPDTBT. PCBM is a fullerene-derivative). They found that the appearance time of the electron–hole pair decreases from 50 to 20 fs when increasing the photon energy from 1.65 to 2.55 eV and attributed this to hot exciton dissociation. Quantum-chemical calculations indicate that in this spectral range there are several excited states that differ regarding the degree of mixing of exciton and CT states. At first sight one would conjecture that the dissociation yield of those different precursor states is also different. However, this notion has been challenged recently. Vandewal et al.[19] found that it does not matter if the primary photons excite the donor, the acceptor or a charge–transfer state. Obviously, there is need for further clarifying work.

In this work we study the field dependence of photogeneration in bilayers of PCPDTBT and PCDTBT with C_{60} as an electron acceptor. The reason for choosing bilayers is that in bilayers the liberated electrons and holes are confined to the acceptor and donor compartments of the diode. Therefore, bimolecular recombination is greatly reduced and the field dependence of the photocurrent under reverse bias is predominately controlled by the charge generation process, i.e., the dissociation of the initially generated electron–hole pair. The yield of pair dissociation saturates at higher fields with the saturation field being determined by the balance between the Coulomb binding energy of the electron–hole pair and the gain of the electrostatic potential due to the applied field. The larger the electron–hole separation of the pair is the lower will be the saturation field that compensates the Coulomb energy. From previous work we know that the saturation field decreases as a function of the effective conjugation length of the polymer chain.[7] This is a plausible result because a large effective conjugation length should facilitate the formation of more loosely bound electron–hole pairs that are easier to completely dissociate. It is straightforward to investigate whether or not an excess energy of the primary excitation has an effect on the size of the dissociating electron–hole pair, monitored via a change of the saturation field as a function of photon energy. Our results will substantiate the notion that excess energy does assist the dissociation of geminately bound electron–hole pair. Importantly, it is the extra electronic rather than vibrational energy associated with a vibronic Franck–Condon state that matters. To substantiate this conclusion we also studied intrinsic photogeneration in single layer PCPDTBT diodes. We find that in PCPDTBT intrinsic photodissociation—albeit inefficient—also increases with excess photon energy. This confirms the conclusion derived from classic molecular crystal work that indicates that it is the extent of the wavefunction function of the donor phase that determines the size of a geminate electron–hole pair and, concomitantly, its subsequent dissociation.

2. Experimental and Theoretical Methods

The low bandgap polymer PCDTBT was synthesized according to the procedure described by Leclerc and co-workers[20] while PCPDTBT was purchased from Sigma-Aldrich. For photocurrent measurements on bilayer assemblies we prepared solar cells. For this, we used patterned ITO substrates that were additionally structured with photoresist in a way to allow for the application homogeneous electric fields up to 1 MV cm^{-1} without risking spurious breakdown effects near the electrode edges.[7] In order to reduce the dark current in the device a 15 nm thick MoO_3 layer (Sigma-Aldrich) was vapor deposited on top of the patterned ITO using a shadow-mask. Afterward, the donor polymer PCPDTBT or PCDTBT is spin-coated from chlorobenzene solution to yield films with a typical thickness of 30 nm. Subsequently, a 30 nm thick layer of C_{60} (American Dye Source Inc.) as acceptor was vapor deposited. Aluminum was vapor deposited as top electrode. The entire device fabrication was done in a glovebox filled with nitrogen atmosphere.

Current–voltage characteristics of the bilayer devices were measured under vacuum at room temperature under variable monochromatic illumination from a 450 W Xenon lamp within a photon energy range between 1.5 to 3.5 eV using a Keithley source–measure unit. The internal electric field was calculated as $F = -(V - V_{oc})/d$ where V is the applied external voltage, V_{oc} is the open circuit voltage determined for each excitation wavelength, and d is the thickness of the polymer-acceptor bilayer. Exemplary current–voltage curves are shown in the Supporting Information.

Finally, the present experimental analyses are corroborated by accurate ab initio Green's function many-body perturbation

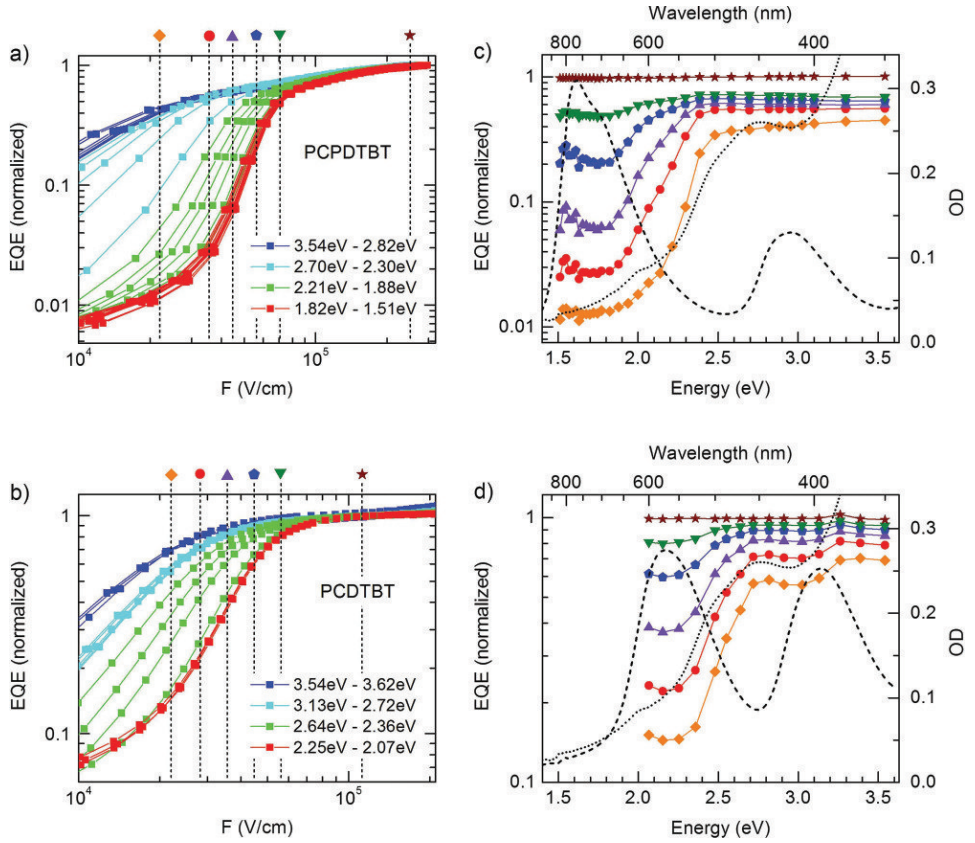

Figure 2. External quantum efficiency (EQE) of the donor–acceptor solar cell, normalized to unity at the saturation field, for a) PCPDTBT and b) PCDTBT parametric in photon energy. On the right side the normalized EQE is shown for a specific field as a function of photon energy (cut through the EQE-curves on the left side, tagged by the dashed line). This is done for several field strengths for c) PCPDTBT and d) PCDTBT. The symbols on the top axis in (a,b) indicate the specific field strength for the corresponding normalized EQE curves in (c,d). On the right ordinate in (c), the optical density of C_{60} (30 nm) (dotted line) and PCPDTBT (30 nm) (dashed line) or PCDTBT (30 nm) (dashed line) are shown.

theory calculations within the framework of the so-called GW and Bethe–Salpeter formalisms,[21] focusing on hot excitations for a model PCBM/PCDTBT complex. The present GW/BSE approach has been recently shown by several groups to describe both localized (Frenkel) and charge–transfer (CT) excitations in excellent agreement with available experimental data or high-level multideterminantal quantum chemistry calculations.[22–25] Our calculations are performed with a large triple-zeta and double-polarization (Gaussian) TZ2P basis using a resolution-of-the-identity approach for the description of the Coulomb integrals and follow a recent study of the low lying excitations in PCBM-polymer complexes where a close agreement between the present Bethe–Salpeter calculations and optimized range-separated hybrids (BNL) TDDFT calculations was observed.[26]

3. Results

The essential information on the role of the photon energy in the photodissociation process in a bilayer diode with PCDTBT and PCPDTBT as donor materials will be inferred from the dependence of the stationary photocurrent as a function of the electric field acting on the geminate electron–hole pair excited and on the photon energy. Since in our diodes the parasitic dark currents are less than 1% of the total current, the latter is identified with the photocurrent. To calculate the field dependence of the yield of photogeneration one has to correct the applied electric field for the built-in field V_{oc}/d where V_{oc} is the open-circuit voltage. V_{oc} is the voltage at which the dissociation and recombination of electron–hole pairs generated at the donor–acceptor interface under zero field electric are exactly balanced thus resulting in a net current of zero. The concentration of those electron–hole pairs depends on their generation rate, i.e., on the light intensity, the optical density of the absorber, and the emission spectrum of the light source, yielding a logarithmic dependence of V_{oc} on the electron–hole pair generation rate.[27,28] For this reason we consider in the following V_{oc} as an experimentally determined input parameter for the individual current–voltage curves parametric in photon quantum energy under reverse bias condition. In the absence of bimolecular recombination the photocurrent then reflects photogeneration in the bilayers as a function of the internal electric field $F = -(V - V_{oc})/d$, and photon energy. The external quantum efficiencies (EQE), i.e., the photocurrent $j(F)$ normalized to the incident light intensity, for a PCPDTBT and a PCDTBT cell with C_{60} as an acceptor as a function of electric field are shown in **Figure 2**a,b. The related dependencies of the EQE as a function of photon energy for different fields

are shown in Figure 2c,d in which the separate optical densities of the donor layers and the C_{60} layer are included. It turns out that EQE characteristics shift to lower values of the electric field with increasing photon energy and feature a saturation effect. It translates into an increase of EQE in the low photon energy range upon raising the electric field. In the case of PCDTBT the increase of EQE with photon energy matches more or less the increase of the OD of the C_{60} layer while for PCPDTBT that increase occurs at lower photon energies already. This is consistent with the bathochromic shift of the absorption spectrum. It is remarkable that—depending on photon energy—EQE(F) can saturate at electric fields F below the build-in field V_{oc}/d which is on the order of 10^5 V cm^{-1} for donor–acceptor thickness of 60 nm and a typical V_{oc} of 0.5–0.8 eV. The saturation field F_{sat} can operationally be determined from the intersection of the tangents to the photocurrent below and above saturation. A plot of the saturation field with photon energy is shown in **Figure 3**. From Figures 2 and 3 it is evident that the field dependence reduces with increasing photon energy.

Complementary to experiments on bilayers we also measured the photocurrent normalized to the number of absorbed photons, i.e. the internal quantum efficiency generation (IQE), in single layer PCPDTBT and PCDTBT diodes, without the C_{60} electron acceptor (**Figure 4**a,b). As expected, the photocurrent is typically two orders of magnitude lower than in bilayers and no saturation is observed at fields up to 8×10^5 V cm^{-1} (**Figure 5**). Obviously, in single layer devices the dissociating electron–hole pairs are more strongly Coulombic bound than those in bilayers diodes but, importantly, at a given electric field the yield also increases with photon energy in a similar fashion as we found with bilayers (Figure 2). For reference, the EQE and donor absorption of the cells presented in Figure 4 are shown in the Supporting Information.

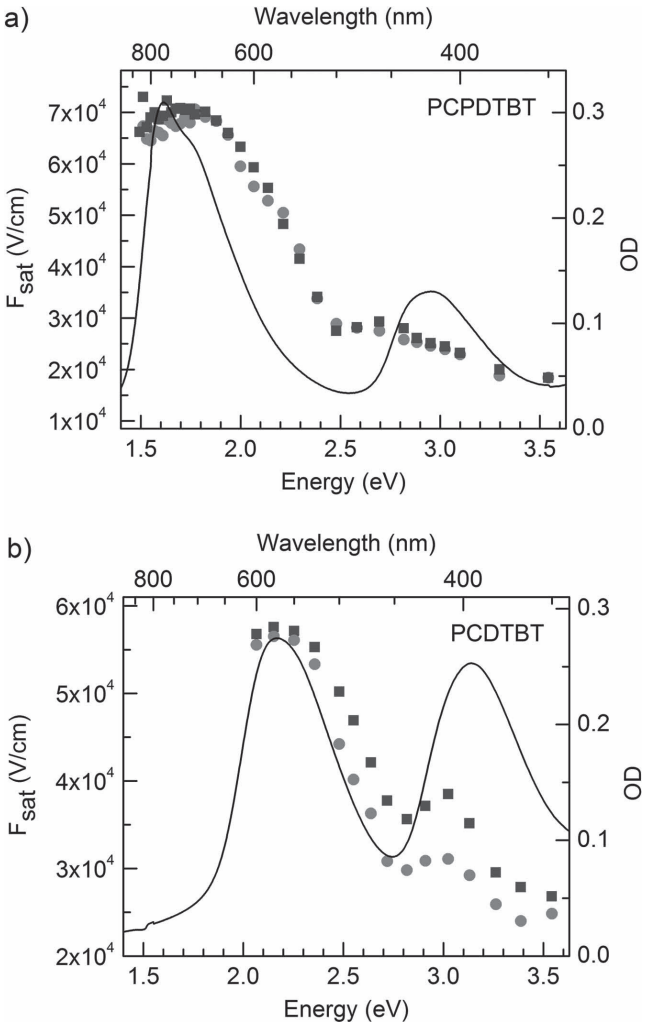

Figure 3. Saturation field F_{sat} as a function of photon energy in donor–acceptor solar cells with C_{60} as acceptor for a) PCPDTBT and b) PCDTBT. Data are shown for several solar cells. The black line indicates the donor absorption.

4. Discussion

4.1. Donor–Acceptor Bilayers: Experiment

In both, single layer cells as well as in donor–acceptor bilayers the photocurrent originates from the dissociation of geminate electron–hole pairs against their Coulomb binding energy. In bilayers, the energetic off-set between the LUMOs and HOMOs of donor and acceptor assists the dissociation process, while in a single layer diode this additional contribution is absent. As a result, the yield of intrinsic photogeneration in a single layer diode is much lower than in a bilayer diode and is often controlled by sensitization due to inadvertent impurities or by exciton-induced charge injection from the electrodes. A measure of how strong or weak an electron–hole pair is Coulomb bound is the electric field strength F_{sat}, at which a photocurrent saturates. Photocurrent saturation occurs when the Coulomb energy of the dissociating electron–hole pair

$$eV_{Coulomb} = \frac{e^2}{4\pi\epsilon_0\epsilon_r} \cdot \frac{1}{r_0} \quad (1)$$

with an initial intrapair separation r_0 is compensated by the applied potential $eF_{sat} \cdot r_0$, i.e.,

$$r_0 = \sqrt{\frac{e}{4\pi\epsilon_0\epsilon_r} \cdot \frac{1}{F_{sat}}} \quad (2)$$

The saturation field is, thus, a measure of the "size" of the electron–hole pair if the simple picture of point-like charges is adopted. This electron–hole separation can be inferred from the data in Figure 3 using Equation (2) (**Figure 6**). Previous experiments on photogeneration in bilayer diodes with conjugated poly-phenylene-type donor polymers with different conjugation length and C_{60} as acceptor indicated that the saturation field scales inversely with the effective conjugation length of the donor polymer, i.e., the more extended the π-electron distribution of the polymer is, the larger is the dissociation yield.[7] However, there is always a finite, non-negligible saturation field even though in some cases it can become comparable to the built-in field under short circuit condition of the diode. Therefore, the generation of free charge carriers is always funneled from precursor geminate pairs. The crucial parameter that

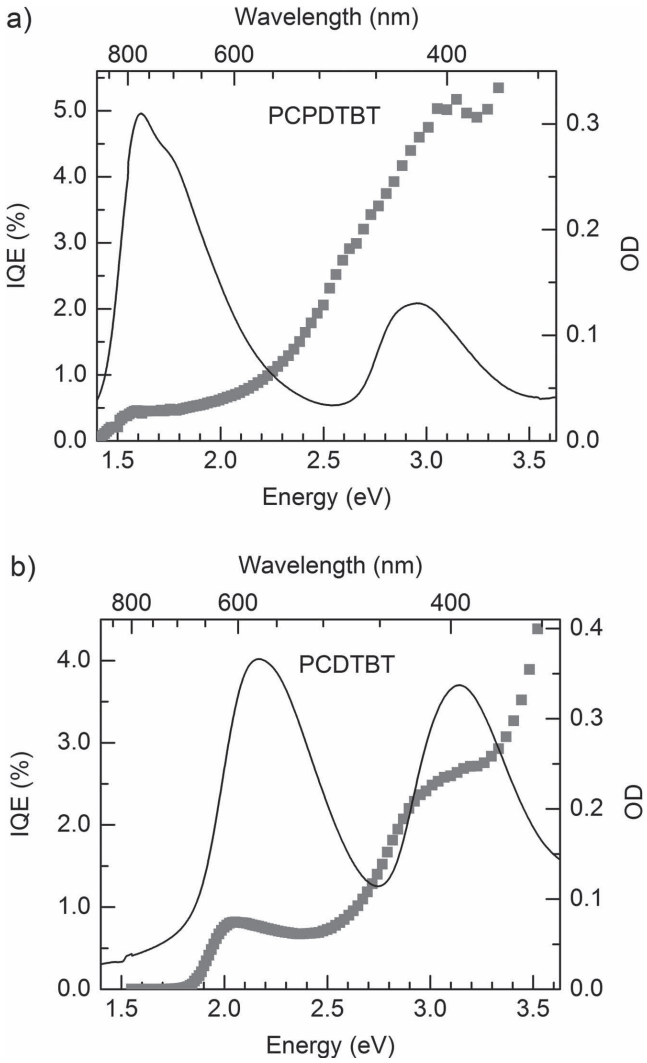

Figure 4. IQE for solar cells without acceptor in the structure a) ITO/MoO_3/30 nm PCPDTBT/Al and b) ITO/MoO_3/40 nm PCDTBT/Al. On the right axis the measured optical density of the polymer used is shown. The IQE was calculated by correcting the EQE for the optical density of the polymer layer and for the transmission of the glass, ITO and MoO_3 layers.

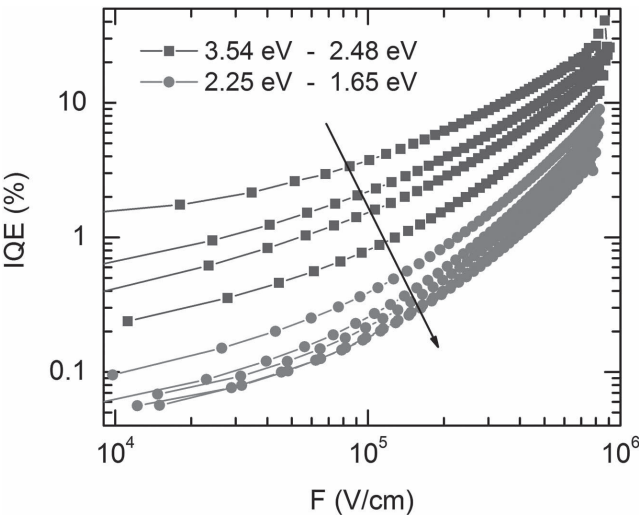

Figure 5. Internal quantum efficiency (IQE) of a monolayer solar cell for a ITO/MoO_3/30 nm PCPDTBT/Al cell as a function of electric field for different photon energies. The arrow indicates decreasing excitation energy.

determines F_{sat} is the delocalisation of the charges constituting the geminate pair.

Figure 3 shows that for diodes with C_{60} acceptor there is a striking correlation between the dependence of the field dependence F_{sat} and the donor absorption spectra. F_{sat} is constant within a photon energy range of 0.4 eV above the S_1–S_0 0–0 transition and decreases with increasing photon energies featuring an intermediate shoulder that correlates with the plateau in the absorption spectrum. It is caused by the superposition of the minimum of the donor spectrum and the onset of the second electronic transition of C_{60}. Although the point charge concept, on which Equation (2) is based on, is certainly only a crude approximation of the separation, r_0, of the electron on C_{60} and the delocalized hole on a conjugated polymer, the decrease of F_{sat} that occurs upon raising the photon energy demonstrates that the electron–hole pairs generated at higher quantum energy are more expanded. When using Equation (2) we end up with a value of 8 nm within a spectral range up to about 0.5 eV above the $S_1 \leftarrow S_0$ 0–0 transition and this increases to 13 nm at $h\nu = 3.5$ eV (Figure 6).

This may be compared to the field dependence of the dissociation yield in the series of polyphenylenes with different conjugation length reported earlier.[7] In that work, we found that the saturation field reduces with increasing conjugation length, that is, when going from the highly disordered DOOPPP to the well-ordered MeLPPP. This translates into an r_0 ranging from 2 nm for DOOPPP—which appears to be a realistic value for a tightly bound electron–hole pair in a donor–acceptor couple—to values up to 9 nm for MeLPPP, clearly reflecting a larger delocalization for this more conjugated polymer. The reduction of F_{sat} with increasing conjugation length also seems to suggest that the increase of the dissociation yield is not associated with entropy effects. The work by Gregg shows that entropy effects can be important in three-dimensional systems in contrast to one-dimensional systems.[29] This is at variance with the observation that F_{sat} reduces when the polymer acquires a more one-dimensional character—as is the case when elongating the conjugated π-system from DOOPPP to MeLPPP. By the same token, more delocalized, and thus more one-dimensional character associated with transitions contribution to the second absorption band, such as the $S_3 \leftarrow S_0$ transition shown in **Figure 7**, implies that entropy effects do not play a significant role here.

Obviously, excess photon energy facilitates photodissociation but the fact that r_0 stays constant within a spectral window of 0.4–0.5 eV above the S_1–S_0 0–0 transition proves that excess vibrational energy has virtually no effect. This is consistent with classic work on crystalline anthracene which shows that the yield increases only when a higher electronic state is reached while it remains constant within the spectral range of the Franck–Condon vibrational progression built on an electronic 0–0 transition.[12] This is a plausible result because the formation of an electron–hole pair from a neutral exciton can be considered as an autoionization process that depends on the

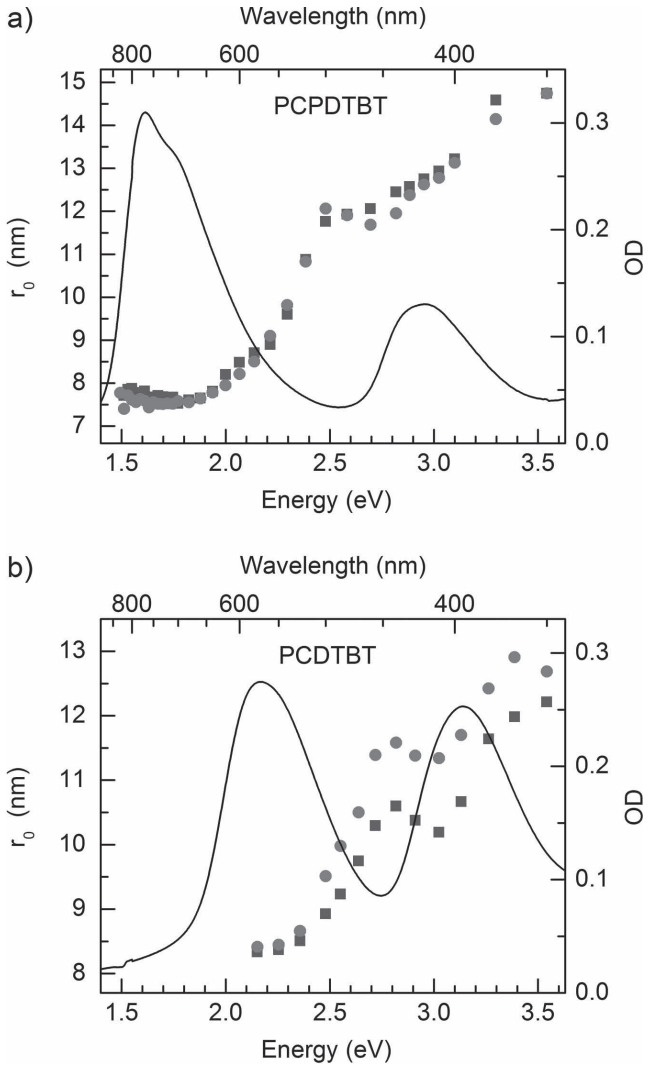

Figure 6. Thermalization radii calculated out of the saturation field F_{sat} as a function of photon energy in donor–acceptor solar cells with C_{60} as acceptor for a) PCPDTBT and b) PCDTBT. Circles and squares indicate different solar cells of the same type. The black line indicates the donor absorption.

wavefunction overlap between initial and final state. It should be indeed independent of an additional vibrational excitation of a chromophore. The observed decrease of F_{sat} and the concomitant increase of the size of the electron–hole pair is therefore a signature of the involvement of higher electronic states.

The conclusion that excess vibrational energy has no effect on photodissociation is consistent with work of Jailaubekov et al.[17] on solar cells with CuPc as electron donor and C_{60}/C_{70}, yet it is in disagreement with the works of Arkhipov et al.[30] who suggest local heating due to vibrational cooling of a higher Franck–Condon state as the origin for increased photogeneration at higher photon energies. At first glance the conclusion that excess photon energy can enhance the dissociation yield is at variance with the work of Vandewal et al.[19] These authors found that the efficiency of charge collection in a chemically very similar PBDTTBT-PCBM solar diode is the same if one excites the charge–transfer transition, the S_1–S_0 0–0 transition or a state at 2.0 eV which is 0.4 eV above the S_1–S_0 0–0 transition. However, based upon our experiments there is no contradiction because the increase of the photocarrier yield starts not until the next higher electronic state. Moreover, the effect of an electronic excess energy on efficiency of photodissociation tends to saturate already at electric fields close to or above the built-in field.

It is important to be aware of the low magnitude of the saturation field for these low-bandgap polymers. If such a device is measured under short-circuit condition, i.e., at the built-in field, the resulting internal quantum efficiency should be nearly flat with photon energy, such as the curves indicated by green triangles in Figure 2c,d.[31] In contrast, in spectroscopic measurements, a film is always measured without a field being present, so that the resulting photogeneration will have a strong dependence on the photon energy such as the curves measured at very low fields that are indicated by the orange diamonds in Figure 2c,d.

4.2. Donor–Acceptor Bilayers: Theory

To explore why a higher electronic state of the donor should assist the separation of the electron–hole pair, we consider quantum chemical calculations. Density functional theory (DFT)/Zerner intermediate neglect of differential overlap (ZINDO) calculations by Granchini at al.[18] have indeed shown that in PCPDTBT there is a S_2–S_0 0–0 transition at 1.88 eV and a S_4–S_0 0–0 transition at 2.32 eV, in addition to the calculated S_1–S_0 0–0 transition at 1.65 eV (which, by the way, is in excellent agreement with experiment). Both transitions overlap with the vibronic Franck Condon progression built on the S_1–S_0 transition.[18] Those transitions carry oscillator strengths of roughly 10% of the S_1–S_0 0–0 transition. Spectroscopic pump–probe experiments by Grancini et al. further demonstrated that the appearance time for the electron–hole pairs formed from precursor neutral excitons decreases from 48 to 38 fs and 22 fs upon raising the photon energy from 1.75 to 1.94 eV and 2.41 eV. They suggest that this is a signature of increasing coupling strength between excitonic states and ionized states that increases the rate of electron transfer to the acceptor. This is associated with an enhanced delocalization of the excited state that controls also the escape of the hole from the sibling charge on the C_{60} acceptor.

In order to support the present experimental findings, and to complement the DFT/ZINDO study by Grancini et al.[18] of the PCPDTBT case,[18] we further perform accurate many-body Green's function Bethe–Salpeter (BSE) calculations of the optical (excitonic) properties of a short PCDTBT polymer taken to be isolated or facing a PCBM acceptor (Figure 7). Due to the cost of these techniques, the PCDTBT polymer we study is composed of 2 monomers, for a total length of about 4.2 nm. Such a simple geometry does not allow discussing the full delocalization of the hole over several polymer units, but it already provides an extremely clear signature of the delocalization for hot donor excitations. However, when comparing experimental and calculated spectra one has to take into account that the calculations pertain to a short oligomer in vacuum. Therefore, the energy scale is shifted to higher values since transition energies increase with decreasing oligomer length.

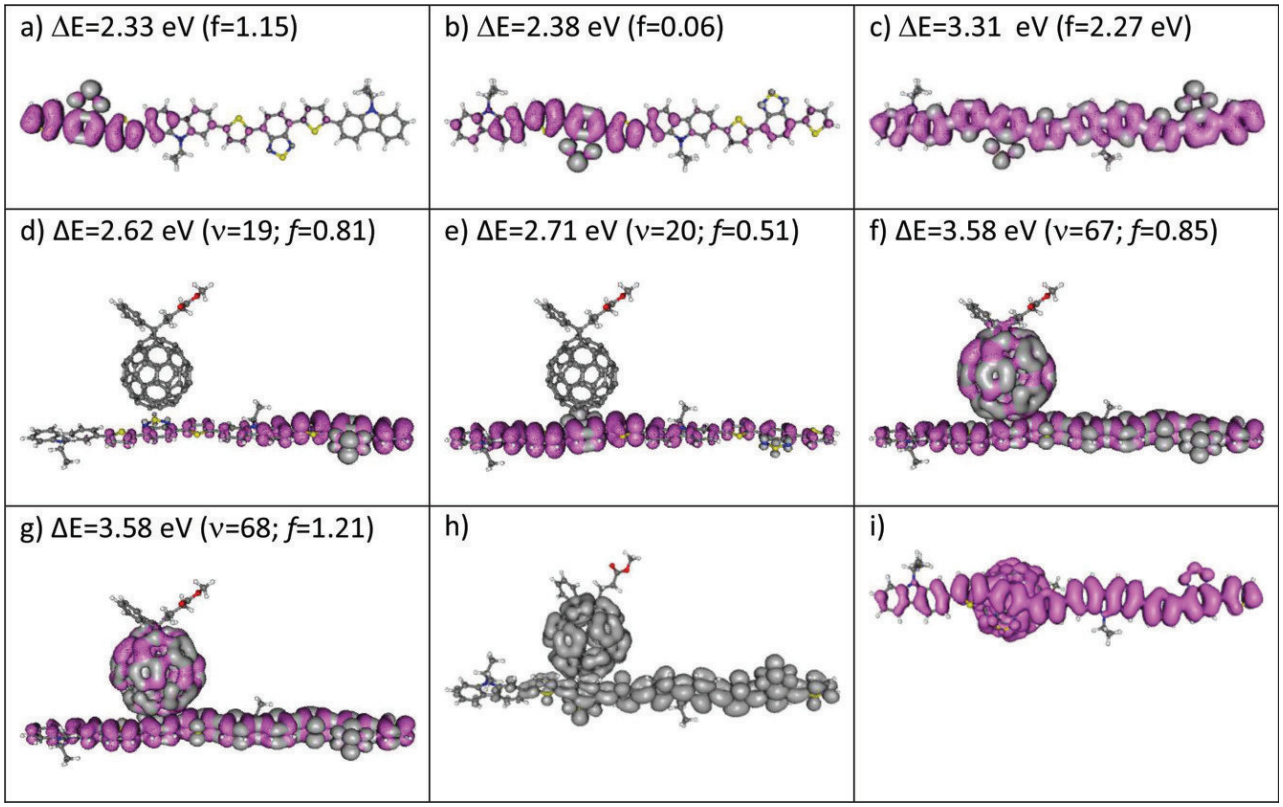

Figure 7. Representation for selected excitations in the PCDTBT polymer and PCDTBT/PCBM complex of the electron-averaged hole density (purple wireframe) and the hole-averaged electron density (solid gray) calculated from the corresponding Bethe–Salpeter electron–hole $\psi^{BSE}_{0\to N}(r_e,r_h)$ excitonic states. a–c) Lowest lying (S_N–S_0) transitions (N = 1, 2) and first dipole-allowed "hot" (S_3–S_0) transition on the isolated polymer. d,e) Lowest lying (S_N–S_0) transitions (N = 1, 2) on the PCDTBT/PCBM complex. f,g) Lowest "hot" dipole allowed excitations with large weight on both the polymer and PCBM. h,i) Electron-only and hole-only distribution for the state represented in (f). For the hole density in (i), we have rotated the complex to better see the polymer. We provide above each picture the absolute excitation energy (ΔE) and oscillator strength f. For the complex, the absolute (ν) index transition is provided (the lowest ν = 1 transition is a pure Frenkel PCBM transition). Isodensity contours have been taken at 1% of the maximum hole or electron density value in all cases.

We present in Figure 7a,b the energy, oscillator strength and excitonic wavefunctions corresponding to the lowest two polymer (S_N–S_0) transitions (N = 1, 2) showing some degree of localization on the benzothiadiazole units.[32] The first higher lying transition with significant oscillator strength is the (S_3–S_0) transition calculated to be at 3.3 eV (Figure 7c). In the absence of environmental (bulk) screening and Stokes shift, it is located about 1 eV above the lowest (S_1–S_0) transition, which compares favorably with the corresponding energy difference measured in solution (≈0.93 eV). The same behavior can be observed in the case of the PCDTBT/PCBM complex. The wavefunction for the lowest lying (S_N–S_0) transitions (N = 1, 2) is represented in Figure 7d,e showing clear similarities with the lowest lying excitations on the corresponding isolated polymer. The next excitations of the complexes exhibiting both a large oscillator strength and a large weight on the polymer are represented in Figure 7f,g. As for the isolated polymer chain, these are again located about 0.8–1.0 eV above the (S_1–S_0) transition. Comparing the complex with the isolated polymer case, we see that hot excitations located at about the same energy above the (S_1–S_0) transition start delocalizing not only over the entire polymer chain but also on the neighboring fullerene as a signature of excess kinetic energy. An analysis of the electron-only (Figure 7h) and hole-only (Figure 7i) distribution for these hot excitations on the complex clearly indicates that these are not charge–transfer states, but really states with the hole (the electron) completely delocalized over the two neighboring molecules. It is worth stressing that these optically accessible excited states are quasidegenerate in energy with a number of charge–transfer states with enhanced electron–hole radii,[26] so that charge separation at higher excitation energy could be favored either through an indirect pathway (i.e., involving a nonadiabatic coupling between the polymer S_3 and hot CT states) or a direct pathway (i.e., through wavefunction mixing in the much higher density of states of a realistic donor–acceptor interface, not captured by the calculations reported here for simple complexes). Obviously, delocalization of the higher excited donor excitations has a great impact on the size of the geminate pair that can subsequently fully dissociate but also the acceptor plays a major role because the strength of coupling depends on both partners.

4.3. Comparison to Single Layer Diodes

Figure 4 shows that there is also photodissociation in single layer PCPDTBT and PCDTBT diodes but it is roughly two

orders of magnitude less efficient than in bilayers. This disparity is even greater in single layer diodes with MEH-PPV and MeLPPP[14–16] that are homo-polymers with unpolar repeat units as compared to donor–acceptor type copolymers. It is straightforward to associate this quantitative difference with the polarity of the donor that affects the size of the geminate electron–hole pair and, consequently, its Coulomb binding energy. In the case of single layer PCPDTBT and PCDTBT diodes, the saturation field of the photocurrent is beyond 10^6 V cm^{-1} (Figure 5). At higher field strength, the photocurrent cannot be measured reliably. Therefore, we can only give an upper limit for r_0. According to Equation (2), $F_{sat} > 10^6$ V cm^{-1} translates into $r_0 = 2$ nm, i.e., a factor of at least 4 lower than the electron–hole pair size in the donor–acceptor assembly. A more concise estimate would require a theory for photodissociation. Fitting the current field characteristic using an Onsager[33] or Onsager–Braun[34] formalism turns out to be unsuccessful. The reason is that those theories are premised on a point charge approximation that is inappropriate for conjugated polymers in which the excited state is more delocalized.[35] Nevertheless, 2 nm appears to be a realistic value for a strongly allowed S_1 state with partial charge character. Recall, on the other hand, that in typical π-conjugated homo-polymers the mean electron–hole separation is around 1 nm.[36]

When raising the photon energy from 1.8 to 3.5 eV the IQE increases by a factor of 30, equivalent to an increase of r_0 by almost by a factor of 2. Importantly, the IQE starts increasing not until an excess energy of about 0.5 eV above the $S_1 \leftarrow S_0$ 0–0 transition is supplied. This is in analogy with the constant saturation field in the bilayers and consistent with the notion that it is the electronic rather than vibronic excess energy that matters. It is also consistent with the spectral dependence of photoconduction in MEH-PPV and MeLPPP.[14–16]

5. Conclusions

Upon photoexciting PCDTBT or PCPDTBT a geminate electron–hole pair is generated that is only weakly Coulomb bound as evidenced by the low saturation field strength of the photocarrier yield. In fact, the electric field that exists in the bilayer due the built-in voltage is already sufficient to liberate the pair from its weak Coulomb potential. We find that dissociation is further facilitated by exciting the donor chromophore into a higher electronic state whose wavefunction is more extended. For the efficiency of the solar cell this has little influence because the intrapair electron separation is already on the order of 10 nm. Therefore, the electric field needed for complete dissociation is comparable to or lower than the built-in electric field. The generated electron–hole pair is therefore essentially free. In this case photodissociation becomes indistinguishable from direct optical excitation from a delocalized to a decoupled charge pair state, even more so if the photon energy is about 1 eV above the S_1–S_0 0–0 transition.[37] Nevertheless, photodissociation is, in its nature, not an instantaneous but a sequential process. This is not only borne out by the field dependent photocurrent measurements shown here, but it has also been demonstrated by the experiments by Grancini et al.[18] They show that upon excitation of the donor material electron–hole pairs are generated from precursor excitons at a rate of order of 2×10^{13} s^{-1}. This is also consistent with ultrafast pump–probe measurements by Herrmann et al.[5] on P3HT/C_{60} bilayer cells structures that unambiguously show the instantaneous appearance of absorption from neutral excitations, while the signature from electron–hole pairs appears only subsequently with a rise time of 120 fs.[5]

We finally comment on the character of "hot" exciton dissociation. The underlying idea concerning hot dissociation is that an excited electron is kicked further away from the donor as the initial photon quantum energy increases. This would imply a larger electron–hole pair separation and a reduced rate for geminate recombination. The present results modify this concept. They demonstrate that it is the spatial extension of the initial excited state wavefunction that is important. After exciting a higher-lying state, the hole and electron are momentarily in a more delocalized and, consequently, in a high mobility state and are therefore able to further escape from each other in the course of a ballistic process rather than a thermalization process.[38] Obviously, the chains themselves should be fairly ordered. Recent spectroscopic work on PCPDTBT in solution shows that there is a transition from a disordered to a more ordered phase and, importantly, the absorption spectra of PCPDTBT films are identical with those of the ordered aggregates.[39]

Supporting Information

Supporting Information is available from the Wiley Online Library or from the author.

Acknowledgements

The authors thank Christina Saller and the group of Peter Strohriegl (University of Bayreuth) for synthesizing and providing PCDTBT for our experiments. The authors acknowledge financial support by the Bavarian State Ministry of Science, Research, and the Arts through the Collaborative Research Network "Solar Technologies go Hybrid" and by the German Science Foundation DFG through the doctoral training center "Photophysics of Synthetic and Biological Multichromophoric Systems" (GRK 1640). X.B. acknowledges support from the French ANR funding agency (Project No. ANR-12-BS04 PANELS) and the supercomputing GENCI program (Curie machine). The work in Mons was supported by the Programme d'Excellence de la Région Wallonne (OPTI2MAT project) and the Belgian National Fund for Scientific Research (FNRS-FRFC). D.B. is a FNRS research director.

Received: October 28, 2014
Revised: December 16, 2014
Published online: January 16, 2015

[1] H. Ohkita, S. Cook, Y. Astuti, W. Duffy, S. Tierney, W. Zhang, M. Heeney, I. McCulloch, J. Nelson, D. D. C. Bradley, J. R. Durrant, *J. Am. Chem. Soc.* **2008**, *130*, 3030.
[2] C. Deibel, T. Strobel, V. Dyakonov, *Phys. Rev. Lett.* **2009**, *103*, 36402.
[3] T. M. Clarke, J. R. Durrant, *Chem. Rev.* **2010**, *110*, 6736.
[4] F. Etzold, I. A. Howard, R. Mauer, M. Meister, T. D. Kim, K. S. Lee, N. S. Baek, F. Laquai, *J. Am. Chem. Soc.* **2011**, *133*, 9469.
[5] D. Herrmann, S. Niesar, C. Scharsich, A. Köhler, M. Stutzmann, E. Riedle, *J. Am. Chem. Soc.* **2011**, *133*, 18220.

[6] F. Paquin, G. Latini, M. Sakowicz, P. L. Karsenti, L. J. Wang, D. Beljonne, N. Stingelin, C. Silva, *Phys. Rev. Lett.* **2011**, *106*, 197401.
[7] C. Schwarz, H. Bässler, I. Bauer, J. M. Koenen, E. Preis, U. Scherf, A. Köhler, *Adv. Mater.* **2012**, *24*, 922.
[8] S. D. Baranovskii, M. Wiemer, A. V. Nenashev, F. Jansson, F. Gebhardt, *J. Phys. Chem. Lett.* **2012**, *3*, 1214.
[9] D. A. Vithanage, A. Devizis, V. Abramavicius, Y. Infahsaeng, D. Abramavicius, R. C. I. MacKenzie, P. E. Keivanidis, A. Yartsev, D. Hertel, J. Nelson, V. Sundstrom, V. Gulbinas, *Nat. Commun.* **2013**, *4*, 2334.
[10] J. D. Servaites, M. A. Ratner, T. J. Marks, *Energy Environ. Sci.* **2011**, *4*, 4410.
[11] R. D. Pensack, J. B. Asbury, *J. Phys. Chem. Lett.* **2010**, *1*, 2255.
[12] R. R. Chance, C. L. Braun, *J. Chem. Phys.* **1976**, *64*, 3573.
[13] N. Geacintov, M. Pope, *J. Chem. Phys.* **1967**, *47*, 1194.
[14] A. Köhler, D. A. dos Santos, D. Beljonne, Z. Shuai, J. L. Bredas, A. B. Holmes, A. Kraus, K. Müllen, R. H. Friend, *Nature* **1998**, *392*, 903.
[15] M. Chandross, S. Mazumdar, *Phys. Rev. B* **1994**, *50*, 14702.
[16] S. Barth, H. Bässler, *Chem. Phys. Lett.* **1998**, *288*, 147.
[17] A. E. Jailaubekov, A. P. Willard, J. R. Tritsch, W. L. Chan, N. Sai, R. Gearba, L. G. Kaake, K. J. Williams, K. Leung, P. J. Rossky, X. Y. Zhu, *Nat. Mater.* **2013**, *12*, 66.
[18] G. Grancini, M. Maiuri, D. Fazzi, A. Petrozza, H. J. Egelhaaf, D. Brida, G. Cerullo, G. Lanzani, *Nat. Mater.* **2013**, *12*, 29.
[19] K. Vandewal, S. Albrecht, E. T. Hoke, K. R. Graham, J. Widmer, J. D. Douglas, M. Schubert, W. R. Mateker, J. T. Bloking, G. F. Burkhard, A. Sellinger, J. M. J. Frechet, A. Amassian, M. K. Riede, M. D. McGehee, D. Neher, A. Salleo, *Nat. Mater.* **2014**, *13*, 63.
[20] N. Blouin, A. Michaud, M. Leclerc, *Adv. Mater.* **2007**, *19*, 2295.
[21] G. Onida, L. Reining, A. Rubio, *Rev. Mod. Phys.* **2002**, *74*, 601.
[22] X. Blase, C. Attaccalite, *Appl. Phys. Lett.* **2011**, *99*, 171909.
[23] C. Faber, I. Duchemin, T. Deutsch, X. Blase, *Phys. Rev. B* **2012**, *86*, 155315.
[24] B. Baumeier, D. Andrienko, Y. C. Ma, M. Rohlfing, *J. Chem. Theory Comput.* **2012**, *8*, 997.
[25] C. Faber, P. Boulanger, I. Duchemin, C. Attaccalite, X. Blase, *J. Chem. Phys.* **2013**, *139*, 194308.
[26] D. Niedzialek, I. Duchemin, T. Branquinho de Queiroz, S. Osella, A. Rao, R. H. Friend, X. Blase, S. Kümmel, D. Beljonne, *Adv. Funct. Mater.* **2014**, DOI: 10.1002/adfm.201402682.
[27] C. M. Ramsdale, J. A. Barker, A. C. Arias, J. D. MacKenzie, R. H. Friend, N. C. Greenham, *J. Appl. Phys.* **2002**, *92*, 4266.
[28] J. C. Blakesley, D. Neher, *Phys. Rev. B* **2011**, *84*, 75210.
[29] B. A. Gregg, *J. Phys. Chem. Lett.* **2011**, *2*, 3013.
[30] V. I. Arkhipov, E. V. Emelianova, S. Barth, H. Bässler, *Phys. Rev. B* **2000**, *61*, 8207.
[31] A. Armin, I. Kassal, P. E. Shaw, M. Hambsch, M. Stolterfoht, D. M. Lyons, J. Li, Z. G. Sho, P. L. Burn, P. Meredith, *J. Am. Chem. Soc.* **2014**, *136*, 11465.
[32] We note, however, that the two lowest lying states are nearly degenerate, leading potentially to resonance states with weight on the two benzothiadiazoles.
[33] L. Onsager, *Phys. Rev.* **1938**, *54*, 554.
[34] C. L. Braun, *J. Chem. Phys.* **1984**, *80*, 4157.
[35] C. Schwarz, S. Tscheuschner, J. Frisch, S. Winkler, N. Koch, H. Bässler, A. Köhler, *Phys. Rev. B* **2013**, *87*, 155205.
[36] J. W. van der Horst, P. A. Bobbert, M. A. J. Michels, H. Bässler, *J. Chem. Phys.* **2001**, *114*, 6950.
[37] N. Banerji, S. Cowan, M. Leclerc, E. Vauthey, A. J. Heeger, *J. Am. Chem. Soc.* **2010**, *132*, 17459.
[38] A. B. Matheson, S. J. Pearson, A. Ruseckas, I. D. W. Samuel, *J. Phys. Chem. Lett.* **2013**, *4*, 4166.
[39] C. Scharsich, F. S. U. Fischer, K. Wilma, R. Hildner, S. Ludwigs, A. Köhler, unpublished.

ADVANCED FUNCTIONAL MATERIALS

Supporting Information

for *Adv. Funct. Mater.*, DOI: 10.1002/adfm.201403784

Does Excess Energy Assist Photogeneration in an Organic Low-Bandgap Solar Cell?

*Tobias Hahn, Johannes Geiger, Xavier Blase, Ivan Duchemin, Dorota Niedzialek, Steffen Tscheuschner, David Beljonne, Heinz Bässler, and Anna Köhler**

Supporting Information to:

Does excess energy assist photogeneration in an organic low band-gap solar cell?

Tobias Hahn[1,3], Johannes Geiger[1,3], Xavier Blase[4], Ivan Duchemin[5], Dorota Niedzialek[2], Steffen Tscheuschner[1,3], David Beljonne[2], Anna Köhler[1,3*] and Heinz Bässler[1,3]

[1] Experimental Physics II, University of Bayreuth, 95440 Bayreuth, Germany

[2] University of Mons, Place du Parc 20, 7000 Mons, Belgium

[3] Bayeuth Institute of Macromolecular Research (BMBF), University of Bayreuth, 95440 Bayreuth, Germany

[4] CNRS and Grenoble-Alpes University, Inst. NEEL, F-38042 Grenoble, France

[5] INAC, SP2M/L sim, CEA Cedex 09, 38054 Grenoble, France.

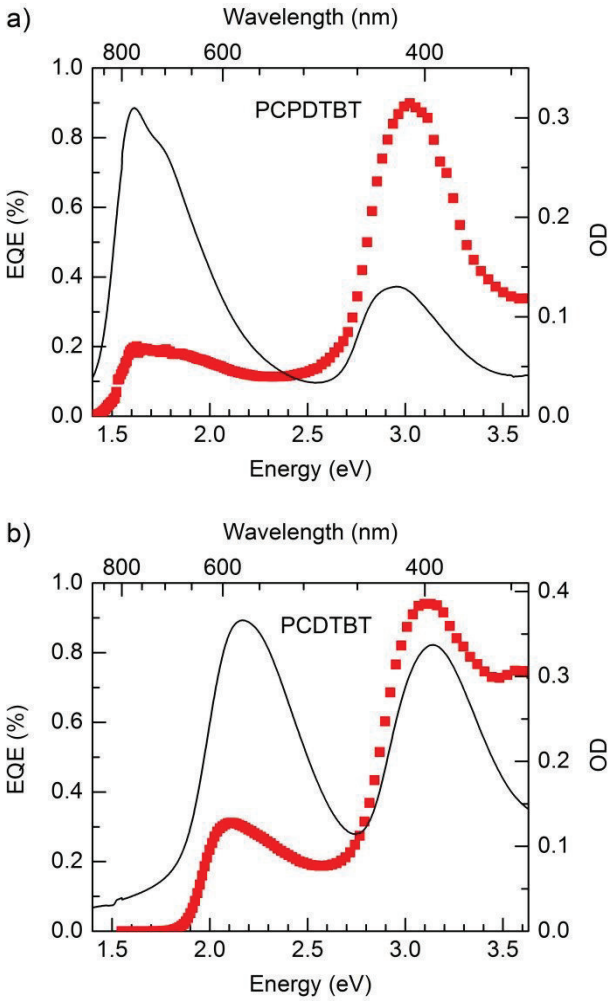

Figure S1: EQE measured under short-circuit condition of the PCPDTBT (a) and the PCDTBT (b) monolayer cells (ITO/MoO_3/30 nm donor/Al) without C_{60} (squares) along with the corresponding donor absorption (solid line).

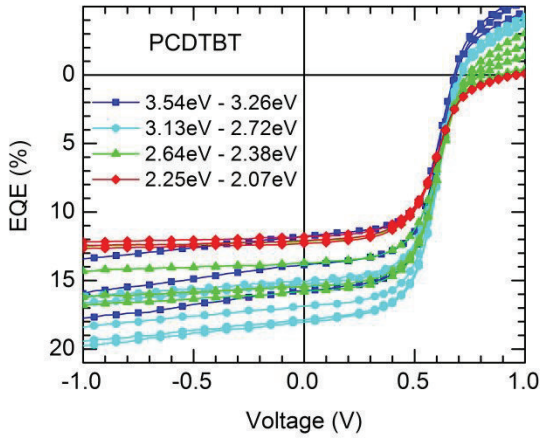

Figure S2: Current-voltage data, shown exemplary for the PCDTBT+C_{60} solar cell. The different symbols indicate measurements taken at different parts of the spectral range.

Appendix: Further Investigations to

"Does Excess Energy Assist Photogeneration in an Organic Low-Bandgap Solar Cell?"

by Tobias Hahn

Introduction

In order to substantiate and advance the data of the publication "Does Excess Energy Assist Photogeneration in an Organic Low-Bandgap Solar Cell?" additional solar cell measurements were done. This was necessary, due to the fact that in the bilayer data of the publication we observed an s-shape which changes with the excitation energy as shown in the supporting information. Furthermore a dependence of the open circuit voltage (V_{oc}) on excitation energy was observed, partly caused by the changes of the s-shape. The resultant energy dependence of V_{oc}, as can be seen in the publication, correlates with the absorption of PCDTBT and the PCPDTBT, showing a kink between the low and the high electronic energy peak. Using the equation $F = -(V - V_{oc})/d$ the energy dependence of V_{oc} influences the shape of the field dependent EQE and consequently the extracted saturation field strength (F_{sat}). The correlation of the s-shape, V_{oc} and the energy dependent F_{sat} is not fully understood yet. Consequently the energy dependence of F_{sat} was checked by additional solar cell measurements.

Using the data and the knowledge from our later publications "Role of Intrinsic Photo-generation in Single Layer and Bilayer Solar Cells with C_{60} and PCBM" and "Monomolecular and Bimolecular Recombination of Electron-Hole Pairs at the Interface of a Bilayer Organic Solar Cell", a well-grounded extended examination of the excess energy issue was possible. New tailored measurements of bilayer solar cells with PCDTBT as donor and thin C_{60} layer (6 nm) as acceptor were able to support and confirm the energy dependence of F_{sat} in the publication. The results are presented in the following section.

Results and discussion

As shown in "Monomolecular and Bimolecular Recombination of Electron-Hole Pairs at the Interface of a Bilayer Organic Solar Cell" an s-shape can appear due to extraction problems at the electrodes (for example at the aluminium C_{60} interface) or due to geminate and non-geminate recombination in thicker donor layers. A dependence of the s-shape on the

excitation energy was not observed. Let us now compare this to the data of the publication on excess energy. An extraction problem at the electrodes can be treated as a structural and morphological problem, which is independent of excitation energy. Due to the fact that the observed s-shape changes with excitation energy, there must be other explanations. Furthermore all solar cells had the same thickness of polymer and C_{60} respectively. Consequently differences in recombination can be excluded, too. To clarify experimentally, whether the s-shape is caused by extraction problems, solar cells were fabricated again using a thin evaporated BCP layer between C_{60} and aluminium. A thin BCP layer is often used as a spacer to prevent chemical reactions of C_{60} and aluminium, that can cause a non-ohmic contact. [1] Using the BCP layer, the s-shape was removed but unfortunately BCP layers also caused a high dark current. A high dark current in forward direction shifts the $j(V)$ curve to lower V_{oc} and can therefore falsify the field dependence of the EQE. A second problem in the solar cells with BCP layer is the large influence of the intrinsic charge generation in the C_{60} layer. As in "Role of Intrinsic Photogeneration in Single Layer and Bilayer Solar Cells with C_{60} and PCBM", we observe a flat saturation of the field dependent EQE for excitation energies below 2.25 eV and a significant slope within the saturation region for higher excitation energies. Consequently, an accurate simultaneous determination of F_{sat} for low and high excitation energies using the tangent method is not possible. Summing up, the experiments with BCP layer did not give meaningful results to verify the observed energy dependence of F_{sat} due to intrinsic effects of the C_{60} layer discussed above. This experimental problem might be solved, if the intrinsic generation in C_{60} can be prevented. Then a proper determination of F_{sat} would be possible for low and high excitation energies, due to a flat saturation in both regimes.

This idea was realized by making bilayer solar cells with very thin C_{60} layers. The structure ITO/MoO_3(15 nm)/PCDTBT(30 nm)/C_{60}(6 nm)/Al(100 nm) was used. As described in "The Role of Intrinsic Photogeneration in Single Layer and Bilayer Solar Cells with C_{60} and PCBM", the intrinsic charge carrier generation in C_{60} is a bulk effect. This means, that a certain volume of C_{60} molecules is necessary, to enable the light induced creation of charge transfer (CT) states in the C_{60} layer. These CT sates can be dissociated and then contribute to the photocurrent. If only a few nanometers of C_{60} are evaporated on the polymer surface, this will rather lead to a doping of the polymer layer surface, than to a C_{60} bulk on the surface. In this case, the intrinsic charge carrier generation does not occur and an excitation energy dependent contribution of the intrinsic generation to the total photocurrent is excluded. The intrinsic charge carrier generation in the polymer-layer is an inefficient process. The resultant contribution to the total photocurrent is one order of magnitude smaller, as shown in Figure 2a. As a consequence mainly the electron hole dissociation at the donor acceptor interface can contribute to the photocurrent because the intrinsic generation of both the polymer and the C_{60} can be neglected. This results in a flat saturation of the photocurrent as presented in Figure 1a.

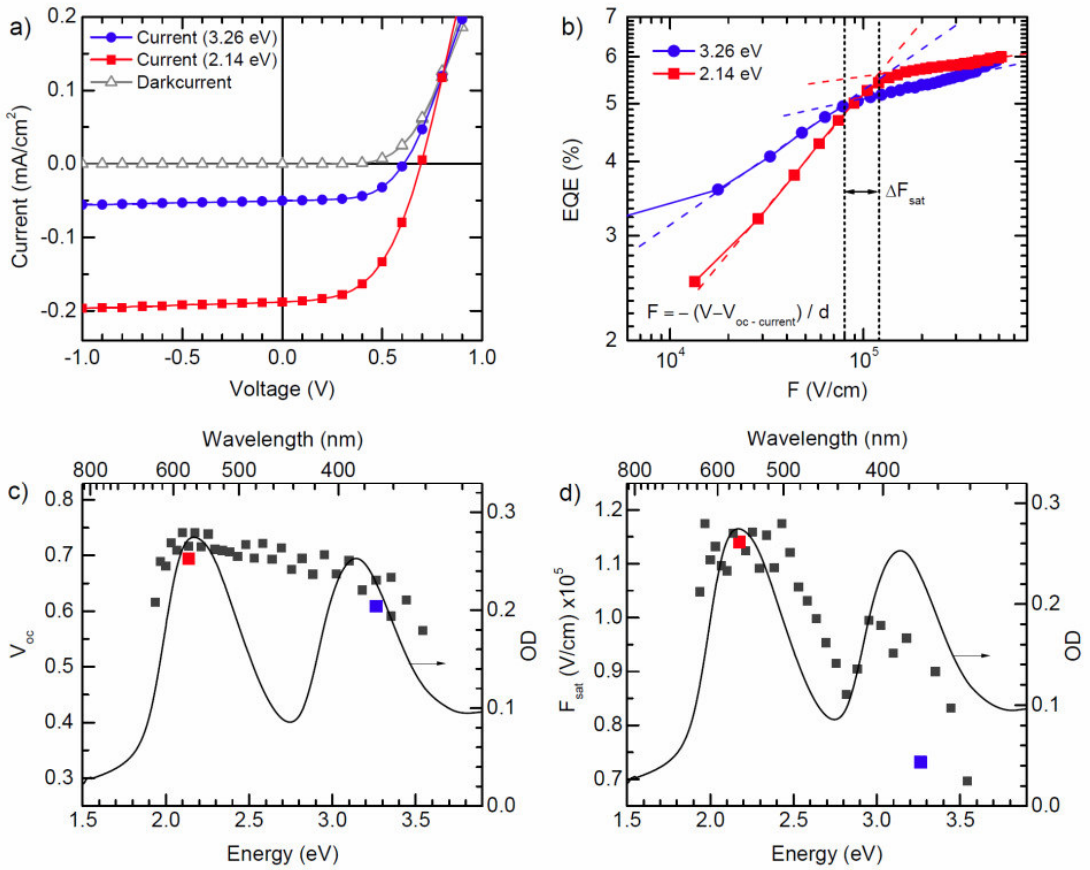

Figure 1: *(a) Representative current-voltage characteristics $j(V)$ for bilayer solar cells with the donor polymer PCDTBT (30 nm) and a 6 nm thick C_{60} acceptor for excitation at 3.26 eV and 2.14 eV (for clarity the measured raw data is shown without any corrections on the used lamp) The structure ITO/MoO_3(15 nm)/PCDTBT(30 nm)/C_{60} (6 nm)/Al(100 nm) was used in the device. (b) Corresponding field dependent EQE, calculated from the photocurrent. The dashed lines are added as guide to the eye to visualize the determining of the saturation field strength (F_{sat}). (c) V_{oc} as a function of excitation energy. Red (2.14 eV) and blue (3.26 eV) squares correspond to V_{oc} of the $j(V)$ characteristic shown in (a), respectively. (d) F_{sat} as a function of excitation energy. Red (2.14 eV) and blue (3.26 eV) squares correspond to F_{sat} as determined from the field dependent EQE curves shown in (b), respectively. For analysis purpose the absorption spectrum of PCDTBT is added in (c) and (d).*

The photocurrent already saturates at positive voltages and the observed saturation is almost horizontal for both the excitation at low (2.14 eV) and high (3.26 eV) photon energies below and above the CT edge of C_{60} at 2.25 eV. Both $j(V)$ curves are parallel in the third quadrant (see Figure 1a). The small remaining slope is attributed to the intrinsic generation in the donor-acceptor lowbandgap polymer PCDTBT. Using $F = -(V - V_{oc})/d$ the field dependent EQE can be calculated as shown in Figure 1b. V_{oc} was extracted from the current-voltage characteristic for each individual excitation energy. As described in the

publication, the saturation field strength F_{sat} can be determined using the tangent method (see Figure 1b). Due to the parallel $j(V)$ curves shown in Figure 1a, a more accurate determination of F_{sat} is now possible for low and high excitation energies. The remaining difference in the saturation-slope due to the intrinsic generation in the polymer layer (emphasized by the logarithmic scale) has no influence on ΔF_{sat}. This can be shown by subtracting the EQE of the intrinsic generation in the polymer layer. Therefore the data of a PCDTBT-only-device was used, which was measured and shown in the publication.

The energy dependence of F_{sat} is supported by the findings shown in Figure 1b. For high excitation energy (3.26 eV) a lower saturation field strength is observed compared to the lower excitation energy (2.14 eV). As discussed in the publication, this can be interpreted by a weaker bound electron hole pair due to the assistance of electronic excess energy. Furthermore, EQE at low electric field strength is enhanced for 3.26 eV in comparison to 2.14 eV. To substantiate these findings, $j(V)$, V_{oc} and F_{sat} were determined for a large number of excitation energies in the absorption range of PCDTBT. V_{oc} and the determined F_{sat} for all $j(V)$ curves are shown in Figure 1c and 1d. Figure 1c shows a constant V_{oc} from the low to the high energy absorption peak of PCDTBT. Since every $EQE(F)$ curve should be corrected on its respective V_{oc}, a constant V_{oc} is of great avail because the calculation of the field is then based on the same zero field condition for all excitation energies. On this basis, a shift in F_{sat} is clear without ambiguity and advantageous for the interpretation of F_{sat}. Figure 1d shows a clear correlation of F_{sat} and the absorption spectra of PCDTBT. The results for PCDTBT are quite similar to that of the publication. Even ΔF_{sat} between low and high excitation energies is in the same range of about $4 \cdot 10^4\, V/cm$. The results are therefore reproducible.

Yet the absolute value of F_{sat} differs. In comparison to the publication, the 6 nm thin C_{60} layer in the bilayer solar cell provides higher F_{sat}. This might be interpreted as a reduced delocalization of the electron in the thin C_{60} layer compared to the 30 nm thick C_{60} layer used in the publication. As already mentioned above, the evaporation of only a few nanometers of C_{60} on the polymer surface will rather lead to a doping of the polymer layer surface, than to a C_{60} bulk on the surface. The absence of bulk delocalization might increase F_{sat}. Furthermore the EQE of the bilayer cell with the thin C_{60} layer is smaller over the whole spectral range. Albeit the total EQE should not affect F_{sat}, the EQE spectra ought to be measured and interpreted. The EQE spectra of C_{60} bilayer cells with 6 nm of C_{60} are shown in Figure 2a. The EQE spectra of the same solar cell with a C_{60} layer of 30 nm thickness, as well as without any acceptor (PCDTBT only device) are shown as reference.

Even though the EQE of the bilayer cells with 6 nm C_{60} is smaller compared to the bilayer cells with 30 nm C_{60}, it is about one order of magnitude higher than the intrinsic generation in the neat PCDTBT solar cell. This implies that charge carrier generation at the donor acceptor interface is working properly. There are different reasons for the smaller EQE compared to the EQE of the bilayer cells with 30 nm C_{60}. In the first place, the intrinsic

charge carrier generation in the C_{60} bulk is missing in the thin sample. To illustrate the intrinsic contribution of the C_{60} in the bilayer cell with the 30 nm C_{60} layer, the EQE of a C_{60} only device is added to the EQE of the bilayer with 6 nm C_{60} (see Figure 2b). At about 3.1 eV the sum has about the same EQE value as the bilayer cell with 30 nm C_{60} (Δ_B in Figure 2b). This is just a rough estimation, because the transmission of the PCDTBT layer and other changes like layer thickness and differences in the internal field from monolayer to bilayer are not considered. Nevertheless, this serves as a hint for the importance of intrinsic charge carrier generation in the C_{60} bulk in bilayer solar cells.

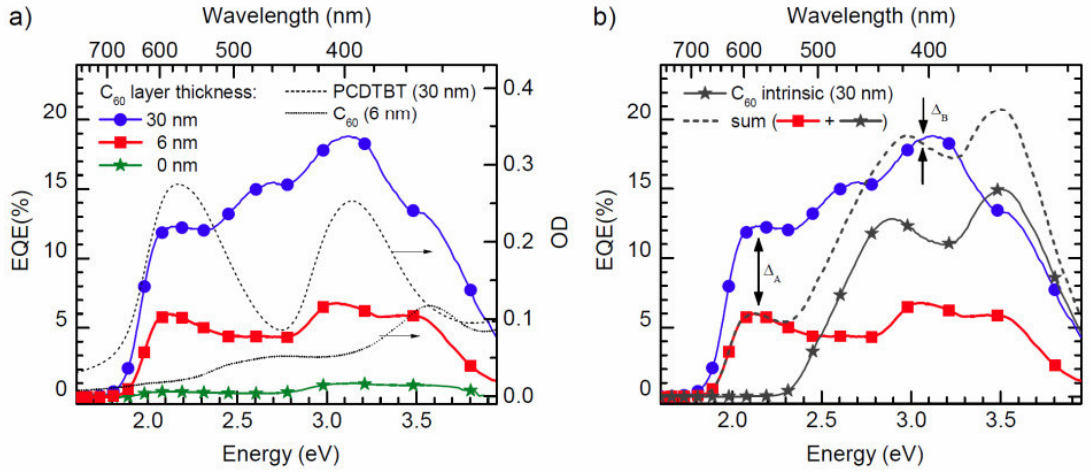

Figure 2: *(a) External quantum efficiency (EQE) of bilayer solar cells with PCDTBT (30 nm) as donor polymer and C_{60} as acceptor with a layer thickness of 30 nm (blue circles) and 6 nm (red squares). The structure ITO/MoO_3(15 nm)/PCDTBT(30 nm)/C_{60} (x nm)/Al(100 nm) is used. Data for a single-layer solar cell of PCDTBT (30 nm) without any acceptor is added (green stars). On the right hand y-axis the optical density (OD) of a 30 nm thick PCDTBT layer and a 6 nm thick C_{60} layer is shown for comparison. (b) EQE data of the bilayer solar cells of (a) compared with the intrinsic EQE of a 30 nm thick C_{60} only device (black stars). For data analysis, the sum of the EQE of bilayer solar cells with a 6 nm layer of C_{60} (red squares) and the intrinsic EQE of the 30 nm thick C_{60} only device (black stars) is shown additionally. Δ_A and Δ_B indicate the EQE difference in the range of the low and high energy peak of the PCDTBT absorption.*

Due to the fact that there is no intrinsic charge carrier generation in C_{60} below an energy of 2.25 eV, the difference Δ_A in Figure 2b cannot be explained by this. Yet we find several other reasons to explain this difference. First of all, the optical-field distribution in the solar cell will change with the layer thickness of C_{60}. [2, 3] Considering that there is a standing wave with a node at the aluminium electrode, the position of the maximal absorption in the active layer will depend on the distance to this node and on the wavelength of the excitation light. For efficient bilayer solar cells it is important, that the position of maximal absorption is at about the donor acceptor interface. Consequently the distance between the

donor acceptor interface and the aluminium electrode, which is the layer thickness of the C_{60}, plays an important role. In the literature it was shown, that for a 30 nm thick layer of C_{70} the position of the maximal absorption is at the position of the donor acceptor interface. [2] For thinner C_{70} or C_{60} layers the donor acceptor interface is shifted away from the position of maximal absorption in the device. Of course, this also depends on the excitation wavelength. This effect might partly explain Δ_A in Figure 2b. Second, excitons which are created in the 30 nm C_{60} layer can partly diffuse towards the donor acceptor interface, dissociate there and contribute to the photocurrent. Considering a C_{60} singlet exciton diffusion length of about 7 nm [4], the use of 6 nm instead of 30 nm C_{60} in the solar cell might reduce this contribution to the photocurrent slightly. Furthermore, the donor acceptor interface of the bilayer cell with 6 nm of C_{60} might differ from the one with 30 nm on top. However, we roughly estimate that incorporation of C_{60} molecules into the polymer film during the evaporation process will end after a few nanometers. [5] Consequently, the difference in donor acceptor interface roughness should not change drastically when going from 6 nm to 30 nm C_{60} layer thickness.

Conclusion

In summary, the data of the bilayer solar cells with a thin C_{60} layer can reproduce and substantiate the energy dependence of F_{sat}, which was found in the publication "Does Excess Energy Assist Photogeneration in an Organic Low-Bandgap Solar Cell?" Crucial in this respect was the possibility to suppress the intrinsic charge carrier generation in the C_{60} bulk by using 6 nm thick C_{60} films, which can rather be seen as doping of the polymer surface. Thus, by preventing bulk generation in the C_{60} layer, only the dissociation at the donor acceptor interface contributes to the photocurrent and a flat saturation can be observed for both low and high excitation energies. This results in an accurate determination of F_{sat}, giving the possibility to analyze field dependent measurements properly. Furthermore, the current voltage characteristics of the bilayer solar cells with 6 nm C_{60} showed no s-shape behavior and a constant V_{oc} for all excitation energies in the range between the position of the low and high energy absorption peak of PCDTBT. This further facilitates an accurate determination of F_{sat} and thus helps to discuss the influence of excess electronic energy. The literature recently supported our findings. [6-8] For instance, in the work of Grancini et al. [6] the influence of excess energy in blend solar cells was verified by measuring and calculating the internal quantum efficiency.

References

[1] Vogel, M.; Doka, S.; Breyer, C.; Lux-Steiner, M. C.;Fostiropoulosa, K. On the Function of a Bathocuproine Buffer Layer in Organic Photovoltaic Cells. *Applied Physics Letters* **2006**, *89*, 163501.

[2] Lee, C. C.; Su, W. C.; Shu, Y. S.; Chang, W. C.; Huang, B. Y.; Lee, Y. Z.; Su, T. H.; Chen, K. T.;Liu, S. W. Decoupling the Optical and Electrical Properties of Subphthalocyanine/C_{70} Bi-Layer Organic Photovoltaic Devices: Improved Photocurrent while Maintaining a High Open-Circuit Voltage and Fill Factor. *Rsc Advances* **2015**, *5*, 5617-5626.

[3] Tress, W.; Merten, A.; Furno, M.; Hein, M.; Leo, K.;Riede, M. Correlation of Absorption Profile and Fill Factor in Organic Solar Cells: The Role of Mobility Imbalance. *Advanced Energy Materials* **2013**, *3*, 631-638.

[4] Fravventura, M. C.; Hwang, J.; Suijkerbuijk, J. W. A.; Erk, P.; Siebbeles, L. D. A.;Savenije, T. J. Determination of Singlet Exciton Diffusion Length in Thin Evaporated C_{60} Films for Photovoltaics. *Journal of Physical Chemistry Letters* **2012**, *3*, 2367-2373.

[5] Schwarz, C.; Milan, F.; Hahn, T.; Reichenberger, M.; Kümmel, S.;Köhler, A. Ground State Bleaching at Donor-Acceptor Interfaces. *Advanced Functional Materials* **2014**, *24*, 6439-6448.

[6] Grancini, G.; Binda, M.; Neutzner, S.; Criante, L.; Sala, V.; Tagliaferri, A.;Lanzani, G. The Role of Higher Lying Electronic States in Charge Photogeneration in Organic Solar Cells. *Advanced Functional Materials* **2015**, *25*, 6893-6899.

[7] Vandewal, K. Interfacial Charge Transfer States in Condensed Phase Systems. *Annual Review of Physical Chemistry, Vol 67* **2016**, *67*, 113-133.

[8] Zhu, X. Y.; Monahan, N. R.; Gong, Z. Z.; Zhu, H. M.; Williams, K. W.;Nelson, C. A. Charge Transfer Excitons at van der Waals Interfaces. *Journal of the American Chemical Society* **2015**, *137*, 8313-8320.

4.5. Role of the effective mass and interfacial dipoles on exciton dissociation in organic donor-acceptor solar cells

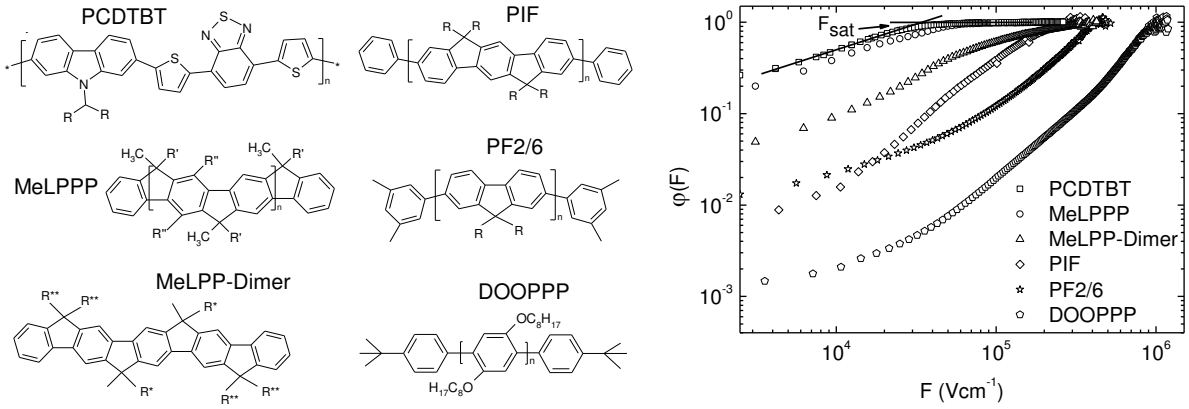

Christian Schwarz, Steffen Tscheuschner, Johannes Frisch, Stefanie Winkler, Norbert Koch, Heinz Bässler, Anna Köhler

Veröffentlicht in

Physical Review B (**2013**), 87, 155205

(DOI: https://doi.org/10.1103/PhysRevB.87.155205)

Role of the effective mass and interfacial dipoles on exciton dissociation in organic donor-acceptor solar cells

Christian Schwarz,[1] Steffen Tscheuschner,[1] Johannes Frisch,[2] Stefanie Winkler,[2,3] Norbert Koch,[2,3] Heinz Bässler,[1] and Anna Köhler[1,*]

[1]*Experimental Physics II and Bayreuth Institute of Macromolecular Research (BIMF), University of Bayreuth, 95440 Bayreuth, Germany*

[2]*Institut für Physik, Humboldt-Universität zu Berlin, 12489 Berlin, Germany*

[3]*Helmholz-Zentrum Berlin für Materialien und Energie GmbH, 12489 Berlin, Germany*

(Received 25 February 2013; published 15 April 2013)

Efficient exciton dissociation at a donor-acceptor interface is the crucial, yet not fully understood, step for obtaining high efficiency organic solar cells. Recent theoretical work suggested an influence of polymer conjugation length and of interfacial dipoles on the exciton dissociation yield. This necessitates experimental verification. To this end, we measured the dissociation yield of several polymer/C_{60} planar heterojunction solar cells up to high electric fields. The results indeed prove that the yield of exciton dissociation depends strongly on the conjugation length of the polymers. Complementary photoemission experiments were carried out to assess the importance of dipoles at the donor-acceptor interfaces. Comparison of exciton dissociation models with experimental data shows that the widely used Onsager-Braun approach is unsuitable to explain photodissociation in polymer/C_{60} cells. Better agreement can be obtained using "effective mass" models that incorporate conjugation length effects by considering a reduced effective mass of the hole on the polymer and that include dielectric screening effects by interfacial dipoles. However, successful modeling of the photocurrent field dependence over a broad field range, in particular for less efficient solar cell compounds, requires that the dissociation at localized acceptor sites is also taken into account.

DOI: 10.1103/PhysRevB.87.155205 PACS number(s): 72.20.Jv, 88.40.jr, 72.80.Le

I. INTRODUCTION

Organic solar cells have now reached power conversion efficiencies above 10%, which is often referred to as the lower limit for industrial mass production.[1] A significant contribution to this advance lies in the optimization of film-processing conditions and device architecture.[2–6] These steps serve to increase the fraction of photogenerated excitons that can dissociate, e.g., by reaching dissociation sites, and effectively reduce inadvertent recombination of electrons and holes.[7] For even more efficient solar cells, fill factor, short circuit current, and open circuit voltage need to be improved by increasing the exciton dissociation yield further.[8] A key step toward this lies in understanding the mechanisms and the material parameters that control how a photogenerated bound electron-hole (e-h) pair (exciton) dissociates into mobile charge carriers. Knowledge of the relevant processes allows for further optimization of film morphology and device architecture and, in particular, for guidelines in the design and choice of suitable high efficiency materials.

Today's organic solar cells involve at least two different types of molecular materials, i.e., a donor compound and an acceptor. In such a donor-acceptor (D-A) system, an exciton is created next to a molecular D-A interface or reaches it within its lifetime. There, it transfers its electron from the excited donor to the ground state acceptor molecule and forms a charge transfer state. This initial charge transfer step usually takes place on an ultrafast timescale.[9,10] Since the dielectric constant of organic semiconductors is typically only 3–4, dielectric screening is weak and the e-h pair is initially bound by its Coulomb potential. To become mobile, the charges need to escape from their mutual Coulombic potential without suffering geminate recombination. In a naïve picture of pointlike charges, they are unbound when they separate to a distance defined as the capture radius, which, in the absence of an electrostatic field, is $r_c = e^2/4\pi\varepsilon_0\varepsilon_r kT$. At that distance, the thermal energy exceeds the Coulomb energy, with typical room temperature values being $r_c \cong 16$ nm for $\varepsilon_r = 3.5$.

The central question is why the e-h pair can overcome the considerable Coulomb potential. One currently discussed possibility is that the excess energy, liberated when the excited donor electron transfers to the acceptor, facilitates complete dissociation. In this case, the yield should depend on the energy difference between the energy of the lowest unoccupied molecular orbital (LUMO) level of the donor and the acceptor. Although there are reports in the literature in favor of this possibility,[11–13] there is strong evidence that alternative dissociation channels must be operative as well. Experimental and theoretical investigations suggest that the degree of delocalization of both an exciton and a charge in a conjugated polymer may be of key importance,[9,12,14–16] the extreme view being the notion that conjugated polymers behave like a one-dimensional inorganic semiconductor with completely delocalized wavefunctions.[17] A more conservative view is that right after its creation, an e-h pair at a D-A interface is in a short-lived extended state with a high, yet finite chance for complete dissociation. Unsuccessful e-h pairs relax in energy and form more tightly bound meta-stable charge transfer states, from which subsequent dissociation attempts may occur.[12] In addition to exciton delocalization, it has emerged that interfacial dipoles may also be conducive to exciton dissociation. Theoretical,[18,19] as well as experimental,[20] evidence for such dipoles seems to correlate with increased photocurrent yields.

To discriminate between the different possibilities, one may compare the experimental photocurrent yields against

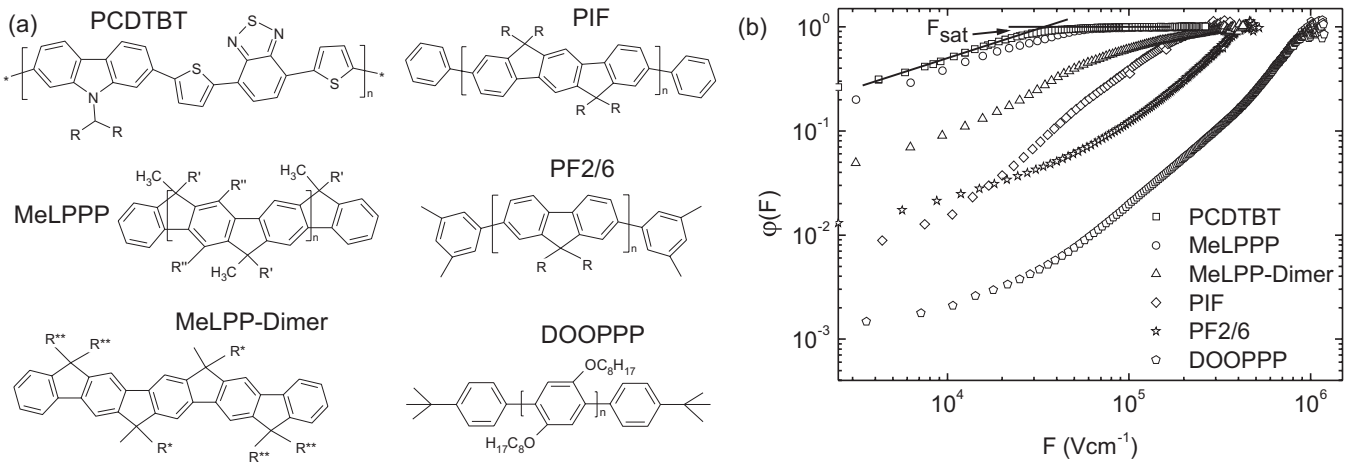

FIG. 1. (a) Chemical structures and abbreviations of the donor polymers (R = 2-ethylhexyl, R′ = 1,4-C_6H_4-*n*-$C_{10}H_{21}$, R″ = -*n*-C_6H_{13}, R* = C_6H_{13}, R** = $C_{10}H_{13}$). (b) External photocurrent quantum yields of bilayer C_{60} devices made with PCDTBT, MeLPPP, MeLPP-dimer, PIF, PF2/6, and DOOPPP, measured at 2.2 eV excitation as a function of the internal field and normalized to unity at the saturation value. For PCDTBT, the tangents whose intersection defines the saturation field F_{sat} are indicated as an example. PCDTBT = Poly[[9-(1-octylnonyl)-9H-carbazole-2,7-diyl]-2,5-thiophenediyl-2,1,3-benzothiadiazole-4,7-diyl-2,5-thiophenediyl], MeLPPP = methyl-ladder-type-poly(*p*-phenylene), MeLPP-dimer = methyl-ladder-type-*p*-phenylene-dimer, PIF = poly(indeno-fluorene), PF2/6=ethyl-hexyl-poly(fluorene), DOOPPP = Di-octyloxy-poly(*p*-phenylene).

predictive models. A classical approach, based on the seminal works by Onsager and Braun, consists in considering the dependence of exciton dissociation on an increasing electric field in the device.[21] A coulombically bound e-h pair requires a certain electric field for complete separation. Above a certain saturation field strength, the yield should become constant when the drop of the electrostatic potential exceeds the Coulomb-binding energy of the e-h pair. If geminate recombination was the dominant recombination process, then the saturation field strength F_{sat} is a measure of the Coulomb-binding energy of an e-h pair and also of the size, i.e., the mean e-h separation of the dissociating e-h pair. While the Onsager-Braun model is frequently employed to interpret organic solar cell performance, its premise of treating the e-h pair as point charges renders its application questionable for materials with extended, delocalized excited states such as polymers. Meanwhile, there are more sophisticated models available. For example, the delocalization of the photogenerated charges can be incorporated explicitly by considering their effective mass.[22–25] Similarly, the screening effect of interfacial dipoles on the Coulomb potential of the e-h pair has been implemented in the theoretical framework.[23,25] So far, however, these models have not yet been compared against experimental data.

Here, we aim to assess the impact of conjugation length and interfacial dipoles on exciton dissociation by comparing simulations of the aforementioned models with experimental data. We recently measured the field dependent photocurrent in a bilayer solar cell in which conjugated phenylene-type donor polymers were combined with a C_{60} acceptor layer. We found that the more ordered, and thus the more conjugated, a polymer chain is, the lower the saturation field strength.[16] To cover a wide range of donor materials in the same series of experiments and under exactly the same experimental conditions, we confirmed the previous experiments on DOOPPP, PIF, and MeLPPP and expanded them to further include PF2/6, a dimer of MeLPPP and the widely used low band-gap material PCDTBT (see Fig. 1 for chemical structure and abbreviations). To obtain information on possible interfacial dipoles, ultraviolet photoelectron spectroscopy (UPS) experiments were carried out for the interfaces of these compounds with C_{60}. The experimental results were analyzed by parameterizing and simulating the existing models. We are able to quantify the effect of charge delocalization, expressed in terms of the effective mass, and of ground state dipoles on the field dependent exciton dissociation. Further, we show that a single mechanism cannot explain the field dependence of the photocurrent, yet it can be modeled adequately by considering a superposition of two processes.

II. EXPERIMENTAL RESULTS

Figure 1 shows the chemical structures of the investigated polymers and the dimer, as well as the relative photocurrent quantum yields $\varphi(F)$ of bilayer devices (with C_{60} as acceptor) as a function of the internal electric field. The key parameter derived from these data is the saturation field strength F_{sat}, defined by the intersection of the tangents to the photocurrent in the regimes of low electric field and high electric field (i.e., at photocurrent saturation) in a double logarithmic plot (see Fig. 1). The existence of the saturation field implies that there is a field-dependent recombination mechanism that can be overcome at high fields. This can be seen by considering that photoexcitation with rate G results in bound or unbound charge carriers. This leads to a photocurrent that is controlled by the competition between a field-dependent escape rate $\mu F/d$ from the recombination zone, with μF being the transport velocity and d the layer thickness, and a recombination rate k_r. The recombination mechanism may, in principle, be geminate or nongeminate. The photocurrent then depends on the field as $j \propto G \cdot \mu F d^{-1}/(\mu F d^{-1} + k_r) = G \cdot 1/(1 + \frac{dk_r}{\mu F})$. Thus, at low fields, the photocurrent will be reduced due to recombination, while at high field, it eventually saturates. We

now argue that, in our case, this recombination is predominantly geminate. As detailed in the Supplemental Material,[26] one can estimate that monomolecular and bimolecular decay become comparable at a critical light intensity of about $2 \cdot 10^{18}$ photons/cm^{2}s. Our photocells were measured at a photon flux of about $4 \cdot 10^{15}$ photons/cm^{2}s, i.e., at an intensity that is 1/500ths of the intensity where bimolecular recombination becomes important. This is consistent with the observation that for all materials the photocurrents depend linearly on the pump intensity I_{ex}. If the carrier would recombine bimolecularly, as were the case for trap-free nongeminate recombination, a dependence such as $j \propto \sqrt{I_{ex}}$ should result. The existence of a saturation field at the light intensities used in our experiment therefore shows that there is a field-dependent geminate-pair recombination mechanism. Such a dominant role of geminate recombination is in agreement with reports by other research groups, even when using higher light intensities.[27] When comparing the polymer MeLPPP and the associated dimer MeLPP, one observes a significant drop of F_{sat} from $4 \cdot 10^4$ V cm^{-1} to $2 \cdot 10^5$ V cm^{-1}. This is the first clear indication that wave-function delocalization in the donor is important. It turns out that the saturation field strength, and thus the binding energy of the interfacial e-h pair, decreases in the order DOOPPP, PF2/6, PIF, MeLPP-dimer, MeLPPP, and PCDTBT (Fig. 1, and Table II further below). For the poly-*p*-phenylene based systems, yet not for the donor-acceptor copolymer PCDTBT, this also correlates with a red-shift of the absorption [Fig. 2(a)].

The red-shift of the optical spectra within a series of structurally related compounds is a well-established signature of increased delocalization of the π-electron system in conjugated oligomers and polymers. A heuristic way to correlate the transition energy of an oligomer or polymer with a certain number of conjugated monomers is provided in the coupled oscillator model of W. Kuhn.[28,29] In the case of poly-*p*-phenylene-type polymers, the coupling elements are identified with phenylene rings. By using fluorescence spectra of ladder-type phenylene oligomers, one can parameterize the chain-length dependence of the transition energy of a chain of perfectly aligned phenylenes.[30] Deviations from chain planarity raise the transition energy and can be translated into an effective conjugation length. This parameterization allows extracting the effective conjugation length of the polymers in both absorption and emission. The two values differ as the excited state geometry is usually more planar than the ground state geometry. In addition, in a film of disordered polymers, there is energy transfer from (shorter) absorbing to (longer) emitting chromophores. In Fig. 2(b), we show the saturation field strengths as a function of the effective conjugation length in absorption and fluorescence for the poly-*p*-phenylene-type systems. The dramatic decrease of F_{sat} with the increasing conjugation length of the polymers proves that the spatial extent of the conjugation length in a π-conjugated polymer has an important bearing of exciton dissociation in our solar cells. We also note that the MeLPP-dimer, which contains five phenylene units so that $1/n = 0.2$, behaves differently. Although F_{sat} for the dimer is four times higher than that for the polymer, one expected a much higher value based upon the parameterization data of the conjugation length. This is evident in Fig. 2(b), where F_{sat} for the dimer is compared to the saturation field strength for the polymers.

Having established that there is a clear dependence of the saturation field strength on the effective conjugation length, we now consider whether there is an influence of interfacial dipoles that exist at the heterojunction in the ground state. To this end, the energy-level line-up at the polymer/C_{60} interfaces was investigated by UPS. C_{60} was sequentially deposited by thermal sublimation in ultrahigh vacuum conditions. After each deposition step, valence band and secondary electron cutoff (SECO) spectra were recorded. The typical SECO evolution upon deposition of C_{60} on the polymer film is shown for the example of PCDTBT in Fig. 3(a). We observe that the initial work function of the pristine PCDTBT film (4.60 eV) is increased to 4.72 eV upon 8 Å C_{60} deposition, and it remains constant for higher C_{60} coverage. The valence spectra show the evolution of C_{60}-derived molecular levels. The valence band onset of pristine PCDTBT is at a binding energy of 0.63 eV below the Fermi level (E_F), as indicated in Fig. 3(a) this yields an ionization energy of 5.23 eV. The position of the PCDTBT valence band onset was found to be independent of the C_{60}

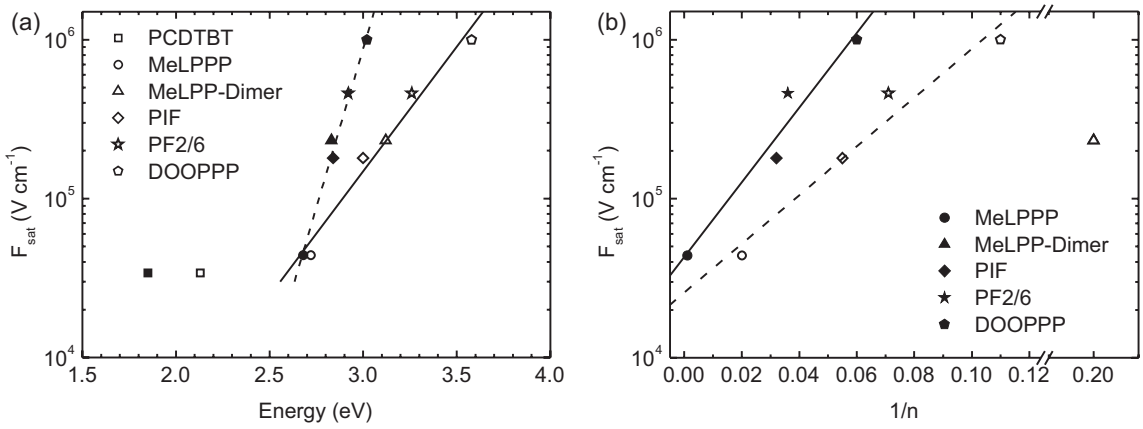

FIG. 2. Saturation field strengths of the bilayer field-dependent photocurrent yields; (a) as a function of the donor absorption energy (empty symbols) and emission energy (filled symbols), (b) as a function of the inverse effective conjugation length of the donors in the ground state geometry (data taken from absorption, empty symbols) and in the excited state geometry (data taken from emission, filled symbols). The lines serve as a guide to the eye.

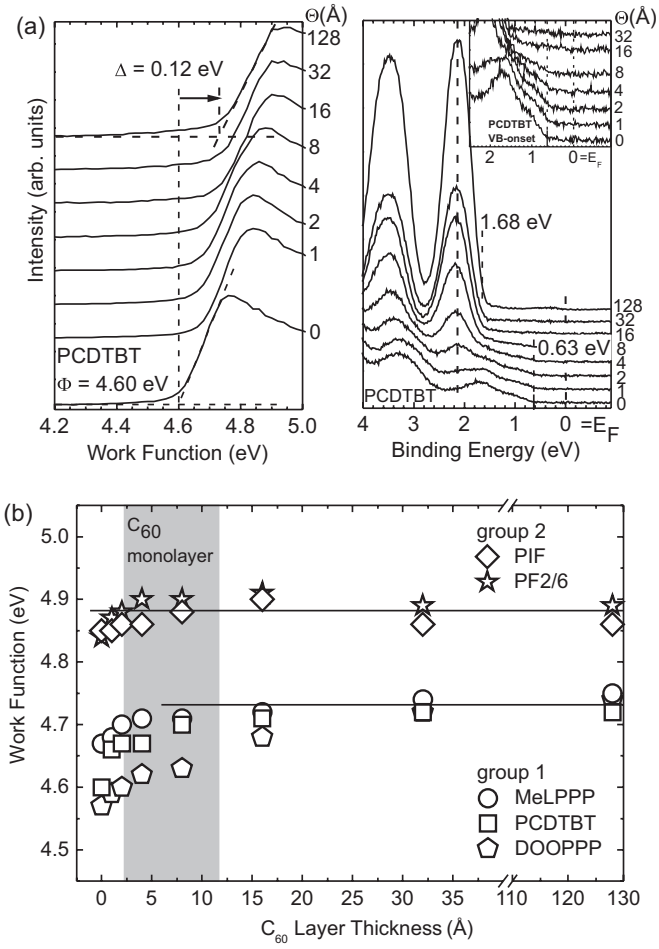

FIG. 3. (a) SECO (left) and low-binding energy region (right) of a 20-nm PCDTBT film spin coated on a PEDOT/PSS-ITO substrate and subsequently deposited C_{60} on top. (b) Work function evolution as a function of subsequent deposited C_{60} coverage. Two groups can be distinguished: group 1 (MeLPPP, PCPTBT, and DOOPPP) Fermi-level pinning of C_{60}-LUMO is found; group 2 (PF2/6 and PIF) vacuum-level alignment is established.

coverage, as it can be observed in the valence band region spectra up to a C_{60} coverage of 8 Å [see close-up spectra in Fig. 3(b)]. The low binding energy onset of emission from the C_{60} highest occupied molecular orbital (HOMO) levels is constant at 1.68-eV binding energy for all coverages. Adding the final work function of 4.72 eV to the energy difference between the C_{60} HOMO onset and the Fermi level yields an ionization energy of 6.40 eV for C_{60}, which is in line with previously reported values.[31,32]

The situation of a constant HOMO position and an increase of the sample work function for the very early stage of interface formation is typical for an interface dipole due to Fermi-level pinning at unoccupied states of C_{60}, i.e., the LUMO level or gap states at slightly lower energy.[33,34] In this scenario, the work function changes until a full monolayer is reached and remains constant for higher film thickness, which we indeed observe beyond 8 Å C_{60} coverage. This coverage corresponds approximately to a monolayer of C_{60} since the diameter of a C_{60} molecule is ∼10 Å.[35] Similar results are obtained for DOOPPP and MeLPPP. In both cases, the initial work function

TABLE I. The ionization energy (IE), the work function Φ of the pristine film, and the change in work function ΔΦ due to the deposition of C_{60}, along with the derived value for the fractional dipole strengths α.

Material	PCDTBT	MeLPPP	PIF	PF2/6	DOOPPP
IE (eV)	5.23	5.28	5.82	5.85	5.22
Φ (eV)	4.60	4.67	4.85	4.84	4.57
ΔΦ (eV)	0.12	0.08	0.02	0.05	0.17
α (10^{-3})	21.4	14.2	3.6	8.9	30.3

of the pristine polymer films increases due to C_{60} deposition. Note that in all three cases, including PCDTBT, the final work function of a multilayer C_{60} deposited film onto the polymer film reaches the same value. Thus, ground state interface dipoles of varying magnitude, dependent on the initial polymer work function, are found (Table I). In contrast, vacuum-level alignment was found at the C_{60}/PIF and C_{60}/PF2/6 interfaces [Fig. 3(b)]. Within accuracy of our measurement (±0.05 eV), the work function of the PIF and PF2/6 polymers film did not change due to C_{60} deposition. The evolution of the sample work function as a function of C_{60} coverage is summarized in Fig. 3(b) for all five different polymers. As indicated in Fig. 3, a transition from vacuum-level alignment to Fermi-level pinning at the polymer/C_{60} interface occurs for a work function of a pristine polymer film below ∼4.75 eV. Nevertheless, Fermi-level pinning at unoccupied states of C_{60} was unexpected because of the C_{60} threshold electron affinity of 4.50 eV in the solid phase[31] (obtained by inverse photoelectron spectroscopy). This is 0.25 eV lower as the obtained transition work function of ∼4.75 eV. This difference can be explained by unoccupied gap states that are created within the C_{60} film due to impurities coming from the spin-coated polymer films or structural defects. The resulting work function values, ionization energies, and work function changes ΔΦ for the five interfaces are summarized in Table I.

From these studies, two key experimental observations emerge.

(i) The electric field strength F_{sat}, at which $\varphi(F)$ saturates decreases by about a factor of 20–30 in the series DOOPPP, PF2/6, PIF, MeLPP-dimer, MeLPPP, and PCDTBT. This correlates with the bathochromic shift of the S_1-S_0 0-0 transition, except for PCDTBT. This is a strong indication that electronic delocalization of the hole residing on the donor is of key importance.

(ii) The photoemission experiments show that there is, indeed, some ground state charge transfer between donor and acceptor, but this effect is relatively weak. In the case of PF2/6, PIF, and MeLPPP, it is barely noticeable. For DOOPPP and PCDTBT, the interfacial potential drop is 170 meV and 120 meV, respectively.

III. ANALYSIS AND DISCUSSION

A. Individual models

One of the most widely applied models to account for exciton dissociation is the Onsager-Braun model, even though it does not account for the effects of effective conjugation length or for interface dipoles.[36,37] The high popularity of

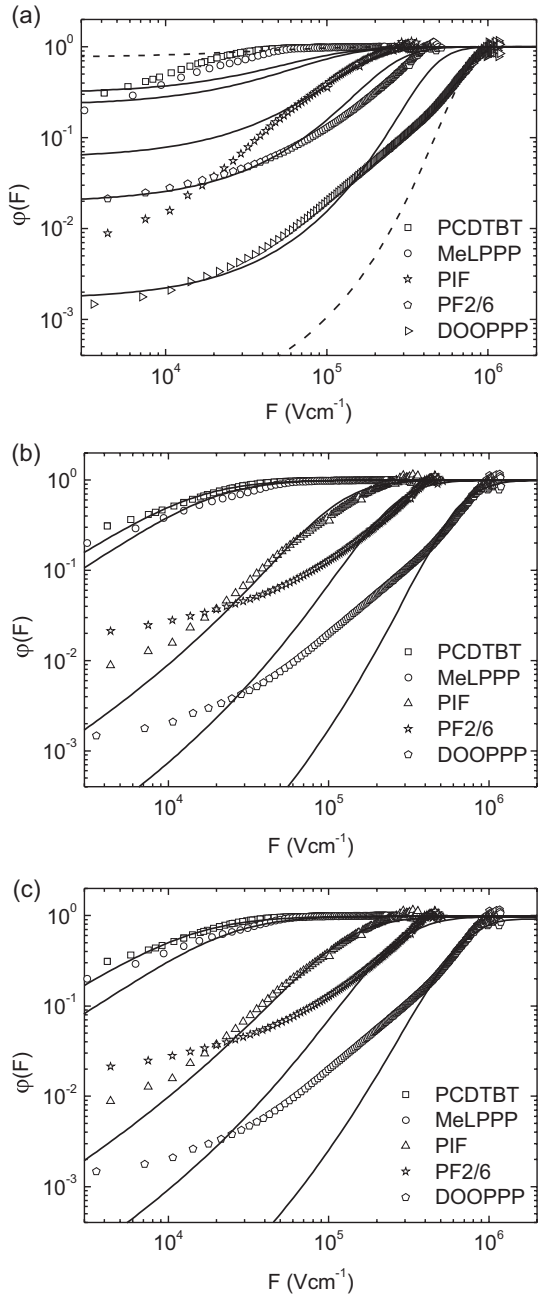

FIG. 4. Comparison of the field-dependent photocurrent yields (symbols) of donor /C_{60} bilayer solar cells with simulations (lines) based on (a) the Braun model [Eqs. (1), (2)], (b) the effective mass model [Eqs. (3)–(5)], and (c) the dipole model [Eqs. (3), (6), and (7)]. The parameters are presented in Table II.

this model warrants a detailed consideration. Onsager's theory for photogeneration in a single component molecular solid rests upon the notion that optical excitation with sufficient energy can autoionize and form a Coulombically bound e-h pair.[38] This pair of pointlike charges can rather fully dissociate in the course of temperature and field-assisted random walk of one carrier in the field of the other, or it may recombine geminately to the ground state. Braun extended this concept to D-A systems in which the lowest excited state is a charge transfer state that can live long enough to make several attempts toward complete dissociation before decaying geminately to the ground state.[39] This dissociation yield is determined by the trade-off between the field-dependent dissociation rate $k_d(F)$ and the field-independent e-h pair decay rate to the ground state k_f, i.e.,

$$\varphi(F) = \frac{k_d(F)}{k_d(F) + k_f} = \frac{1}{1 + k_f k_d(F)^{-1}}. \quad (1)$$

The theory predicts a strong field dependence of the dissociation rate $k_d(F)$, that is,

$$k_d(F) = \frac{3\mu e}{4\pi\varepsilon_0\varepsilon_r r_0^3} \exp\left(\frac{-\Delta E}{kT}\right) \frac{J_1(2\sqrt{-2b})}{\sqrt{-2b}} \quad \text{with}$$
$$b = \frac{e^3 F}{8\pi\varepsilon_0\varepsilon_r k^2 T^2}. \quad (2)$$

Here, J_1 is the Bessel function of order one, F is the electric field, μ is the sum of the mean electron and hole mobility, $\Delta E = e^2/4\pi\varepsilon_0\varepsilon_r r_0$ is the Coulombic-binding energy of the e-h pair, which is controlled by the initial intrapair separation r_0. Inserting (2) into (1) allows simulating the field dependence of the dissociation yields and comparing it with the experimental data; this is shown in Fig. 4(a). For the simulation, we employed $\varepsilon_r = 3.5$ and we used the Bessel function J_1 and not the frequently employed approximation $(1 + b + b^2/3 + b^3/18 + ...)$, as the deviations become significant in the regime of high field strengths that is of interest here. The free parameters in the simulation are the intrapair separation r_0 and the ratio μ/k_f; they are listed in Table II.

We find that the Onsager-Braun model yields unsatisfactory results in two respects. First, and most importantly, the field dependence for the compounds with low F_{sat}, MeLPPP, and PCDTBT, cannot be reproduced at all, and for the remaining compounds, agreement between the experimental data and the Onsager-Braun fits is poor. The main reason for this is that the field dependence predicted by the Braun model is steeper than the experimentally found one. For illustration, if the simulation parameters are adjusted so that there is not an overall agreement with the experimental curve but rather the value of the saturation field is matched [dashed in Fig. 4(a)], one finds that for the regime of low-field strengths, the Onsager-Braun model underestimates the photocurrent yield for DOOPPP while it overestimates it for PCDTBT. Second, the simulation parameters required are unphysical. While the values obtained for r_0 in the nm range are plausible, the values inferred for μ/k_f imply either charge mobility or a lifetime that are too high to be consistent with existing knowledge. Consider, for example, PCDTBT, where $\mu/k_f = 2 \cdot 10^{-8}$ cm^2 V^{-1}. The lifetime at zero electric field is $\tau_0 = [k_f + k_d(0)]^{-1}$. $k_d(0)$ can be evaluated as $k_d(0) = \frac{\mu e}{\varepsilon_0\varepsilon_r}\frac{3}{4\pi r_0^3}\exp(\frac{-\Delta E}{kT})$. Taking μ to be dominated by the hole mobility, and using a value of $1 \cdot 10^{-4}$ cm^2/Vs,[40] one obtains $k_d(0) = 1.3 \cdot 10^3$ s^{-1}, $k_f = 5 \cdot 10^3$ s^{-1}, and $\tau_0 = 158\mu$s. Similar calculations can be carried out for the other polymers in Table II. From this estimate, one can see first that $k_d(0) < k_f$, so that $\tau_0 \approx 1/k_f$, and, more importantly, the values for τ_0 range from 6 μs (for MeLPPP, based upon $\mu = 2 \cdot 10^{-3}$ cm^2/Vs) to more than 30 ms (for DOOPPP, assuming $\mu < 10^{-5}$ cm^2/Vs, which is an upper limit for the hole mobility in highly disordered polymers). Typical lifetimes for charge transfer states between

TABLE II. Fit parameter for different individual models, along with the experimentally measured saturation field strength F_{sat}.

Material	PCDTBT	MeLPPP	PIF	PF2/6	DOOPPP	MeLPP-dimer
F_{sat} [Vcm^{-1}]	$3.4 \cdot 10^4$	$4.4 \cdot 10^4$	$1.8 \cdot 10^5$	$4.6 \cdot 10^5$	$1.0 \cdot 10^6$	$2.3 \cdot 10^5$
Onsager-Braun model[a]						
r_0 [nm]	1.03	1.02	0.92	0.86	0.80	1.02
μ/k_f [10^{-12} m^2 V^{-1}]	2.0	1.5	1.3	1.1	0.3	0.50
Effective mass model (numerical)						
m_{eff}/m_e	0.060	0.067	0.110	0.170	0.300	0.115
$\tau_0 \nu_0 \exp(-2\gamma r)$	3910	3830	3500	100	40	3830
Effective mass model (parabolic approximation)						
m_{eff}/m_e	0.060	0.067	0.110	0.170	0.300	0.115
$\tau_0 \nu_0 \exp(-2\gamma r)$	60	65	40	37	12	65
Dipole model						
m_{eff}/m_e	0.117	0.109	0.130	0.250	1.000	0.20
$\tau_0 \nu_0 \exp(-2\gamma r)$	60	65	40	37	12	65

[a]For the solid lines in Fig. 4(a). See Supplemental Material[26] for the dashed lines.

conjugated polymers and C_{60} derivatives tend to be up to few tens of nanoseconds.[37,41–43] Thus, the Braun model is clearly inadequate to describe the field dependence of exciton dissociation in conjugated polymers. In the same way, we found the mathematically more rigorous treatment of the Onsager-Braun model presented recently by Wojcik and Tachiya[44] to be inappropriate for these conjugated polymers.

Why should the Onsager-Braun treatment be an unsuitable model for conjugated polymer systems when it has been shown to be highly successful for molecular donor-acceptor crystals? One difference between aromatic molecules such as the polyacenes and the conjugated polymers used in today's solar cells is the degree of charge and exciton delocalization. The experimental results clearly show that the photodissociation yield increases with the effective conjugation length of the polymers. A way to explicitly include the effects due to conjugation has been presented by Arkhipov *et al.* by considering the effective mass of a hole on a polymer chain.[22,23] The original motivation for this effective mass model was the observation of a very weak temperature dependence of the photocurrent in MeLPPP that was incompatible with the predictions of the Onsager-Braun model.[45] Such weak temperature dependence has more recently been confirmed for bilayers[46] as well as blends.[47] In order to account for the lack of temperature activation for a well-conjugated polymer like MeLPPP, Arkhipov suggested there should be an additional term that reduces the energy needed to separation of electron and hole.

The central idea of Arkhipov's model is simple. After photoexcitation of the polymer donor, the electron is transferred to the acceptor, and the hole remains on the polymer chain. The two carriers are bound by their mutual Coulomb potential. The hole on the polymer is delocalized within the effective conjugation length, i.e., it can be viewed to carry out zero-point quantum oscillations in the Coulomb potential due to the electron [Fig. 5(a)]. This quantum oscillation is associated with an energy that depends on the effective mass m_{eff} of the hole. This kinetic energy assists the hole in overcoming the Coulomb potential. The effective mass is introduced here in a heuristic way as a measure for the electronic coupling within the polymer chain that depends on intrachain disorder. A low relative effective mass implies a highly delocalized hole. Arkhipov applied this effective mass model to two different situations. One case comprises the situation of a donor doped with only few acceptors;[22] the other considers an extended interface between donor and acceptor, where dark interfacial dipoles prevail.[23] This idea of the effective mass model has been taken up and developed further by the Baranovskii group. A particularly elegant formulation of the effective mass model has been presented by Nenashev and coworkers, and we have therefore applied the Nenashev formulation to our data.[24] Nenashev considers the polymer as a set of one-dimensional chains that are placed parallel to the polymer fullerene interface. The electric field is acting orthogonal to the interface. The geometry of this model is illustrated in Fig. 5(b). The chains are numbered from 1 to n, starting at the interface, with spacing r. The electron on the fullerene is taken as immobile while the hole on the polymer is taken to hop. The dissociation yield $\varphi(F)$ is controlled by the rates for the recombination of the e-h pair, $k_r = 1/\tau_0$, where τ_0 is the lifetime of the e-h pair, and by the rate for dissociation k_d

$$\varphi(F) = \frac{k_d}{k_d + k_r} = \frac{\tau_0}{\tau_0 + k_d^{-1}} = \frac{\tau_0}{\tau_0 + \sum_{n=1}^{N-1} a_{n\to n+1}^{-1} \exp\left(\frac{E_n - E_1}{kT}\right)}. \quad (3)$$

Here, $a_{n\to n+1}$ is the Miller-Abrahams hopping rate of the hole,

$$a_{n\to n+1} = \nu_0 \exp(-2\gamma r) \begin{cases} \exp\left(-\frac{E_{n+1}-E_n}{kT}\right) & E_{n+1} > E_n \\ 1 & E_{n+1} \leqslant E_n \end{cases} \quad (4)$$

ν_0 and γ take their usual meaning as frequency factor and as a measure for the electronic coupling, respectively. The hopping and dissociation process is controlled by energy of the hole on each chain, E_n, which results from the Coulomb potential due to the electron, from the potential of the applied field and from the zero-point oscillation along the conjugated segment within

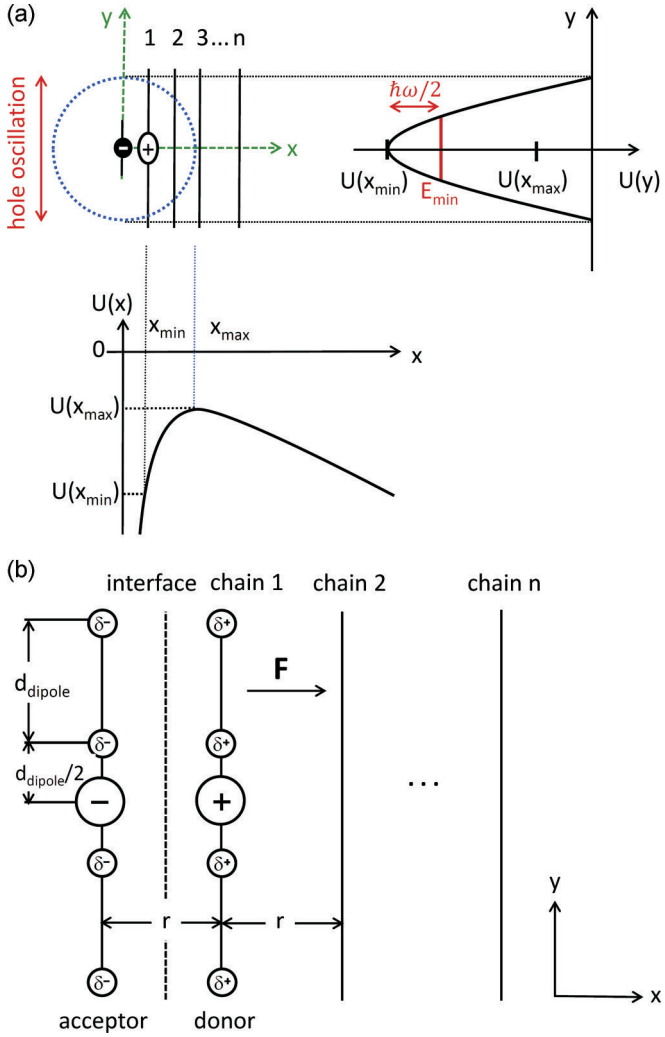

FIG. 5. (Color online) Schematic illustrating electron-hole dissociation at the bilayer interface with an electron on C_{60} at $x = 0$ and a hole on a polymer chain. The chains are assumed parallel to the interface and are labeled 1 to n. (a) The hole on the polymer chain executes a zero-point oscillation along the y direction inside the Coulomb well set up by the electron. The potential along x direction is due to the Coulomb field from an electron at $x = 0$ and a constant applied electric field in x direction. The energy of the hole located at $x_{\min}$ is raised by a zero-point oscillation energy $\hbar\omega/2$, $E_{\min} = U(x_{\min}) + \hbar\omega/2$. To escape, the energy barrier between $E_{\min}$ and $U(x_{\max})$ needs to be overcome. The potential along the y direction is approximated by a parabola. (b) Detailed geometry at the donor-acceptor interface. In the effective mass model, $\delta^+ = \delta^- = 0$. In the dipole model, interfacial ground state dipoles δ^+ and δ^- modify the potential and assist the hole's escape. For simplicity, we used $d_{\text{dipole}} = r$ in our modeling.

the Coulomb potential. As detailed in the original paper by Nenashev, it can be calculated solving the Schrödinger equation

$$-\frac{\hbar^2}{2m_{\text{eff}}}\frac{d^2\psi}{dy^2} + U_n\psi = E_n\psi_n, \tag{5}$$

with

$$U_n = -\frac{e^2}{4\pi\varepsilon_0\varepsilon_r}\frac{1}{\sqrt{y^2 + x_n^2}} - eFx_n, \quad x_n = nr.$$

The dependence of the dissociation rate on the electric field and on the effective mass is thus included implicitly via the hole energy E_n. To implement the Nenashev formalism, we solved (5) numerically and inserted the resulting E_n in (4) and (3), so that $\varphi(F)$ could be calculated parametric in the relative effective mass m_{eff}/m_e and in the product of the e-h pair lifetime with the isoenergetic hopping parameter $\tau_0\nu_0\exp(-2\gamma r)$. The resulting curves with optimized parameters listed in Table II [as "effective mass model (numerical)"] are compared to the experimental data in Fig. 4(b).

In contrast to the Onsager-Braun model, the agreement of the simulated and experimental field dependence is quite satisfactory over the entire field range for the more delocalized compounds PCDTBT, MeLPPP, and PIF. For the compounds with shorter conjugation length, simulation and experiment match only at high fields, and one finds that experimentally there is an additional photocurrent quantum-yield contribution at low field strength. Before we address this additional contribution, let us discuss the values obtained for the parameters. If we know the isoenergetic jump rate $\nu_0\exp(-2\gamma r)$, we can derive the lifetime τ_0 of the geminate e-h pair from the $\tau_0\nu_0\exp(-2\gamma r)$ value.

As an estimate, we consider first the jump rate of an electron from an optically excited donor to a silicon nanoparticle as an acceptor in a P3HT/Si solar cell, which was recently reported.[9] Using ultrafast pump-probe spectroscopy, Herrmann and coworkers showed that the exciton state, created instantaneously during the rise of the laser pulse, decays to yield a polaron signal. The time constant of the exciton decay and the concomitant polaron rise was found to be 120 fs, corresponding to a jump rate of $8 \cdot 10^{12}$ s^{-1}. This jump rate associated with the initial charge transfer step can be taken as the rate for an isoenergetic jump. Second, one may argue that the rate for an isoenergetic jump should be of the same range of that of a charge carrier in an ordered organic solid. There, the charge carrier mobility is around 1 cm^2/Vs.[48] By using the Einstein ratio between mobility μ and the carrier diffusion constant D, $\mu/D = e/kT$, and assuming isotropic diffusion in a cubic system, where $D = \frac{1}{6}a^2[\nu_0\exp(-2\gamma r)]$, with a typical lattice constant for a crystal of 0.6 nm, one ends up with an estimate of the jump rate of $4 \cdot 10^{13}$ s^{-1}. Adopting a representative value for $\tau_0\nu_0\exp(-2\gamma r) \cong 3800$ and a jump rate of about $4 \cdot 10^{13}$ s^{-1} thus yields a lifetime of about 95 ps for the geminate e-h pair, which is a realistic lifetime.

The relative effective masses obtained from the simulation decrease in line with the increase in conjugation length of the compounds. This confirms the notion that improved electronic coupling along the polymer chain is crucial for improving the dissociation efficiency. However, the values for the relative effective masses m_{eff}/m_e range from 0.3 for DOOPPP to 0.060 for PCDTBT, which is rather low. For comparison, for polydiacetylene, which is the most ordered conjugated polymer that is known, electroreflectance measurements by Weiser and Möller yielded an effective mass of 0.05 m_e,[49] and theoretical calculations by Van der Horst placed its effective mass at 0.1 m_e.[50] In the more disordered compounds studied here, the effective mass can be expected to be somewhat higher. Thus, in summary, while the incorporation of the conjugation lengths' effects through the effective mass leads to an improved description of the charge dissociation process, in particular for

the well-delocalized compounds, the values required for the effective mass to account for the dissociation are too low.

The fact that there must be an additional factor that contributes to efficient exciton dissociation at the D-A interface had already been noticed by Arkhipov a decade ago.[23] This was prompted by the observation that in a D-A system, the dissociation yield increases abruptly above a critical acceptor concentration.[51] Dissociation yields exceeding 50% at moderate electric field strengths, as well as the usually weak temperature and field dependence, were taken as an indication that the Coulomb attraction between carriers within a short geminate pair must be effectively screened or counterbalanced. To allow for such a screening, Arkhipov *et al.* invoke the existence of a layer of dipoles that exist in the dark (i.e., in the ground state) at the interface between donors and acceptors with different electron affinities. There are experimental and theoretical results in favor of this notion.[18–20] Arkhipov thus extended the effective mass model to account for the effect of dipoles.[23] We refer to the resulting model as the dipole model.

Arkhipov considered a bilayer system where photoexcitation results in a hole on the first chain adjacent to the interface and an electron on the acceptor on the other side of the interface [Fig. 5(b)]. Suppose there is an additional partial positive charge on the donor chain 1 and a partial negative one on the acceptors, caused by interfacial dipoles. The hole executes zero-point oscillations, as described previously, for the effective mass model, but now these oscillations occur within the Coulomb potential modified by the fractional positive charges, thus raising the energy of the hole on chain 1. A jump of the hole to chain 2 is favorable for two reasons. First, the attractive Coulomb force to the negative sibling charge is partially shielded due to the positive fractional charges on chain 1. Second, on chain 2, the energy of the zero-point oscillations is diminished since the Coulomb potential there is wider and shallower (as there are no fractional charges on chain 2). Both effects will reduce the energy needed to overcome the attractive Coulomb potential. Note that this mechanism requires internal interfaces that can exist in a bilayer system or in a blend system where phase separation occurs. In the model by Arkhipov, the interfacial dipoles are, however, not formed in a donor phase doped by a low concentration of acceptors.

Meanwhile, Wiemer *et al.*[25] improved the theoretical treatment and showed that the existence of a dipole layer has a profound effect. For the practical implementation, we follow the formulation by Wiemer, though for simplicity, we used a square grid with the distance between the chains equal to the distance between the dipoles equal to r. As before, the dissociation yield $\varphi(F)$ is given by (3) and (4). The hole energy E_n is given by the sum of its kinetic energy and potential energy,

$$E_n = E_{p,n} + E_{k,n}, \quad \text{where} \quad E_{p,n} = U(x_n,y)|_{y=0} \quad \text{and}$$
$$E_{k,n} = \frac{1}{2}\hbar\omega = \frac{\hbar}{2\sqrt{m_{\text{eff}}}}\sqrt{\frac{d^2}{dy^2}U(x_n,y)|_{y=0}}, \tag{6}$$

which uses a parabolic approximation for the energy of the zero-point oscillations. The potential energy is modified compared to (5) by considering the effect of dipoles with fractional strength α.

$$U(y,x_n) = \frac{e^2}{4\pi\varepsilon_0\varepsilon_r}\frac{-1}{\sqrt{x_n^2+y^2}} + \frac{e^2}{4\pi\varepsilon_0\varepsilon_r}\left(\sum_{j=-N/2}^{N/2}\frac{\alpha}{\sqrt{(x_n-r)^2+\left(y-\left(j+\frac{1}{2}\right)r\right)^2}} + \sum_{i=-N/2}^{N/2}\frac{-\alpha}{\sqrt{x_n^2+\left(y-\left(i+\frac{1}{2}\right)r\right)^2}}\right) - eFx_n. \tag{7}$$

The number N of dipoles we used is 200. For r we took 0.92 nm as before, and values for the dipole fraction α were derived from the work function difference $\Delta\Phi$ obtained from the photoemission experiments (Table I). The change in work function $\Delta\Phi$ can be related to the fractional dipole strength α at the interface using the Helmholtz equation for interfacial dipoles. When $\Delta\Phi$ is measured in eV, the strength of an interfacial dipole can be expressed as $\varepsilon_0\varepsilon_r\frac{\Delta\Phi}{e} = ep\sigma$, where $p = \alpha er$ is the dipole moment and σ is the area density of dipoles, $\sigma = 1/r^2$, with σ being the fractional dipole. This yields $\alpha = \varepsilon_0\varepsilon_r r\Delta\Phi/e$. Using the measured values for $\Delta\Phi$ and taking $\varepsilon_r = 3.5$ and $r = 0.92$ nm, we arrive at the rather low values for α up to 0.03 listed in Table I. Inserting (7) into (6) allows us to simulate the dissociation yield $\varphi(F)$ using (3) and (4) as before. The resulting curves shown in Fig. 4(c) are very similar to those of the pure effective mass model in two respects, noting, however, that the values for the effective masses are larger (vide infra). First, we can reproduce the field dependence and, in particular, the decrease of F_{sat} in the polymer series, from DOOPPP to PCDTBT. Second, the comparison of experimental and theoretical efficiencies still indicates that at lower electric fields the model predicts lower yields than experimentally measured.

To compare the simulation parameters of the dipole model with the effective mass model, we need to take a little detour. In the effective mass model, we could use accurate values for E_n by solving the Schrödinger Equation (5) numerically. This is valuable and needed when evaluating the resulting simulation parameters quantitatively. In the dipole model (6), a numerical solution to E_n was not possible, and the quantization energy needs to be approximated by a harmonic oscillator [$U(y)$ in Fig. 5(a)]. Since we want to directly compare how the incorporation of dipoles affects the simulation and its associated parameters, we have first repeated the simulations to the effective mass model using also the harmonic oscillator approximation (Eq. 12 in Ref. 24), while keeping the effective masses equal to those obtained with the numerical solution [Table II, "effective mass model (parabolic approximation)"]. The resulting field dependence of the photocurrent yield is identical to Fig. 4(b) and is therefore not shown. Changes caused by the parabolic approximation are manifested in the different values obtained for the factor $\tau_0\nu_0\exp(-2\gamma r)$, which reduces by one to two orders of magnitude and shall not be considered any further. Having used the same level of approximation and very similar values for $\tau_0\nu_0\exp(-2\gamma r)$, we can now consider the impact of including the dipoles on the effective masses (Table II, dipole model). We find m_{eff}/m_e still decreases from DOOPPP to MeLPPP, yet the values are

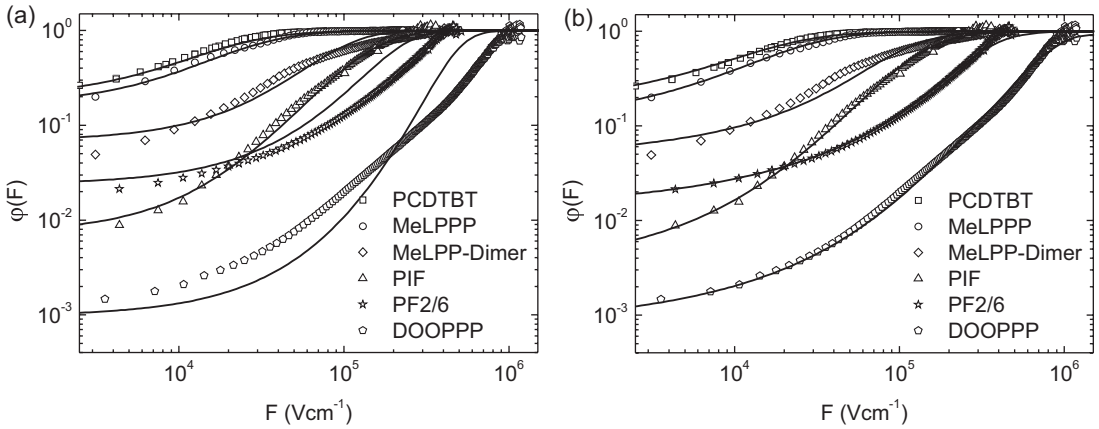

FIG. 6. Comparison of the field-dependent photocurrent yields (symbols) of donor /C_{60} bilayer solar cells with simulations (lines) based on (a) the combination of dipole model with Braun model, and (b) the combination of dipole model with dopant assisted dissociation model. The parameters are presented in Table III.

higher and more realistic than those needed when the dipoles are ignored. Thus, we have seen that charge dissociation in the more efficient, well-delocalized polymers PCDTBT, MeLPPP, and PIF can be described well by taking into account the effects from both, zero-point oscillations and interfacial dipoles. For the efficient polymers with shorter conjugation length, PF2/6 and DOOPPP, there is an additional photocurrent at lower fields that is not yet included in the modeling.

B. Combined models

We now attend to the additional contribution to the dissociation yield observed experimentally at lower electric fields. It is tempting to consider localized charge transfer states as candidates for the additional contribution. To test this hypothesis we tried to fit that extra contribution employing the Onsager-Braun model, i.e., we combined the dipole model and the Onsager-Braun model as $\varphi(F) = \varphi_{\text{dipole}}(F) + (1 - \varphi_{\text{dipole}}(F))\varphi_{\text{Onsager-Braun}}(F)$. As is evident in Fig. 6(a) and Table III, this was unsuccessful. To reproduce the yield at low electric fields, one had to invoke parameters that lead to a lower saturation field than experimentally observed, and, vice versa, if the saturation field is reproduced, the yields at low field cannot be matched. We therefore abandoned the Braun model (and its modification by Tachiya) to describe our results.

As a second option, we explored the idea of *dopant-assisted carrier photogeneration* at C_{60} molecules that may have diffused into the polymer donor layer.[52] The field dependence of the photocurrent resulting from such a process has been worked out by Arkhipov in 2003 as a variation of the effective mass model.[22] Arkhipov *et al.* consider a polymer film containing a low dopant concentration. The idea is again that the electron is transferred to the dopant, leaving behind a hole that oscillates coherently in the conjugated polymer segment. Due to the isolated, localized nature of the dopant, no interfacial dipoles are considered, which is in contrast to the situation of an extended dopant layer forming an interface. Note that while the dopant concentration is low and dopants are isolated within the polymer matrix, the concentration needs to be sufficient to allow for trap-to-trap motion of the electrons to the electrode in order for this process to result in a photocurrent.

If an exciton initially happens to be on a conjugated polymer segment adjacent to an individual C_{60} molecule at a distance r, then the probability w for it to dissociate into free carriers is given by the product of the probability for the electron to transfer to the C_{60}, w_t, multiplied by the probability for the hole to escape from the mutual Coulomb potential, w_{esc}. For an exciton with lifetime τ_0 and a tunneling rate to C_{60} given by $k_t = \nu_0 \exp(-2\gamma r)$, this yields

$$w_t = \frac{k_t}{k_t + \tau_0^{-1}} = \frac{1}{1 + (\nu_0\tau_0)^{-1}\exp(2\gamma r)}. \tag{8}$$

Similarly, w_{esc} is given by considering the escape rate $k_{\text{esc}} = \nu_0 \exp\left(-(U_{\max} - E_{\min})/kT\right)$ and the recombination rate, which is equal to the tunneling rate k_t. Thus,

$$w_{\text{esc}} = \frac{k_{\text{esc}}}{k_{\text{esc}} + k_t} = \frac{1}{1 + \exp(-2\gamma r)\exp\left(\frac{U_{\max} - E_{\min}}{kT}\right)}. \tag{9}$$

The potential U considered here is the sum of Coulomb potential and electric field, as expressed in (5). As indicated in Fig. 5(a), $U_{\max}$ is the maximum value of the potential. $E_{\min}$ is the energy of the hole. Analogous to (6), it can be expressed as the sum of the potential energy at the hole position $x_{\min}$ and the zero-point oscillation energy, so that $E_{\min} = U(x_{\min}) + 0.5\hbar\omega$. To facilitate the calculations, the parabolic approximation is used for ω analogous to (6). The difference between $U_{\max}$ and $E_{\min}$ is the height of the barrier that the hole needs to overcome in order to escape. The probability for dissociation at a site at distance r is then

$$w(r) = \frac{1}{1 + (\nu_0\tau_0)^{-1}\exp(2\gamma r)} \cdot \frac{1}{1 + \exp(-2\gamma r)\exp\left(\frac{U_{\max} - E_{\min}}{kT}\right)}. \tag{10}$$

Arkhipov considers that the dopants are distributed randomly so that the probability of finding the nearest dopant over the distance r from a conjugated segment is determined by the Poisson distribution $P(r) = 2\pi r l N_d \exp\left(-\pi l N_d (r^2 - r_{\min}^2)\right)$.

TABLE III. Fit parameter for different combined models

Material	PCDTBT	MeLPPP	PIF	PF2/6	DOOPPP	MeLPP-dimer
			Dipole model + Onsager-Braun model			
m_{eff}/m_e (dipole)	0.125	0.110	0.135	0.310	1.180	0.180
$\tau_0\nu_0 \exp(-2\gamma r)$	39	40	39	38	12	40
r_0 [nm]	0.92	0.92	0.92	0.92	0.92	0.92
$\mu\tau[10^{-12}\ \text{m}^2\ \text{V}^{-1}]$	5.00	4.00	0.15	0.40	0.02	1.50
			Dipole model + dopant model			
m_{eff}/m_e (dipole)	0.125	0.110	0.135	0.310	1.180	0.180
$\tau_0\nu_0 \exp(-2\gamma r)$	39	40	39	38	12	40
m_{eff}/m_e (dopant)	0.125	0.133	0.250	0.490	1.300	0.340
$\tau_0\nu_0$ [10^3]	55	36	22	15	8	36
γ [nm^{-1}]	2.8	3.0	4.0	4.0	7.0	6.3
$\tau_0\nu_0 \exp(-2\gamma r)$[a]	318	120	14	9	0.02	0.3
r_{min} [nm]	0.60	0.60	0.60	0.63	0.70	0.60
lN_d [$10^{18}\ \text{m}^{-2}$]	1.32	1.98	4.86	1.32	3.6	1.8

[a]Calculated from the parameters $\tau_0\nu_0$ and γ, using $r = 0.92$ nm.

r_{min} is the smallest possible distance between dopant and chain, l is the conjugation length, and N_d is the dopant concentration. The overall dissociation yield $\varphi(F)$ is then obtained by integrating $P(r)w(r)$ over space [Eq. (8) in Ref. 22]. By combining the dipole model with the dopant-assisted model, the experimental data can be fitted in a perfect manner, giving the parameters in Table III. The high quality of fit for all polymers considered over the entire field range is very satisfying [Fig. 6(b)].

We shall consider the values obtained for the parameters. The two physical processes that are combined here in the fashion $\varphi(F) = \varphi_{\text{dipole}}(F) + (1 - \varphi_{\text{dipole}}(F))\varphi_{\text{dopant}}(F)$ are (i) the dissociation at an interface between an extended polymer phase and an extended C_{60} phase, where interfacial dipoles can form, and (ii) the dissociation at localized polymer/C_{60} sites that arise from the diffusion of individual C_{60} molecules into the polymer phase. It is gratifying that the values for the effective mass inferred from the data for both processes are close (Table III). Those values should, indeed, be similar because both processes are based upon the concept of a hole oscillating within the conjugated segment of the polymer. They differ insofar that, at the extended interface, the oscillation happens in the Coulomb well modified by the interfacial dipoles, yet at always the same distance from the C_{60}. In contrast, for the dopant-assisted dissociation process, the Coulomb potential is only due to the geminate charges, yet the polymer–C_{60} distance varies, and thus the position of the hole within the potential well. At this point, it is appropriate to consider the numerical error that might arise if the built-in potential, used to calculate the internal field, was 100 meV or 200 meV lower than the open-circuit voltage $V_{\text{oc}}^{\text{photo}}$ determined for the photocurrent. Repeating the fits for such a case (see Supplemental Material[26]) shows that the effective masses change by up to 30%, yet they remain within the error margin indicated in Fig. 7. In view of the large variation of effective mass between the compounds, this variation obtained when using a different built-in potential is not significant.

We now turn to the remaining parameters. To evaluate whether the values obtained for lN_d are reasonable, consider a conjugation length l of about 10 nm and take the result of $lN_d = 2 \cdot 10^{18}\ \text{m}^{-2}$ obtained for MeLPPP as representative example. This translates into a dopant concentration of $N_d = 2 \cdot 10^{20}\ \text{cm}^{-3}$. A typical concentration of molecules in a molecular crystal is about $4 \cdot 10^{21}\ \text{cm}^{-3}$ (using, for anthracene, a density of 1.2 g/cm^3, a molar mass of 178g, and Avogadro's number). Assuming a similar concentration of conjugated segments (chromophores) here, this would suggest a doping concentration of about 5%. This is a realistic value. Similarly, the value obtained for r_{min} is plausible. Considering the values for the product of the lifetime and probability in detail is not meaningful. As discussed previously, they are underestimated due to the technical need of using the parabolic approximation for the potential. Nevertheless, it is encouraging that their trend and magnitude is consistent with that obtained for the effective mass model when also using the parabolic approximation.

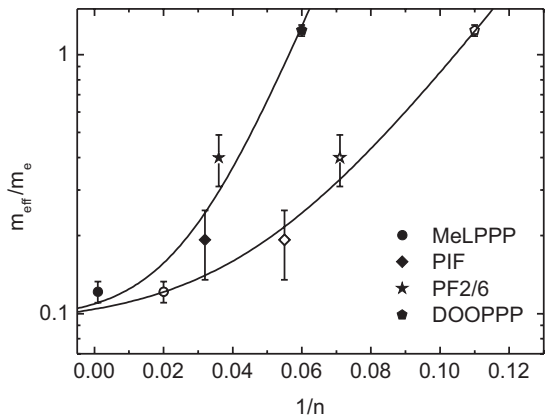

FIG. 7. The dependence of the relative effective masses on the inverse effective conjugation length of the donors for the ground state geometry (data taken from absorption, empty symbols) and for the excited state geometry (data taken from emission, filled symbols). The effective masses are taken from the dipole model (Table II) and the dipole model + dopant model (Table III), with the error bar indicating the spread of values between these models. The solid lines are fits to an exponential curve with a baseline, as described in the text.

Overall, the combination of experiment and modeling demonstrates that taking into account the effect of conjugation length by an effective mass approach is essential for an appropriate description of the dissociation process. In this context, it is useful to recall that the degree of delocalization can be quantified through the effective conjugation length. It is the number of repeat units over which an excitation, be it an exciton or a charge carrier, is coherently coupled considering, though, that there is, on average, no sharp boundary between different conjugated segments but rather a gradual local decrease of the coupling strength. In this sense, the effective mass should be viewed as an average effective mass that depends on the size of coherently coupled repeat units. The concept of a conjugation length-dependent effective mass is confirmed by Fig. 7. It shows the variation of the values for the effective mass inferred from the data fits on the reciprocal effective conjugation lengths taken from either the absorption or fluorescence spectra. The effective mass decreases roughly exponentially toward a value of about $0.1\,m_e$ at infinite conjugation length. This value is in good agreement with both experiment[49] and theory[50] on perfect π-conjugated chains. Empirically, the dependence of the relative effective mass on the effective conjugation lengths in either the ground state geometry (i.e., for the energy taken from the $S_1 \leftarrow S_0$ 0-0 transitions seen in absorption) or the excited state geometry (i.e., for the energy taken from the $S_1 \rightarrow S_0$ 0-0 transitions seen in fluorescence) can be expressed as

$$\frac{m_{\text{eff}}}{m_e} = 0.090 + 0.014 \cdot e^{\frac{40}{n}} \tag{11a}$$

for the excited state geometry, and

$$\frac{m_{\text{eff}}}{m_e} = 0.095 + 0.014 \cdot e^{\frac{74}{n}} \tag{11b}$$

for the ground state geometry.

This is an entirely empirical relationship, obtained for the poly(*p*-phenylene) type polymers, since for these materials the parameterization of transition energy versus conjugation lengths is known.[30]

IV. CONCLUSIONS

The present experiments on polymeric donor/C_{60} bilayer systems demonstrate that measuring the photocurrent over a broad range of electric field provides a unique source of information on the elementary step of photodissociation.

(i) The existence of a saturation field confirms the notion that mobile charge carriers originate from the dissociation of geminately bound e-h pairs. These are generated by a preceding ultrafast charge transfer step. [9,10]

(ii) The experiments show that the Coulomb-binding energy, evidenced by F_{sat}, scales inversely with the conjugation length of the donor polymer. If that conjugation length is large, the Coulomb-binding energy is small, and the built-in potential of the solar cell can be sufficient to break up all initially generated geminate e-h pairs. This is the case desired for solar cell applications, and it is associated with a high fill factor. Here, this is realized for MeLPPP and PCDTBT, with the latter having a far more suitable optical gap for actual solar cell applications. In contrast, if the conjugation length is short, the hole cannot overcome the Coulomb barrier and will recombine eventually with its sibling electron. The recombination can be prevented, and escape from the Coulomb well can be assisted by supplying additional activation energy, for example, in the form of an infrared light pulse as demonstrated by Bakulin *et al.*[12]

(iii) Photoemission measurements and modeling show that in a bilayer device, the dissociation process can be facilitated by a weak ground state dipole layer that exists at the donor-acceptor interface and that screens the Coulomb potential.

(iv) Except for electric field strengths that are much lower than the saturation field strengths, the experimental results can be quantitatively explained in terms of a model that was set up by Arkhipov *et al.* and subsequently refined and extended by Nenashev *et al.*[22–25] The key idea is that the hole on the e-h pair is delocalized within a segment of the π-conjugated polymer and executes zero-point oscillations within the Coulomb potential well of the localized electron at the C_{60}. The energy of those zero-point oscillations is controlled by the effective mass of the hole.

(v) When modeling the experimental results, we find that the effective mass correlates inversely with the effective conjugation length, i.e., the larger the conjugation lengths, the smaller the effective mass and, concomitantly, the Coulomb-binding energy of the dissociating e-h pair.

(vi) The present results show there is also an additional photogeneration channel. It originates from the dissociation of e-h pairs at individual C_{60} molecules that diffused into the donor layer. The description of this process is also based on an effective mass model except for the absence of the interfacial dipole layer. This channel is relevant at low fields for polymers with short conjugation lengths. In systems with large effective conjugation lengths of the polymeric donor, this contribution of dopant-assisted dissociation becomes virtually negligible.

V. EXPERIMENTAL METHODS

MeLPPP, MeLPP-dimer, PIF, PF2/6, and DOOPPP were synthesized by the group of U. Scherf, as described elsewhere.[53–56] PCDTBT was bought from "1-material." The structure formulae for the materials are given in Fig. 1. For photocurrent measurements, bilayer solar cell devices were fabricated using structured ITO-coated glass substrates in a special device architecture that eliminates edge effects.[16] This allows applying electric fields up to 1.3 MV/cm without risking spurious breakdown effects. For the series of solar cells reported here, 50–60-nm-high conductive PEDOT:PSS (Sigma Aldrich, neutral pH) was spin coated on top of the ITO and heated up to 180 °C for 30 min. Onto this, 40-nm-thick polymer films were spin coated from filtered chlorobenzene solutions (5.0–7.5 mg/ml) and annealed at 80 °C for 10 min to remove any residual solvent. This was followed by vapor deposition of a 40-nm layer of C_{60} (99.9% purity, AmericainDyeSourceInc). A 100-nm vapor-deposited layer of aluminum as a top electrode completed the diode structure.

Current-voltage curves were measured under monochromatic illumination at 2.2 eV (570 nm) from a 150 W Xenon lamp at 1.5 mW/cm^2. At this wavelength, the light is absorbed by the C_{60} acceptor while the polymer donors are not excited, except for the low-bandgap polymer PCDTBT. The photocurrent was determined by measuring the dark current

and the total current under illumination and then subtracting the dark current from the total current under illumination. This is done after each data point before stepping to the next voltage step. The solar cells were evaporated under a vacuum of $5 \cdot 10^{-7}$ mbar at room temperature. A Keithley 236 source-measure unit was used to record current and applied voltage. The internal electric field was calculated as $|F| = (V - V_{bi})/d$, where V is the applied external voltage, V_{bi} is the built-in field, taken as $V_{bi} = V_{oc}^{photo}$ unless stated otherwise. V_{oc}^{photo} is the open-circuit voltage determined for the photocurrent (i.e., after subtracting the dark current from the total current).

Its value is slightly higher than that of the usual open-circuit voltage, V_{oc}, where the total current (dark current + photocurrent) is zero. d is the active film thickness determined using a Dektak surface profilometer. The relative photocurrent quantum yield $\varphi(F)$ corresponds to the photocurrent per illuminated light intensity, both normalized to unit area. $\varphi(F)$ is normalized to unity at the high field saturation value. In our earlier work,[16] we have confirmed that $\varphi(F)$ indeed is on the order of unity at the high field saturation value by considering the absorption coefficient and modeling the exciton diffusion to the interface. The incident light intensities were recorded with a calibrated Hamamatsu S1337-33BQ photodiode, and the absorption of the films was measured using a Cary 5000 absorption spectrometer.

For UPS studies, the polymer samples were spincoated on PEDOT:PSS coated ITO glass substrates from chlorobenzene solutions (2 mg/ml, 25 rps), similar as previously described.

C_{60} was vacuum sublimed (base pressure $p = 3 \cdot 10^{-9}$ mbar) from resistively heated glass crucibles. The mass thickness of the layers was monitored using a quartz crystal microbalance [$\rho(C_{60}) = 1.6$ g/cm^3]. The UPS measurements were performed using a multitechnique ultra high vacuum (UHV) apparatus (base pressure: $1 \cdot 10^{-10}$ mbar) and a Helium discharge lamp ($h\nu = 21.22$ eV). The initial photon flux was attenuated by a factor of ~100 using a silicon filter to avoid irradiation damage of the sample. All spectra were recorded at room temperature and normal emission using a hemispherical Specs Phoibos 100 energy analyzer with 90 meV energy resolution. To determine the work function, the SECO was recorded with the sample biased at -10 V to clear the analyzer work function. Binding energies are reported relative to the Fermi-level spectra, and the error of energy values is estimated to be ± 0.05 eV.

ACKNOWLEDGMENTS

We thank the group of Prof. Ullrich Scherf for supplying the ladder type polymers and dimer and Prof. J. P. Rabe for providing access to a photoelectron spectroscopy setup. This work was supported by the GRK 1640 and the SPP1355 of the Deutsche Forschungsgemeinschaft (DFG), the Helmholtz-Energie-Allianz "Hybrid-Photovoltaik," and the network "SolTechGoHybrid" of the Bayerische Staatsministerium für Wissenschaft, Forschung und Kunst.

*Corresponding author: anna.koehler@uni-bayreuth.de

[1] Heliatek, http://www.heliatek.com/wp-content/uploads/2013/01/130116_PR_Heliatek_achieves_record_cell_effiency_for_OPV.pdf, 2013.
[2] L. Müller-Meskamp, Y. H. Kim, T. Roch, S. Hofmann, R. Scholz, S. Eckardt, K. Leo, and A. F. Lasagni, Adv. Mater. **24**, 906 (2012).
[3] C. Müller, T. A. M. Ferenczi, M. Campoy-Quiles, J. M. Frost, D. D. C. Bradley, P. Smith, N. Stingelin-Stutzmann, and J. Nelson, Adv. Mater. **20**, 3510 (2008).
[4] J. Y. Kim, K. Lee, N. E. Coates, D. Moses, T. Q. Nguyen, M. Dante, and A. J. Heeger, Science **317**, 222 (2007).
[5] C. Deibel and V. Dyakonov, Rep. Prog. Phys. **73**, 096401 (2010).
[6] R. H. Friend, M. Phillips, A. Rao, M. W. B. Wilson, Z. Li, and C. R. McNeill, Faraday Discuss. **155**, 339 (2012).
[7] J. L. Brédas, J. E. Norton, J. Cornil, and V. Coropceanu, Acc. Chem. Res. **42**, 1691 (2009).
[8] J. Nelson, Mater Today **14**, 462 (2011).
[9] D. Herrmann, S. Niesar, C. Scharsich, A. Köhler, M. Stutzmann, and E. Riedle, J. Am. Chem. Soc. **133**, 18220 (2011).
[10] F. Etzold, I. A. Howard, R. Mauer, M. Meister, T. D. Kim, K. S. Lee, N. S. Baek, and F. Laquai, J. Am. Chem. Soc. **133**, 9469 (2011).
[11] T. M. Clarke and J. R. Durrant, Chem. Rev. **110**, 6736 (2010).
[12] A. A. Bakulin, A. Rao, V. G. Pavelyev, P. H. M. van Loosdrecht, M. S. Pshenichnikov, D. Niedzialek, J. Cornil, D. Beljonne, and R. H. Friend, Science **335**, 1340 (2012).
[13] T. G. J. van der Hofstad, D. Di Nuzzo, M. van den Berg, R. A. J. Janssen, and S. C. J. Meskers, Adv. Energy Mater **2**, 1095 (2012).
[14] C. Deibel, T. Strobel, and V. Dyakonov, Phys. Rev. Lett. **103**, 036402 (2009).
[15] A. Köhler, D. A. dos Santos, D. Beljonne, Z. Shuai, J. L. Brédas, A. B. Holmes, A. Kraus, K. Müllen, and R. H. Friend, Nature **392**, 903 (1998).
[16] C. Schwarz, H. Bässler, I. Bauer, J. M. Koenen, E. Preis, U. Scherf, and A. Köhler, Adv. Mater. **24**, 922 (2012).
[17] A. J. Heeger, Chem. Soc. Rev. **39**, 2354 (2010).
[18] S. Verlaak, D. Beljonne, D. Cheyns, C. Rolin, M. Linares, F. Castet, J. Cornil, and P. Heremans, Adv. Funct. Mater. **19**, 3809 (2009).
[19] A. Ojala, A. Petersen, A. Fuchs, R. Lovrincic, C. Pölking, J. Trollmann, J. Hwang, C. Lennartz, H. Reichelt, H. W. Höffken, A. Pucci, P. Erk, T. Kirchartz, and F. Würthner, Adv. Funct. Mater. **22**, 86 (2012).
[20] H. Aarnio, P. Sehati, S. Braun, M. Nyman, M. P. de Jong, M. Fahlman, and R. Österbacka, Adv. Energy Mater **1**, 792 (2011).
[21] R. R. Chance and C. L. Braun, J. Chem. Phys. **59**, 2269 (1973).
[22] V. I. Arkhipov, E. V. Emelianova, and H. Bässler, Chem. Phys. Lett. **372**, 886 (2003).
[23] V. I. Arkhipov, P. Heremans, and H. Bässler, Appl. Phys. Lett. **82**, 4605 (2003).
[24] A. V. Nenashev, S. D. Baranovskii, M. Wiemer, F. Jansson, R. Österbacka, A. V. Dvurechenskii, and F. Gebhard, Phys. Rev. B **84**, 035210 (2011).

[25]M. Wiemer, A. V. Nenashev, F. Jansson, and S. D. Baranovskii, Appl. Phys. Lett. **99**, 013302 (2011).
[26]See Supplemental Material at http://link.aps.org/supplemental/10.1103/PhysRevB.87.155205 for (i) an estimate of the critical photon density at which geminate and non-geminate recombination become comparable, (ii) more parameters for the Braun model, (iii) the photocurrent yield and fits to the MeLPP-Dimer, (iv) parameters and fits to the combined Dipole model + Dopant model using different values for the built-in field.
[27]B. P. Rand, D. Cheyns, K. Vasseur, N. C. Giebink, S. Mothy, Y. P. Yi, V. Coropceanu, D. Beljonne, J. Cornil, J. L. Brédas, and J. Genoe, Adv. Funct. Mater. **22**, 2987 (2012).
[28]W. Kuhn, Helv. Chim. Acta **31**, 1780 (1948).
[29]J. Gierschner, J. Cornil, and H. J. Egelhaaf, Adv. Mater. **19**, 173 (2007).
[30]S. T. Hoffmann, H. Bässler, and A. Köhler, J. Phys. Chem. B **114**, 17037 (2010).
[31]K. Akaike, K. Kanai, H. Yoshida, J. Tsutsumi, T. Nishi, N. Sato, Y. Ouchi, and K. Seki, J. Appl. Phys. **104**, 023710 (2008).
[32]J. Niederhausen, P. Amsalem, A. Wilke, R. Schlesinger, S. Winkler, A. Vollmer, J. P. Rabe, and N. Koch, Phys. Rev. B **86**, 081411 (2012).
[33]S. Braun, W. R. Salaneck, and M. Fahlman, Adv. Mater. **21**, 1450 (2009).
[34]H. Ishii, K. Sugiyama, E. Ito, and K. Seki, Adv. Mater. **11**, 605 (1999).
[35]M. Körner, F. Loske, M. Einax, A. Kühnle, M. Reichling, and P. Maass, Phys. Rev. Lett. **107**, 016101 (2011).
[36]A. C. Morteani, P. Sreearunothai, L. M. Herz, R. H. Friend, and C. Silva, Phys. Rev. Lett. **92**, 247402 (2004).
[37]D. Veldman, Ö. Ipek, S. C. J. Meskers, J. Sweelssen, M. M. Koetse, S. C. Veenstra, J. M. Kroon, S. S. van Bavel, J. Loos, and R. A. J. Janssen, J. Am. Chem. Soc. **130**, 7721 (2008).
[38]L. Onsager, Phys. Rev. **54**, 554 (1938).
[39]C. L. Braun, J. Chem. Phys. **80**, 4157 (1984).
[40]K. K. H. Chan, S. W. Tsang, H. K. H. Lee, F. So, and S. K. So, Org. Electron. **13**, 850 (2012).
[41]R. A. Marsh, J. M. Hodgkiss, and R. H. Friend, Adv. Mater. **22**, 3672 (2010).
[42]C. S. Ponseca, A. Yartsev, E. Wang, M. R. Andersson, D. Vithanage, and V. Sundström, J. Am. Chem. Soc. **134**, 11836 (2012).
[43]J. Kirkpatrick, P. E. Keivanidis, A. Bruno, F. Ma, S. A. Haque, A. Yarstev, V. Sundström, and J. Nelson, J. Phys. Chem. B **115**, 15174 (2011).
[44]M. Wojcik and M. Tachiya, J. Chem. Phys. **130**, 104107 (2009).
[45]S. Barth, H. Bässler, U. Scherf, and K. Müllen, Chem. Phys. Lett. **288**, 147 (1998).
[46]A. Petersen, A. Ojala, T. Kirchartz, T. A. Wagner, F. Würthner, and U. Rau, Phys. Rev. B **85**, 245208 (2012).
[47]N. Christ, S. W. Kettlitz, S. Valouch, J. Mescher, M. Nintz, and U. Lemmer, Org. Electron. **14**, 973 (2013).
[48]M. Pope and C. E. Swenberg, *Electronic Processes in Organic Crystals and Polymers* (Oxford University Press, New York, 1999).
[49]G. Weiser and S. Möller, Phys. Rev. B **65**, 045203 (2002).
[50]J. W. van der Horst, P. A. Bobbert, M. A. J. Michels, and H. Bässler, J. Chem. Phys. **114**, 6950 (2001).
[51]C. Im, W. Tian, H. Bässler, A. Fechtenkötter, M. D. Watson, and K. Müllen, J. Chem. Phys. **119**, 3952 (2003).
[52]D. E. Markov, E. Amsterdam, P. W. M. Blom, A. B. Sieval, and J. C. Hummelen, J. Phys. Chem. A **109**, 5266 (2005).
[53]M. Grell, W. Knoll, D. Lupo, A. Meisel, T. Miteva, D. Neher, H. G. Nothofer, U. Scherf, and A. Yasuda, Adv. Mater. **11**, 671 (1999).
[54]S. P. Huang, G. S. Huang, and S. A. Chen, Synth. Met. **157**, 863 (2007).
[55]U. Scherf and K. Müllen, Makromol Chem-Rapid **12**, 489 (1991).
[56]S. Setayesh, D. Marsitzky, and K. Müllen, Macromolecules **33**, 2016 (2000).

Supporting Information to

On the Role of the Effective Mass and Interfacial Dipoles on Exciton Dissociation in Organic Donor-Acceptor Solar Cells

Christian Schwarz, Steffen Tscheuschner, Johannes Frisch, Stefanie Winkler, Norbert Koch, Heinz Bässler, and *Anna Köhler**

C. Schwarz, S. Tscheuschner, H. Bässler, A. Köhler,

Experimental Physics II and Bayreuth Institute of Macromolecular Research (BIMF)

University of Bayreuth

95440 Bayreuth, Germany

E-mail: Anna.Koehler@uni-bayreuth.de

J. Frisch, S. Winkler, N. Koch

Institut für Physik

Humboldt-Universität zu Berlin

The critical photon density at which geminate and non-geminate recombination become comparable can be estimated roughly as follows.

The rate equation for the density of photogenerated charges n is given by

$$\frac{dn}{dt} = 0 = G - \frac{n}{\tau_{tr}} - \gamma n^2 \qquad (1)$$

where γ is the bimolecular recombination coefficient, τ_{tr} is the transit time i.e. the inverse of the rate constant for getting the charges through the film to the electrodes. G is the generation rate per cm^3, i.e. the photon flux (photons/cm^2) divided by the penetration depths.
The quadratic equation if (1) can be solved as

$$n = -\frac{1}{2\gamma\tau_{tr}} + \sqrt{\frac{G}{\gamma} + \left(\frac{1}{2\gamma\tau_{tr}}\right)^2} \qquad (2)$$

which may be written as

$$n = \frac{1}{2\gamma\tau_{tr}}\left[-1 + \sqrt{1 + (2\tau_{tr})^2 G\gamma}\right]. \qquad (3)$$

γ is a material constant that is the same, independent of illumination intensity. Two cases can be distinguished. First, consider the case of a very low photon flux, i.e. low generation rate, so that $(2\tau_{tr})^2 G\gamma << 1$. Developing the root leads to

$$\frac{n}{\tau_{tr}} = G \qquad \text{for} \qquad (2\tau_{tr})^2 G\gamma << 1. \qquad (4)$$

This is identical to the result one obtains from (1) if bimolecular recombination is negligible. The other case is that of a very high generation rate, so that $(2\tau_{tr})^2 G\gamma >> 1$. The number of 1 under the root and in front of the root can then be neglected, leading to

$$n = \sqrt{\frac{G}{\gamma}} \qquad \text{for} \qquad (2\tau_{tr})^2 G\gamma >> 1. \qquad (5)$$

This is the same than would be obtained from (1) if bimolecular decay dominates. We now consider the number of charges getting out of the device, n/τ_{tr}. For high generation rate, this is

$$\frac{n}{\tau_{tr}} = \frac{1}{\tau_{tr}}\sqrt{\frac{G}{\gamma}} \quad \text{for} \qquad (2\tau_{tr})^2 G\gamma >> 1. \qquad (6)$$

From (4) and (6), the effects of monomolecular decay and bimolecular decay are equal if,

$$G = \frac{1}{\gamma\tau_{tr}^2}. \qquad (7)$$

The transit time is given by $\tau_{tr} = d / \mu F$, with d being the film thickness and F the electrical field across the film. The rate constant for bimolecular recombination can be taken from the Langevin condition

$$\frac{\gamma}{\mu} = \frac{e}{\varepsilon_0 \varepsilon_r} \quad . \tag{8}$$

Inserting this into equation 7 gives

$$G = \frac{\varepsilon_0 \varepsilon_r \mu F^2}{e d^2} . \tag{9}$$

Typical parameters of F = 10^5 V/cm, μ = 10^{-3} cm^2/Vs, d = 100 nm imply that $G = 2 \cdot 10^{23}\ cm^{-3}s^{-1}$ is the volume generation rate at which bimolecular and monomolecular decay become comparable. If we presume that every photon absorbed generates an electron (and a hole), and that absorption is linear, then for a film thickness of 100 nm, the critical photon flux G_A is

$$G_A = 2 \cdot 10^{18}\ cm^{-3}s^{-1} \tag{10}$$

In our experiments, we used monochromatic illumination at 570 nm from a Xenon lamp. The intensity at the position of the solar cell was 1.5 mW/cm^2. This corresponds to a photon flux of about $4 \cdot 10^{15}$ photons/cm^2s, i.e. the intensity used in our experiment is 1/500 of the intensity at which bimolecular recombination becomes important.

Table S1 : Parameters for the Braun model, comparison of dashed and solid lines in Fig. 4a

	PCDTBT dashed	PCDTBT solid	DOOPPP dashed	DOOPPP solid
r_0 [nm]	1.03	1.03	0.80	0.80
$\nu\tau$ [10^{-12}m^{2}V^{-1}]	2.0	15.0	0.30	0.02

Fig. S1 : Photocurrent yield and fits to the MeLPP-Dimer

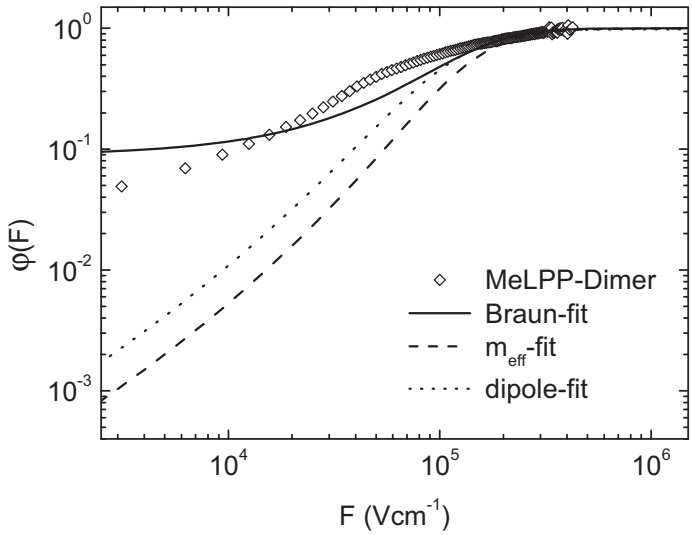

Fits of the experimental external quantum yields of bilayer MeLPP-Dimer/C_{60} devices with different models. The fit parameters are shown in the paper.

In order to assess the impact of the uncertainty in determining the built-in field, we have repeated the combined fit (Dipole model + Dopant model), using the same parameters in Table 3 except for the effective mass, for the case $V_{bi} = V_{oc}^{photo}$ - 100 meV, $V_{bi} = V_{oc}^{photo}$ - 200 meV. The resulting parameters for are compared in Table S2.

Table S2:

	DOOPPP		PIF		MeLPPP	
	m_{eff}/m_e (dipol)	m_{eff}/m_e (dopant)	m_{eff}/m_e (dipol)	m_{eff}/m_e (dopant)	m_{eff}/m_e (dipol)	m_{eff}/m_e (dopant)
$V_{bi} = V_{oc}^{photo}$	1.180	1.300	0.135	0.250	0.110	0.133
$V_{bi} = V_{oc}^{photo}$ - 100meV	1.200	1.000	0.160	0.190	0.115	0.110
$V_{bi} = V_{oc}^{photo}$ - 200meV	1.300	0.900	0.160	0.175	0.110	0.100

The corresponding fits (lines) to the data (symbols) are shown here for different V_{bi}:

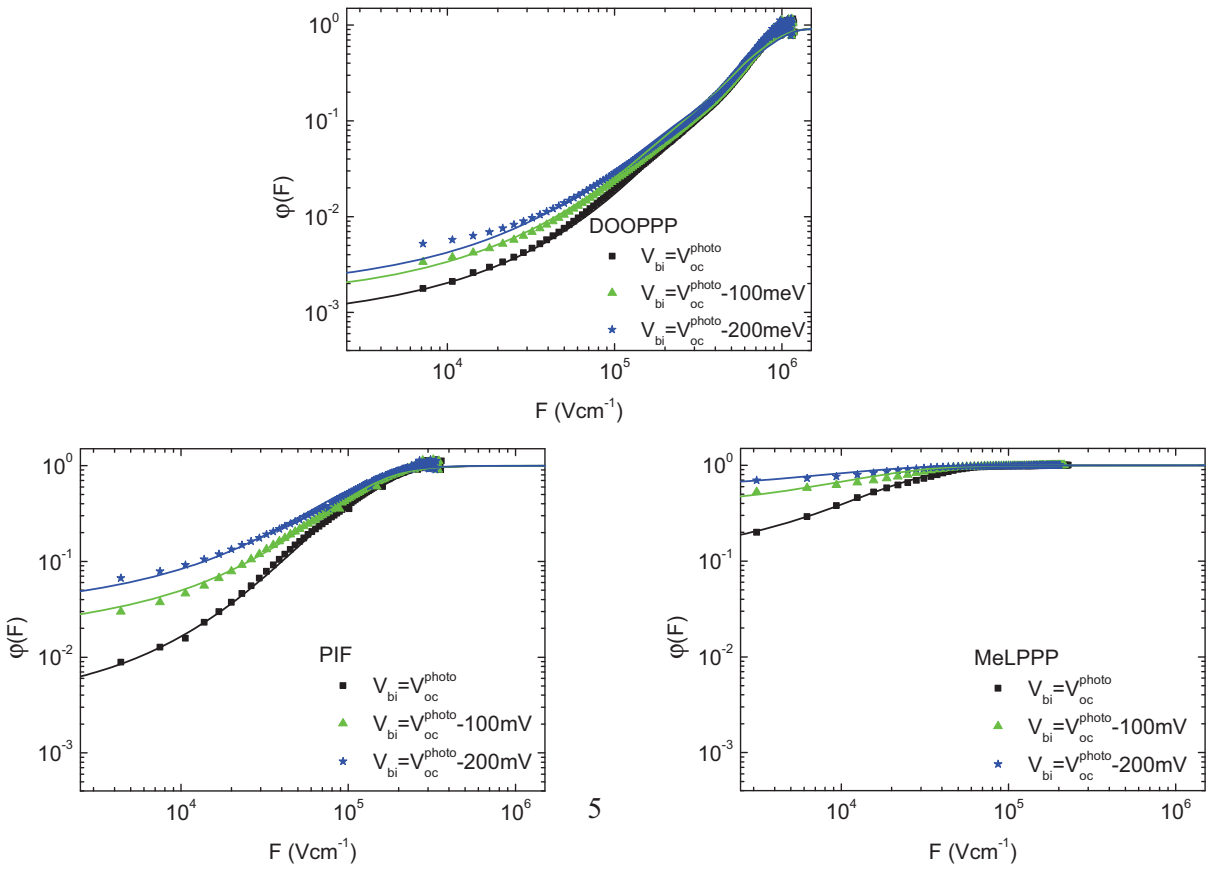

4.6. A Combined Theoretical and Experimental Study of Dissociation of Charge Transfer States at the Donor-Acceptor Interface of Organic Solar Cells

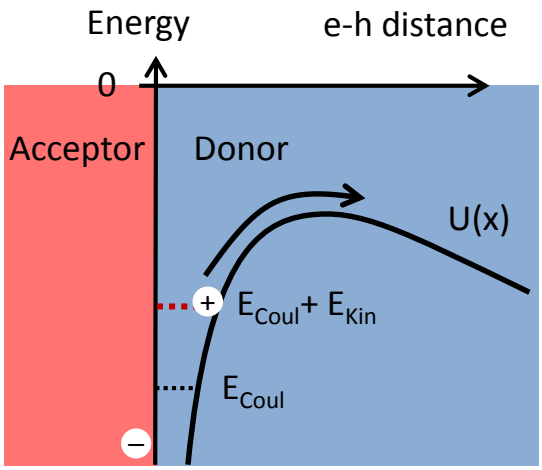

Steffen Tscheuschner, Heinz Bässler, Katja Huber, Anna Köhler

Veröffentlicht in

Journal of Physical Chemistry B (**2015**), 119, 10359-10371

(DOI: https://doi.org/ 10.1021/acs.jpcb.5b05138)

THE JOURNAL OF PHYSICAL CHEMISTRY B

Article

pubs.acs.org/JPCB

A Combined Theoretical and Experimental Study of Dissociation of Charge Transfer States at the Donor−Acceptor Interface of Organic Solar Cells

Steffen Tscheuschner,[†] Heinz Bässler,[‡] Katja Huber,[†] and Anna Köhler*[,†,‡]

[†]Experimental Physics II, University of Bayreuth, D-95440 Bayreuth, Germany

[‡]Bayreuth Institute of Macromolecular Research (BIMF), University of Bayreuth, D-95440 Bayreuth, Germany

Supporting Information

ABSTRACT: The observation that in efficient organic solar cells almost all electron−hole pairs generated at the donor−acceptor interface escape from their mutual coulomb potential remains to be a conceptual challenge. It has been argued that it is the excess energy dissipated in the course of electron or hole transfer at the interface that assists this escape process. The current work demonstrates that this concept is unnecessary to explain the field dependence of electron−hole dissociation. It is based upon the formalism developed by Arkhipov and co-workers as well as Baranovskii and co-workers. The key idea is that the binding energy of the dissociating "cold" charge-transfer state is reduced by delocalization of the hole along the polymer chain, quantified in terms of an "effective mass", as well as the fractional strength of dipoles existent at the interface in the dark. By covering a broad parameter space, we determine the conditions for efficient electron−hole dissociation. Spectroscopy of the charge-transfer state on bilayer solar cells as well as measurements of the field dependence of the dissociation yield over a broad temperature range support the theoretical predictions.

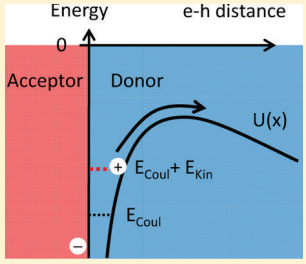

1. INTRODUCTION

The power conversion efficiency of organic solar cells (OSCs) has passed the 10% limit which is considered as a benchmark for future technical application.[1−4] Translating this power conversion efficiency into the probability that an absorbed photon creates a free electron−hole pair indicates that the internal quantum efficiency of this process has to be close to 100%. Considering that in organic solids dielectric screening is weak, as evidenced by dielectric constants of typically only 3−4, this is a remarkable phenomenon and requires an explanation.

Photon absorbers in such highly efficient OSCs are either bulk or bilayer donor−acceptors assemblies. When exciting—usually—the donor of the donor−acceptor couple, the excited electron is transferred to the acceptor, thus creating a coulomb-bound electron−hole pair. If the electron−hole separation was comparable to the intermolecular spacing, typically 1 nm, the coulomb binding energy would be about 0.48 eV, i.e., almost 20 times the thermal energy kT at room temperature. This is in striking disagreement with the fact that in efficient organic solar cells the dissociation yield is virtually field independent.[5] Liberation of the pair from its mutual coulomb potential should be a quite unlikely process unless (i) the separation of the electron−hole pair is much larger than the intermolecular spacing,[6] (ii) there is screening of the coulomb potential,[7] or (iii) the collapse of the geminate pair is kinetically hindered.

One possibility to explain why the recombination of the electron−hole pair could be kinetically hindered (option iii) rests on the Onsager−Braun formalism.[8] It takes into account that a charge-transfer (CT) state has a lifetime that is much longer than the jump time of a single charge carrier because the orbital overlap within the electron−hole pair is weak. In molecular crystals, typical lifetimes of the CT states are in the nanosecond range, whereas the jump times for charges are in the sub-picosecond range. Therefore, the pair can make many attempts to escape from the coulomb well, and this enhances the probability for eventual dissociation. Experimental results on OSCs with a small molecular donor−acceptor system prepared by vapor deposition have indeed been explained successfully on the basis of the Onsager−Braun concept.[9,10] There is consensus, however, that a data analysis for systems containing π-conjugated polymers as donor materials would require lifetime and jump time values as fit parameters that are unphysical.[11,12]

This failure of the Onsager−Braun concept for polymeric systems suggests that this is in some way related to the delocalization of the chains' π orbitals. It is intuitively plausible that once the pair's partners are more spread out the coulomb binding energy is diminished. This was considered by Deibel and co-workers in Monte Carlo simulations on the exciton dissociation.[13] A mathematical formalism to quantitatively incorporate this effect has been initially suggested by Arkhipov et al.,[7] and it has been further developed by the Baranovskii group.[14] In this model, shown schematically in Figure 1, the energy of the electron−hole pair is considered to consist of two contributions, i.e., a potential energy as well as a kinetic energy. The latter arises from the delocalization of the pair's electronic

Received: May 29, 2015
Revised: July 15, 2015
Published: July 15, 2015

DOI: 10.1021/acs.jpcb.5b05138
J. Phys. Chem. B 2015, 119, 10359−10371

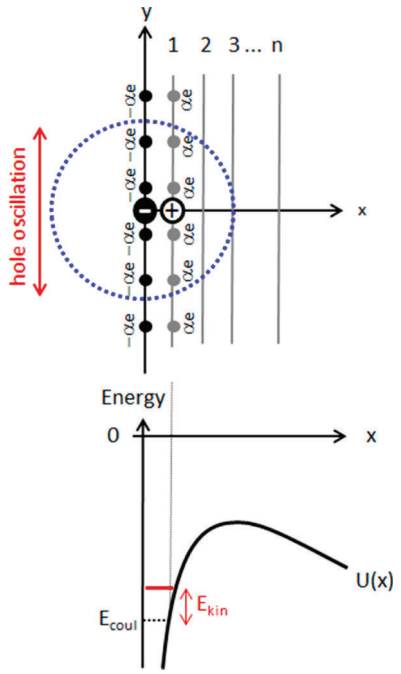

Figure 1. Top panel: Schematic illustrating the model for electron–hole dissociation at a bilayer interface (at $x = 0$) with the electron on the acceptor at $(x, y) = (0, 0)$ and with the hole on the polymer chain. An electric field is applied along the x-direction. Equidistant fractional charges αe on the interfacial layer are taken into account. The blue dotted circle indicates the coulomb capture radius within which the hole oscillates along the chain in the y-direction. Bottom panel: Schematic of the associated potential energy at $y = 0$. The energy of the hole in the potential, E_{coul}, is reduced by the contribution E_{kin} resulting from the zero-point oscillation along the chain.

wave functions. If, say, the hole is located on a donor chain and spread out coherently over several π-conjugated repeat units, then it can be considered to oscillate back and forth over the conjugated chain. This oscillation takes place within the coulomb potential of the electron located on the acceptor. The "kinetic" energy in the Arkhipov–Baranovskii formalism is the energy associated with this zero-point oscillation of the delocalized hole in the potential of the electron. Therefore, the binding energy of the pair is not simply the difference between the potential energies of the dissociated charge carriers of the pair and the coulomb-bound pair. Rather, the binding energy is further reduced by the energy of the zero-point oscillation along the chain (Figure 1). Evidently, the escape of the electron–hole pair is facilitated by that zero-point oscillation. The energy of the zero-point oscillation scales with the electronic coupling along the chain. This implies that the efficiency of an organic solar cell with π-conjugated donor materials should increase when its excited states—and consequently also its charged states—are more delocalized. Studies on bilayer organic solar cells with donor films made of poly(p-phenylene)s with different conjugation lengths and with a C_{60} film as an acceptor support this reasoning.[15] Meanwhile, there is growing attention on the importance of delocalization effects in polymeric solar cells.[6,16−18]

As already mentioned (option ii), the efficiency of an organic solar cell can also be improved when the coulomb potential is screened. This is the case, for example, if there are dipoles at the donor–acceptor interface in a bilayer diode or in a bulk heterojunction. Owing to the difference between the electronegativities of the donor and acceptor, there can be some fractional electron transfer to the acceptor interface in the dark.[19,20] When a photoexcited electron of the donor is transferred to the acceptor, that electron will feel some repulsion due to already existing fractional electron distribution so that, in effect, the coulomb potential is screened and the coulomb binding energy of the electron–hole pair is diminished. This effect has been incorporated into the Arkhipov–Baranovskii formalism by simply superimposing the potential of interfacial dipoles with the coulomb potential of the electron–hole pair.[7,21]

The Arkhipov–Baranovskii formalism has been confirmed through experimental data on photodissociation in bilayer solar cells made with various acceptors such as C_{60} or trinitrofluorenone, combined with a range of π-conjugated polymers as donor materials. In particular, an analysis carried out on a systematic series of solar cells made with a layer of C_{60} evaporated onto a layer of π-conjugated polymer showed that both on-chain delocalization and interfacial dielectric screening due to dark dipoles contribute to the organic solar cell efficiency.[17] On the basis of the theoretical concepts to rationalize dissociation of geminate pairs in polymeric organic solar cells developed by Arkhipov et al. and the Baranowskii group, we studied in the current work systematically how the dissociation yield depends on the delocalization of a charge carrier in the donor, on the strength of dark dipoles at an internal interface, and on the lifetime jump-time product of the electron–hole pair as a function of the applied electric field and temperature. To allow for further comparison of the Arkhipov–Baranovskii formalism with experimental data, we also measured the temperature dependence of the dissociation yield in a MeLPPP/C_{60} diode as well as the spectra of electroluminescence under forward bias conditions. These spectra provide a measure of the binding energy of relaxed electron–hole pairs at the donor–acceptor interface. The excellent agreement between theory and experiment indicates that there is no need to invoke dissociation of hot electron–hole pair states in efficient polymeric organic solar cells provided that the hole on the donor chain is delocalized and has, concomitantly, a low effective mass.

The paper is structured as follows. After introducing the reader to the central ideas of the Arkhipov–Baranovskii formalism in section 3, we consider which range of values needs to be adopted for the pertinent parameters so that the model is of relevance to common bilayer OSCs. In this context, we also comment on the approximations used in previous work. In section 4, we demonstrate first how the electron–hole pair binding energy, and thus the dissociation yield, is affected by the delocalization of the hole along the chain and by the presence of interfacial dipoles. Next, pertinent experiments are presented. The discussion in section 5 first focuses on comparing the experimental results with the predictions of the model before expounding its implications. The concluding outlook also discusses limitations of the current model.

2. EXPERIMENTAL DETAILS

We measured the field dependent steady state photocurrent in a bilayer OSC consisting of a spin coated 30 nm thick MeLPPP donor layer and a vapor deposited 30 nm thick C_{60} layer as an electron acceptor. The sample was sandwiched between MoO_3-covered ITO (indium–tin–oxide) and Al electrodes. It was mounted in a temperature controlled cryostat operating within a temperature regime of 400 and 5 K. Illumination was

DOI: 10.1021/acs.jpcb.5b05138
J. Phys. Chem. B 2015, 119, 10359−10371

provided by a xenon lamp, dispersed by a monochromoator. Total current under illumination and dark current were recorded and subtracted from each other after each data point measurement to give the photocurrent.

In another set of experiments, we determined the open circuit voltage (V_{oc}) of a MeLPPP/C_{60} diode as well as that of a diode with DOOPPV as a donor layer as a function of temperature and at different light intensities. Under forward bias, i.e., $V > V_{oc}$, the samples operate as light emitting diodes. The electroluminescence spectrum was recorded using a monochromator/photocell unit with a cutoff photon energy of 1.32 eV (950 nm).

3. THE THEORETICAL MODEL

3.1. Key Features of the Model. We pursue the Arkhipov–Baranovskii formalism as detailed in refs 17 and 22. In essence, we consider a donor–acceptor bilayer model system in which the donor moieties are parallel chains of π-conjugated polymers on top of a layer of C_{60}, as sketched in Figure 1. In order to make the model as simple as possible, disorder effects have been disregarded. We implicitly assume that the energy levels of the donor and acceptor are such that a coulomb-bound electron–hole pair with a finite lifetime is generated upon exciting either the donor or the acceptor. We further make the assumption that the electron remains stationary while the hole executes a random walk among the donor chains under action of a (built-in or externally applied) electric field that is directed perpendicular to the chains. In the course of this diffusive hopping process, the hole may eventually escape from the coulomb well or recombine geminately with the electron. The key features of the formalism are that (i) the energy of the electron–hole pair is the sum of a potential term and a kinetic term, the latter being associated with the zero-point oscillation of the hole in the coulomb potential, and that (ii) the coulomb potential may be screened by dipoles that exist at the donor and acceptor interface already in the dark.

Thus, we consider chains of infinite length and with an interchain separation of $d = 1$ nm. The chains directly at the interface consist of repeat units than can carry a factional charge αe, with fractional countercharges on the C_{60} side establishing a dipole layer. From earlier work,[23] we know that in the relevant temperature range charge carrier hopping can be satisfactorily described by the Miller–Abrahams mechanism; i.e., the jump rate $\nu_{ij}(F)$ for nearest neighbor jumps between chains i and $j = i \pm 1$ is given by

$$\nu_{ij}(F) = \nu_0 e^{-2\gamma r_{ij}} \begin{cases} \exp - \dfrac{E_j(F) - E_i(F)}{kT} & E_j(F) > E_i(F) \\ 1 & E_j(F) < E_i(F) \end{cases} \tag{1}$$

where ν_0 is the prefactor rate, γ is the inverse localization radius, and r_{ij} is the distance between two hopping sites, i.e., between two adjacent chains. We adopt the Rubel et al. algorithm[24] for the field-dependent rate $k_d(F)$ to reach chain number n

$$k_d(F)^{-1} = \sum_{i=1}^{n-1} \nu_{ij}(F)^{-1} \exp \frac{E_i(F) - E_1(F)}{kT} \tag{2}$$

$k_d(F)$ is the dissociation rate, provided that chain n is well outside the coulomb capture radius. Assuming an intrinsic lifetime τ_0 of the initial electron–hole pair, the field-dependent probability $p(F)$ for the dissociation of the interfacial electron hole pair is given by the rate equation

$$p(F) = \frac{k_d(F)}{k_d(F) + \tau_0^{-1}} = \frac{1}{1 + (\tau_0 k_d(F))^{-1}} \tag{3}$$

The approach taken is thus analogous to that of Onsager and Braun. However, the dissociation rate $k_d(F)$ includes contributions from the delocalization of the hole wave function and from the shielding of the coulomb potential by interfacial dipoles. These contributions are incorporated implicitly through the dependence of $k_d(F)$ on the energy $E_n(F)$ of the hole on chain n. These energies can be obtained by solving the Schrödinger equation for the wave function $\psi_n(x_n, y)$ of the hole on chain n in the potential $U_n(x_n, y)$. The coordinate system refers to Figure 1, with the electron located at the position $(x_n, y) = (0, 0)$. Thus, the direction along x gives the distance between the electron and the center of the hole wave function, and the direction along y corresponds to the direction along the chain

$$\left[-\frac{\hbar^2}{2m_{\text{eff}}} \frac{\partial^2}{\partial y^2} + U_n(x_n, y) \right] \psi_n(x_n, y) = E_n \psi_n(x_n, y) \tag{4a}$$

with

$$U_n(x_n, y) = -\frac{e^2}{4\pi\epsilon_0\epsilon_r \sqrt{y^2 + x_n^2}} - eFx_n + \frac{e^2}{4\pi\epsilon_0\epsilon_r} \sum_{j=-N/2}^{N/2} \left(\frac{\alpha}{\sqrt{(x_n - r)^2 + \left(y - \left(j + \frac{1}{2}\right)r\right)^2}} + \frac{-\alpha}{\sqrt{x_n^2 + \left(y - \left(j + \frac{1}{2}\right)r\right)^2}} \right) \tag{4b}$$

This electrostatic potential $U_n(x_n, y)$, in which the hole oscillates, is an essential ingredient of the theory. The first term in eq 4b expresses the attraction of the sibling electron, the second term results from the (superimposed applied and built-in) electric field present in the film, and the third term incorporates interfacial electrostatic effects. Since $U_n(x_n, y) = 0$ for a sufficiently large distance x_n from the interface, it follows that the energy E_n of the hole on chain n in the absence of an electric field is identical to the binding energy of the geminate electron–hole pair. In earlier work, we calculated the binding energies by approximating the electrostatic potential along the chain as harmonic.[17] Following Wiemer et al.,[22] we eliminate this shortcoming now by solving the Schrödinger equation numerically.

3.2. Evaluation of the Parameter Space Relevant to Polymer-Based Bilayer Cells. Besides the dielectric constant ϵ_r, the Arkhipov–Baranovskii model contains three parameters. One parameter is the coupling strength between the constituent repeat units of the chain, parametrized here through the effective mass of the hole, m_{eff}. A second one is the magnitude of any interfacial electrostatic effects, expressed through the fractional dipole strength α, and the final parameter is the product $\tau_0\nu_0 e^{-2\gamma r_{ij}}$ of the lifetime τ_0 of the initial electron–hole pair with the hopping rate $\nu_0 e^{-2\gamma r_{ij}}$ for energetically

DOI: 10.1021/acs.jpcb.5b05138
J. Phys. Chem. B 2015, 119, 10359–10371

downward jumps. Unless stated otherwise, our calculations were performed using $\epsilon_r = 3$, though we also explored the effect of varying the dielectric constant by increasing ϵ_r from 3 to 6. We now consider the range of physically meaningful values for the parameters m_{eff}, α, and $\tau_0\nu_0 e^{-2\gamma r_{ij}}$.

The electronic coupling between repeat units cannot be less than the van der Waals coupling encountered in molecular crystals, and it cannot exceed the strength of the covalent coupling encountered in a perfectly π-conjugated chain. Thus, the effective mass on the hole on the donor chain is limited, on the one hand, by that for a molecular crystal and that of a perfect conjugated polymer on the other hand. Cyclotron resonance experiments on an anthracene crystal yield $m_{eff}/m_e \cong 10$, while electro-reflection experiments on a perfect π-conjugated chain of crystalline polydiacetylenes gave $m_{eff}/m_e \cong 0.05$.[25,26] The latter value is consistent with calculation for π-conjugated polymers based on a solution of the Bethe–Salpeter equation. For MeLPPP and PPV, the calculated m_{eff}/m_e values are 0.058 and 0.048.[27] It is straightforward to conjecture that m_{eff}/m_e should increase as a chain becomes distorted and concomitantly less conjugated. This is borne out by our earlier work showing that for polymeric, phenylene-based OSCs there is indeed an exponential correlation between the effective mass and the inverse effective conjugation length of the chain.

The experiments by Schwarz et al.[17] already demonstrated that the field dependence of the photodissociation yield of organic solar cells with conjugated polymers as donor materials is consistent with the Arkhipov–Baranovskii model, and an exponential dependence of this field dependence on the effective mass has been observed. The quantitative analysis has been premised, though, upon the notion that the potential in which the hole oscillates within the polymer chain is harmonic which is certainly a very crude approximation. Wiemer et al.[22] eliminated this shortcoming by solving the relevant Schrödinger equation numerically. They applied the modified algorithm to the case of dipole enhanced electron–hole pair dissociation assuming the fractional charge displacement of $\alpha = 0.1$ or 0.2. Koehler et al.[28] invoked an even larger value of $\alpha = 0.4$. However, photoelectron spectroscopy on a series of poly-phenylenes[17] indicates that the drop of the electrostatic potential due to the interfacial dipole is in the range from 0.08 to 0.17 eV only. On the basis of a diameter of a C_{60} molecule of roughly 1 nm,[29] this translates into $\alpha = 0.014–0.03$, i.e., about an order of magnitude lower than the values taken by Wiemer and by Koehler. Note that $\alpha = 0.1$ would be equivalent to an interfacial potential drop of 0.55 eV which even exceeded the binding energy of an electron–hole pair with an intrachain separation of 1 nm. Thus, to address the effect that interfacial dipoles have on dissociation, we shall routinely consider the range of the fractional dipole strength α from 0 to 0.02.

Regarding the lifetime hopping rate product, in a system devoid of disorder, the maximum value of τ_0 is the intrinsic lifetime of the initial electron–hole pair which is in the range 1–10 ns. Information on the maximum jump rate of the hole can be inferred from pump–probe experiments. From the experiments of Herrmann et al. and of Grancini et al.,[30,31] we know that the transfer time of an electron from a donor chain to an acceptor is on the order of 100 fs; i.e., the maximum jump rate cannot exceed 10^{13} s^{-1}. The same value is attained when translating a charge carrier mobility of 1 $cm^2/(V\ s)$ measured in an ordered organic solid, e.g., a molecular crystal, into a jump rate using the Einstein ratio between mobility diffusivity, $eD = \mu kT$, and considering that in a 3D system the diffusivity is $D = a^2[6\nu_0 \exp(-2\gamma r)]^{-1}$, with a being the jump distance. On the basis of these estimates, we shall in the following consider a range of the $\tau_0\nu_0 e^{-2\gamma r_{ij}}$ product of 3–10.000. Unless stated, the remaining values of the model are temperature $T = 300$ K, interchain distance $d = 1$ nm, donor–acceptor distance = 1 nm, dipole–dipole distance = 1 nm, and number of dipoles N = 200.

4. RESULTS

4.1. Theoretical Results. Before embarking on a description of the results of the theoretical treatment, we estimate the error made in our previous work when approximating the potential of the electron–hole pair as harmonic along the polymer chain, rather than solving the Schrödinger equation numerically.[17] In Figure 2, the field

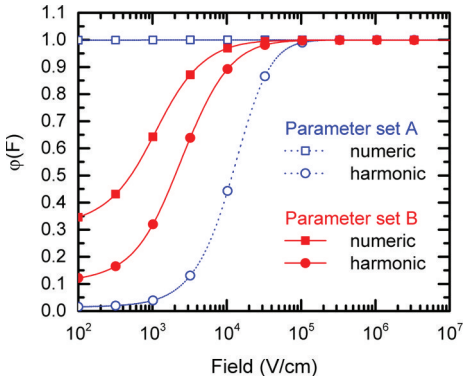

Figure 2. Field dependence of the dissociation probability $\varphi(F)$ obtained by solving eq 4 numerically (lines with square symbols) or by using a harmonic approximation (lines with circles) for two sets of parameters: (A) $m_{eff}/m_e = 1$, $\alpha = 0.1$, $\tau_0\nu_0 e^{2\gamma r_{ij}} = 10.000$, $d = 0.6$ nm; (B) $m_{eff}/m_e = 0.125$, $\alpha = 0.02$, $\tau_0\nu_0 e^{2\gamma r_{ij}} = 1.000$, $d = 1.0$ nm. All other values of the model are identical.

dependences of the dissociation probabilities $\varphi(F)$ obtained in the harmonic approximation and using the numeric solution are compared using two different sets of parameters. Wiemer et al.[22] showed that using the harmonic approximation has a dramatic effect for the parameters $m_{eff}/m_e = 1$, $\alpha = 0.1$, $\tau_0\nu_0 e^{-2\gamma r_{ij}} = 10.000$, and $d = 0.6$ nm. In Figure 2, this choice of values is denoted as parameter set A. However, when using parameters that are typical for well-conjugated polymers such as MeLPPP, the simple harmonics approximation does provide a reasonable semiquantitative description of the dissociation process. For the experimentally based parameter set B, $m_{eff}/m_e = 0.125$, $\alpha = 0.02$, $\tau\nu_0 e^{-2\gamma r_{ij}} = 1.000$, and $d = 1.0$ nm, the dissociation probability $\varphi(F)$ increases by only a factor of about 2 when going to the numerical approximation. Throughout this work, in which we explore a broad range of parameters, we shall employ the numerical solution of the Schrödinger equation.

Having established the computational framework, we can calculate the energy and wave function of the hole within the overall potential. Figure 3a illustrates how the squared modulus of the hole wave function spreads out along the chain with increasing distance to the sibling electron for $m_{eff} = 0.1m_e$ in the absence of an electric field and interfacial dipoles. When increasing the effective mass, this spreading reduces, as illustrated in the Supporting Information in Figure S1. It is gratifying that the delocalization of the hole, that oscillates on a

DOI: 10.1021/acs.jpcb.5b05138
J. Phys. Chem. B 2015, 119, 10359–10371

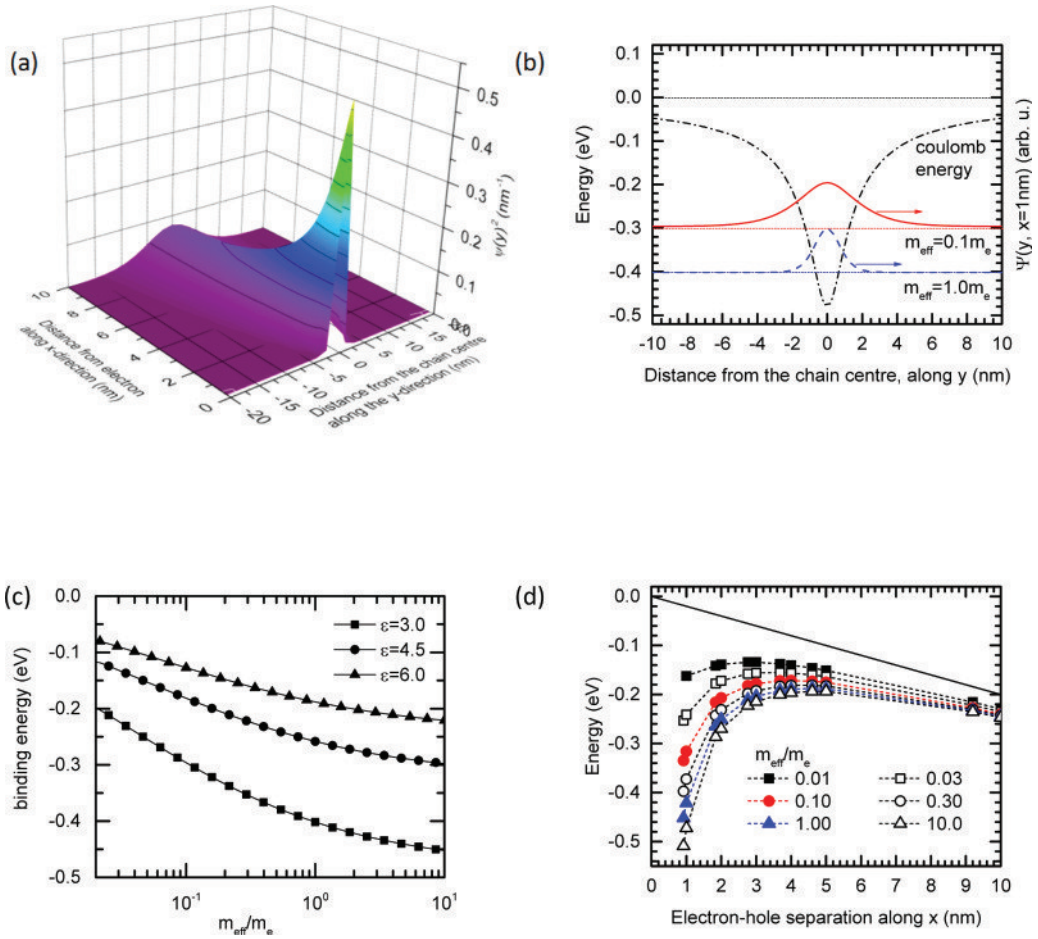

Figure 3. (a) The probability density $|\psi_n(y)|^2$ of measuring a hole along a chain in the coulomb potential of the electron for an effective mass of $m_{eff} = 0.1m_e$ at a distance x from the interface. $\psi_n(y, x_n)$ is the solution of eq 4 in the absence of a field and interfacial dipoles ($F = 0$ and $\alpha = 0$). (b) The energies E_1 (dotted line, left axis) and wave functions $\psi_1(y, x_1 = 1\ \text{nm})$ (right axis) obtained as solution to eq 4 for the cases $m_{eff} = 0.1m_e$ (solid red line) and $m_{eff} = 1.0m_e$ (dashed blue line) for a hole on chain 1, i.e., at $x_1 = 1$ nm, in the absence of a field and interfacial dipoles ($F = 0$ and $\alpha = 0$). For illustration, the coulomb energy along that chain is also indicated as a black dash-dotted line. (c) The binding energy of the initial electron hole pair as a function of the hole effective mass, parametric in the dielectric constant ε. It is derived as E_1 for $F = 0$ and $\alpha = 0$. (d) The energies E_n (symbols) obtained for the wave functions $\psi_n(y = 0, x_n)$ of the hole as a function of perpendicular distance x from the interface, where the electron is located, parametric in the effective mass. The values are calculated considering the superimposed action of the coulomb field of the electron and of an electric field $F = 2 \times 10^5$ V/cm, yet in the absence of interfacial dipoles ($\alpha = 0$). The dotted lines are to guide the eye. The change of potential energy due to the electric field is indicated by the black solid line.

polymer chain within the coulomb potential of a C_{60} counteranion, is consistent with electron spin resonance (ESR) and electron nuclear double resonance (ENDOR) experiments in P3HT:PCBM blends.[32] In such experiments, the delocalization is assessed by the magnitude of the interaction between the spin of the unpaired electron and the magnetic moments of the protons that decreases as the delocalization increases. The difference in spread of the hole wave function with effective mass is also evident in Figure 3b. This figure further shows the energy of a hole on chain 1 for two different effective masses, in the absence of an electric field and interfacial dipoles. This is the energy that needs to be overcome to dissociate the electron hole pair. It is evident how this binding reduces with decreasing effective mass. The reason is the contribution of the kinetic energy of the hole oscillating in the potential well. The critical dependence of the binding energy on effective mass, parametric in the dielectric constant, is displayed in Figure 3c. With increasing effective mass, the binding energies obtained using $\epsilon_r = 3$ approach the value of 0.48 eV that corresponds to the value for localized point charges at 1 nm distance. Figure 3d indicates how the energy of the hole evolves with distance from the electron in the presence of an electric field. The maximum of this $E_n(x)$ curve, which indicates the point at which the hole drifts toward dissociation rather than recombination, moves closer to the electron with reducing effective mass. It is also evident that in the limit of a low effective mass the electron−hole pair potential becomes flat. This implies that dissociation should be field saturated and temperature independent. In this limit, dissociation approaches the situation that exists in an inorganic semiconductor device.

Figure 4 shows the probability $\varphi(F)$ that a geminate electron−hole pair dissociates into a pair of coulombically unbound charges as a function of the electric field at 300 K and parametric in the relative effective mass of the hole on the polymer chain for lifetime hopping rate products of 35 and 3000. From low to high field values, $\varphi(F)$ increases until it saturates at a field F_{sat}, defined by the intersection of slope of the low field part of $\varphi(F)$ and the extrapolated horizontal high field part. In a picture of point charges, F_{sat} is a measure for the binding energy of the initial geminate pair. We find that F_{sat}

DOI: 10.1021/acs.jpcb.5b05138
J. Phys. Chem. B 2015, 119, 10359−10371

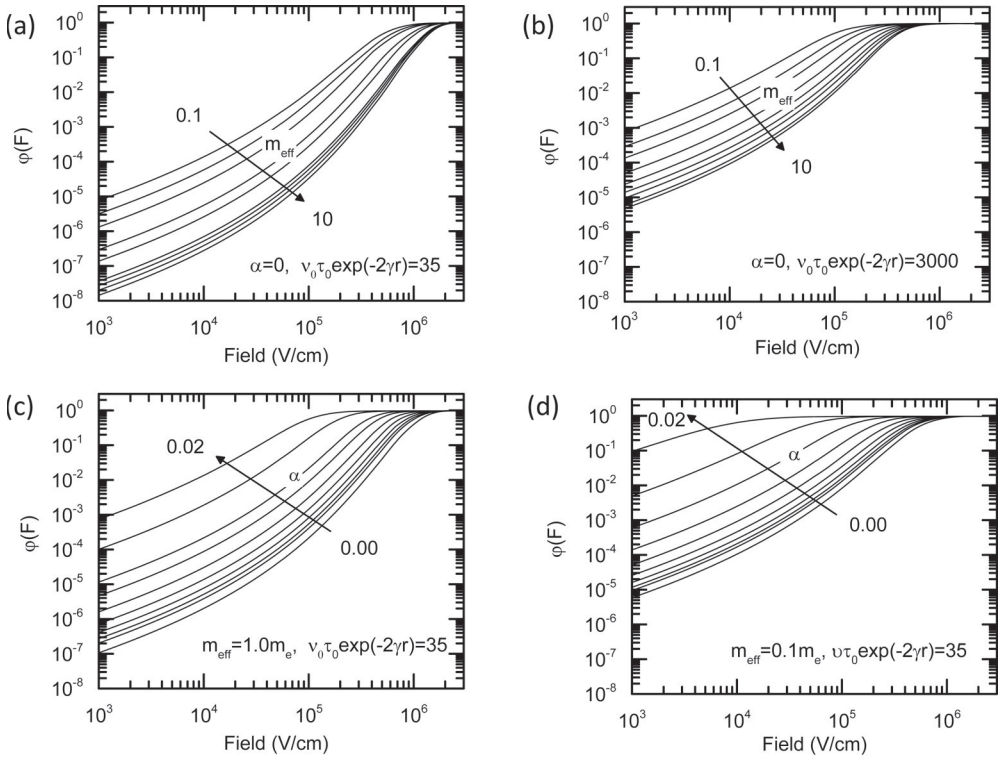

Figure 4. Dissociation probability as a function of the electric field in the device parametric in the effective mass (a) with $\alpha = 0$ and $\nu_0\tau_0 \exp(-2\gamma r) = 35$ and (b) with $\alpha = 0$ and $\nu_0\tau_0 \exp(-2\gamma r) = 3000$ and parametric in the partial dipole strength (c) for $m_{eff} = 1.0m_e$ and $\nu_0\tau_0 \exp(-2\gamma r) = 35$ and (d) for $m_{eff} = 0.1m_e$ and $\nu_0\tau_0 \exp(-2\gamma r) = 35$. The effective masses in parts a and b are $m_{eff}/m_e = 0.1, 0.2, 0.3, 0.6, 1.0, 2.0, 3.0, 6.0, 10$. The partial dipole strengths in parts c and d are $\alpha = (0.0, 1.0, 1.4, 2.1, 3.2, 4.6, 6.8, 10.0, 14.7, 21.5) \times 10^{-3}$.

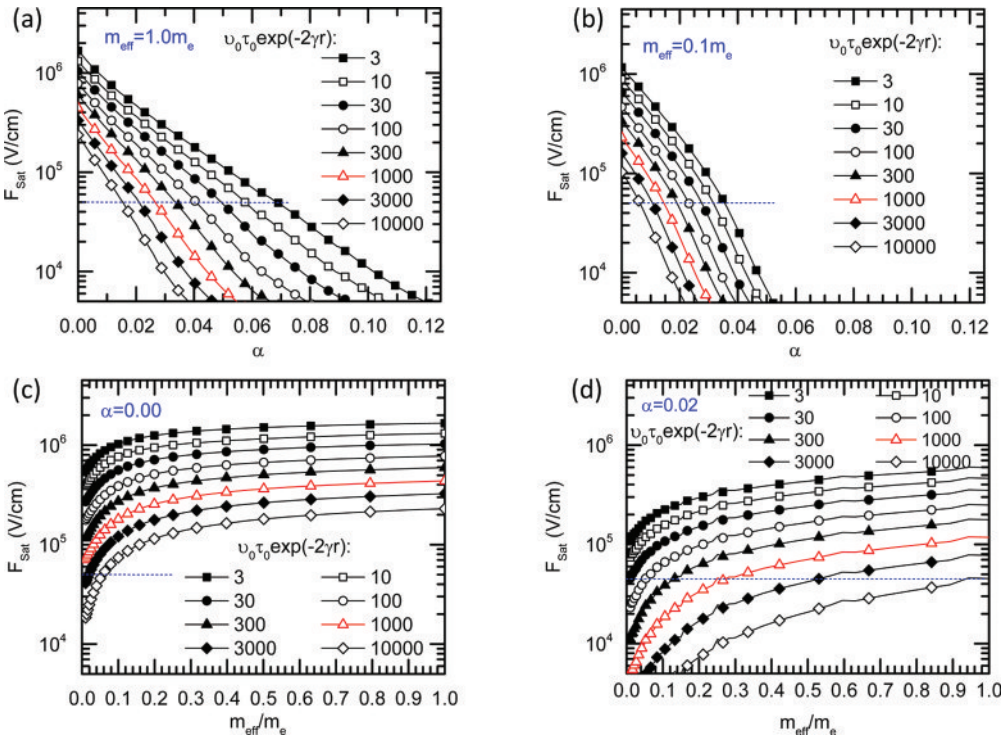

Figure 5. Saturation field F_{sat} parametric in the lifetime hopping rate product (a) for an effective mass of $1.0m_e$ as a function of fractional dipole strength, (b) for an effective mass of $0.1m_e$ as a function of fractional dipole strength, (c) in the absence of any dipole as a function of effective mass, and (d) for a fractional dipole strength $\alpha = 0.02$ as a function of effective mass. The curve for the lifetime hopping rate product of 1000, corresponding to frequent experimental values, is highlighted in red color. The blue dashed line indicates a saturation field of 5×10^4 V/cm, corresponding to a typical value for the built-in field in organic solar cells.

DOI: 10.1021/acs.jpcb.5b05138
J. Phys. Chem. B 2015, 119, 10359−10371

decreases with decreasing effective mass for a constant lifetime hopping rate product (Figure 4a). The entire family of $\varphi(F)$ curves shifts to lower fields when the lifetime hopping rate product increases (Figure 4b). The reason is that when increasing either the initial pair lifetime or the hopping rate the charges can make several attempts to escape, thus increasing their chances. This idea had already been implemented in the Onsager–Braun formalism for the dissociation of charge transfer states with finite lifetime. Increasing the electrostatic potential offset at the interface by increasing the fractional charge α qualitatiavely has the same effect as reducing the effective mass (Figure 4c). When combining a finite interfacial charge with a low effective mass, the dissociation yield becomes virtually field independent for field strengths above 5×10^4 V/cm, corresponding to the typical strength of the built-in field in organic solar cells with a thickness of 100 nm and an open-circuit voltage of 0.5 V (Figure 4d). The character of the $\varphi(F)$ dependene is consistent with the earlier work of Nenashew et al. and Schwarz et al.[14,17] Quantitative deviations are due to implementing the numerical solution of eq 4.

A requirement for an efficient organic solar cell is that the built-in field of the diode should suffice to dissociate most of the electron–hole pairs. In order to find the parameter space in which this condition can be satisfied, we calculated the saturation field F_{sat} as a function of the effective mass, the fractional dipole strength, and the lifetime hopping rate product at ambient temperature. In Figure 5a,b, we show that F_{sat} decreases almost exponentially with increasing dipole strength for different lifetime hopping rate products. The slope of this evolution increases with reducing effective mass. Complementary data on the variation of F_{sat} with the effective mass for a fixed dipole strength are plotted in Figure 5c,d. Evidently, an experimentally desirable F_{sat} value of 5×10^4 V/cm can only be realized in the presence of a finite interfacial dipole. When considering a realistic value of 1000 for $\tau_0\nu_0 e^{-2\gamma r_{ij}}$, one has to invoke a fractional dipole strength exceeding 0.025 for an effective mass of $1.0m_e$, while a α-value exceeding 0.015 suffices when the effective mass is reduced to $0.1m_e$. When using an α-value of 0.02, i.e., in the range of the values found experimentally for the donor polymers PCDTBT and MeLPPP with the acceptor C_{60},[17] a saturation field of 5×10^4 V/cm can be attained for any polymer with an effective mass below $0.25m_e$, which is the case for many well-conjugated polymers. Regarding the dependence on $\tau_0\nu_0 e^{-2\gamma r_{ij}}$, it is straightforward that F_{sat} should decrease with increasing electron–hole pair lifetime and hopping rate, yet it is remarkable that the slope of the log F_{sat} versus m_{eff}/m_e dependence increases dramatically with decreasing effective mass.

The Arkhipov–Baranovskii formalism predicts how the dissociation yield should depend on temperature. Pertinent results are plotted on an Arrhenius scale in Figure 6a for a fixed electric field. A more detailed field dependence is given in the Supporting Information (Figure S2). A near Arrhenius-like temperature dependence prevails in the absence of interfacial electrostatic effects for an effective mass of $1.0m_e$, consistent with the predictions of thermally activated dissociation by the Onsager–Braun model for a localized point charge. The activation energy is 0.23 eV. Adding screening through a moderate fractional dipole strength of $\alpha = 0.02$ to a system with an effective mass of $1.0m_e$ remarkably reduces the activation energy to 0.14 eV for temperatures below 250 K. The same effect results when, instead of screening the field, the kinetic energy of the hole is increased by delocalization, i.e., for the

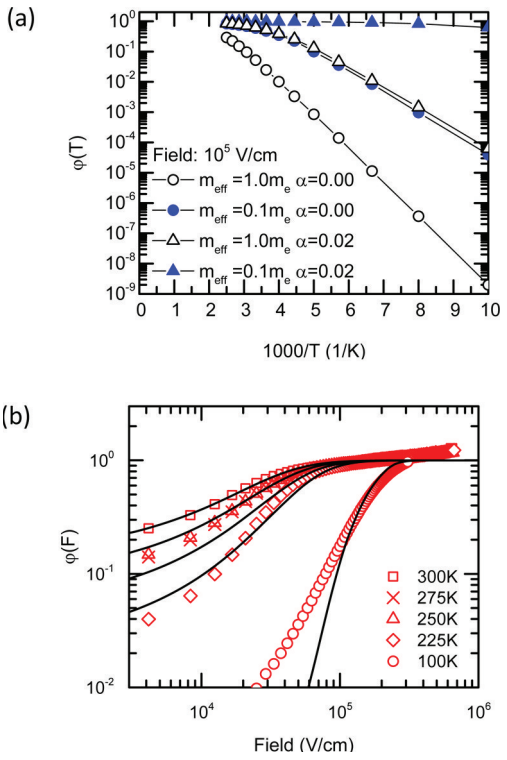

Figure 6. (a) The calculated dissociation probability $\varphi(F)$ as a function of inverse temperature for an effective mass of $1.0m_e$ (open symbols) and $0.1m_e$ (full sumbols) in the absence of an interfacial dipole (circles) and for dipoles with $\alpha = 0.02$ (triangles). (b) The measured photocurrent yield (red symbols), normalized to unity at the saturation field, for an organic solar cell in the layer structure ITO/MoO_3/30 nm polymer/30 nm C_{60}/Al. Also shown is the dissociation probability $\varphi(F)$ calculated for $m_{eff} = 0.112m_e$, $\alpha = 0.0142$, and $\tau\nu_0 e^{-2\gamma r_{ij}} = 2500$ for different temperatures.

parameters $\alpha = 0.0$ and $m_{eff} = 0.1m_e$. Above 250 K, the temperature dependence of $\varphi(F)$ disappears, since the hopping rate increases such that the dissociation probability approaches unity, even though the individual jumps are still thermally activated (cf. eqs 1–3). The dissociation becomes fully independent of temperature for $m_{eff} = 0.1m_e$ and $\alpha = 0.2$. In this case, the effect of screening the coulomb potential by interfacial dipoles combines with the additional kinetic energy due to the zero-point oscillation of the hole in the potential well, so that further thermal energy is not required to allow for dissociation. The data in Figure 6 are obtained for a fixed field strength of 5×10^5 V/cm. This activation energy decreases for even higher fields, as shown in the Supporting Information. When the electric field is essentially absent, such as for a field strength of 3×10^3 V/cm, activation energies of 0.30 eV result for $m_{eff} = 0.1m_e$ and $\alpha = 0.00$. They reduce to 0.12 eV for $m_{eff} = 0.1m_e$ and $\alpha = 0.02$, i.e., typical parameters for a good solar cell polymer (see the Supporting Information, Figure S2).

4.2. Comparison to Experimental Results. The temperature dependence calculated in the framework of the Arkhipov–Baranovskii formalism is compared in Figure 6b to experimental results for the field dependence of the photocurrent in a MeLPPP/C_{60} bilayer organic solar cells upon cooling from 300 to 100 K. At moderate fields, the current decreases strongly with decreasing temperature, yet it remains almost temperature independent in the saturation regime. The temperature dependence of these experimental results can be

DOI: 10.1021/acs.jpcb.5b05138
J. Phys. Chem. B 2015, 119, 10359–10371

fitted using a fixed set of input parameters for all temperatures, i.e., $m_{eff} = 0.112m_e$, $\alpha = 0.0142$, $\varepsilon = 3.5$, $\tau_0\nu_0 e^{-2\gamma r_{ij}} = 2500$, and $d = 0.92$ nm. For temperatures below 100 K, the measured current in the low field regime exceeds the value predicted by the model. We attribute this to the neglect of disorder in the model.

As mentioned above, the model allows calculating the energy by which the hole on chain 1 is bound to its sibling electron on C_{60}. This can be compared to the experimentally determined binding energy E_b of the charge transfer state. If the charge transfer energy E_{CT}, the ionization potential I_P^D of the donor, and the electron affinity E_A^A of the acceptor are known, the binding energy of the charge transfer states results as $E_b = (I_P^D - E_A^A) - E_{CT}$. In Figure 7, results are summarized that allow estimating the charge transfer state energy E_{CT} for the polymers MeLPPP and DOOPPV. Having an effective hole mass of $0.1m_e$ and $1.1m_e$, respectively,[17] these two polymers are representative for a well conjugated and a poorly conjugated chain. Figure 7a shows the electroluminescence (EL) measured in a bilayer MeLPPP/C_{60} device under forward bias, while the photocurrent spectrum is displayed in Figure 7b. The EL spectrum reveals two features, one with a maximum at 1.67 eV and one peaking at 1.38 eV, whose relative intensities depend on the applied voltage and thus on the cell current. The 1.67 eV feature is readily assigned to fluorescence from C_{60}. We consider that the lower energy feature originates from the radiative recombination of electrons and holes injected from the electrodes and can therefore be attributed to emission from the interfacial charge transfer state. The photocurrent spectrum falls steeply from 1.7 eV, the energy of the C_{60} S_1 state, to lower energies, with a prominent shoulder centered at about 1.48 eV. We attribute this weak photocurrent with direct excitation of the charge-transfer state between MeLPPP and C_{60}. The intersection between the normalized EL and EQE spectra at about 1.44 eV (Figure S3, Supporting Information) can be taken as the 0−0 position of the CT state, implying that the reorganization energy is about 50 meV (=0.5(1.48 − 1.38 eV)). To substantiate this assignment, we have also measured the temperature dependence of the open-circuit voltage $V_{oc}(T)$ in the MeLPPP/C_{60} device under illumination (Figure 7c). $V_{oc}(T)$ should extrapolate to E_{CT}, the energy of the charge transfer state, in the limit of zero temperature.[33,34] The fact that $V_{oc}(T)$ extrapolates to 1.35 eV, i.e., close to the maximum observed in the electroluminescence, supports the assignment of the 1.37 eV emission to a charge transfer state. Observing emission from C_{60} in the EL spectra requires an explanation. At first glance, there should be no electroluminescence from C_{60} because electrons had to overcome an energy barrier of roughly 1 eV between the ionization potentials of MeLPPP and C_{60}. It appears that at an electric field as large as 7×10^5 V/cm in combination with disorder driven level spreading facilitates leakage of holes into the C_{60} layer that can recombine with electrons injected from the Al cathode. The fact that the relative contribution of the electroluminescence coming from C_{60} increases with forward bias supports this reasoning.

For a DOOPPV/C_{60} bilayer diode, $V_{oc}(T)$ extrapolates toward about 1 V. Consistent with this, we could not observe any electroluminescence feature within our experimental range from the visible range down to 1.2 eV other than that from C_{60}. Evidently, any charge transfer state emission is below 1.2 eV, indicating that the charge transfer state must be strongly bound. Therefore, we estimate $E_{CT} = 1.1 \pm 0.1$ eV. We note that, as discussed in detail further below, the model neglects explicit consideration of disorder. However, disorder is included implicitly through the higher value of the effective mass in DOOPPP.

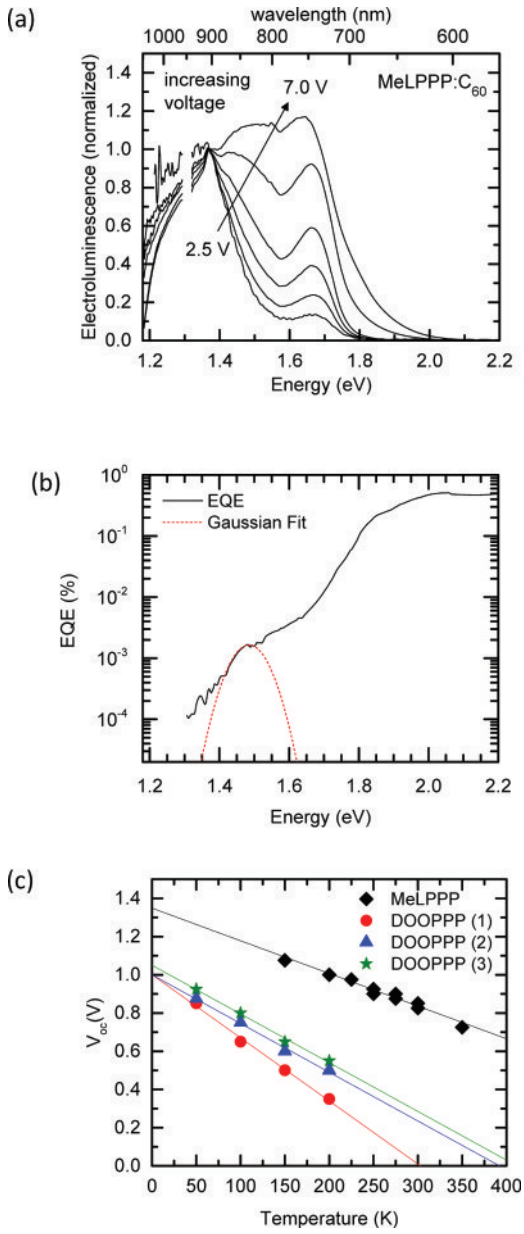

Figure 7. (a) The room-temperature electroluminescence spectra of a bilayer device in the structure ITO/MoO_3/30 nm MeLPPP/30 nm C_{60}/Al taken for increasing applied voltages (2.5, 3.5, 4.0, 5.0, 6.0, and 7.0 V). The data are normalized to unity at 1.38 eV. The lack of data near 1.35 eV is due to a detector defect in that spectral range. (b) The photocurrent quantum yield (EQE) of the same device (black solid line). The dashed red curve indicates a fit to a Gaussian centered at 1.48 eV with a full width at half-maximum of 110 meV. (c) The open-circuit voltages as a function of temperature taken of bilayer solar cells of ITO/PEDOT:PSS/30 nm polymer/30 nm C_{60}/Al with either MeLPPP (black diamond) or DOOPPV (circle, triangle, star) as polymer. The solid lines indicate a linear extrapolation. The DOOPPV cells were measured at three slightly different light intensities.

5. DISCUSSION

5.1. The Appropriateness of the Model. Schwarz et al. already demonstrated that the Arkhipov−Baranovskii formalism

DOI: 10.1021/acs.jpcb.5b05138
J. Phys. Chem. B 2015, 119, 10359−10371

is a suitable approach to describe the dissociation of interfacial electron−hole pairs by comparing the calculated field dependent dissociation probability to photocurrent measurements on bilayer solar cells made with a range of π-conjugated polymers as donor materials and C_{60} as the acceptor.[15,17] In that work, the potential along the chain was approximated as harmonic rather than solving the Schrödinger equation with the full potential numerically. However, from Figure 2, it is evident that the deviations due to the approximation are tolerable for the experimentally relevant parameter range. Before discussing the implications of the Arkhipov−Baranovskii formalism, it is however worthwhile to deliberate how it relates to the experimentally observed temperature dependence of the photocurrent, the binding energy of the charge transfer state, and the delocalization of the hole wave function.

In organic solar cells, the photodissociation process is frequently observed to be only weakly dependent on temperature.[35−37] This is an intriguing effect that cannot be explained with models presuming thermally activated dissociation such as that by Onsager and Braun[8] or that by Barker et al.[38] As mentioned in the Introduction, if dissociation was thermally activated, it should be associated with an activation energy of about 0.5 eV for an electron hole pair with an intrapair separation of 1 nm in the absence of a field. Petersen et al.[37] suggested a field dependent tunnel process to increase the intrapair separation. This would allow for a concomitant decrease of the activation energy of the electron−hole pair. In the Arkhipov−Baranovskii model, such an assumption is not necessary. The results in Figure 6b show that the weak temperature dependence of the photocurrent in a MeLPPP/C_{60} bilayer diode can be fully accounted for in the Arkhipov−Baranovskii model by using a fixed set of parameters and varying only the temperature, in the range from 300 to 225 K. In this framework, the weak thermal activation arises because the coulomb energy of an even electron−hole pair with 1 nm separation is diminished by the energy of the zero-point oscillation of the electron−hole pair and by dipolar screening. This effect is illustrated in Figure 6a for a moderate field of 1×10^5 V/cm.

In our opinion, the virtually identical experimental and calculated field dependences of the photocurrent over a range of temperatures provide conclusive evidence for the applicability of the current model. At temperatures below 225 K, the experimentally observed photocurrent exceeds the prediction by theory. This deviation can be ascribed to the neglect of disorder in the model. In the presence of disorder, a charge carrier does not always need to overcome the activation energy given by the difference between the site energy and the center of the DOS. Rather, it can also already migrate among lower energy sites, so that the actual activation energy is diminished. This effect is particularly relevant at lower temperatures.[39,40]

Independent support for the strength of the Arkhipov−Baranovskii model comes from comparing the binding energy of an electron−hole pair predicted by the model with that derived from experimental values. The binding energy E_b of a charge transfer state is the difference between the energies of the electron and holes at infinite separation—given by the ionization potential I_P^D of the donor and the electron affinity E_A^A of the acceptor and the optical transition energy of the charge transfer state E_{CT}. Thus, $E_b = (I_P^D - E_A^A) - E_{CT}$. The electron affinity of C_{60} can be inferred from cyclic voltammetry. Suzuki et al.[41] reported a value of −1.13 V for the reduction potential of C_{60} in dichlorobenzene solution with the ferrocene/ferrocenium couple as an internal reference. Since the potential of the Fc/Fc^+ couple relative to the vacuum level is −4.8 eV,[42] E_A^A for an C_{60} in solution should be −3.67 eV. Provided that the solvation energy of the ion in dichlorobenzene solution is identical to the polarization energy of C_{60}^- in a solid, one can adopt this value for the electron affinity of a C_{60} film. In reality, E_A^A of a solid film is expected to be slightly less. The reason is that the polarization energy of a C_{60} anion in a bulk C_{60} film is less than the ionic contribution to solvation in a polar solvent. However, one can compare this above value for E_A^A with the known electron affinity of a C_{60} anion in the gas phase which is 2.69 eV.[43] The difference between the gas phase and the solution values, i.e., 1.02 eV, represents the solvation energy. Knowing that the electronic polarization of an electron in an apolar molecular crystal is near 1 eV, this indicates that we can safely use $E_A^A = 3.65 \pm 0.05$ eV for the electron affinity of a C_{60} film.[44]

The ionization potential I_P^D of the donor polymers can be taken from the photoionization threshold of a donor film. Values for the well conjugated polymers MeLPPP and PCDTBT are 5.28 and 5.23 eV, while the less conjugated DOOPPV has 5.22 eV.[17] The energy of the charge transfer state at the MeLPPP/C_{60} interface can be estimated from Figure 7 to be E_{CT} = 1.43 eV. This yields a binding energy of $E_b = 0.20 \pm 0.05$ eV, as summarized in Table 1. The charge-transfer energy for PCDTBT with fullerene can be estimated using results by Provencher et al. on PCDTBT/$PC_{70}BM$ blend diodes.[45] These authors reported on a low energy emission relative to the fluorescence of the neat donor that is assigned to emission from a charge transfer state. Upon optical excitation, the maximum of this low energy emission is at 1.45 eV, while in EL it is at 1.35 eV. The minor bathochromic shift in electroluminescence relative to photoluminescence is likely due to the fact that in electroluminescence charge carriers can execute more jumps within the energetic landscape before recombination takes place than optically generated short-lived excitons can. Neglecting the relaxation energy and using 1.45 eV as a lower limit for E_{CT} yields an upper limit of $E_b \leq 0.13 \pm 0.05$ eV for PCDTBT. For DOOPPV, the absence of a charge transfer transition in a DOO-PPV/C_{60} diode above 1.2 eV is a strong indication that electron−hole pairs are strongly bound. This is consistent with an extrapolation of the open circuit voltage toward 0 K that yields $V_{oc}(T = 0) = 1.0$ eV. Using this as an estimate of E_{CT} translates into a value of 0.57 ± 0.05 as an estimate for the binding energy.

Table 1. Summary of the Ionization Potentials I_P^D of the Polymers, the Electron Affinity E_A^A of C_{60}, the Estimate Taken for the Energy of the Charge Transfer State E_{CT}, and the Resulting Binding Energy E_b

	MeLPPP	DOOPPV	PCDTBT
I_P^D [17]	5.28 eV	5.22 eV	5.23 eV
E_A^A	3.65 ± 0.05 eV	3.65 ± 0.05 eV	3.65 ± 0.05 eV
E_{CT}	1.43 eV	1.1 ± 0.1 eV	1.45 eV
E_b	0.20 ± 0.05 eV	0.47 ± 0.15 eV	≤0.13 ± 0.05 eV

We can compare these experimentally based values with theoretical predictions for the energy of the hole on chain 1 at 1 nm. The values of 0.4 and 0.3 eV are shown in Figure 3 for effective masses of $1.0m_e$ and $0.1m_e$, respectively, for the case of $\alpha = 0$ (and using $\epsilon_r = 3.0$). For MeLPPP and PCDTBT, values of $m_{eff} = 0.1m_e$ and $\alpha = 0.02$ need to be employed.[17] This yields

DOI: 10.1021/acs.jpcb.5b05138
J. Phys. Chem. B 2015, 119, 10359−10371

a binding energy of 0.14−0.22 eV using ϵ_r = 4.5 down to ϵ_r = 3.0. For DOOPPV, pertinent values are m_{eff} = 1.1m_e and α = 0.03. With these parameters, the Arkhipov−Baranovskii model gives a binding energy of 0.32 ± 0.1 eV. The key point to take away from this comparison between the experimentally derived values of the binding energy and those calculated by the model is not the degree to which the values match. In fact, some deviation is expected due to the neglect of disorder in the present model. Rather, the reasonable agreement indicates that this model is consistent with experiment. This implies that the underlying concept of additional energy terms due to the charge delocalization and due to interfacial electrostatics is suitable and appropriate to describe the dissociation process.

5.2. Implications of the Model. The concept elaborated above is premised upon the implicit notion that optical excitation generates a relaxed ("cold") electron−hole pair. It ignores any excess energy that either the hole or electron may initially possess right after charge transfer at the donor−acceptor interface. The fact that the theoretical results—based upon considering only "cold" electron−hole pairs—are consistent with experiment demonstrates that "hot" electron−hole pairs do not contribute significantly, if at all, to the photodissociation process. This is consistent with the results of Vandewal et al.[46] and Albrecht et al.[47] that show that the yield of electron−hole pair dissociation is independent of how the pair had initially been generated, i.e., upon optical excitation of either the donor or acceptor or via direct optical excitation of the charge transfer state.

At first glance, this conclusion seems at variance of the work of Grancini et al.[30] These authors found that the appearance time of the radical cation upon exciting the PCPDTBT donor in a PCPDTBT/PCBM bulk heterojunction decreases from 50 to 20 fs when the incident photon energy increases from 1.65 to 2.55 eV. The explanation of this effect is that within this spectral range different electronic states are accessed that differ regarding the degree of mixing of donor exciton states and donor−acceptor CT states. It is worth bearing in mind that the experiments by Grancini et al. were optical experiments conducted on a thin film, i.e., in the absence of any field. In contrast, the measurements by Vanderwal et al. and by Albrecht et al. were carried out on devices, where a superimposed built-in field and an applied (reverse or forward) field prevail that is already sufficient to dissociate all "cold" electron−hole pairs, so that the effect of additional "hot" dissociation may not be discernible. Nevertheless, if there was an initial ultrafast dissociation process, it could be implemented in our current work by invoking an ultrafast lifetime of the dissociating electron−hole pair. However, this would imply a very low value of the lifetime hopping rate product such as about 1. As is evident from Figure 5a and b, for such a low $\tau_0\nu_0 e^{-2\gamma r_{ij}}$ value, the saturation field is lower than the built-in field only if there is a fractional charge displacement of 0.04 at an effective mass of m_{eff} = 0.1m_e or of 0.8 for m_{eff} = 1.0m_e. This does not seem realistic. Consistent with the work of Vandewal et al., we therefore conclude that the energy dissipated when an initially hot charge transfer state cools down has only a minor effect for the entire dissociation process.

Even so, there is experimental evidence that the efficiency of organic solar cells can depend on the offset between the LUMOs of donors and acceptors, and thus on the energy dissipated when the donor electron is transferred to the acceptor LUMO.[48,49] A possible explanation to resolve this puzzle could be that there is usually a correlation between LUMO−LUMO offset and the difference between the electronegativities of the donor and acceptor. Such an increase could enhance the fractional charge displacement at the interface in the dark, i.e., increase α, which, in turn, will lower the saturation field for electron−hole pair dissociation and, concomitantly, increase the cell efficiency.

It is obvious that the binding energy of the charge-transfer state at a donor−acceptor interface is a crucial parameter that controls the yield of the dissociation process. In the current work, we show that there is a direct link between that binding energy and the degree of delocalization of the hole on the donor phase and the interfacial electrostatics via fractional charge transfer at the donor−acceptor interface in the dark. This is illustrated by the strikingly different performance of diodes with either DOOPPV or MeLPPP as donors. On the basis of a V_{oc} of only 1 V and the absence of a charge-transfer emission above 1.2 eV, the binding energy of the charge-transfer exciton in DOOPPV should be about 0.47 ± 0.15 eV (see Table 1). Such a large value of the binding energy of the charge transfer state is consistent with the observation that the saturation field of the dissociation yield is large as 1 MV/cm while the saturation field of the MeLPPP/C_{60} diode is about 4 × 10^4 V/cm only.[15] The obvious reason why DOOPPV behaves very different from MeLPPP is that DOOPPV is a highly disordered polymer—as evidenced by the blue-shifted absorption spectrum—with a substantially larger effective hole mass as compared to well-ordered MeLPPP. Interestingly, photoemission spectroscopy[17] indicated that the fractional interfacial charge displacement, quantified by α, of DOOPPV/C_{60} is comparable if slightly larger than that of a MeLPPP/C_{60} diode. This proves that the larger binding energy of electron−hole pairs in DOOPPV/C_{60} as compared to MeLPPP/C_{60} must solely be due to the larger effective hole mass of DOOPPV.

In passing, it is interesting to display the field dependence of the yield of electron−hole pair dissociation against the voltage applied on the diode parametric in the effective mass in the absence of interfacial dipoles. The data shown in Figure 8 refer

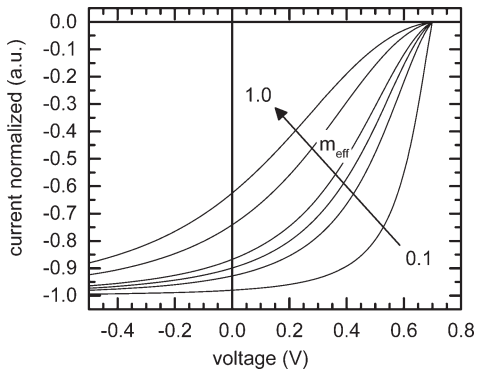

Figure 8. Current−voltage characteristics obtained for a bilayer cell of 60 nm thickness and an open-circuit voltage of 0.7 eV with the parameters α = 0.02 and $\nu_0\tau_0 \exp^{-2\gamma r}$ = 3000 for m_{eff}/m_e = 0.100, 0.215, 0293, 0.341, 0.541, and 1.00.

to an assumed built-in potential of 0.7 V and a presumed diode thickness of 60 nm. It is remarkable that current−voltage curves feature an inflection point, i.e., acquire an s-shape, upon increasing the effective mass, although neither bimolecular charge recombination nor detrimental electrode effects can occur. This demonstrates that observing an s-shape in experimental $j(V)$ curves[50] cannot be taken as a stringent

DOI: 10.1021/acs.jpcb.5b05138
J. Phys. Chem. B 2015, 119, 10359−10371

signature of loss of charge carriers due to nongeminate recombination but may also—and often will—reflect field dependent charge generation. Figure 8 further documents how important the value of the effective mass and the fractional dipole strength are for the shape of the current−voltage curve. For an interfacial dipole with $\alpha = 0.02$, a reasonably good fill factor of 0.58% is obtained with an effective mass of $m_{eff} = 0.1m_e$. In contrast, an unrealistically low effective mass of $m_{eff} = 0.016m_e$ would be required to obtain the same fill factor in the absence of an interfacial dipole, $\alpha = 0.00$ (Figure S4, Supporting Information).

6. OUTLOOK

The intention of the current work was to quantify how delocalization as well as fractional charge displacement at the interface affect photogeneration in organic solar cells employing the Arkhipov−Baranovskii model. It covers a large parameter space and shows that the predictions of the model are consistent with representative experiments. We are aware that the model is simple and ignores several aspects of real world organic solar cells. For instance, the model implies that the coulomb potential is generated by a spatially fixed electron presuming that this is located at a fullerene site. Meanwhile, it is well established that electrons in a C_{60} film or domain are quite mobile.[6] Conceivably, a motion of the sibling electron will further decrease coulomb attraction of the electron−hole pair. The same is expected if the electron delocalizes over several fullerene molecules of a crystalline domain. This effect will be dealt with in future work.

A serious shortcoming of the present model is that any disorder effects have been disregarded up to now. Disorder roughens the energy landscape and alters charge migration. Depending on the relative amounts of disorder, thermal energy, and field strength and direction, disorder can enhance or reduce electron−hole dissociation.[39,40] Thus, the implementation of disorder effects into the already very successful present model is expected to further improve quantitative agreement with experiment. In this context, it is interesting to note that organic solar cells with low-band-gap-type donors such as PCDTBT feature exceptionally high power conversion efficiencies.[6] Recent spectroscopic studies showed that these polymers are prone to local crystallization.[51] The associated improved inter- as well as intrachain ordering might establish a two-dimensional network of hole transport near the donor−acceptor interface. A combined spectroscopic, structural, and photoelectric study could provide a quantitative link for a structure−property relation.

A straightforward application of the current model to bulk heterojunction diodes is hampered by the fact that the Arkhipov−Baranovskii model describes electron−hole pair dissociation in an ideal bilayer assembly in which the electric field acts perpendicular to the interface with the arrangement of the polymer chains parallel to the interface. This disregards the effect of a finite component of electric field along the chain that may facilitate dissociation. In a bulk heterojunction diode, there is a distribution of electric fields acting on inter- as well as intrachain transport. In this case, the escape process of the electron−hole pair should be three-dimensional rather than one-dimensional, as currently seen in the Arkhipov−Baranovskii approach. This effect needs be implemented into the theory in future work.

In summary, the current work demonstrates that the Arkhiov−Baranovskii model is able to capture the essential features of the electron−hole dissociation process, thus yielding a field and temperature dependence of the dissociation probability that is in good agreement with photocurrent results on bilayer diodes. The delocalization of the hole along the polymer backbone and the electrostatic landscape at the interface are identified as major parameters controlling the dissociation process. Further directions in which to expand this model are indicated.

■ ASSOCIATED CONTENT

Supporting Information

The squared modulus of the hole wave function spreads out along the chain with increasing distance to the sibling electron for $m_{eff} = 1.0m_e$ and $m_{eff} = 0.1m_e$. The dependence of the photogeneration yield $\varphi(T)$ on the temperature. Comparison of the EQE and the EL of a MeLPPP device. The current−voltage characteristics obtained for a bilayer cell with no interfacial dipoles. The Supporting Information is available free of charge on the ACS Publications website at DOI: 10.1021/acs.jpcb.5b05138.

■ AUTHOR INFORMATION

Notes

The authors declare no competing financial interest.

■ ACKNOWLEDGMENTS

Financial support is acknowledged by the German Science Foundation DFG for the GRK 1640 and the Bavarian Ministry of Education and Research for the Research initiative “Solar Technologies go Hybrid”.

■ REFERENCES

(1) Green, M. A.; Emery, K.; Hishikawa, Y.; Warta, W.; Dunlop, E. D. Solar Cell Efficiency Tables (Version 42). *Prog. Photovoltaics* **2013**, *21*, 827−837.

(2) Hoke, E. T.; Vandewal, K.; Bartelt, J. A.; Mateker, W. R.; Douglas, J. D.; Noriega, R.; Graham, K. R.; Frechet, J. M. J.; Salleo, A.; McGehee, M. D. Recombination in Polymer:Fullerene Solar Cells with Open-Circuit Voltages Approaching and Exceeding 1.0 V. *Adv. Energy Mater.* **2013**, *3*, 220−230.

(3) Kyaw, A. K. K.; Wang, D. H.; Gupta, V.; Zhang, J.; Chand, S.; Bazan, G. C.; Heeger, A. J. Efficient Solution-Processed Small-Molecule Solar Cells with Inverted Structure. *Adv. Mater.* **2013**, *25*, 2397−2402.

(4) He, Z. C.; Zhong, C. M.; Su, S. J.; Xu, M.; Wu, H. B.; Cao, Y. Enhanced Power-Conversion Efficiency in Polymer Solar Cells Using an Inverted Device Structure. *Nat. Photonics* **2012**, *6*, 591−595.

(5) Foertig, A.; Kniepert, J.; Gluecker, M.; Brenner, T.; Dyakonov, V.; Neher, D.; Deibel, C. Nongeminate and Geminate Recombination in PTB7: PCBM Solar Cells. *Adv. Funct. Mater.* **2014**, *24*, 1306−1311.

(6) Gelinas, S.; Rao, A.; Kumar, A.; Smith, S. L.; Chin, A. W.; Clark, J.; van der Poll, T. S.; Bazan, G. C.; Friend, R. H. Ultrafast Long-Range Charge Separation in Organic Semiconductor Photovoltaic Diodes. *Science* **2014**, *343*, 512−516.

(7) Arkhipov, V. I.; Heremans, P.; Bässler, H. Why is Exciton Dissociation so Efficient at the Interface Between a Conjugated Polymer and an Electron Acceptor? *Appl. Phys. Lett.* **2003**, *82*, 4605−4607.

(8) Braun, C. L. Electric-Field Assisted Dissociation of Charge-Transfer States as a Mechanism of Photocarrier Production. *J. Chem. Phys.* **1984**, *80*, 4157−4161.

(9) Goliber, T. E.; Perlstein, J. H. Analysis of Photogeneration in a Doped Polymer System in Terms of a Kinetic-Model for Electric-Field-Assisted Dissociation of Charge-Transfer States. *J. Chem. Phys.* **1984**, *80*, 4162−4167.

DOI: 10.1021/acs.jpcb.5b05138
J. Phys. Chem. B 2015, 119, 10359−10371

(10) Peumans, P.; Forrest, S. R. Separation of Geminate Charge-Pairs at Donor-Acceptor Interfaces in Disordered Solids. *Chem. Phys. Lett.* **2004**, *398*, 27−31.
(11) Veldman, D.; Ipek, O.; Meskers, S. C. J.; Sweelssen, J.; Koetse, M. M.; Veenstra, S. C.; Kroon, J. M.; van Bavel, S. S.; Loos, J.; Janssen, R. A. J. Compositional and Electric Field Dependence of the Dissociation of Charge Transfer Excitons in Alternating Polyfluorene Copolymer/Fullerene Blends. *J. Am. Chem. Soc.* **2008**, *130*, 7721−7735.
(12) Christ, N.; Kettlitz, S. W.; Valouch, S.; Mescher, J.; Nintz, M.; Lemmer, U. Intensity Dependent but Temperature Independent Charge Carrier Generation in Organic Photodiodes and Solar Cells. *Org. Electron.* **2013**, *14*, 973−978.
(13) Deibel, C.; Strobel, T.; Dyakonov, V. Origin of the Efficient Polaron-Pair Dissociation in Polymer-Fullerene Blends. *Phys. Rev. Lett.* **2009**, *103*, 036402.
(14) Nenashev, A. V.; Baranovskii, S. D.; Wiemer, M.; Jansson, F.; Osterbacka, R.; Dvurechenskii, A. V.; Gebhard, F. Theory of Exciton Dissociation at the Interface between a Conjugated Polymer and an Electron Acceptor. *Phys. Rev. B: Condens. Matter Mater. Phys.* **2011**, *84*, 035210.
(15) Schwarz, C.; Bässler, H.; Bauer, I.; Koenen, J. M.; Preis, E.; Scherf, U.; Köhler, A. Does Conjugation Help Exciton Dissociation? A Study on Poly(p-phenylene)s in Planar Heterojunctions with C60 or TNF. *Adv. Mater.* **2012**, *24*, 922−925.
(16) Bakulin, A. A.; Rao, A.; Pavelyev, V. G.; van Loosdrecht, P. H. M.; Pshenichnikov, M. S.; Niedzialek, D.; Cornil, J.; Beljonne, D.; Friend, R. H. The Role of Driving Energy and Delocalized States for Charge Separation in Organic Semiconductors. *Science* **2012**, *335*, 1340−1344.
(17) Schwarz, C.; Tscheuschner, S.; Frisch, J.; Winkler, S.; Koch, N.; Bässler, H.; Köhler, A. Role of the Effective Mass and Interfacial Dipoles on Exciton Dissociation in Organic Donor-Acceptor Solar Cells. *Phys. Rev. B: Condens. Matter Mater. Phys.* **2013**, *87*, 155205.
(18) van der Hofstad, T. G. J.; Di Nuzzo, D.; van den Berg, M.; Janssen, R. A. J.; Meskers, S. C. J. Influence of Photon Excess Energy on Charge Carrier Dynamics in a Polymer-Fullerene Solar Cell. *Adv. Energy Mater.* **2012**, *2*, 1095−1099.
(19) Bredas, J. L.; Norton, J. E.; Cornil, J.; Coropceanu, V. Molecular Understanding of Organic Solar Cells: The Challenges. *Acc. Chem. Res.* **2009**, *42*, 1691−1699.
(20) Clarke, T. M.; Durrant, J. R. Charge Photogeneration in Organic Solar Cells. *Chem. Rev.* **2010**, *110*, 6736−6767.
(21) Wiemer, M.; Nenashev, A. V.; Jansson, F.; Baranovskii, S. D. On the Efficiency of Exciton Dissociation at the Interface between a Conjugated Polymer and an Electron Acceptor. *Appl. Phys. Lett.* **2011**, *99*, 013302.
(22) Wiemer, M.; Koch, M.; Lemmer, U.; Pevtsov, A. B.; Baranovskii, S. D. Efficiency of Exciton Dissociation at Internal Organic Interfaces beyond Harmonic Approximation. *Org. Electron.* **2014**, *15*, 2461−2467.
(23) Fishchuk, I. I.; Kadashchuk, A.; Hoffmann, S. T.; Athanasopoulos, S.; Genoe, J.; Bässler, H.; Köhler, A. Unified Description for Hopping Transport in Organic Semiconductors Including both Energetic Disorder and Polaronic Contributions. *Phys. Rev. B: Condens. Matter Mater. Phys.* **2013**, *88*, 125202.
(24) Rubel, O.; Baranovskii, S. D.; Stolz, W.; Gebhard, F. Exact Solution for Hopping Dissociation of Geminate Electron-Hole Pairs in a Disordered Chain. *Phys. Rev. Lett.* **2008**, *100*, 196602.
(25) Burland, D. M. Cyclotron-Resonance in a Molecular Crystal-Anthracene. *Phys. Rev. Lett.* **1974**, *33*, 833−835.
(26) Weiser, G. Stark-Effect of One-Dimensional Wannier Excitons in Polydiacetylene Single-Crystals. *Phys. Rev. B: Condens. Matter Mater. Phys.* **1992**, *45*, 14076−14085.
(27) van der Horst, J. W.; Bobbert, P. A.; Michels, M. A. J.; Bässler, H. Calculation of Excitonic Properties of Conjugated Polymers Using the Bethe-Salpeter Equation. *J. Chem. Phys.* **2001**, *114*, 6950−6957.
(28) Koehler, M.; Santos, M. C.; da Luz, M. G. E. Positional Disorder Enhancement of Exciton Dissociation at Donor/Acceptor Interface. *J. Appl. Phys.* **2006**, *99*, 053702.
(29) Körner, M.; Loske, F.; Einax, M.; Kuhnle, A.; Reichling, M.; Maass, P. Second-Layer Induced Island Morphologies in Thin-Film Growth of Fullerenes. *Phys. Rev. Lett.* **2011**, *107*, 016101.
(30) Grancini, G.; Maiuri, M.; Fazzi, D.; Petrozza, A.; Egelhaaf, H. J.; Brida, D.; Cerullo, G.; Lanzani, G. Hot Exciton Dissociation in Polymer Solar Cells. *Nat. Mater.* **2013**, *12*, 29−33.
(31) Herrmann, D.; Niesar, S.; Scharsich, C.; Köhler, A.; Stutzmann, M.; Riedle, E. Role of Structural Order and Excess Energy on Ultrafast Free Charge Generation in Hybrid Polythiophene/Si Photovoltaics Probed in Real Time by Near-Infrared Broadband Transient Absorption. *J. Am. Chem. Soc.* **2011**, *133*, 18220−18233.
(32) Niklas, J.; Mardis, K. L.; Banks, B. P.; Grooms, G. M.; Sperlich, A.; Dyakonov, V.; Beaupre, S.; Leclerc, M.; Xu, T.; Yu, L. P.; Poluektov, O. G. Highly-Efficient Charge Separation and Polaron Delocalization in Polymer-Fullerene Bulk-Heterojunctions: A Comparative Multi-Frequency EPR and DFT Study. *Phys. Chem. Chem. Phys.* **2013**, *15*, 9562−9574.
(33) Blakesley, J. C.; Neher, D. Relationship between Energetic Disorder and Open-Circuit Voltage in Bulk Heterojunction Organic Solar Cells. *Phys. Rev. B: Condens. Matter Mater. Phys.* **2011**, *84*, 075210.
(34) Koster, L. J. A.; Mihailetchi, V. D.; Ramaker, R.; Blom, P. W. M. Light Intensity Dependence of Open-Circuit Voltage of Polymer: Fullerene Solar Cells. *Appl. Phys. Lett.* **2005**, *86*, 123509.
(35) Deibel, C.; Dyakonov, V. Polymer-Fullerene Bulk Heterojunction Solar Cells. *Rep. Prog. Phys.* **2010**, *73*, 096401.
(36) Grzegorczyk, W. J.; Savenije, T. J.; Dykstra, T. E.; Piris, J.; Schins, J. M.; Siebbeles, L. D. A. Temperature-Independent Charge Carrier Photogeneration in P3HT-PCBM Blends with Different Morphology. *J. Phys. Chem. C* **2010**, *114*, 5182−5186.
(37) Petersen, A.; Ojala, A.; Kirchartz, T.; Wagner, T. A.; Wurthner, F.; Rau, U. Field-Dependent Exciton Dissociation in Organic Heterojunction Solar Cells. *Phys. Rev. B: Condens. Matter Mater. Phys.* **2012**, *85*, 245208.
(38) Barker, J. A.; Ramsdale, C. M.; Greenham, N. C. Modeling the Current-Voltage Characteristics of Bilayer Polymer Photovoltaic Devices. *Phys. Rev. B: Condens. Matter Mater. Phys.* **2003**, *67*, 075205.
(39) Emelianova, E. V.; van der Auweraer, M.; Bässler, H. Hopping Approach Towards Exciton Dissociation in Conjugated Polymers. *J. Chem. Phys.* **2008**, *128*, 224709.
(40) Zimmerman, J. D.; Xiao, X.; Renshaw, C. K.; Wang, S. Y.; Diev, V. V.; Thompson, M. E.; Forrest, S. R. Independent Control of Bulk and Interfacial Morphologies of Small Molecular Weight Organic Heterojunction Solar Cells. *Nano Lett.* **2012**, *12*, 4366−4371.
(41) Suzuki, T.; Maruyama, Y.; Akasaka, T.; Ando, W.; Kobayashi, K.; Nagase, S. Redox Properties of Organofullerenes. *J. Am. Chem. Soc.* **1994**, *116*, 1359−1363.
(42) Pommerehne, J.; Vestweber, H.; Guss, W.; Mahrt, R. F.; Bässler, H.; Porsch, M.; Daub, J. Efficient 2-Layer Leds on a Polymer Blend Basis. *Adv. Mater.* **1995**, *7*, 551−554.
(43) Betowski, L. D.; Enlow, M.; Riddick, L.; Aue, D. H. Calculation of Electron Affinities of Polycyclic Aromatic Hydrocarbons and Solvation Energies of their Radical Anion. *J. Phys. Chem. A* **2006**, *110*, 12927−12946.
(44) Faist, M. A.; Kirchartz, T.; Gong, W.; Ashraf, R. S.; McCulloch, I.; de Mello, J. C.; Ekins-Daukes, N. J.; Bradley, D. D. C.; Nelson, J. Competition between the Charge Transfer State and the Singlet States of Donor or Acceptor Limiting the Efficiency in Polymer:Fullerene Solar Cells. *J. Am. Chem. Soc.* **2012**, *134*, 685−692.
(45) Provencher, F.; Sakowicz, M.; Brosseau, C. N.; Latini, G.; Beaupre, S.; Leclerc, M.; Reynolds, L. X.; Haque, S. A.; Leonelli, R.; Silva, C. Slow Geminate-Charge-Pair Recombination Dynamics at Polymer: Fullerene Heterojunctions in Efficient Organic Solar Cells. *J. Polym. Sci., Part B: Polym. Phys.* **2012**, *50*, 1395−1404.
(46) Vandewal, K.; Albrecht, S.; Hoke, E. T.; Graham, K. R.; Widmer, J.; Douglas, J. D.; Schubert, M.; Mateker, W. R.; Bloking, J. T.;

DOI: 10.1021/acs.jpcb.5b05138
J. Phys. Chem. B 2015, 119, 10359−10371

Burkhard, G. F.; Sellinger, A.; Frechet, J. M. J.; Amassian, A.; Riede, M. K.; McGehee, M. D.; Neher, D.; Salleo, A. Efficient Charge Generation by Relaxed Charge-Transfer States at Organic Interfaces. *Nat. Mater.* **2014**, *13*, 63−68.
(47) Albrecht, S.; Vandewal, K.; Tumbleston, J. R.; Fischer, F. S. U.; Douglas, J. D.; Frechet, J. M. J.; Ludwigs, S.; Ade, H.; Salleo, A.; Neher, D. On the Efficiency of Charge Transfer State Splitting in Polymer: Fullerene Solar Cells. *Adv. Mater.* **2014**, *26*, 2533−2539.
(48) Ohkita, H.; Cook, S.; Astuti, Y.; Duffy, W.; Tierney, S.; Zhang, W.; Heeney, M.; McCulloch, I.; Nelson, J.; Bradley, D. D. C.; Durrant, J. R. Charge Carrier Formation in Polythiophene/Fullerene Blend Films Studied by Transient Absorption spectroscopy. *J. Am. Chem. Soc.* **2008**, *130*, 3030−3042.
(49) Servaites, J. D.; Ratner, M. A.; Marks, T. J. Organic Solar Cells: A new Look at Traditional Models. *Energy Environ. Sci.* **2011**, *4*, 4410−4422.
(50) Wagner, J.; Gruber, M.; Wilke, A.; Tanaka, Y.; Topczak, K.; Steindamm, A.; Hormann, U.; Opitz, A.; Nakayama, Y.; Ishii, H.; Pflaum, J.; Koch, N.; Brütting, W. Identification of Different Origins for S-Shaped Current Voltage Characteristics in Planar Heterojunction Organic Solar Cells. *J. Appl. Phys.* **2012**, *111*, 054509.
(51) Scharsich, C.; Fischer, F. S. U.; Wilma, K.; Hildner, R.; Ludwigs, S.; Köhler, A. Revealing Aggregate Formation in PCPDTBT by Optical Spectroscopy. *J. Polym. Sci., Part B: Polym. Phys.* **2015**, DOI: 10.1002/polb.23780.

DOI: 10.1021/acs.jpcb.5b05138
J. Phys. Chem. B 2015, 119, 10359−10371

Supporting information to

A Combined Theoretical and Experimental Study of Dissociation of Charge Transfer States at the Donor-Acceptor Interface of Organic Solar Cells

Steffen Tscheuschner[1], Heinz Bässler[2], Katja Huber[1], Anna Köhler[1,2*]

[1] Experimental Physics II, University of Bayreuth,D- 95440 Bayreuth, Germany

[2] Bayreuth Institute of Macromolecular Research (BIMF), University of Bayreuth, D-95440 Bayreuth, Germany

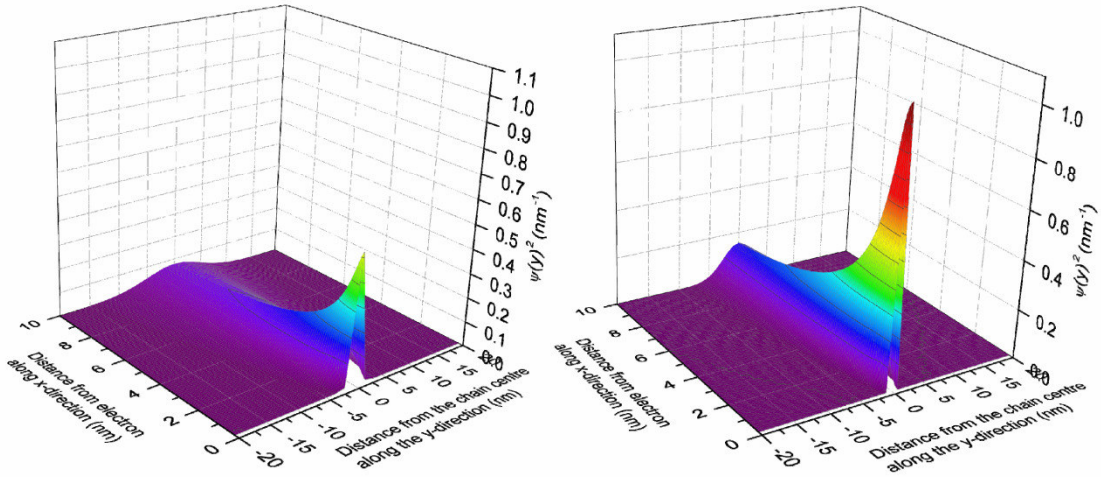

Figure S1 – The square modulus of the hole wavefunction $\psi_n(x_n, y)$ along the chain as a function of distance from the interface for m_{eff}=0.1m_e (left) and for m_{eff}=1.0m_e (right). The total area under the wavefunction is normalized to unity. The colour indicates the amplitude of $|\psi_n(x_n, y)|^2$.

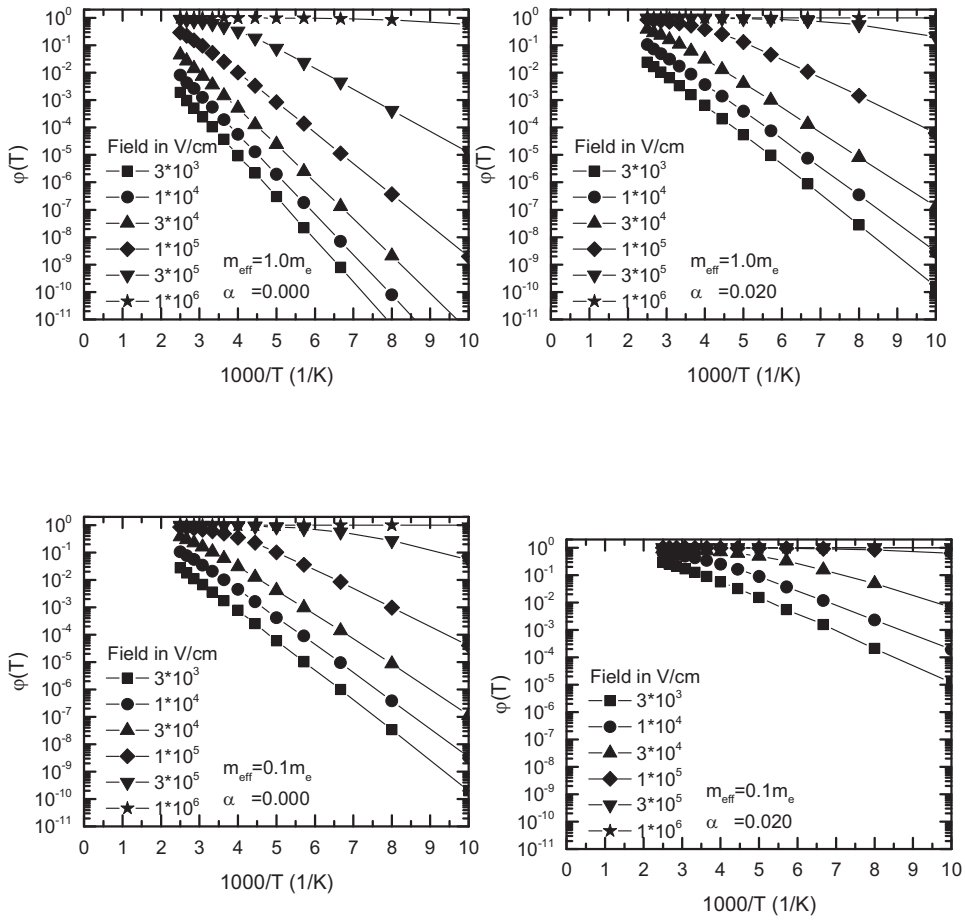

Figure S2

The dependence of the photogeneration yield $\varphi(T)$ on temperature plotted logarithmically versus inverse temperature for different field strength across the device (a) for $m_{eff} = 1.0m_e$, α =0.00, (b) for $m_{eff} = 1.0m_e$, α =0.02, (c) for $m_{eff} = 0.1m_e$, α =0.00, (d) for $m_{eff} = 0.1m_e$,α =0.02. When the electric field is essentially absent, such as for field strength of 3 x 10^3 V/cm, activation energies are 0.30 eV (a), 0.21 eV (b), 0.24 eV (c) 0.12 eV (d).

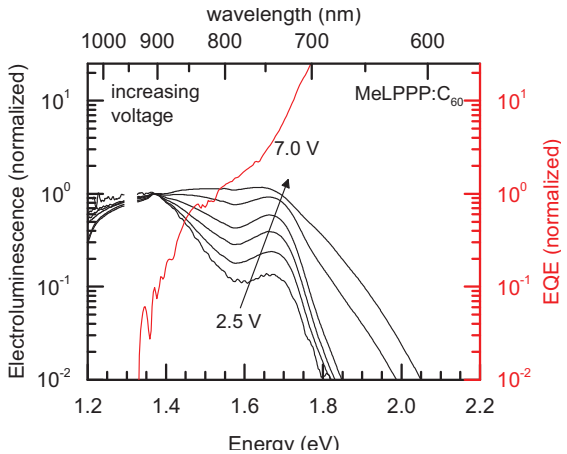

Figure S3

The EQE (red colour) and EL (black colour) spectra taken from a ITO/MoO_3/30 nm MeLPPP/30nm C_{60}/Al device, both displayed on a semilogarithmic scale. The EL spectra were taken for driving voltages from 2.5 V to 7.0 V.

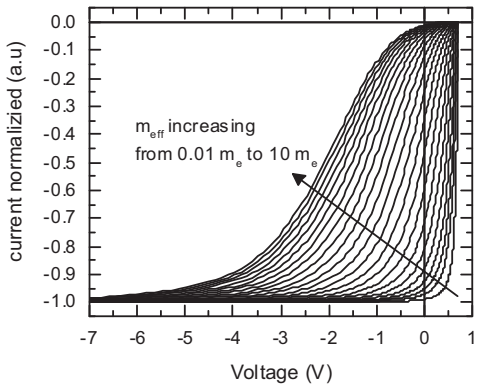

Figure S4

The current-voltage characteristics obtained for a bilayer cell of 60 nm thickness and open-circuit voltage of 0.7 eV with the parameters α =0.00,$\nu_0\tau_0 \exp -2\gamma r = 3000$, $\frac{m_{eff}}{m_e}$is increased from 0.01 onwards by a factor of 1.36.

Anhang A Iodine Migration and its Effect on Hysteresis in Perovskite Solar Cells

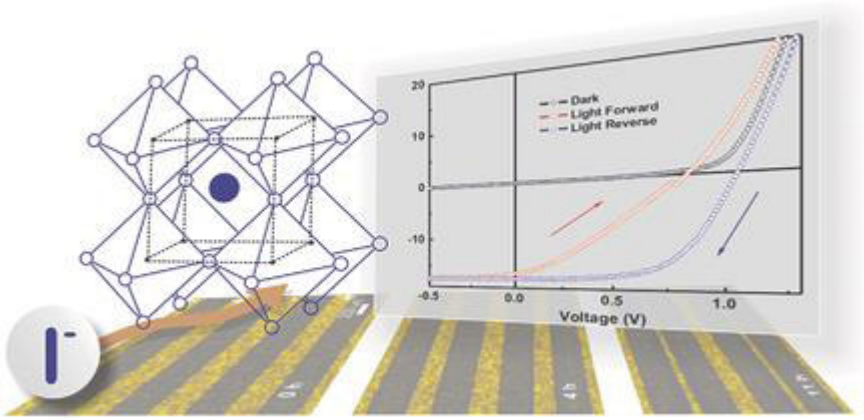

Cheng Li, Steffen Tscheuschner, Fabian Paulus, Paul E. Hopkinson, Johannes Kiessling, Anna Köhler,Yana Vaynzof, Sven Hüttner

Veröffentlicht in

Advanced Materials (**2016**), 28, 2446-2454

(DOI: https://doi.org/10.1002/adma.201503832)

ADVANCED MATERIALS
www.advmat.de

Materials Views
www.MaterialsViews.com

Iodine Migration and its Effect on Hysteresis in Perovskite Solar Cells

*Cheng Li, Steffen Tscheuschner, Fabian Paulus, Paul E. Hopkinson, Johannes Kießling, Anna Köhler, Yana Vaynzof, and Sven Huettner**

The past few years have witnessed a dramatic development of inorganic–organic halide organometal perovskite solar cells, which have captured the attention of the scientific community due to their high power conversion efficiencies[1] and simple fabrication processes.[2,3] Besides further improving the conversion efficiency[4] and stability,[5] important device related questions still need to be answered:[6,7] the hysteresis behavior, i.e., the discrepancy of the performance between two voltage-sweeping directions when performing a current–voltage (*J–V*) measurement. The possible origins include ferroelectricity,[8,9] low frequency capacitance,[10] trap states in the bulk,[11] interfacial dipoles,[12] as well as mobile ion screening.[13–15] Several groups have fabricated devices without significant hysteresis, for example, by using mesoporous TiO_2 layers instead of a compact TiO_2 layer,[16] solvent annealing to obtain large crystalline grains,[17] as well as a fullerene passivation method.[18]

Although there are several proposed mechanisms, recently more and more attention is focused on the role of ions/vacancies migration under an electrical field.[15,19–21] (1) The characterized decay time scale in perovskite solar cells is on a second timescale[22] (also see Figure S6, Supporting Information), while the ferroelectric domain polarization/depolarization process is much faster, in the picosecond range.[23,24] In addition, piezoresponse force microscopy[13,25] results also suggested that polarization switching in $CH_3NH_3PbI_3$ is unlikely to be the dominant reason for the hysteresis behavior. (2) By transient photovoltage and capacitance measurements, O'Regan et al.[26] proved that *J–V* curve hysteresis is not associated with the change of recombination rate and charge separation efficiency. (3) Simple trapping and detrapping of charges at defects in the bulk or at the interface is also unlikely to be the main mechanism due to the long duration and large magnitude of the current decay.[19] However, the trapping/detrapping process associated with migrating defects, such as iodine interstitials,[15,27] which can be driven by an electrical field, may play an important role in the hysteresis.

In brief, we used three different methods to reveal the underlying processes relating to hysteresis. First we employed electroabsorption (EA) spectroscopy, a noninvasive in situ characterization approach[28,29] to determine the built-in potential (V_{BI}) in solar cell devices. In a second experiment we applied a staircase voltage profile to these devices and measured the time dependent current at a series of temperatures in order to study the activation energy of the migrating species in perovskite based devices. In the last experiment we used X-ray photoemission spectroscopy (XPS) measurements to study the redistribution of elements within laterally configured devices after long-term electrical biasing. Our results suggest that the hysteresis in *J–V* curves originates from the interfacial barrier associated with the drift of iodide ions or the respective interstitial under an electrical field.

Figure 1a shows the scheme of a FTO/compact TiO_2/$CH_3NH_3PbI_{3-x}Cl_x$/Spiro-OMeTAD/Ag planar perovskite solar cell. As a p-i-n structure,[30,31] photogenerated electrons are collected by a FTO (fluorine doped tin oxide) electrode through a compact TiO_2 layer, and the holes by an Ag electrode through a layer of Spiro-OMeTAD (2,2′,7,7′-Tetrakis-(*N*,*N* -di-4-methoxyphenylamino)-9,9′-spirobifluorene), acting respectively as electron and hole transport layers (ETL/HTL). The ionization energy and the electron affinity of materials were estimated according to values reported in literature[1,14] and measurement of the optical bandgap (Figure S1, Supporting Information). The *J–V* curves of a $CH_3NH_3PbI_{3-x}Cl_x$ perovskite solar cell under AM 1.5G illumination in forward and reverse voltage sweeps are shown in Figure 1b. As shown in **Table 1**, there is a shift in V_{oc} of 0.22 V and a significant difference in the performance between the two sweeping directions. Note that the red dashed line depicts the extension of the *J–V* curve during

Dr. C. Li, J. Kießling, Prof. S. Huettner
Macromolecular Chemistry I
University of Bayreuth
Universitätstr. 30, 95447 Bayreuth, Germany
E-mail: sven.huettner@uni-bayreuth.de
S. Tscheuschner, Prof. A. Köhler
Experimental Physics II
University of Bayreuth
Universitätstr. 30, 95447 Bayreuth, Germany
F. Paulus
Organic Chemistry Institute
Im Neuenheimer Feld 270
Heidelberg University
69120 Heidelberg, Germany
Dr. P. E. Hopkinson, Prof. Y. Vaynzof
Kirchhof Institute for Physics
Im Neuenheimer Feld 227
Heidelberg University
69120 Heidelberg, Germany
Dr. P. E. Hopkinson, Prof. Y. Vaynzof
Centre for Advanced Materials
Im Neuenheimer Feld 225
Heidelberg University
69120 Heidelberg, Germany

DOI: 10.1002/adma.201503832

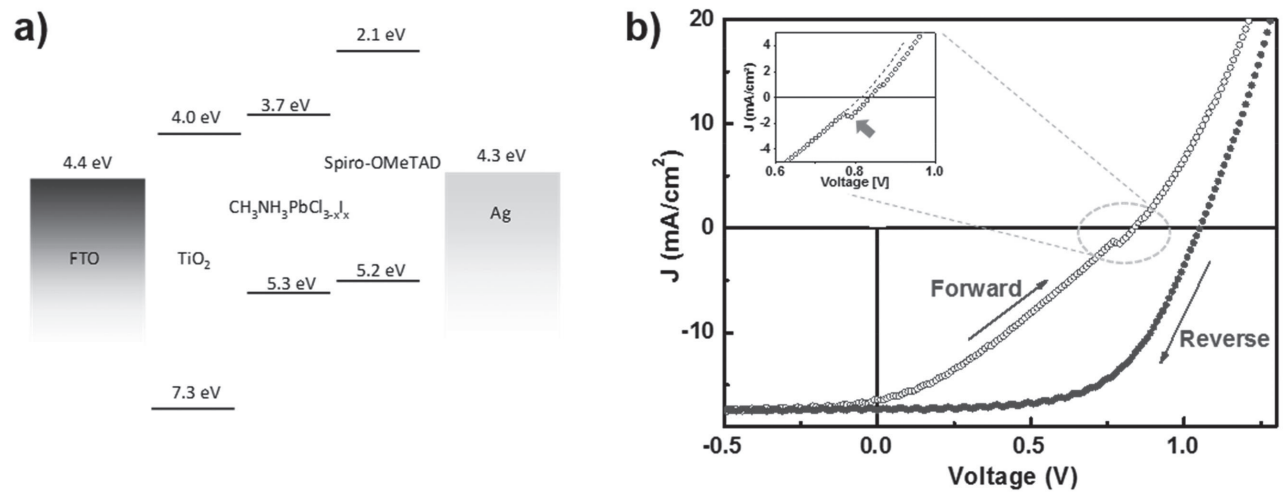

Figure 1. a) Energy diagram of a FTO/compact TiO_2/$CH_3NH_3PbI_{3-x}Cl_x$/Spiro-OMeTAD/Ag perovskite solar cell. b) Current–voltage (J–V) curve of a perovskite solar cell under AM 1.5G illumination. The arrows indicate the directions of applied external voltage (forward and reverse sweeping). Inset shows the kink in the J–V curve in detail. The dashed line is the extension of the J–V curve below ≈0.75 V, and the grey arrow indicates the shift of the curves near the flat-band condition. The scanning speed is 0.9 V s^{-1}.

the forward voltage sweep below 0.75 V, based on a single junction diode equation.[32] The inset in Figure 1b shows a magnification of the area around 0.75 V, and the shift of V_{oc} between the dashed extension line and the measured curve and the emerging kink will be discussed in the course of this work. This kink has been frequently observed in several papers, especially during fast scanning.[7,22,33] In addition, unlike the reverse sweep, in the forward sweep, the fill factor is significantly reduced and tends to look "S-curved" near V_{oc} implying that during forward sweeps there may exist injection barriers associated with interfacial dipoles at the perovskite/HTL or ETL interface,[34] or capacitive charging/discharging effects during the scanning process.[26,35]

To understand the origin of the hysteresis in $CH_3NH_3PbI_{3-x}Cl_x$ perovskite solar cells in more detail, we carried out the EA measurement in forward and reverse sweeping directions. We used an EA setup as described in detail in previous papers.[36,37] In brief, the absorption of materials can be modulated by an external electrical field due to the Stark effect. Here, a superposition of DC and AC voltages was applied to the device and the change in intensity of the reflective probe light, ΔR, was monitored by a silicon photodetector connected to a lock-in amplifier. According to the classical Stark effect theory,[38] the shift of the energy (ΔE) produced by the electrical field (F) arises from both the change of dipole moment ($\Delta\mu$) and polarizability (Δp)

$$\Delta E(F) \propto -\Delta\mu F - \frac{1}{2}F\Delta pF \quad (1)$$

Table 1. Device performance parameters of a FTO/compact TiO_2/$CH_3NH_3PbI_{3-x}Cl_x$/Spiro-OMeTAD/Ag perovskite solar cell, during the forward and reverse sweeping, respectively.

Sweep direction	J_{sc} [mA cm^{-2}]	V_{oc} [V]	FF [%]	PCE [%]
Forward	16.22	0.83	30.2	4.3
Reverse	17.62	1.05	60.1	12.0

The change in the absorption coefficient $\Delta\alpha$ or EA signal $\Delta R/R$, which is a function of ΔE, can be expressed by a Taylor expansion truncated by the quadratic term[39]

$$\Delta\alpha \propto \frac{\Delta R}{R} \propto \frac{\partial\alpha}{\partial E}\Delta E + \frac{1}{2}\frac{\partial^2\alpha}{\partial E^2}\Delta E^2 \quad (2)$$

By inserting Equation (1) into Equation (2), the lineshape of the EA spectrum can be regarded as a linear combination of the spectra resembling the first and second derivative of the unperturbed absorption spectrum. Two possible conditions can be considered:[38–40] (1) If there is no permanent dipole, i.e., only dipole moments induced by an external electrical field, the whole absorption spectrum will shift towards a lower energy. As a consequence, the change of absorption $\Delta\alpha$, or the EA spectrum $\Delta R/R$, exhibits a first derivative lineshape. (2) If permanent dipoles exist, $\Delta\mu F$ dominates Equation (2). Assuming $\Delta\mu > 0$, dipole moments that are aligned with the external electrical field will decrease in energy, while those aligned against the field will experience an increase in energy. As a result, the EA spectrum resembles a second derivative lineshape.

A typical EA spectrum of a $CH_3NH_3PbI_{3-x}Cl_x$ perovskite solar cell is shown in **Figure 2**, which overlaps well with the features of the second derivative of the unperturbed absorbance spectrum of the perovskite film. In addition, Wu et al.[28] have shown that these features are unaffected when using different ETL and HTL layers. This suggests that this EA response is mainly related to permanent dipoles within the bulk of the perovskite layer.

O'Regan et al.[26] proposed that the J–V curve hysteresis is ascribed to the band offset at the interface. Tress et al.[21] suggested that the hysteresis is due to the screening of build-in field by ionic migration, changing the effective difference in work functions of two contacts. Leguy et al.[24] proposed a similar decrease of work functions difference due to an alignment of ferroelectric domains. Therefore, to characterize the built-in potential within the device, we carried out DC dependent EA

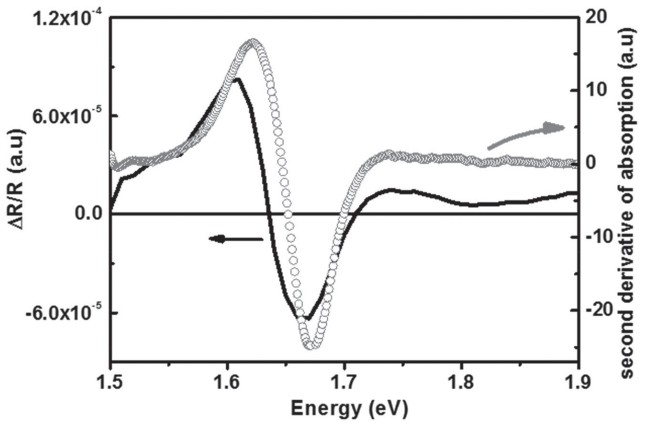

Figure 2. Comparison between EA spectrum of a $CH_3NH_3PbI_{3-x}Cl_x$ perovskite solar cell (black) and second derivative of $CH_3NH_3PbI_{3-x}Cl_x$ absorption spectrum (open symbols). Applied DC and AC voltage in EA measurement are –2 V and 1 V, respectively, and the AC frequency is 2.01 kHz.

measurements. The EA response ($\Delta R/R$) at the first harmonic of the applied AC bias is[37]

$$\left.\frac{\Delta R}{R}\right|_{\omega} \propto \chi(h\nu)V_0V_{AC}\sin(\omega t) = \chi(h\nu)(V_{DC}-V_{BI})V_{AC}\sin(\omega t) \quad (3)$$

Here, $\chi(h\nu)$ is the electric susceptibility of the materials, a function of the photon energy $h\nu$, while V_{DC} and V_{AC} are the applied external DC and AC voltages, respectively. V_{BI} is the built-in potential in the device and V_0 is the internal DC voltage. Based on the standard metal–insulator–metal model, the built-in potential V_{BI} relies on the work function difference between two electrodes.[41] Herein, according to Equation (3), V_{BI} can be determined by finding the nulling voltage V_{null} ($V_{null} = V_{DC} - V_{BI}$), when the EA signal is zero.

The spectra of the perovskite solar cell under a series of external DC voltages are shown in **Figure 3**a. The features of peaks located at 1.62 and 1.66 eV are nearly field-independent, while the amplitudes are proportional to the external DC voltage. In addition, at $V_{DC} = 0$ V an EA signal is still presented, indicating the nonzero built-in potential in the device. During the forward scan, from –2 to 0 V, the built-in potential is estimated as 1.0 ± 0.1 V (linear fit of 5 points at 1.66 eV in Figure 3a, indicated by the dashed line). Since the Spiro-OMeTAD is highly doped with a lithium salt, we can assume that the work function approaches the valance band (or highest occupied molecular orbital).[42] Therefore, the obtained V_{BI} can be regarded as approximately the work function difference between the TiO_2 and the Spiro-OMeTAD layer[3] which corresponds to a p-i-n structure as used in the theoretical description of EA.[13,36]

Figure 3b shows the DC dependent EA signal at a photon energy of 1.66 eV in forward and reverse sweeping direction, respectively. By sweeping from –2.5 to 2 V we obtain a $V_{BI} = 1.0 \pm 0.1$ V, which is consistent with the spectra under a series of external DC voltages in Figure 3a. We notice that for voltages above +1 V, the EA signal exhibits a deviation from its linear relationship. This originates from the large charge injection and electroluminescence of this perovskite solar cell at higher positive voltages (Figure S5, Supporting Information). By reverse sweeping from 2 to –2.5 V, the device exhibits a V_{BI} of 1.3 ± 0.1 V, showing a shift of V_{BI} of 0.3 ± 0.1 V, reflecting the shift of V_{OC} as seen in Figure 1b. This reduction of V_{BI} is also consistent with the observation in rate-dependent J–V curve hysteresis measurement (Figure S3, Supporting Information).[21] This result implies a change of the effective work function of Spiro-OMeTAD and TiO_2 during sweeping. This change is shown in Figure S10 (Supporting Information) and can be caused by a modulation of the interfacial barrier.[43,44] In the negative voltage region, we notice that the EA response in the reverse curve (blue) deviates from a linear relationship, and the EA signal drops to near zero at ≈–1 V. We also observe that when applying larger negative voltages (greater than –3 V), both the forward and reverse curves merge (not shown here). We propose that this behavior is a further indication for ionic migration, i.e., the drift of ions within the bulk under a negative electrical field. This migration results in the redistribution of ions and disturbs the internal electrical

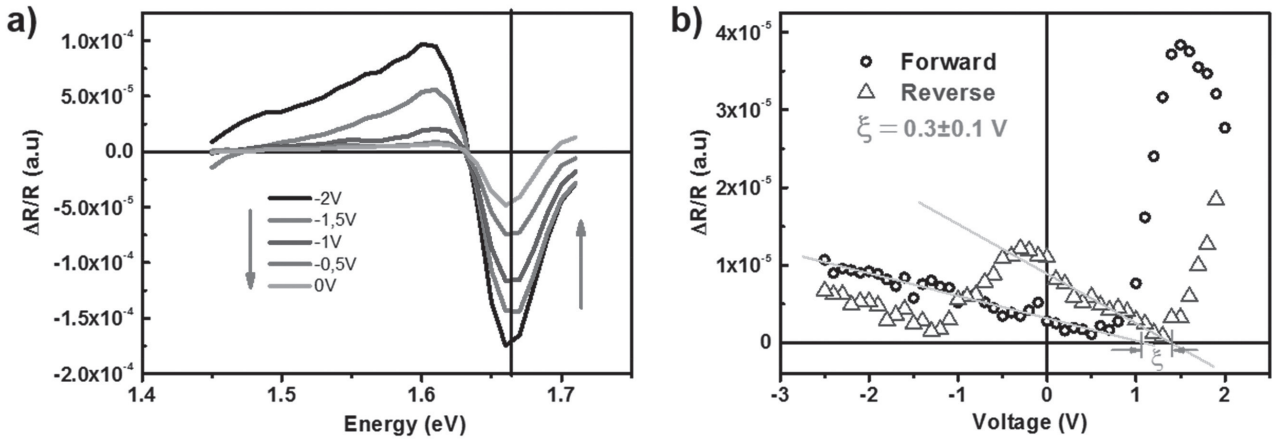

Figure 3. a) EA spectra of a perovskite solar cell under a series of DC voltages. The dashed line indicates the photon energy 1.66 eV selected for the DC voltage dependent EA characterization. The arrows show the order of applied external DC voltages. b) DC dependent EA signal at 1.66 eV, in the forward and reverse sweeping, respectively. Gray solid lines are linear fits of the EA signal to obtain the built-in potential. ξ is the shift of the built-in potential between forward and reverse sweeping directions. $V_{AC} = 1$ V, and AC frequency is 2.01 kHz. The FTO layer was grounded and the external voltage was applied to the Ag layer.

field, leading to the deviation of the standard EA signal.[45] This process is also time dependent and would automatically lead to a change of capacitance during the switching.[22,35]

Temperature dependent electrical measurements enable us to investigate the nature of the ionic species, such as the activation energy.[10,15,19,27,46,47] According to the chemical diffusion theory, if the transient curve fits an exponential behavior, it implies a chemical diffusion process is involved.[15,48] By applying subsequent voltage steps between −2 and 2 V, each step lasting for 40 s with an absolute step size of 0.5 V, we monitor the dynamic process of the electrical current response. As in a typical diode, the current densities in the negative voltage region are negligible (in both sweeping directions). In the positive region, time t dependent current density curves at different voltage steps can be fitted by a single exponential function $e^{-t/\tau}$ (Figure S7, Supporting Information). We observe that as the temperature decreases, the decay time increases, which is in good agreement with the observation in temperature dependent chronophotoamperometry measurement.[19] Therefore, this behavior is consistent with the chemical diffusion theory as mentioned above and suggests ions migration during the J–V curve measurement. In detail, Nian et al.[47] presented that the resistivity of perovskite materials exhibits an exponential relationship with the concentration of defects/ions at the interface. Even though the influence of diffusion and drift may be more complex, the good match with a monoexponential function suggests that we can assume a linear increase of the ion concentration with their migration velocity. Hence, the electrical current decay time τ can be considered to be proportional to the reciprocal of the velocity of ions.

We studied the decay time τ constant at 1.5 V, both in forward and reverse sweeping at different temperatures. **Figure 4**c,d plots $\ln(\tau)$ against $1000/T$ and within the margin of error, the curves between 200 and 300 K approximately show a straight line. The material undergoes a phase transition from a tetragonal to an orthorhombic phase[49] at ≈160 K, which is why the point at 150 K does not fit the same temperature dependency. This phase transition, has also been observed in temperature dependent capacitance measurement,[35] UV–vis absorbance spectra[50] and photoluminescence spectra.[51]

The movement of ions within the bulk of a material, especially in traditional perovskite materials (ABO_3), has been intensively investigated.[52] This linear relationship between $\ln(\tau)$ and $1/T$ suggests that the movement of ions is facilitated by a hopping mechanism among the atomic lattices under an external electrical field.[53] Vineyard presented an absolute rate theory in 1957, which describes an individual defect jump rate[53] of ions Γ in solids excited by thermal activation

$$\Gamma = \Gamma_0 e^{-\Delta E/k_B T} \tag{4}$$

Here, ΔE is the activation energy required to hop from one equilibrium site to the neighboring one, T is the absolute

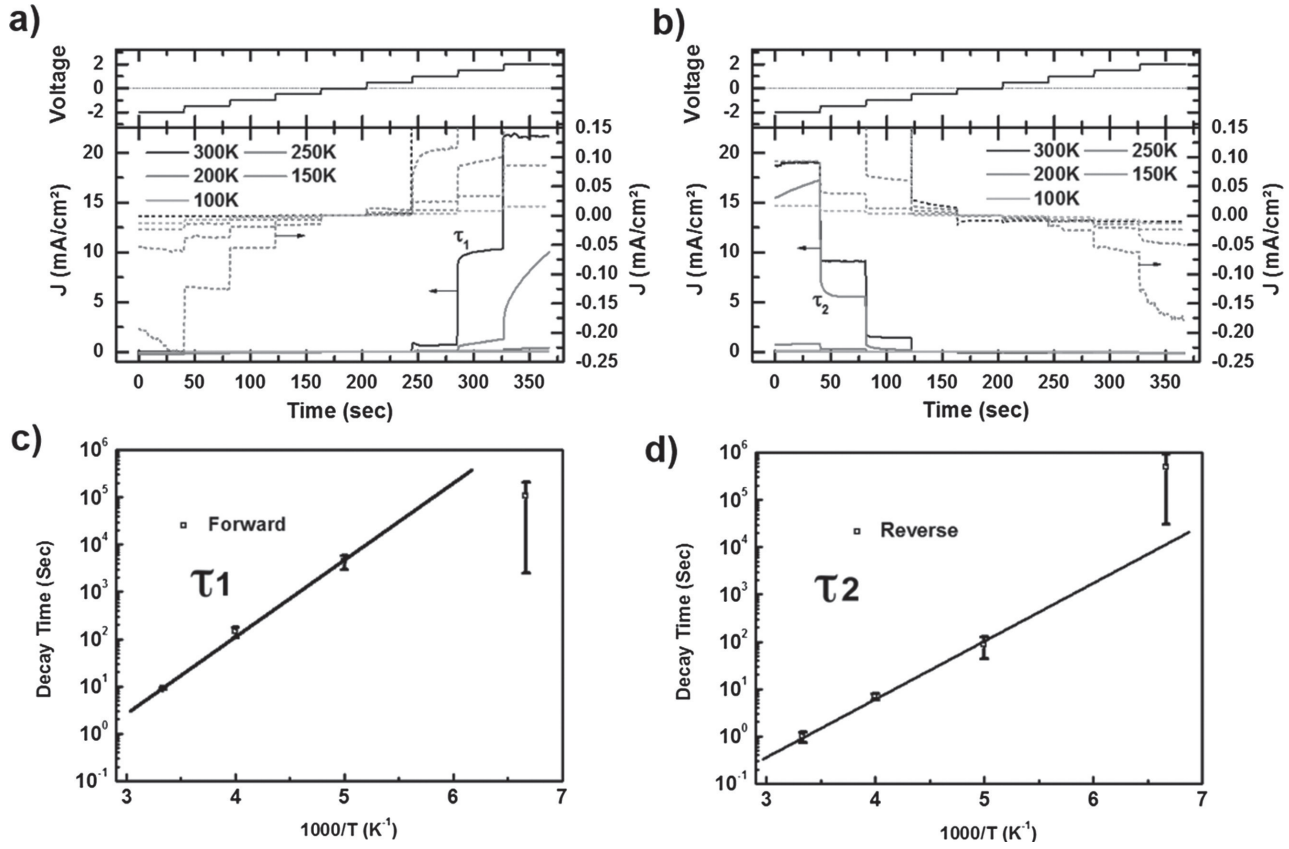

Figure 4. a,b) Temperature dependent current density against time curve of a perovskite solar cells in dark during the forward and reverse sweeping, respectively. c,d) The decay time τ at 1.5 V during forward and reverse sweeping against 1000/T, respectively. The solid lines are the linear fitting curves of first three points (300, 250, and 200 K).

temperature, and k_B is the Boltzmann constant. Plotting $\ln(\tau)$ versus $1000/T$ (Figure 4c) generates a slope of $\Delta E/k_B = 3630$ K, resulting in a thermal activation energy of about 0.31 eV, while in Figure 4d the slope $\Delta E/k_B = 2659$ K, leads to an activation energy of about 0.23 eV. The discrepancy between these two activation energies may be ascribed to the concentration gradient of ions in the vicinity of the interfaces. These activation energies obtained are consistent with previous calculations between 0.16 and 0.33 eV.[20,54] We note that there are differences between our measurements and other reported results. Baumann et al.[55] obtained an activation energy through thermally stimulated current measurement around 0.5 eV. Eames et al.[19] found an activation energy around 0.6 eV through experimental and computational studies. Yang et al.[15] obtained an activation energy of 0.43 eV through temperature conductivity measurements. Almora et al.[35] calculated the activation energy of 0.45 eV by temperature dependent capacitance measurement. We propose that theses differences can be explained by the different fabrication methods used such as either long time annealing[15,19] or two-step fabrication,[55] which lead to different crystalline quality. Our extracted activation energies are very close to the lately reported theoretical calculations by Azpiroz et al.[20]and Haruyama et al.[54]

To study the redistribution of ions after long-term biasing, we used in a further experiment a lateral set of electrodes to apply a bias (**Figure 5**c) and subsequently analyzed the sample with XPS. XPS enables us to quantify the amount of a certain element in the vicinity of the surface. The I/Pb ratio in the as-prepared device between the two electrodes is ≈3.03, consistent with the stoichiometry of the perovskite materials. After biasing at 1 V for 30 min, the ratio of I/Pb becomes 5.65 ± 0.93 at the positive electrode and 2.29 ± 0.04 at the ground electrode (averaged over four separated pairs of electrodes).

In order to investigate the distribution of I and Pb ions between the electrodes (separated laterally by 200 µm as depicted in Figure 5 c), we measured the ratio of I/Pb at nine positions across the electrode pair after biasing at 1 V for 30 min (spot size ≈50 µm). At the positive electrode, in Figure 5f, the I/Pb ratio is 5.57, indicating an accumulation of I^- ions on that side. The ratio of I/Pb decreases across the electrode pair and at the negative electrode, the ratio of I/Pb is around 2.59, implying a lack of the iodide ions (or accumulation of iodide vacancies) there. After 6 h disconnection of the

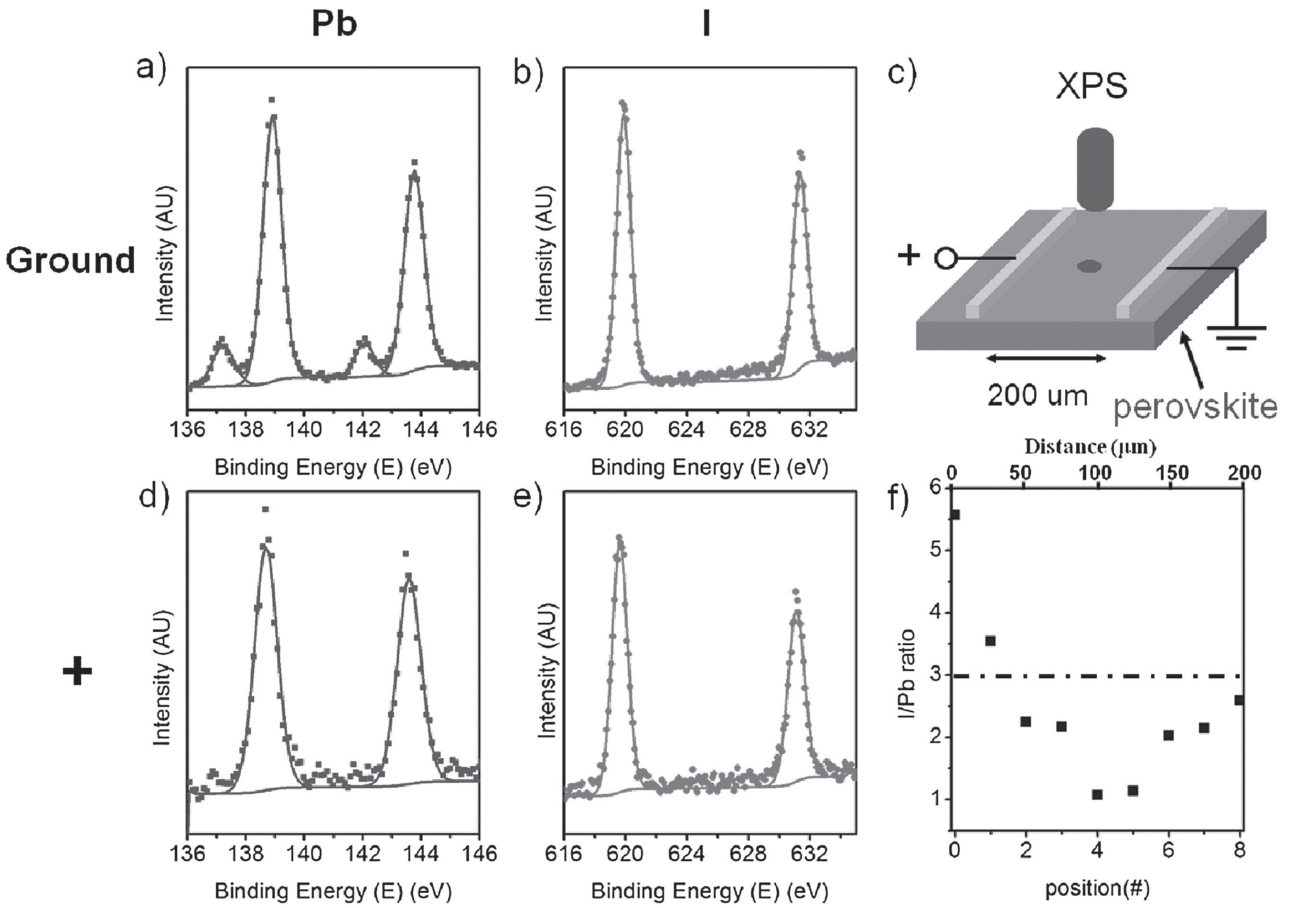

Figure 5. X-ray photoemission spectroscopy (XPS) result of a lateral $CH_3NH_3PbI_{3-x}Cl_x$ device. a,b) XPS spectra of Pb and I in the vicinity the ground electrode, respectively. d,e) The XPS spectra of Pb and I in the vicinity the positive electrode, respectively. c) Illustration of the set-up for characterization of elements distribution using a lateral structure. The applied DC voltage is 1 V for 30 min. The lateral distance between two electrodes is 200 µm. f) Distribution of the ratio of I/Pb between the electrode pairs after applying bias between two lateral electrodes. Position 0 is near the positive electrode and position 8 is near the ground electrode. The dashed line indicates the stoichiometry of perovskite, around 3.

external bias, the ratio of I/Pb at the positive electrode becomes ≈3 again (not shown here). Because the activation energy of Pb ions is very high, ≈2.31 eV,[19] we can assume that this change of I/Pb ratio is only due to the migration of iodide ions. Hence, this change of I/Pb ratio before and after biasing indicates that iodide ions can be driven by an external electrical bias, and these ions can diffuse back to the equilibrium states. This result is fitted nicely into the theoretical calculations of Duan et al.[27] and Azpiroz et al.,[20] in which the defect states in perovskite such as mobile iodide ions or iodine interstitials are the contributing species to the hysteretic behavior. Note that, as shown in Figure 5a, there are two sets of peaks for the Pb 4*f* visible in the XPS spectrum of Pb at the ground electrode and the ratio of I/Pb increases again. This suggests that a decomposition (i.e., electrochemical reaction) of the perovskite material under long term bias starts at this electrode (Figure S9, Supporting Information). A similar observation was recently reported by Fravola et al.[56] investigating the field-induced and photoinduced self-doping chemistry in perovskite films.[56] Kim et al.[57] proposed that the two sets of Pb 4*f* originate from the decomposition of the perovskite materials. Once iodine is no longer within the perovskite crystal structure, these iodide ions may not migrate under this electrical field, and leading to the increase of I/Pb ratio towards ≈3 near the ground electrode. In addition, the increase in the I/Pb ratio is also caused by the relatively large spot size (50 μm) of the XPS measurement.

The absence of hysteresis in FTO/TiO_2/Spiro-OMeTAD/Ag device, as shown in Figure S2 (Supporting Information), suggests that TiO_2 and Spiro-OMeTAD layers are not the main origin of hysteresis in perovskite solar cells. Several groups have proposed the energy band bending due to the migration of ions within the perovskite bulk.[19,21,58] Here, the results presented above suggest a mechanism for the hysteresis seen in perovskite solar cells during forward and reverse voltage sweeping. At the interfaces of $CH_3NH_3PbI_{3-x}Cl_x$ perovskite, two type-II heterojunctions are formed at the $CH_3NH_3PbI_{3-x}Cl_x/TiO_2$ and $CH_3NH_3PbI_{3-x}Cl_x$/Spiro-OMeTAD interfaces, respectively.[3,12] We can assume that due to the high doping level in the Spiro-OMeTAD layer,[42] the Fermi level of TiO_2 is approaching its conduction band (Figure S2, Supporting Information) and relatively high conductivity of TiO_2 layer (Figure S4, Supporting Information), the band bending in both layers is negligible as illustrated in the energy diagram in **Figure 6**a. Furthermore, V_{BI} measured in EA measurement is determined in the reversed bias region, as shown in Figure 3b, in which the overall current is small. In this respect, the perovskite solar cell can be considered as a multilayer capacitor, and TiO_2 layer serves as a dielectric layer in series with the perovskite layer. The dielectric constant of TiO_2, around 100,[59] is much higher than the one of perovskite materials, which is between 18 and 36.[9,35,60] Concerning the thickness of TiO_2 (≈50 nm) and perovskite (≈400 nm), most of the voltage drops within the perovskite layer in the reversed bias region. This has been observed, for example, using Kelvin probe force microscopy by mapping the potential distribution in the perovskite solar cells.[31]

When a positive bias is applied at the Spiro-OMeTAD layer while the TiO_2 layer is grounded, iodide ions I^- are driven towards the $CH_3NH_3PbI_{3-x}Cl_x$/Spiro-OMeTAD interface, leaving iodine vacancies at the opposite electrode. These changes lead to band bending within the $CH_3NH_3PbI_{3-x}Cl_x$ layer in the proximity of the two interfaces as shown in Figure 6b. In this case, the electron and hole injection/extraction improves by tunneling through these narrow interfacial barriers.[44] Thus positive charges accumulate at the TiO_2/perovskite interface and cause compensating negative charges to accumulate at the TiO_2 layer resulting in an upshift of the effective work function of TiO_2 (the Fermi level moves towards the vacuum level). The same happens at the Spiro-OMeTAD layer, with the only difference that the work function shifts downwards (the Fermi level moves away from the vacuum level).[44] Consequently, the built-in potential (which originates from the effective work function difference between the p- and n-type collection layers) experiences an increase with a concomitant decrease of the local injection barriers at these interfaces due to local band bending (Figure S10, Supporting Information). In addition, bimolecular recombination, which is strongly related with the built-in field in the bulk will also significantly decrease.[36,61] This results in an increase of open circuit voltage V_{oc} and enhancement of the device performance, as illustrated in Figure 1b.

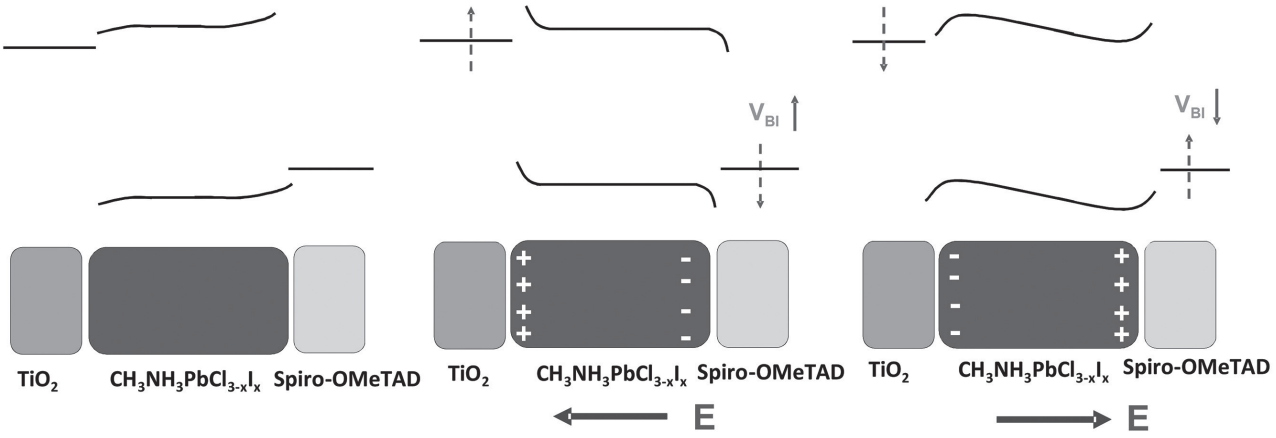

Figure 6. Schematic diagrams of band bending in the perovskite solar cells under electrical fields. The dashed arrows indicate the direction of the effective work function movement. *E* presents the direction of the external electrical field.

Conversely, when applying a negative bias to the Spiro-OMeTAD layer, negatively charged iodide ions, are driven towards the perovskite/TiO_2 interface. In this respect, this change in the distribution of iodide ions alters the band alignment as shown in Figure 6c, resulting in the formation of larger injection barriers at the two perovskite interfaces. These two interfaces hinder the charge injection/extraction due to the formation of interfacial barriers. In addition, the accumulated ions effectively shift down the work function of TiO_2 and shifts up that of the Spiro-OMeTAD, causing a decrease of both the effective built-in potential and the open circuit voltage.

We can now give an explanation for the kink in the *J–V* curve as shown in Figure 1b (indicated by the blue circle) which is usually visible in forward sweeping[7] (and of course depends on the scanning speed). Coming from a negative bias the flat band condition is reached at this point. No electrical field is prevalent at this stage and ion diffusion (no drift) rearranges the built-in potential, which in return shifts V_{oc}.

The presented results imply that improving the crystallinity and quality of the perovskite layer may significantly reduce the density of mobile ions, thereby decreasing the hysteretic behavior. This is consistent with recently reported methods using solvent annealing or mesoporous TiO_2 layers.[16,17]

With these results we can give a concise interpretation of the ion migration, which is dominated by iodide ions. We note that the complete picture of ion movement might be much more complicated due to the coupling between charge transport and ion migration, strong spin–orbit coupling and atomic lattice distortions.[62] The accumulation of ions at the interfaces might further enhance the generation of local defects/interstitials in the lattice, resulting in an enhancement of ions movement through drift and diffusion.[63] In addition, the polycrystalline structure of the perovskite film can also complicate the mechanism owing to complex boundary conditions.[64] In this work, we cannot absolutely rule out the contribution of ferroelectricity of perovskites on the hysteresis, it may play a minor role on the behavior and has not been observed thus far. Methylammonium ions may have to be considered as well[11,12,20] and are subject of further investigation, however, our results clearly show that the migration of iodine plays the major role.

In this article, we investigated the mechanism that mainly contributes to the hysteresis in planar FTO/compact TiO_2/$CH_3NH_3PbI_{3-x}Cl_x$/Spiro-OMeTAD/Ag perovskite solar cells. Through DC dependent EA spectra, temperature dependent electrical measurement and XPS characterization, we can attribute the hysteresis to the modulation of interfacial barriers at $CH_3NH_3PbI_{3-x}Cl_x$/Spiro-OMeTAD and TiO_2/$CH_3NH_3PbI_{3-x}Cl_x$. This modulation is caused by the migration of iodide ions/interstitials driven by an external electrical bias leading to shift in the effective work function at the respective electrodes. By removing these defects related ions, it is likely that we can further enhance the solar cells performance and decrease the hysteretic behaviors. This investigation should contribute to the fundamental understanding of hybrid organic–inorganic material, paving the path for their further development and large-scale industrial application.

Experimental Section

Spiro-OMeTAD was purchased from Merck company, all the other chemicals were purchased from Sigma-Aldrich and were used as received.

Preparation of $CH_3NH_3PbI_{3-x}Cl_x$ Precursor: CH_3NH_3I was synthesized at room temperature for 2.5 h by reacting methylamine (CH_3NH_2, 33 wt% in ethanol) and hydroiodic acide (HI, 57 wt% in water with stabilizer). The ethanol was removed by a rotary evaporator, and the white powder was washed with diethyl ether. Then the product was further dried on hotplate at 70°C and stored in a nitrogen glovebox.

$CH_3NH_3PbI_{3-x}Cl_x$ Perovskite Solar Cells Fabrication and J–V Curve Characterization: Fluorine-doped tin oxide (F:SnO_2) coated glass was patterned by Zn power and HCl solution. FTO glasses were washed successively with acetone, 2% hellmanex diluted in deionized water, deionized water, and isopropanol for 10 min each. A compact TiO_2 layer was deposited by spraying a solution of titanium diisopropoxide bis(acetylacetonate) (0.6 mL) in ethanol (21.4 mL) at 450 °C for 90 min in ambient atmosphere. CH_3NH_3I and lead chloride ($PbCl_2$) were dissolved in anhydrous *N*,*N*-dimethylformamide at 3:1 molar ratio to make a mixture. This perovskite solution was spin-coated at 2000 rpm for 60 s. After drying in a nitrogen glovebox for ≈30 min, the as-spun films were annealed at 100 °C for 90 min. Spiro-OMeTAD solution was prepared by dissolving 72.3 mg Spiro-OMeTAD, 26.3 µL lithium-bis(trifluoromethanesulfonyl)imide (Li-TFSI) solution (520 mg Li-TFSI in 1 mL acetonitrile), and 43.2 µL 4-tert-butylpyridine in 1 mL chlorobenzene. This hole transport layer was deposited by spin-coating at 4000 rpm for 30 s. All device fabrication steps were carried out within a nitrogen filled glovebox. Finally, a 150 nm silver electrode was deposited by thermal evaporation in a chamber with a pressure of 1×10^{-6} mbar. The effective electrode area was 9 mm^2 or 16 mm^2.

J–V measurements were performed under inert environment with a Keithley 2400 source measure unit under 100 mW cm^{-2} illumination from an AM 1.5 solar simulator. The active area of 4 and 9 mm^2 were defined by the overlap of a black mask aperture area, the FTO and the evaporated top electrode. The light intensity was calibrated before by a Si detector. There was no biasing process prior the scanning, we scanned from 2 to −1 V and then measured the reverse scanning continuously. The delay time was 0.01, 0.05, 0.1, and 1 s, respectively. During the delay time, the voltage was kept constant. The step was 0.01 V. Number of power line cycles (NPLC) was 0.1.

EA Characterization: The light source was installed within a monochromator illuminator (Oriel Company). The light going through the monochromator (SPEX 1681B, Horiba Scientific) illuminated the device and was reflected back from the silver electrode onto a photodiode (HUV-4000B, EG&G Judson). A dual channel lock-in amplifier (SR 830 from Stanford Research Systems) was used to bias the device with a DC and an AC voltage and monitored the AC amplitude of the EA signal from the photodiode. In parallel the DC amplitude of the EA signal was recorded with a digital multimeter (HP34401A). For all the electrical experiment, the FTO electrode was connected to the ground, and Ag electrode was applied external voltages.

XPS Experiment: Heavily doped silicon substrates with a 300 nm oxide layer were cleaned successively with acetone, deionized water, and isopropanol for 10 min each in an ultrasonic bath. Then CH_3NH_3I and lead chloride ($PbCl_2$) were dissolved in anhydrous *N*,*N*-dimethylformamide at 3:1 molar ratio. This perovskite solution was spin-coated at 3000 rpm for 60 s. After drying in a nitrogen glovebox for ≈30 min, the as-spun films were annealed at 100 °C in a glovebox for 90 min. Finally, the devices were transferred into an evaporation chamber, and 150 nm of silver was deposited by thermal evaporation through a shadow mask within a chamber pressure of 1×10^{-6} mbar. The electrode distance was 200 µm and the interdigitating electrode geometry provided a ratio between width *W* and length, *W*/*L* of 500. A bias was applied to the devices in a nitrogen glovebox.

The samples were then transferred to the ultrahigh vacuum chamber of the Thermo Scientific ESCALAB 250Xi XPS system. The XPS measurements were carried out using a XR6 monochromated Al k_α

source ($h\nu$ = 1486.6 eV) using a 50 µm spot size. The measurements were collected between the Ag electrodes in steps of 30 µm.

Supporting Information

Supporting Information is available from the Wiley Online Library or from the author.

Acknowledgements

The authors gratefully acknowledge the financial support from the Bavarian frame work program Solar Technologies Go Hybrid. The authors are grateful to Fabian Panzer, Tanaji Gujar and Thomas Unger for valuable discussions.

Received: August 6, 2015
Revised: October 2, 2015
Published online: January 29, 2016

[1] H. Zhou, Q. Chen, G. Li, S. Luo, T. B. Song, H. S. Duan, Z. Hong, J. You, Y. Liu, Y. Yang, *Science* **2014**, *345*, 542.
[2] J. Burschka, N. Pellet, S.-J. Moon, R. Humphry-Baker, P. Gao, M. K. Nazeeruddin, M. Grätzel, *Nature* **2013**, *499*, 316.
[3] M. A. Green, A. Ho-Baillie, H. J. Snaith, *Nat. Photonics* **2014**, *8*, 506.
[4] N. J. Jeon, J. H. Noh, W. S. Yang, Y. C. Kim, S. Ryu, J. Seo, S. I. Seok, *Nature* **2015**, *517*, 476.
[5] a) G. Niu, X. Guo, L. Wang, *J. Mater. Chem. A* **2015**, *3*, 8970; b) C.-C. Chueh, C.-Z. Li, A. K. Y. Jen, *Energy Environ. Sci.* **2015**, *8*, 1160.
[6] a) M. D. McGehee, *Nat. Mater.* **2014**, *13*, 845; b) E. L. Unger, E. T. Hoke, C. D. Bailie, W. H. Nguyen, A. R. Bowring, T. Heumuller, M. G. Christoforo, M. D. McGehee, *Energy Environ. Sci.* **2014**, *7*, 3690.
[7] H. J. Snaith, A. Abate, J. M. Ball, G. E. Eperon, T. Leijtens, N. K. Noel, S. D. Stranks, J. T.-W. Wang, K. Wojciechowski, W. Zhang, *J. Phys. Chem. Lett.* **2014**, *5*, 1511.
[8] J. M. Frost, K. T. Butler, F. Brivio, C. H. Hendon, M. Van Schilfgaarde, A. Walsh, *Nano Lett.* **2014**, *14*, 2584.
[9] J. M. Frost, K. T. Butler, A. Walsh, *APL Mater.* **2014**, *2*, 081506.
[10] H. S. Kim, N.-G. Park, *J. Phys. Chem. Lett.* **2014**, *5*, 2927.
[11] X. Wu, M. T. Trinh, D. Niesner, H. Zhu, Z. Norman, J. S. Owen, O. Yaffe, B. J. Kudisch, X.-Y. Zhu, *J. Am. Chem. Soc.* **2015**, *137*, 2089.
[12] G. Xing, B. Wu, S. Chen, J. Chua, N. Yantara, S. Mhaisalkar, N. Mathews, T. C. Sum, *Small* **2015**, *11*, 3606.
[13] Z. Xiao, Y. Yuan, Y. Shao, Q. Wang, Q. Dong, C. Bi, P. Sharma, A. Gruverman, J. Huang, *Nat. Mater.* **2015**, *14*, 193.
[14] Z.-K. Tan, R. S. Moghaddam, M. L. Lai, P. Docampo, R. Higler, F. Deschler, M. Price, A. Sadhanala, L. M. Pazos, D. Credgington, F. Hanusch, T. Bein, H. J. Snaith, R. H. Friend, *Nat. Nanotechnol.* **2014**, *9*, 687.
[15] T.-Y. Yang, G. Gregori, N. Pellet, M. Grätzel, J. Maier, *Angew. Chem. Int. Ed.* **2015**, *54*, 7905.
[16] N. J. Jeon, J. H. Noh, Y. C. Kim, W. S. Yang, S. Ryu, S. I. Seok, *Nat. Mater.* **2014**, *13*, 897.
[17] W. Nie, H. Tsai, R. Asadpour, A. J. Neukirch, G. Gupta, J. J. Crochet, M. Chhowalla, S. Tretiak, M. A. Alam, H.-L. Wang, *Science* **2015**, *347*, 522.
[18] Y. Shao, Z. Xiao, C. Bi, Y. Yuan, J. Huang, *Nat. Commun.* **2014**, *5*, 5784.
[19] C. Eames, J. M. Frost, P. R. F. Barnes, B. C. O'Regan, A. Walsh, M. S. Islam, *Nat. Commun.* **2015**, *6*, 7497.
[20] J. M. Azpiroz, E. Mosconi, J. Bisquert, F. De Angelis, *Energy Environ. Sci.* **2015**, *8*, 2118.
[21] W. Tress, N. Marinova, T. Moehl, S. M. Zakeeruddin, M. K. Nazeeruddin, M. Gratzel, *Energy. Environ. Sci.* **2015**, *8*, 995.
[22] R. S. Sanchez, V. Gonzalez-Pedro, J.-W. Lee, N.-G. Park, Y. S. Kang, I. Mora-Sero, J. Bisquert, *J. Phys. Chem. Lett.* **2014**, *5*, 2357.
[23] J. M. Frost, K. T. Butler, A. Walsh, *APL Mater.* **2014**, *2*, 081506.
[24] A. M. A. Leguy, J. M. Frost, A. P. McMahon, V. G. Sakai, W. Kockelmann, C. Law, X. Li, F. Foglia, A. Walsh, B. C. O'Regan, J. Nelson, J. T. Cabral, P. R. F. Barnes, *Nat. Commun.* **2015**, *6*, 7124.
[25] Z. Fan, J. Xiao, K. Sun, L. Chen, Y. Hu, J. Ouyang, K. P. Ong, K. Zeng, J. Wang, *J. Phys. Chem. Lett.* **2015**, *6*, 1155.
[26] B. C. O'Regan, P. R. F. Barnes, X. Li, C. Law, E. Palomares, J. M. Marin-Beloqui, *J. Am. Chem. Soc.* **2015**, *137*, 5087.
[27] H.-S. Duan, H. Zhou, Q. Chen, P. Sun, S. Luo, T.-B. Song, B. Bob, Y. Yang, *Phys. Chem. Chem. Phys.* **2015**, *17*, 112.
[28] X. Wu, H. Yu, L. Li, F. Wang, H. Xu, N. Zhao, *J. Phys. Chem. C* **2015**, *119*, 1253.
[29] V. Roiati, E. Mosconi, A. Listorti, S. Colella, G. Gigli, F. De Angelis, *Nano Lett.* **2014**, *14*, 2168.
[30] H. A. Abbas, R. Kottokkaran, B. Ganapathy, M. Samiee, L. Zhang, A. Kitahara, M. Noack, V. L. Dalal, *APL Mater.* **2015**, *3*, 016105.
[31] V. W. Bergmann, S. A. L. Weber, F. Javier Ramos, M. K. Nazeeruddin, M. Grätzel, D. Li, A. L. Domanski, I. Lieberwirth, S. Ahmad, R. Berger, *Nat. Commun.* **2014**, *5*, 5001.
[32] a) J. You, Y. M. Yang, Z. Hong, T.-B. Song, L. Meng, Y. Liu, C. Jiang, H. Zhou, W.-H. Chang, G. Li, Y. Yang, *Appl. Phys. Lett.* **2014**, *105*, 183902; b) J.-H. Im, I.-H. Jang, N. Pellet, M. Grätzel, N.-G. Park, *Nat. Nanotechnol.* **2014**, *9*, 927.
[33] a) D. A. Egger, E. Edri, D. Cahen, G. Hodes, *J. Phys. Chem. Lett.* **2015**, *6*, 279; b) J. Wei, Y. Zhao, H. Li, G. Li, J. Pan, D. Xu, Q. Zhao, D. Yu, *J. Phys. Chem. Lett.* **2014**, *5*, 3937; c) B. Wu, K. Fu, N. Yantara, G. Xing, S. Sun, T. C. Sum, N. Mathews, *Adv. Energy Mater.* **2015**, *5*, 1500829.
[34] A. Kumar, S. Sista, Y. Yang, *J. Appl. Phys.* **2009**, *105*, 094512.
[35] O. Almora, I. Zarazua, E. Mas-Marza, I. Mora-Sero, J. Bisquert, G. Garcia-Belmonte, *J. Phys. Chem. Lett.* **2015**, *6*, 1645.
[36] C. Li, D. Credgington, D.-H. Ko, Z. Rong, J. Wang, N. C. Greenham, *Phys. Chem. Chem. Phys.* **2014**, *16*, 12131.
[37] T. M. Brown, R. H. Friend, I. S. Millard, D. J. Lacey, T. Butler, J. H. Burroughes, F. Cacialli, *J. Appl. Phys.* **2003**, *93*, 6159.
[38] G. U. Bublitz, S. G. Boxer, *Annu. Rev. Phys. Chem.* **1997**, *48*, 213.
[39] L. Sebastian, G. Weiser, H. Bässler, *Chem. Phys.* **1981**, *61*, 125.
[40] F. W. Vance, R. D. Williams, J. T. Hupp, *Int. Rev. Phys. Chem.* **1998**, *17*, 307.
[41] I. H. Campbell, T. W. Hagler, D. I. Smith, J. P. Ferraris, *Phys. Rev. Lett.* **1996**, *76*, 1900.
[42] R. Schölin, M. H. Karlsson, S. K. Eriksson, H. Siegbahn, E. M. J. Johansson, H. Rensmo, *J. Phys. Chem. C* **2012**, *116*, 26300.
[43] C. Li, G. J. Beirne, G. Kamita, G. Lakhwani, J. Wang, N. C. Greenham, *J. Appl. Phys.* **2014**, *116*, 114501.
[44] I. H. Campbell, B. K. Crone, *Appl. Phys. Lett.* **2006**, *88*, 172113.
[45] J. C. De Mello, N. Tessler, S. C. Graham, R. H. Friend, *Phys. Rev. B* **1998**, *57*, 12951.
[46] L. K. Ono, S. R. Raga, S. Wang, Y. Kato, Y. Qi, *J. Mater. Chem. A* **2015**, *3*, 9074.
[47] Y. B. Nian, J. Strozier, N. J. Wu, X. Chen, A. Ignatiev, *Phys. Rev. Lett.* **2007**, *98*, 146403.
[48] I. Yokota, *J. Phys. Soc. Jpn.* **1961**, *16*, 2213.
[49] a) H.-S. Kim, S. H. Im, N.-G. Park, *J. Phys. Chem. C* **2014**, *118*, 5615; b) A. Poglitsch, D. Weber, *J. Chem. Phys.* **1987**, *87*, 6373.
[50] V. D'Innocenzo, G. Grancini, M. J. P. Alcocer, A. R. S. Kandada, S. D. Stranks, M. M. Lee, G. Lanzani, H. J. Snaith, A. Petrozza, *Nat. Commun.* **2014**, *5*, 3586.

[51] H.-H. Fang, R. Raissa, M. Abdu-Aguye, S. Adjokatse, G. R. Blake, J. Even, M. A. Loi, *Adv. Funct. Mater.* **2015**, *25*, 2378.
[52] M. B. Salamon, M. Jaime, *Rev. Mod. Phys.* **2001**, *73*, 583.
[53] G. H. Vineyard, *J. Phys. Chem. Solids* **1957**, *3*, 121.
[54] J. Haruyama, K. Sodeyama, L. Han, Y. Tateyama, *J. Am. Chem. Soc.* **2015**, *137*, 10048.
[55] A. Baumann, S. Väth, P. Rieder, M. C. Heiber, K. Tvingstedt, V. Dyakonov, *J. Phys. Chem. Lett.* **2015**, *6*, 2350.
[56] L. A. Frolova, N. N. Dremova, P. A. Troshin, *Chem. Commun.* **2015**, *51*, 14917.
[57] Y.-H. Kim, H. Cho, J. H. Heo, T.-S. Kim, N. Myoung, C.-L. Lee, S. H. Im, T.-W. Lee, *Adv. Mater.* **2015**, *27*, 1248.
[58] Y. Zhao, C. Liang, H. Zhang, D. Li, D. Tian, G. Li, X. Jing, W. Zhang, W. Xiao, Q. Liu, F. Zhang, Z. He, *Energy Environ. Sci.* **2015**, *8*, 1256.
[59] R. A. Parker, *Phys. Rev.* **1961**, *124*, 1719.
[60] M. Samiee, S. Konduri, B. Ganapathy, R. Kottokkaran, H. A. Abbas, A. Kitahara, P. Joshi, L. Zhang, M. Noack, V. Dalal, M. Samiee, S. Konduri, B. Ganapathy, R. Kottokkaran, *Appl. Phys. Lett.* **2014**, *105*, 153502.
[61] C. G. Shuttle, R. Hamilton, B. C. O'Regan, J. Nelson, J. R. Durrant, *Proc. Natl. Acad. Sci. USA* **2010**, *107*, 16448.
[62] J. Even, L. Pedesseau, J.-M. Jancu, C. Katan, *J. Phys. Chem. Lett.* **2013**, *4*, 2999.
[63] Z.-H. Wang, Y. Yang, L. Gu, H.-U. Habermeier, R.-C. Yu, T.-Y. Zhao, J.-R. Sun, B.-G. Shen, *Nanotechnology* **2012**, *23*, 265202.
[64] W. D. Dane, S. M. Vorpahl, S. D. Stranks, H. Nagaoka, G. E. Eperon, M. E. Ziffer, H. J. Snaith, D. S. Ginger, *Science* **2015**, *348*, 683.

ADVANCED MATERIALS

Supporting Information

for *Adv. Mater.*, DOI: 10.1002/adma.201503822

Iodine Migration and its Effect on Hysteresis in Perovskite Solar Cells

*Cheng Li, Steffen Tscheuschner, Fabian Paulus, Paul E. Hopkinson, Johannes Kießling, Anna Köhler, Yana Vaynzof, and Sven Huettner**

Supporting Information:

Iodine Migration and its Effect on Hysteresis in Perovskite Solar Cells

Cheng Li[1)], Steffen Tscheuschner[2)], Fabian Paulus[3)], Paul Hopkinson[4,5)], Johannes Kießling[1)], Anna Köhler[2)], Yana Vaynzof[4,5)], Sven Huettner[1)*]

1) Macromolecular Chemistry I, University of Bayreuth, Universitaetstr. 30, 95447 Bayreuth, Germany
2) Experimental Physics II, University of Bayreuth, Bayreuth, Germany
3) Organic Chemistry Institute, Im Neuenheimer Feld 270, Heidelberg University, 69120 Heidelberg, Germany
4) Kirchhof Institute for Physics, Im Neuenheimer Feld 227, Heidelberg University, 69120 Heidelberg, Germany
5) Centre for Advanced Materials, Im Neuenheimer Feld 225, Heidelberg University, 69120 Heidelberg, Germany
*) Author to whom correspondence should be addressed. Electronic address: Sven.Huetttner@uni-bayreuth.de

Absorption and Photoluminescence Spectroscopy

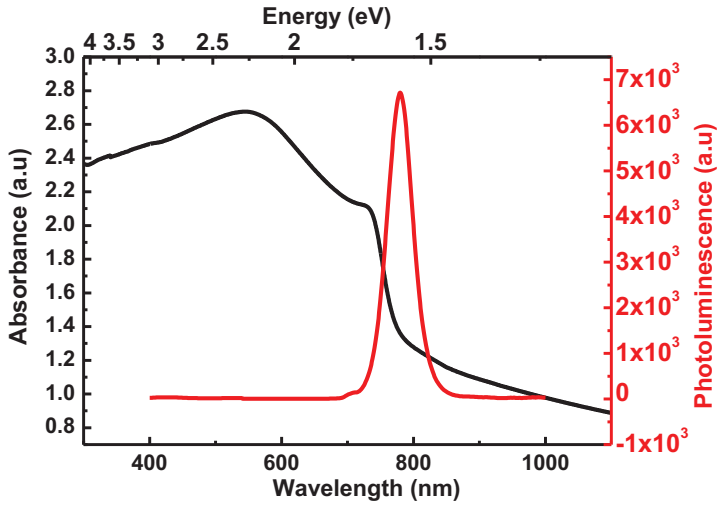

Figure S1. Absorption and photoluminescence spectra of $CH_3NH_3PbI_{3-x}Cl_x$ perovskite on quartz substrate.

The absorption and photoluminescence spectra of $CH_3NH_3PbI_{3-x}Cl_x$ perovskite thin film on glass substrate are shown in Figure S1. The absorption edge is located at around 780 nm, which is consistent with previous papers.[1] The excitation wavelength is 350 nm and the PL peak is centered at around 769 nm.

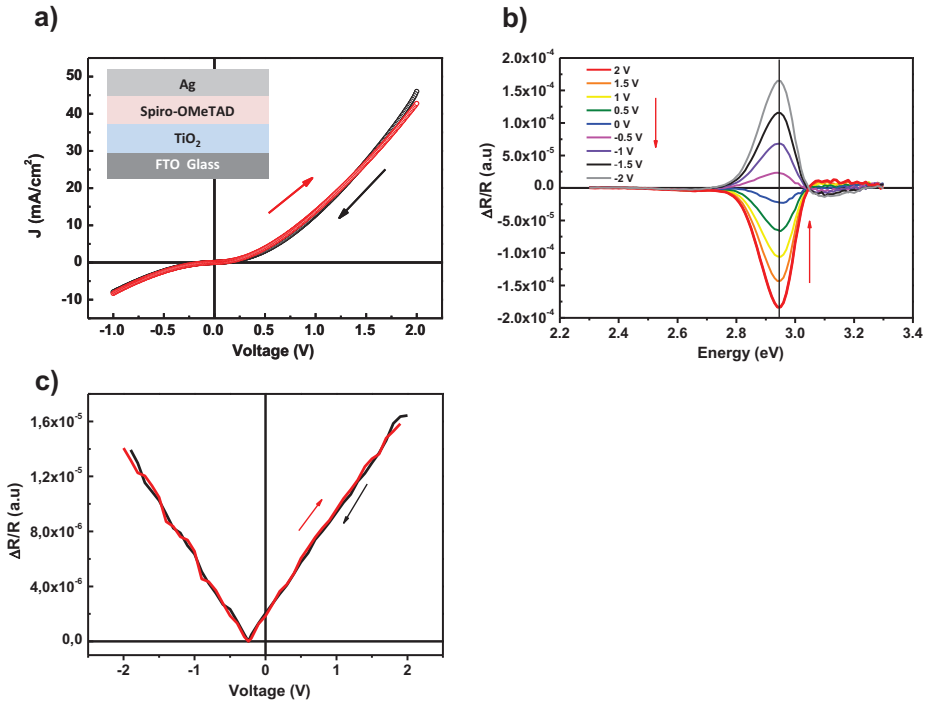

Figure S2. a) *J-V* curve of a FTO/compact TiO_2/Spiro-OMeTAD/Ag device in forward and reverse sweeping. Inset is the structure of the device. b) The DC dependence of EA spectra. Arrows indicate the directions of applying voltage. The line at 2.94 eV indicates the energy of light for the DC dependence EA signal. Red arrows indicate the order of applied voltage. c) The DC dependence EA signal at 2.94 eV, in the forward and reverse sweeping. Arrows show the direction of applying voltages. The AC amplitude is 1 V. The frequency of AC voltage is 2.01 kHz.

Figure S2a shows the current-voltage curves of a FTO/TiO_2/Spiro-OMeTAD/Ag device, which indicates there is no hysteresis phenomena between forward and reverse sweeping. Figure S2b shows the DC dependence of EA spectra between 2.3 and 3.3 eV. Figure S2c shows the DC dependence of EA signal at 2.94 eV. The built-in potential of 0.2±0.1 V is obtained, which is consistent with the work function difference between TiO_2 and Ag electrodes.[2] Hence, this indicates that the Fermi level of TiO_2 is approaching its conduction band (4.0 eV), assuming the work function of Ag is 4.3 eV. In addition, this result shows that there is no hysteresis in the forward and reverse sweeping of the EA signal. These results verify that only the perovskite layer is associated with both hysteresis effects in EA and *J-V* curves.

Scanning speed dependent of J-V curve measurement

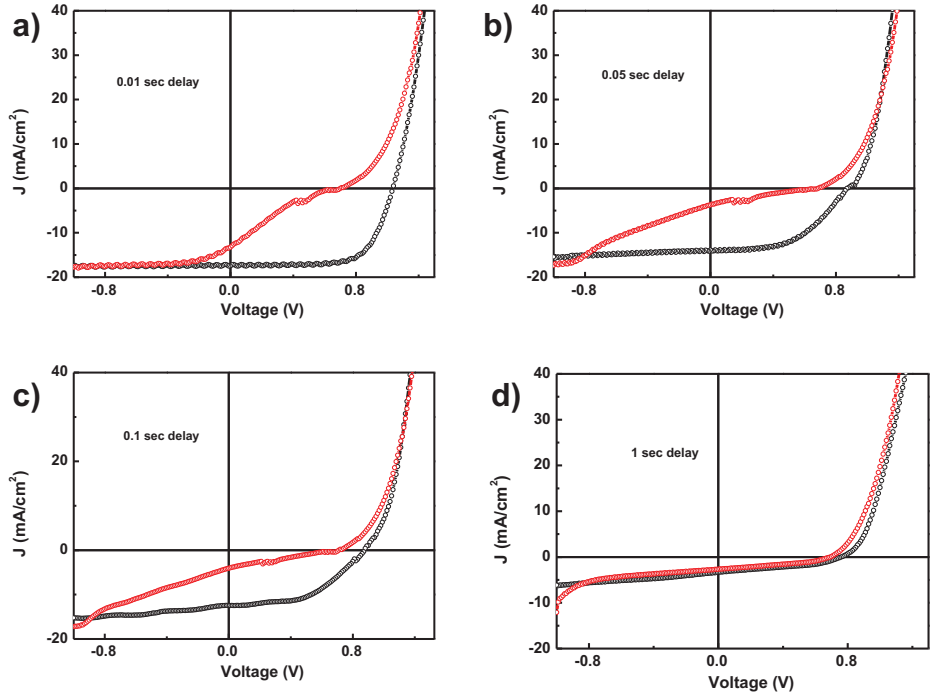

Figure S3. J-V curve measurement with different delay times, a) 0.01 Sec, b)0.05 Sec, c) 0.1 Sec and d) 1 Sec.

The J-V curve measurement, there is no prior biasing process, we scan from 2v to -1V and then measure the reverse scanning continuously. We used Keithley 2400 sourcemeter. The delay time is 0.01 sec, 0.05 sec, 0.1 sec, and 1 sec, respectively, with step of 0.01 V. That means during measurement, before change to the next voltage point, the voltage was kept 0.01 sec, 0.05 sec, 0.1 sec and 1 sec, respectively. The results are consistent with other papers.[3] With increasing the delay time, the current decrease, and the difference between forward and reverse decreases.

Conduction measurement of TiO_2 layer.

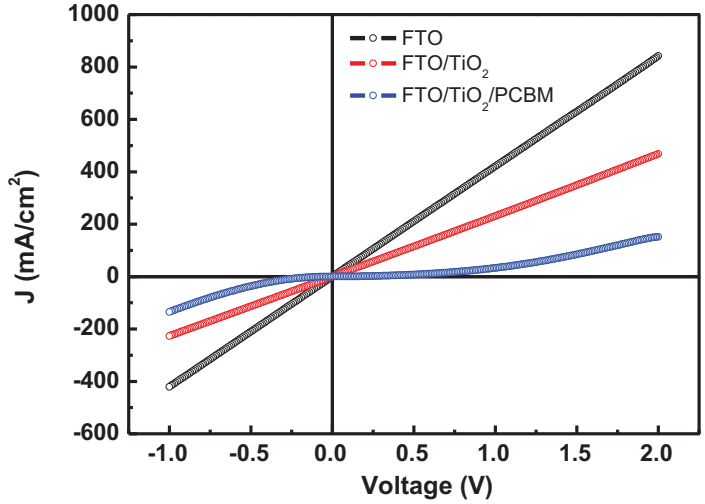

Figure S4. *J-V* curve measurement of FTO/Ag, FTO/TiO_2/Ag and FTO/TiO_2/PCBM/Ag measurement.

The thickness of FTO, TiO_2 and PCBM are 120nm, 50 nm and ~50 nm respectively. Based on the *J-V* plot, we can obtain the dc conductivity σ of different layers.[4]

$$I = \sigma A d^{-1} V \quad (1)$$

where, I is the current, A is the effective electrode area, d is the thickness and V is the voltage applied between two electrodes.

For pure FTO the conductivity is 0.005 mS/cm and FTO/TiO_2 0.001 mS/cm. Considering the geometry of FTO/Ag device, the conductivity of FTO is underestimated. While the high conductivity of TiO_2 may be ascribe to the diffusion of Ag into TiO_2, so we make the FTO/TiO_2/PCBM to protect the TiO_2 layer. In this device the conductivity significantly decreases, which is ascribed to the interfacial barrier between TiO_2 and Ag or PCBM layer as well as the resistance of PCBM layer. However, we can obtain the similar order of magnitude of current amplitude in the large positive voltage. Hence, it indicates that the conductivity of TiO_2 layer is quite high, and it is consistent with the previous EA result (Figure S2) on the Fermi level of TiO_2

Electroluminescence

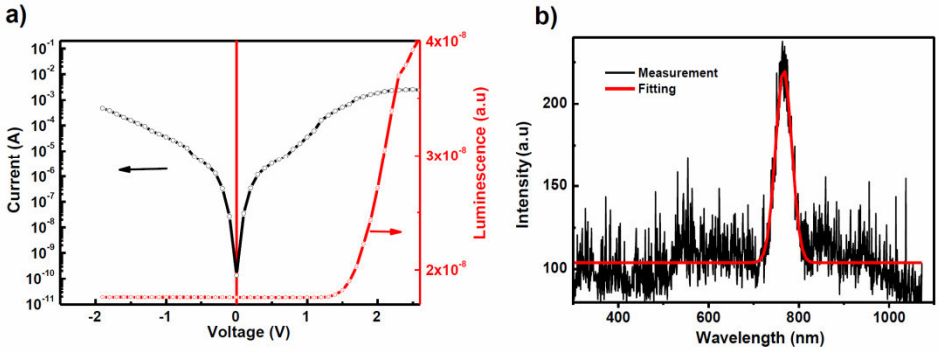

Figure S5. a) Combined current (black) and electroluminescence amplitude (measured by a photodetector) (red) versus voltage characteristics of the perovskite solar cell. The device turns on at 1.3 V. The direction of applying voltage is from -2 V to 2.5 V. b) Electroluminescence spectrum of the perovskite solar cell, and the fitting curve based on Gaussian function.

Figure S3a shows the current and luminescence characteristic of a FTO/TiO_2/perovskite/Spiro-OMeTAD/Ag device in reverse sweeping. This result indicates that this solar cell can function, even though as a very poor, as a light emitting diode and generates infrared light through electroluminescence. The turn on voltage is around 1.3 V, which is consistent with the DC dependent EA signal. Figure S3b shows the emission spectrum of the FTO/compact-TiO_2/perovskite/Spiro-OMeTAD/Ag device when applying +2 V, which is consistent with the result of Z. Tan, *et al.*[1]

Bias Stress and Current Dynamics

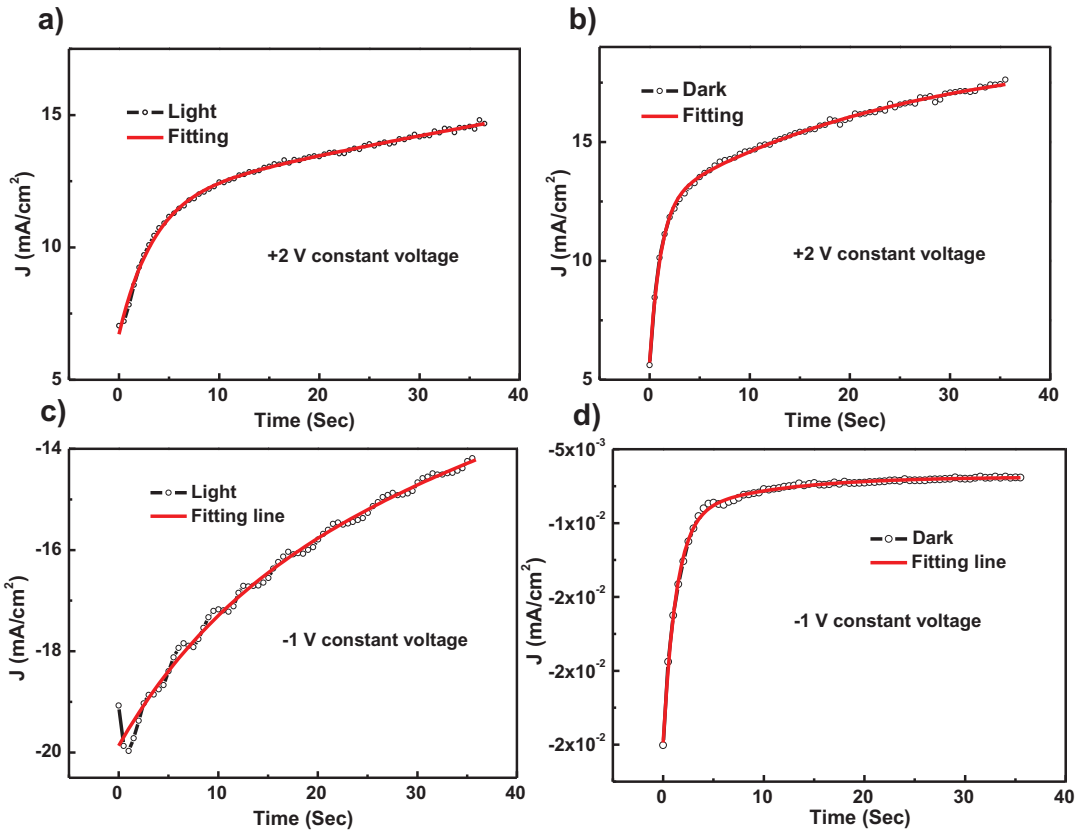

Figure S6. a) and b) The time dependent current density of the perovskite solar cell when applying constant +2 V under AM 1.5G and dark, respectively. c) and d) The time dependent current density of the perovskite solar cell when applying constant -1 V under AM 1.5G and dark, respectively. Red curves are the fitting lines based on exponential functions. FTO layer is connected to the ground.

Figures S4a and S4b show the current density dynamics of the perovskite solar cell when applying a constant voltage of +2 V, under AM 1.5G illumination and dark condition, respectively. Figures S4c and S4d show the current density dynamics when applying constant -1 V bias under AM 1.5G and dark condition, respectively. All the curves can be fitted using a bi-exponential function, τ_1 is in the order of ~1 sec and τ_2 is in order of magnitude of 100 sec. It indicates that under electrical stress, two distinct processes occur, *i.e.* a fast and a much slower one. Note that, in the temperature dependent measurement, the dynamic processes are fitted by single exponent function, the slow processes are not observed during applying the step voltages. In general these ions can be considered as individual point defects within a matrix of stoichiometric atoms. For perovskite materials[5], but also for binary oxide

materials,[6] there are strong interactions among defects, which perform as ordered or collective clusters rather than free isolated points. The energy for the migration of these clusters is much larger than the one for individual isolated vacancies. In addition, the movement of these individual defects might further lead to the rearrangement of the local atomic lattice. This can give rise to the separation of the cluster into single isolated defects or smaller size clusters. At low temperature, this slow process, *i.e.* the movement of larger clusters, might play a minor role for the hysteresis effect. Therefore, a single exponential function can sufficiently describe the dynamics. The detailed microscopic reason will be subject to further investigations.

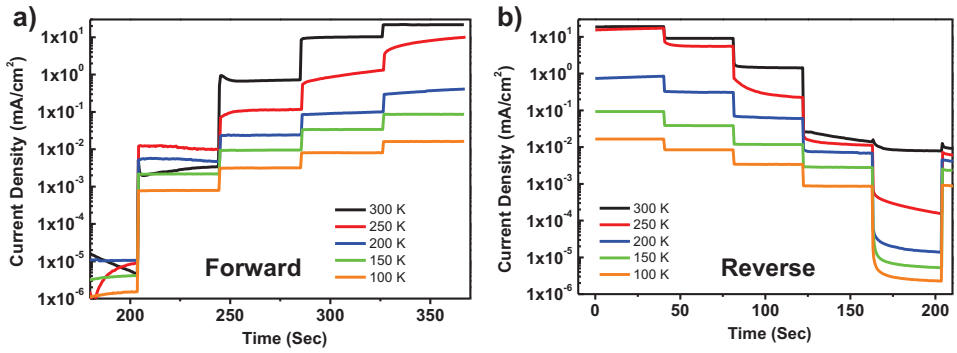

Figure S7. a) and b) Temperature dependent current density versus time of a perovskite solar cells in dark during the forward and reverse sweeping in log scale, respectively.

X-ray Phototelectron Spectroscopy

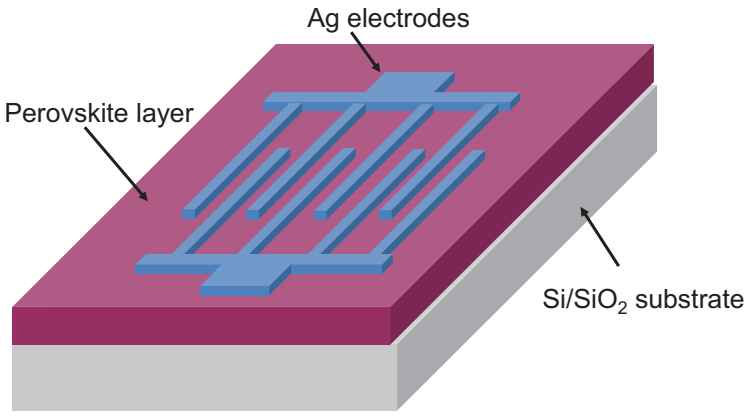

Figure S8. Schematic of the structure of a laterally configured device for XPS measurement to characterize the distribution of ions within the channel after a electrical stress.

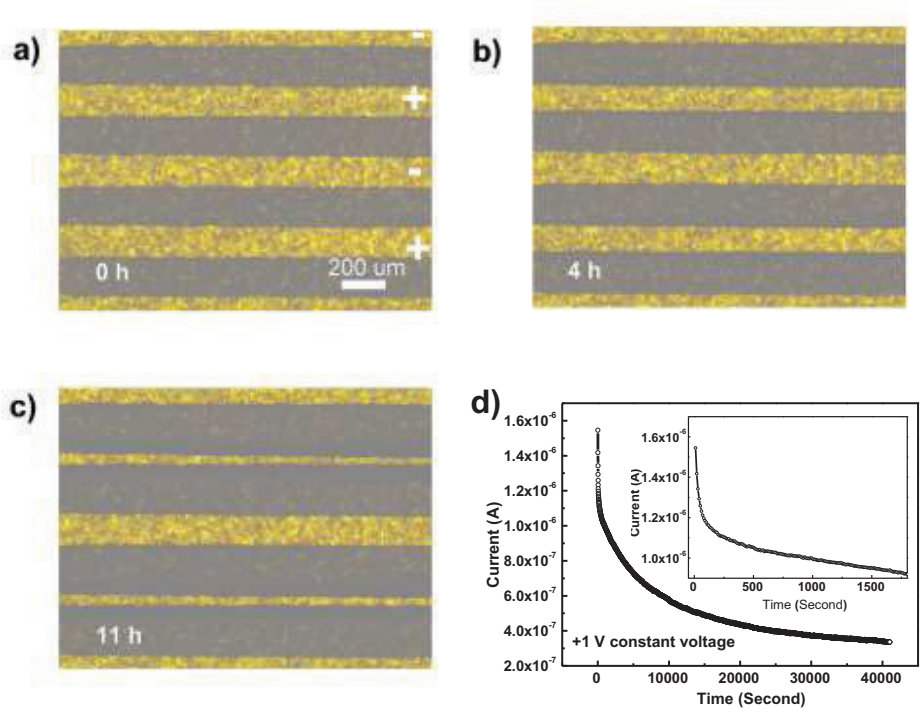

Figure S9. a) to c) *In-situ* microscopy snapshots while applying a voltage, showing the change of the anode material. We suggest that the change of the width of Ag anode (positive voltage), is an electrochemical reaction between I with Ag during the biasing process. The applied constant voltage is +1 V. (d) The time dependency of the current during the biasing process shows single exponential decay behavior. The inset is the time dependent current behavior in 30 min.

Modulation of Interfacial Barrier

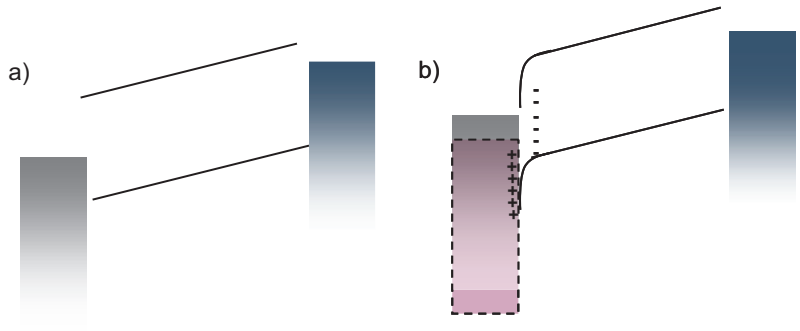

Figure S10. Schematic energy diagram of a device before a) and after b) charges accumulate at the interface. After charges accumulate at the interface, compensating positive charges accumulated at the electrode. As a consequence, the *effective* work function of the electrode shifts due to interfacial dipoles, leading to the change of the built-in potential of the devices. In the mean time, the local interfacial barrier decreases, enhancing the hole injection/extraction.

References

[1] Z.-K. Tan, R. S. Moghaddam, M. L. Lai, P. Docampo, R. Higler, F. Deschler, M. Price, A. Sadhanala, L. M. Pazos, D. Credgington, F. Hanusch, T. Bein, H. J. Snaith, R. H. Friend, *Nat. Nanotechnol.* **2014**, 9, 687.
[2] M. A. Green, A. Ho-Baillie, H. J. Snaith, *Nat. Photon.* **2014**, 8, 506.
[3] L. K. Ono, S. R. Raga, S. Wang, Y. Kato, Y. Qi, *J. Mater. Chem. A* **2015**, 3, 9074; R. S. Sanchez, V. Gonzalez-Pedro, J.-W. Lee, N.-G. Park, Y. S. Kang, I. Mora-Sero, J. Bisquert, *J. Phys. Chem. Lett.* **2014**, 5, 2357.
[4] J. Obrzut, K. A. Page, *Phys. Rev. B* **2009**, 80, 195211.
[5] Z.-H. Wang, Y. Yang, L. Gu, H.-U. Habermeier, R.-C. Yu, T.-Y. Zhao, J.-R. Sun, B.-G. Shen, *Nanotechnology* **2012**, 23, 265202.
[6] C. Zhang, A. Michaelides, D. A. King, S. J. Jenkins, *Phys. Rev. B* **2009**, 79, 075433; S. Park, H.-S. Ahn, C.-K. Lee, H. Kim, H. Jin, H.-S. Lee, S. Seo, J. Yu, S. Han, *Phys. Rev. B* **2008**, 77, 134103.

Danksagung

Zunächst möchte ich mich bei Frau Prof. Dr. Anna Köhler bedanken, die mir die Möglichkeit gegeben hat an ihrem Lehrstuhl zu promovieren und mir dabei die Möglichkeit gegeben hat meine Persönlichkeit zu entfalten. Ebenso danken möchte ich dafür, dass Sie mich so bei der Erstellung, Korrektur und Einreichung meiner Publikationen so Tatkräftig unterstützt haben. Ich werde ebenfalls nicht vergessen wie Sie sich eingesetzt haben, damit ich an Konferenzen wie die „Gordon-Research-Konferenz“ in Italien sowie dem „MRS-Spring-Meeting“ in den USA teilnehmen durfte. Ich möchte mich für die schöne Zeit am Lehrstuhl bedanken!

Ein weiterer Dank geht an Prof. Dr. Heinz Bässler, der mich immer unterstützt hat. Insbesondere sind hier die stets fruchtbaren, lehrreichen und interessante Diskussionen in „ihrem Kämmerchen“ zu erwähnen. Hierbei haben Sie Ihr gesammeltes Fachwissen und Ihre Erfahrung zur Verfügung gestellt. Auch dafür möchte ich mich bedanken.

Ganz herzlich möchte ich dem Graduierten Kolleg 1640 danken im Rahmen dessen ich meine Promotion durchführen durfte. Hierbei sind neben der zusätzlichen finanziellen Unterstützung auch meine Mentoren, alle beteiligten Professoren sowie alle Mit-Promovierende zu erwähnen, die mich während meiner Promotion immer unterstützt haben.

Des Weiteren möchte ich mich bei meinen langjährigen Bürokollegen Tobias Hahn bedanken, der mich immer unterstützt hat. Ich finde es gut, wie du meine Marotten die ganze Zeit ausgehalten hast und (hoffentlich) immer noch froh bist bei mir in „unserem Kämmerchen“ zu sitzen. Zusätzlich möchte ich mich noch für die interessanten Konferenzen, die wir gemeinsam besucht haben, bedanken. Auf noch eine lange, gute und erfolgreiche Zusammenarbeit, solange du noch an der Uni bist. ;-)

Ebenso möchte ich mich bei Julian Kahle der mich mit seinem Fachwissen und seiner Kompetenz immer unterstützt hat. Ich hoffe du führst das Solarzellenerbe erfolgreich fort. Du hattest ja jetzt genug Zeit dich damit vertraut zu machen, am Anfang unter meiner Obhut, dann als Kollegen und am Ende unter deiner Führung.

Ich möchte mich auch bei Alexander Rudnick bedanken, der mich insbesondere am Montag immer motiviert hat das Spiegelrätsel zu lösen, damit die grauen Zellen nach dem Wochenende wieder hochfahren.

Ein ganz besonderer Dank geht auch an meine Studenten Julian Kahle (2x), Markus Dauth, Johannes Ress und Michael Reitz, die ich betreuen durfte. Ihr habt mich immer weitergebracht und wo es ging unterstützt.

Bedanken möchte ich mich auch bei meinen Kollegen Markus Reichenberger, Tobias Meier, Thomas Unger, Stefan Wedler, Fabian Panzer, Christina Saller und Exkollege und Exbetreuer Christian Schwarz bedanken.

Bedanken möchte ich mich auch bei Frank Schirmer, Irene Bauer, Thomas Vogtmann, Michaela Fischer, Thomas Dabisch und Melanie Kummer für die großartige Unterstützung während meiner gesamten Promotion.

Nicht zu vergessen ist hier die Kaffeerunde, welche versucht hat mich immer aufzumuntern. Natürlich darf ich natürlich nicht unser blödes Gewaaf vergessen zu erwähnen, ohne welches so mancher Tag nur halb so lustig gewesen wäre.

Ein herzlicher Dank geht auch an die Mittagskickerrunde, welche mich nach dem Mittagessen immer wieder gefordert hat, sei es bei einem Spielstand von 9-9, 0-0 oder 9-0. Es hat mir immer Freude bereitet das entscheidende Tor zum 10-9, 1-0 oder 9-1 zu schießen. Nur noch mehr Freude macht da eigentlich das 10-0.

Ein großer herzlicher Dank geht auch an meine Familie die mich schon mein ganzes Studium unterstützt hat und mir immer Mut gegeben haben weiter zu machen. Ihr habt mir das Physikstudium ermöglicht und damit auch diese Promotion. Vielen Dank.

Auch wenn es für dich immer so aussieht, dass du ganz am Ende kommst, bist du für mich immer an erster Stelle. Deswegen möchte ich mich hier an dieser Stelle von ganzem Herzen bei dir bedanken, meine liebe Frau, dass du nie an mir gezweifelt und immer zu mir gehalten hast. Eva Tscheuschner ich möchte mit allem was ich habe bei dir bedanken, dafür, dass du mir immer ein Lächeln auf meinen Mund gezaubert hast und mich bei allem, was ich gemacht habe, unterstützt hast. Du gibst mir Kraft und Mut für jeden neuen Tag. Du bist die Liebe meines Lebens, ich danke dir dafür.

Erklärung

Hiermit erkläre ich mich einverstanden, dass die elektronische Fassung meiner Dissertation unter Wahrung meiner Urheberrechte und des Datenschutzes einer gesonderten Überprüfung hinsichtlich der eigenständigen Anfertigung der Dissertation unterzogen werden kann.

(§ 8 S. 2 Nr. 6 PromO)

Hiermit versichere ich eidesstattlich, dass die Dissertation selbständig verfasst und keine anderen als die von mir angegebenen Quellen und Hilfsmittel benutzt habe.

(§ 8 S. 2 Nr. 8 PromO)

Hiermit erkläre ich, dass ich nicht bereits versucht habe eine Dissertation einzureichen oder mich einer Doktorprüfung zu unterziehen.

(§ 8 S. 2 Nr. 9 PromO)

Hiermit erkläre ich, dass ich bisher keine Hilfe von gewerblichen Promotionsberatern bzw. Promotionsvermittlern in Anspruch genommen habe und diese auch künftig nicht in Anspruch nehmen werde.

(§ 8 S. 2 Nr. 10 PromO)

Bayreuth, den 22.12.2016

Steffen Tscheuschner